University of Bath

PHD

Investigation into track parameters for simulation of electrified railway systems

Carpenter, David C.

Award date:
1993

Awarding institution:
University of Bath

Link to publication

Alternative formats
If you require this document in an alternative format, please contact:
openaccess@bath.ac.uk

General rights
Copyright and moral rights for the publications made accessible in the public portal are retained by the authors and/or other copyright owners and it is a condition of accessing publications that users recognise and abide by the legal requirements associated with these rights.

- Users may download and print one copy of any publication from the public portal for the purpose of private study or research.
- You may not further distribute the material or use it for any profit-making activity or commercial gain
- You may freely distribute the URL identifying the publication in the public portal ?

Take down policy
If you believe that this document breaches copyright please contact us providing details, and we will remove access to the work immediately and investigate your claim.

Download date: 11. May. 2021

Investigation into Track Parameters for Simulation of Electrified Railway Systems

submitted by David C. Carpenter
for the degree of Doctor of Philosophy
of the University of Bath

1993

COPYRIGHT

Attention is drawn to the fact that copyright of this thesis rests with its author. This copy of the thesis has been supplied on condition that anyone who consults it is understood to recognise that its copyright rests with its author and that no quotation from the thesis and no information derived from it may be published without the prior written consent of the author.

This thesis may be made available for consultation within the University Library and may be photocopied or lent to other libraries for the purposes of consulation.

UMI Number: U057695

All rights reserved

INFORMATION TO ALL USERS
The quality of this reproduction is dependent upon the quality of the copy submitted.

In the unlikely event that the author did not send a complete manuscript
and there are missing pages, these will be noted. Also, if material had to be removed,
a note will indicate the deletion.

UMI U057695
Published by ProQuest LLC 2013. Copyright in the Dissertation held by the Author.
Microform Edition © ProQuest LLC.
All rights reserved. This work is protected against
unauthorized copying under Title 17, United States Code.

ProQuest LLC
789 East Eisenhower Parkway
P.O. Box 1346
Ann Arbor, MI 48106-1346

UNIVERSITY OF BATH
LIBRARY
33 2 DEC 1993
5075533

Summary

The use of electronic train control systems and power electronic control for traction on electric railways is well established. The application of such systems has increased the awareness of the effects of electromagnetic interference with regard to system safety and reliability. One approach to assuring electromagnetic compatibility between subsystems is by circuit simulation studies. This requires the establishment of an accurate electrical model for the whole traction network. Of importance in this modelling procedure is the representation of the rail track. This thesis reports on the results of research to accurately define the track self and mutual impedances and admittances.

The material properties of the complete track structure are examined. The electromagnetic properties of rail material are determined, by measurement, testing and modelling methods. The ground plane and track bed also have significant effects in such studies and the results from the examination of the electromagnetic properties of ballast, soil and sleepers are reported.

The influences of material properties on the track transmission line parameters are described in terms of series impedance behaviour and shunt admittance behaviour. These parameters have been measured, estimated from approximate analytical methods and modelled by appropriate numerical techniques.

Applications of the derived track transmission line parameters are described. A matrix method has been used and this is explained in detail. Case studies are given with typical design problems considered and the usefulness of the simulator in such studies of the interaction of traction and signalling systems is outlined.

Acknowledgements

I should like to thank Dr. R.J. Hill for his constant and enthusiastic interest, support and guidance throughout the period of research and in the writing of this thesis.

Also I should like to acknowledge the support given by the Directors of Vector Fields Limited who have actively encouraged this research by providing computer facilities for finite element analysis and the writing of the thesis.

In addition I should like to thank Prof. D. Roger and Dr. P. Leonard for their help in using finite element software.

Contents

List of Figures

List of Tables

Abbreviations

μ	permeability
σ	conductivity
ϵ	permittivity
a.f.	audio–frequency
a.c.	alternating current
A.I	artifical intelligence
A.T.	autotransformers
A.T.C.	automatic train control
A.T.O.	automatic train operation
A.T.P.	automatic train protection
A.T.S.	automatic train supervision
A.W.S.	automatic warning system
B	flux density
B–H	flux density verses magnetic field strength
B.A.R.T.	Bay Area Rapid Transit
B.T.	booster transformers
C.A.D.	computer aided design
C.D.A.	critical damping adjustment
C.S.I.	current source inverters
d.c.	direct current
D.L.R.	Docklands Light Railway
D.O.T.	Department of Transportation
E.M.C.	electromagnetic compatibility
E.M.I.	electromagnetic interference

E.M.T.D.C.	Electromagnetic Transient Simulation Program
E.M.T.P.	Electromagnetic Transients Program
E.P.R.I.	Electric Power Research Institute
F.D.M.	finite difference method
F.E.	Finite Element
F.E.M.	finite element method
F.F.T.	fast fourier transform
F.S.K.	frequency shift keying
G.M.D.	geometric mean difference
G.M.R.	geometric mean radius
G.T.O.	gate turn off switch
H	magnetic field strength
Hmax	maximum magnetic field strength
L.U.	London Underground
M.T.R.C.	Mass Transit Railway Corporation
P.W.M.	phase width modulation
S.N.C.F.	Societe Nationale des Chemins de Fer
S.P.I.C.E.	Simulation Program with Integrated Circuit Emphasis
'T','PI'	circuit connection descriptions
U.M.T.A.	Urban Mass Transit Administration
V.S.I.	voltage source inverters
W.M.A.T.A.	Washington Metropolitan Area Transit Authority

Notation

α	temperature coefficient
α_{circ}	$j\omega\sigma\mu^*$
$\alpha_n(z)$	nth Taylor series coefficient
δ, δ_{eff}	(effective) skin depth
ϵ	permittivity
Γ	the gamma function
$[\gamma]$	modal propagation constants matrix
γ	modal propagation constant
γ_{xn}	substitution variable
γ_{comm}, γ_{diff}	modal propagation constants
$[\mathbf{\Lambda}]$	eigenvalue matrix
λ	substitution variable
λ_i	ith mode eigenvalue
μ	permeability
μ^*	complex permeability
μ'	real part of permeability
μ''	imaginary part of permeability
$\mu_{\Delta AC}$	small signal AC permeability
$\mu_{\Delta DC}$	delta permeability
μ_{area}	permeability of elliptical B–H model
μ_{Bo}	permeability of fundamental flux density B–H model
μ_{diff}	differential permeability
μ_{eff}	effective permeability
μ_i	initial permeability

μ_{inc}	incremental permeability
μ_{max}	maximum permeability
μ_n	normal permeability
μ_o	permeability of free space
ω	frequency
Φ	flux
ϕ	substitution variable
ρ, ρ_{20}	resistivity (at 20° C)
σ	conductivity
σ_{circ}	conductivity of circular conductor
σ_e, σ_{gnd}	ground conductivity
σ_{FEM}	conductivity of F.E.M. model
τ	travel time
[**A**]	[**Y**].[**Z**] resultant matrix
$A(\lambda)$	substitution variable
A_{FEM}	area of F.E.M. model
A, A_1, A_2, A_u, a	constants
a_a, b_a, c_a, d_a	experimental circuit constants
a_a', b_a', c_a', d_a'	experimental circuit constants
a_e, a_{eq}	equivalent radius
a_n	$\alpha_n(o)$
a_{rad}	radius
ΔB	change in flux density
B	flux density
B_1, B_2, B_u	constants

B_o	fundamental component of flux density
b	constant
b_{eff}	effective susceptance
b_{ie}	conductor–to–ground susceptance
b_{ij}	inter–conductor susceptance
b_{meas}	measured susceptance
C	capacitance
C_{ie}	conductor–to–ground capacitance
C_{mij}	mutual capacitance
c	constant
d	circuit separation
d_x	ground layer interface depth
d_{rail}	rail separation
E	electric field strength
$e_m(t),\ E_s$	source voltage
$[\mathbf{F}]$	matrix of F_{ij} elements
F_{ij}	experimental circuit constants
${}_1F_1$	degenerate hypergeometric function
$[\mathbf{G_{node}}]$	conductance matrix
G	conductance
$g(\lambda)$	arbitrary function of λ
g_{eff}	effective conductance
g_{ie}	conductor–to–ground conductance
g_{ij}	mutual conductance
g_{meas}	measured conductance

ΔH	change in magnetic field strength
H	magnetic field strength
H_{mn}	magnetic field strength at node nm for F.D.M.
h	transmission line constant dependent on Z_n and R
h_λ	small fraction of λ
$h_k,\ h_m,\ h_t$	height of conductor above ground
h_s	spacial step length for F.D.M.
[I]	phase current vector
$[\mathrm{I^m}]$	modal current vector
$[\mathrm{I_{node}}]$	current vector for simulation
Ipk	peak current of chopper circuit
I_{int}	rail current in F.E.M. model
I_k	Norton current for node k
I_l	load current
I_n	phase current for rail n
${I_n}^m$	modal current for mode n
$I_{na},\ I_{nb},\ I_{nc}$	rail currents
$I_{OB},\ I_{1B}$	bessel functions
$I_s,\ I_a,\ I_b$	source currents
$i_{mn}(t)$	current flowing between nodes m and n at time t
J	current density
$J_m,\ J_{xs}$	substitution variables
J_o	bessel function
J_s	elemental current density

$[\mathbf{K}]$	reflection coefficient matrix
K_{1B}	bessel function
k	kernel function
L	inductance
l	transmission line length
l_{circ}	inductance of circular conductor
l_r	test track length
$l_{int-FEM}$	internal inductance by F.E.M.
$[\mathbf{M}]$	general matrix M
$det[\mathbf{M}]$	determinant of matrix M
$M_{pq}(z)$	whittaker function
p	time step length for F.D.M.
$Q_e(r),\ Q(r)$	mutual resistance
R	resistance
R_c	conductor resistance
R_e	earth resistance
$R_p,\ r_p$	probe spacing
r	radial distance
r_{circ}	circular conductor radius
r_{DF}	$p/(\sigma\mu h_s{}^2)$
$r_{int-FEM}$	internal resistance by F.E.M.
r_{nm}	mutual resistance between conductors n and m
$[\mathbf{T}]$	eigenvector matrix
T	absolute temperature
T_{im}	ith eigenvector

Δt	simulation time step
$[\mathbf{U}]$	unit matrix
$u(r)$	variable of potential function
$[\mathbf{V}]$	phase voltage vector
$[\mathbf{V^m}]$	modal voltage vector
$[\mathbf{V_{node}}]$	voltage vector for simulation
V, V_{Zb}	potential difference
$V(N)$	potential of probe N
V_s, V_a, V_b, V_c	source voltages
$V_k(t)$	voltage at node k at time t
V_l	load voltage
V_n	phase voltage for rail n
$V_n{}^m$	modal voltage for mode n
V_{node}	voltage vector for simulation
$v(\lambda, z)$	variable of potential function
X_c	conductor reactance
X_e	earth reactance
X_g	geometry reactance
$x1$	probe spacing
x_{nm}	mutual reactance between conductors n and m
$[\mathbf{Y}]$	phase admittance matrix
$[\mathbf{Y^m}]$	modal admittance matrix
Y_{eff}	effective admittance
Y_o	bessel function
y_{ij}, Y_{nm}	phase admittance between conductors n (i) and m (j)

Y_{ie}	conductor–to–ground admittance
Y_{im}	modal admittance of mode i
Y_{mij}	mutual admittance
Y_X, Y_Y, Y_Z	admittances
$Y_{meas:K}$	measured admittance
y_{shunt}	shunt admittance
$[\mathbf{Z}]$	phase impedance matrix
$[\mathbf{Z^m}]$	modal impedance matrix
$[\mathbf{Z_o}]$	characteristic impedance matrix
Z_{circ}	impedance of circular conductor
Z_{ext-s}, $Z_{ext-self}$	external self impedance
Z_{im}	modal impedance of mode i
Z_{int}	internal impedance
Z_N	norton impedance
Z_o	line characteristic impedance
Z_{oi}	modal characteristic impedance of mode i
Z_{rail}	impedance of rail
z_B, Z, Z_a, Z_b, Z_{Li}	impedance
z_{ij}, Z_{nm}	phase impedance between conductors n (i) and m (j)
z_{nm}	total rail impedance element
z_{series}	series impedance

Chapter 1

Introduction

The introduction of power electronic traction converters and computer–based train control systems on electric railways has been wide–spread. Such advances have increased the awareness of the effects of electromagnetic interference with regard to system safety and reliability. One approach to achieving electromagnetic compatibility assurance between subsystems is by circuit simulation studies in the microsecond and millisecond timescales. This requires the establishment of an accurate electrical model for the whole traction network. A vital part of this modelling is the representation of the rail track. This thesis reports on the results of research aimed at defining in detail the track self and mutual impedances and admittances.

1.1 An Overview of Electric Traction and Train Signalling Systems

The use of electricity for traction and signalling in railway operations is taken for granted. Electric drives with the power source concentrated at discrete points and the energy transmitted by conductors provide an economic method of train propulsion to the moving vehicles. Economic and ecological pressures, as well as operational considerations, have caused both urban and main–line operators to turn to electric traction since the source of pollution may be removed from densely populated regions to remote sites.

Due to the increased demand on train operators to improve service by increasing capacity or frequency especially at peak traffic times, the need for more advanced signalling has become apparent. This has been encouraged by a rapid evolution in electrical and electronic signalling technology. The need to ensure compatibility between traction drives and signalling systems is well understood. However, achieving such compatibility is a complicated engineering process. To understand this further the variety of traction and signalling systems used in practice must be examined.

1.1.1 Electric Traction Systems.

The choice of electric, rather than diesel based, traction is made on overall operational cost effectiveness. In most cases, commuter traffic will benefit from electric traction. For long distance traffic, the construction and maintenance of overhead supply systems may become uneconomic. If the traffic density is low diesel traction is chosen.

Electric traction supplies may be d.c. or a.c. This together with the different types of traction motors and converters, leads to a range of possibilities in traction systems as shown in Table 1.1. The trade–offs of transmission efficiency and motor controllability for various voltage levels and supply types are only clear for the extreme cases. That is urban railways which use low and medium voltage d.c. and high speed railways which use high voltage a.c. power transmission.

The standard voltage levels for d.c. supplies are 600 V, 750 V, 1.5 kV, although voltages up to 3 kV are used. For voltages less than 1 kV, the power is supplied by a rail running along the side the track. The train connects to this *third rail* by a power supply pick–up or *shoe*. Although the normal return path is through the running rails, there are notable exceptions such as the L.U. (London Underground) system and the Red Line on the

Table 1.1: Traction Drives and Converters

Power Supply	Traction Motor	Converter	Notes
D.C.	D.C. Series	Resistance controller (cam)	
	D.C. Separately Excited	D.C. – D.C. Chopper	
D.C.	Induction	V.S.I.	(1)
		Chopper – C.S.I.	
		Chopper – V.S.I.	(2)
D.C.	Synchronous	Chopper – C.S.I.	(3)
A.C. (l.f.)	Universal	Tapchanger	(4)
A.C. (power freq.)	D.C. Series	Tapchanger – rectifier	
	D.C. Separately Excited	Controlled phase rectifier	
A.C. (power freq.)	Induction	Pulse converter – V.S.I.	(1)(5)
A.C. (power freq.)	Synchronous	Rectifier – C.S.I.	(3)

Notes:–

(1) Expected to be the standard system in the future.

(2) Early models : later used P.W.M. to vary D.C. link voltage.

(3) France only : dual system trains.

(4) Germany, Austria, Switzerland, Norway, Sweden use 16.66 Hz.

(5) Also l.f. used – 16.66 Hz.

C.S.I. – Current Source Inverter

V.S.I. – Voltage Source Inverter

Milan Subway, which both have a fourth rail, laid in the centre of the track to provide a return path for the traction current. D.c. systems use a catenary feed when the supply voltage is in excess of 1000 V (typically 1.5 or 3 kV).

A.c. supplied traction systems typically have the power supplied by an overhead *catenary.* Power collection is made via train roof–mounted sliding pickups or *pantographs.* The specifications of this type of system vary substantially from country to country but the power is generally at high voltages, with a standard set at 25 kV[1]. Supply frequencies in use include 16.66, 25, 50 and 60 Hz. The lower frequencies are left over from the 1920s when a.c. commutator motors where used for traction[2]. The basic feeding system consists of substations supplying the catenary with the return current path along the running rails. More sophisticated systems include booster transformer and autotransformer feed circuits; the larger capital costs of these being offset by the increase in transmission efficiency and reduction in electromagnetic interference from induced track–side voltages.

The initial attractiveness of d.c. powered trains was that d.c. traction motors could be used with simple cam control. Until recently d.c. motors were used in a.c.–fed systems using phase converters with rectifiers. With the development of thyristors, simple effective controllers became available. Modern traction drives use inverter–fed three-phase a.c. motors. These were first developed for d.c.–fed railways and later applied to a.c.–fed railways using an a.c. – d.c. line converter feeding the d.c. link. The advantages of a three–phase induction motor is that it does not have a commutator or slip rings and has a higher power–to–weight ratio than the d.c. machines. An additional advantage is that, regenerative braking is available although the process may also be

[1] 50 kV has been tried on some railways in North America and South Africa.

[2] The $16\frac{2}{3}$ is derived from $\frac{1}{3}\times$ 50 Hz for ease of generation.

achieved using d.c. — d.c. chopper drives but is not often implemented due to the need to establish inverting d.c. substations. Studies have shown that cost savings through the regeneration of power may be significant. For example, the New York Subway System has chosen inverter–fed control for all new rolling stock, purely on economic grounds. The new generation traction drives for a.c. supplied systems have pulse (four quadrant) a.c. – d.c. converters feeding 3–phase a.c. motors. These drives also can provide regenerative breaking but, because traffic is generally less frequent on a typical main–line system, the additional capital costs in providing the necessary harmonic protection in substations are not always recoverable in operational savings.

1.1.2 Train Signalling Systems.

Although there are current international projects to standardise signalling systems[3], there are many variations in train signalling which essentially provide a solution to the same train control problem. There always will be a need for detection of train position and velocity. Also data transmission of safety information i.e. through line side signal or cab signalling always will be required.

There are three common methods of train detection. The first is a count of the train axles passing a point, or more often a number of points. These devices are known as *Axle Counters.* It is a precise, if inflexible, approach to determining train location. Axle counters are usually mechanical treadles or magnetic circuit devices which are attached to the rails. The presence of train wheels passing then activates the devices. The second approach is to use conductors, positioned between the running rails, usually with the conductor crossing repeatedly. These crossing points are used by train–mounted systems to detect position by phase reversal of the detected signal. The third method of train

[3]Examples of these are EURET and EUROCAB which are European Community Funded.

detection is known as the *Track Circuit.* In this system the track is divided into section lengths termed track circuits. Within a track circuit, the running rails are used as a transmission line. With a transmitter at one end of the track circuit and a receiver at the other end, a train is known not to be present while a signal is detected. If the receiver does not detect a signal, then either a train has been detected with the axles short–circuiting the transmission line, or the signalling system has failed. The *fail–safe* principle is inherent in this method. The first two methods are not inherently fail safe.

The practical implementation of the track circuit depends on the type of power supply to the traction drives. In the case of a d.c. traction supply, the track circuit system must use an a.c. signal. The running rails must be electrically continuous within each track circuit and so the ends of the track circuits are separated by block joints if they operate at power frequencies or by tuned circuits if they operate at audio frequencies. For an a.c. traction supply, it is sometimes possible to use d.c. track circuit signals. The track circuits must be physically isolated by inserting block joints in one rail, so the traction return current flows along one rail with the d.c. track circuit current along both rails. The *insulated rail joints* which isolate the d.c. track circuits are generally known to be mechanically unreliable and this has resulted in the development of a.c. traction supplied systems using audio frequency excitation with tuned electrical circuit joints to delineate adjacent track circuits. In this case, the operating frequencies in adjacent track circuits must include a suitable spectral separation for correct operation.

Many track circuit frequencies are in use with typical values for power frequencies of 33.33, 50, 60, 100 Hz, 125Hz. For example,L.U. use 33.33 and 125 Hz, whilst 100 Hz is found on the AMTRAK (the USA National Passenger Railway)[4] north east corridor. Audio frequencies in the range of 2 to 20 kHz have been chosen by many rapid transit

[4]This system uses insulated rail joints.

operators, such as Singapore Mass Transit and Washington Metropolitan Mass Transit Authorities.

There are also many methods of transmitting the control information to the train. Several main–line methods are simply magnetic devices laid in the track to repeat signal aspects giving a visual message to the driver. An example is the AWS (Automatic Warning System) technique operated by British Rail. A more sophisticated system is the INDUSI transmission system in use in Germany.

A number of wider bandwidth automatic transmission methods have been developed to transfer data to the cab, when the train is either stationary or moving, using the principle of inductive transmission of coded information. An example of this is the original system installed on the D.L.R. (Docklands Light Rail) operating in London. The problem of on–the–move information transfer has been solved by passive static *beacons* or active transponders positioned between the running rails. Beacons allow one–way information transmission from track–to–train, whereas transponders can be configured for two way transmission.

The natural extension of this is to have a continuous data transmission system, allowing flexible operation with full two–way data exchange. The Vancouver Skytrain and the Singapore Mass Transit System both have a range of sophisticated communication systems.

1.1.3 Automatic Train Control.

Train control can be considered as a set of nested feedback control loops, as illustrated in Figure 1.1. Effective track–to–train and train–to–track data transmission is necessary for full implementation of such a control system.

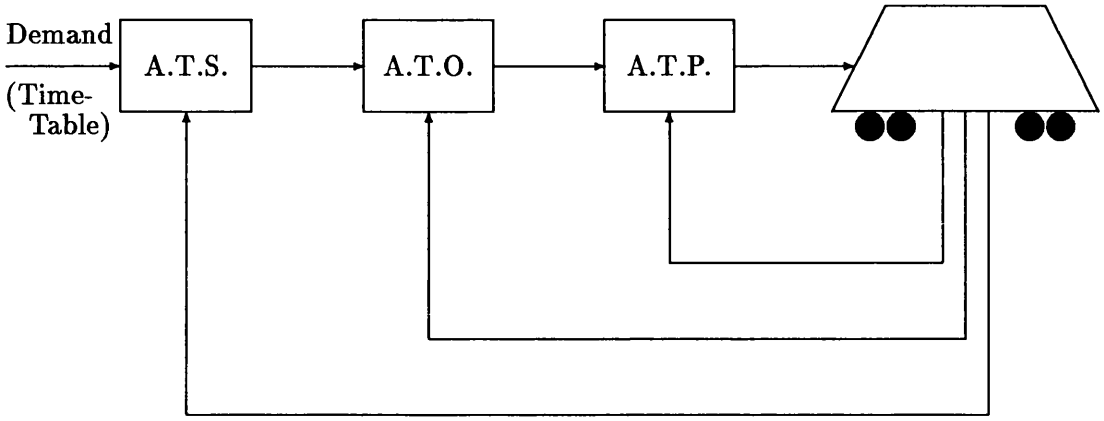

Figure 1.1: Nested Loops Forming an Automatic Train Control System

Safe train operation is controlled by A.T.P. (automatic train protection), the inner–most loop. It must be the over–riding mechanism such that, if it is unsafe to proceed, the train speed is reduced and the train may eventually be stopped. This system includes fail–safe track occupancy detection, safe transmission of speed limit information, train position and speed monitoring, door closure status information and traction drive–braking supervision (for operation within a defined safety margin).

The next control loop outside A.T.P. is A.T.O. (automatic train operation). This might include normal door opening operation, control of speed and braking to operate to the timetable and accurate (stopping) positioning at station platforms. Generally it covers all *non–vital* functions local to the train.

The outermost control loop is A.T.S. (automatic train supervision). This represents control of the overall system and can be used to meet a particular service specification e.g. to maximise passenger throughput at peak traffic periods. Also as a supervisory

system, control of other *cost functions* can be achieved e.g. optimisation of energy demand or consumption. Using A.T.S, the parameters to be optimised can be changed automatically, depending on the most pressing requirement at the time.

1.2 The Requirement for Simulation in Electrified Railway Systems

Considering the complexity and number of variations in electric traction and signalling methods, especially when combined into one system, it can be seen that computer aided analysis should be a powerful tool for the design and fault analysis of such systems. Simulation can be carried out in microsecond, millisecond, second or tens of seconds timescale, depending on the problem to be solved. For example, for traffic flow studies, in the tens of seconds timescale, an initial system design could be achieved by passenger flow considerations and then the detailed design could be optimised by simulation. For power flow studies in the seconds timescale, the simulator would need to have the capability of modelling both power system and signalling operation. For E.M.C. studies in the microsecond and millisecond timescale, the simulator would need to model electrical parameters very accurately.

This thesis is concerned with electrical simulation for E.M.C. studies. To achieve a useful electrical model for such an application, the rail track can be treated as a distributed power line. The difficulty is that the rails and earth in an of electrified track system exhibit unusual, non–linear properties. Hence the track modelling must consider the material properties (conductivity, permeability and permittivity) in detail.

1.2.1 Electric Traction and Power Supply Considerations

In the second timescale, simulators may be used to optimise power flow. For a simulator to be useful in a practical sense, it must allow for both d.c. and a.c. supply systems. Verified commercial software is available for the simulation of industrial power distribution systems. These simulators may be applied to single–phase a.c. and d.c. traction supply systems, with some software modifications, since they are capable of representing power electronic circuits, including train–borne traction systems.

1.2.2 Signalling System Considerations

One application of train signalling simulation is in track circuit design. Track circuit optimisation must include the choice of signal frequency and magnitude, with respect to variations in ballast and soil conditions, the proximity of other track circuits and the presence of E.M.I. (electromagnetic interference) from traction supplies.

Most track circuit designs have evolved from continuous development of existing systems. It follows that in most cases the design can normally be refined further by the use of simulation.

1.2.3 Electromagnetic Interference in Train Systems

E.M.I. within any system is defined as the presence of an unwanted signal within the operational range of the receptor system. E.M.I. may result from a number of coupling effects, including magnetic induction, conduction, electric induction or radiation. The design process in any system should ensure E.M.C. (electromagnetic compatibility) between individual subsystems.

A line of track circuits within the same running rails are usually electrically coupled because traction power current must pass through many track circuits to return to the substation. Thus signalling power from one track circuit will couple with other track circuits, as filters do not have ideal characteristics. The method of coupling is usually inductive and conductive, since the signals rarely exceed mid–range audio–frequencies, making radiative E.M.I. much less significant. Also with relatively low voltages, capacitive coupling is usually not significant[5]. The actual coupling mechanism is often open to speculation as detailed studies are rarely undertaken[6]. Also coupling via track side cables or track–bed re–enforcing structures cannot be excluded especially when 25 or 50 kV systems are used, since capacitive effects may be significant. Adjacent track circuits also can exhibit electromagnetic coupling through crosstalk (by inductive coupling), as the tracks are only a few metres apart, whereas the circuits may be up to 1 km in length. The problem of E.M.I. between track circuits is that unsafe failures may occur e.g. where a train axle shunts a transmitted signal but significant power, at the same frequency couples from traction equipment on another track to keep the receiver energised thus indicating a state of unoccupancy.

It is good practice to provide complete spectral separation between traction and signalling frequencies to alleviate E.M.I. However, harmonics generated by power control circuits in traction systems still may produce significant power at or near the track circuit frequencies if faults arise in equipment.

The problem of both the wanted track circuit currents and the unwanted power harmonics occurring at similar frequencies is further emphasised if they share the same conduction path, which happens in the case of the running rails. In addition, since sig-

[5]Capacitive coupling may be significant when spikes of e.m. noise are generated from trains to track circuits.

[6]Studies are generally undertaken when a specific problem arises.

nalling currents are small (e.g 5 A) compared to traction currents (e.g. 1000 A)[7], power supply harmonics may be of the same order of magnitude as the signalling currents.

The effect of E.M.I. from traction power systems into circuits other than signalling also may be significant, for example, on telecommunication systems in main–line railways and rapid transit systems.

The most cost effective way to avoid E.M.I. is at the design stage, by careful choice of power/signal levels and operating frequencies in all subsystems. Spacial, temporal and spectral separation requires careful pre–selection and their interaction and interdependency in railway electrical systems indicates that complex design procedures must be invoked. This implies the extensive use of computer based simulators reliant on accurate system modelling

1.3 Electrical Representations of Track Structure

The central feature of electrical traction simulators is an electrical equivalent model of the track. The track structure (i.e. rails, power conductors and track bed) may be represented in a number of ways in electric circuit terms. It is possible to represent the track as discrete or *lumped* components. With two parallel rails, there will be inductive coupling between the rails and between each rail and ground (when ground currents flow) so that inductance always must be included in time varying analyses.

Since the rails are in contact with the sleepers, ballast and hence ground, conduction paths must exist between the rails, sleepers, ballast and ground. The rails also exhibit capacitance between each other and the ground. To allow for a variable length of track, the discrete component electrical model necessarily would represent a defined unit length

[7]This value is typically for a 700 kW train at 700 V

of track.

In a more general case when multiple tracks may be long, the discrete component model might become rather cumbersome. The physical layout of track tends to leads to a transmission line representation as a more useful modelling technique. The electrical behaviour of the track may be represented by distributed transmission line parameters, enabling the exploitation of telecommunication and power system transmission theory.

For a two–rail single track study, it may be acceptable for some purposes to consider the track as a simple two wire transmission line. The proximity of the ground will have an influence on the electrical characteristics of the track and must be included if unbalanced conditions are to be modelled. For 3– or 4–rail systems and those with catenary and multiple tracks, the simple two–wire model is insufficient. A multiple rail track system must be considered as a multi–wire transmission line with more extensive analysis due to the interaction between lines.

1.4 Scope and Bounds of Research and Thesis

This thesis reports on a study undertaken to analyse rail track as a multiple–wire transmission line. To achieve this analysis, a detailed investigation of the equivalent electrical track parameters was carried out. The research programme concentrated on the effects of rail material and lossy ground with their influence on the electrical parameters. The work includes theoretical analysis, experimental measurement and numerical modelling in an attempt to obtain a complete physical understanding of the processes involved.

Case studies of signalling systems and traction signal harmonic propagation along the track have been included to illustrate the use of the track parameters (obtained from

the research programme results) in simulations. Signalling equipment specifications and characteristics such as track circuit transmitter and receiver circuits have been included where appropriate; this has been supplied by several manufacturers and operators of railway systems, or obtained by measurement.

1.4.1 Thesis Outline.

The thesis initially reviews previous published work. This provides an overview of earlier track modelling studies and discusses the advantages and disadvantages of the methods used. The rail material is significant in the conduction process and reports on studies into magnetic material properties have been included in the literature review. In a similar manner, previous work on the electrical properties of ground has been examined to provide an understanding of the influence of ballast, soil etc. Other relevant literature has also been considered. A critical appraisal of alternative simulation methods is given. This describes the benefits of the choice of multiple–wire transmission line modelling, compared to the alternatives available.

Following this the material properties of the complete track structure are examined. The magnetic and electrical properties of rail material are determined, by measurement, testing and modelling methods. The ground plane and track bed also have a significant effect on the track electrical parameters, and a study of ballast, soil and sleepers has been undertaken.

Then the influences of material properties on the transmission line parameters are considered. The transmission line parameter study is separated into the series resistance and inductance behaviour and the shunt conductance and capacitance behaviour. These parameters have been measured, estimated from approximate analytical methods and

modelled by appropriate numerical techniques with further tests to confirm the results.

The thesis continues by describing the application of the derived transmission line parameters. A matrix method, analogous to a power system multimode transmission line method, has been used and this is explained in detail. Case studies are given with typical design problems considered and the usefulness of the simulator in such studies of the interaction of traction and signalling systems is outlined. To conclude the thesis, the overall results, together with modelling methods are discussed and appropriate conclusions drawn. Further work is suggested.

Chapter 2

Review of Literature

In examining the features and techniques that might be considered in the development of a track model for a microsecond, millisecond or second timescale simulator which could assist in the analysis of E.M.I. problems in electrified railways, it has been essential to consider a wide range of published studies. Also a number of general background areas associated with electrified railways have been included. The areas covered are traction power supply systems and drives, train signalling and control, E.M.I./E.M.C., evaluation of track parameters and simulation techniques.

2.1 Traction Power Supply Systems and Drives

2.1.1 A.C. Traction Supplies

A.c.–supplied traction systems are most often used for main–line railways and are associated with longer distance operation than d.c. systems. To prove that there are always exceptions to rules, Sykes [1] describes the d.c. electrification of the 150 km London to Bournemouth main–line which did not use an a.c. system since it was treated as an extension to an existing system.

There has been much work reported on the analysis of a.c. traction power systems performance. Glover, Kusko and Peeran [2], for example, describe a method of analysing train voltages for new railroad electrification systems at 25 kV, 50 kV and 60 Hz. The analysis can be carried out with or without booster or autotransformers. The power

supply system analysis is required to aid the determination of optimum substation spacing, catenary feed configuration, requirement for auxiliary transformers and equipment ratings. The train voltage analysis ensures that train performance specifications can be met. This report puts emphasis on catenary and return rail impedances with detailed calculations given. It is shown that accurate resistance and reactance values, for running rails improves the accuracy of calculations. However, only approximate, well–known evaluations are given, with internal rail reactance left to unspecified measurement.

General reviews of a.c. electrified railway power supply systems have been given by Suddards [3], and Spenny and Kusko [4], whilst specific applications and implementations are described in other papers [5, 6, 7]. Although these provide practical details of systems in operation, there is only limited information in terms of the analyses used.

Bozkaya et al. [8] and Mellitt et al. [9] provide a detailed examination of the comparative merits of auxiliary transformers. It is shown how B.T.s (booster transformers) are used to draw current up to a return conductor, away from the track and so reduce rail and earth currents. One aim of this design is to reduce induced voltages in line–side metallic conductors. The B.T. method is used mainly on conventional 25 kV systems with a transformer spacing limitation of between 2–5 km. From the viewpoint of the reduction of E.M.I. from earth currents, the A.T. (autotransformer) system also achieves a similar objective. A.T.s are used with a 25–0–25 kV power system; 25 kV is applied between catenary and rails with the aid of an auxiliary feeder and a 50 kV power supply. Since most standard train–borne equipment is developed for a 25 kV rating, the 25–0–25 kV method is preferred to a 0–50 kV system. The work also gives a detailed comparison between the performance of B.T. and A.T. systems, showing simulation results of earth currents.

Machczynski [10] gives a mathematical analysis of currents and voltages in earth–return

circuits for a.c. traction supplies. The practical application of this analysis is for determining induced voltages in parallel cables and example calculations are given. The paper is concerned with the determination of harmful effects of power electronic converter traction supplies on other systems.

Kneschke [11] [12] has shown how relatively simple circuit theory and power system analysis can be used to determine substation distribution. A base substation spacing is used and this is followed by examination of the parameters that affect the final substation spacing. Single–end, double–end and centre–fed systems with booster and autotransformers are all considered.

As stated in Chapter 1, commercial software is available to analyse industrial power supply systems. Cesario et al. [13] have shown that it is possible to apply a commercial package to traction power supply simulation. The paper explains the difficulties in simulating traction systems using E.M.T.P. (Electromagnetic Transients Programme) but states that complex elements can be incorporated into the model. Two case studies are given for the Dorsale–Sarda railway line in Sardinia, Italy and for the Carajas line in Brazil. Although the package has standard *built in* models for many components and subsystems, the actual values used, and the type of models used for these components (and those developed by the authors) is not made clear.

With the demand for more rapid main–line trains, European railway operators have been developing power supply and catenary systems to operate trains at speeds in excess of 350 km per hour. Harprecht et al. [14] present a paper illustrating the modifications and extensions to standard German Federal Republic Railway equipment to achieve these higher speeds. Much test data is presented to illustrate the operation of a high–speed train.

2.1.2 D.C. Traction Supplies

Since the d.c. traction supply system is most often used in rapid transit operation, it is usually characterised by shorter distances between stations compared with main–line operation. This tends to imply that the load on the supply, from the train, is normally smaller than for main–line systems. However, train starting loads may occur more frequently.

De Koranyi [15] describes the system requirements that arise when designing a d.c. power supply for rapid transit systems. He states that the aim of a design, whether for a new system or for a modernisation contract, is to optimise substation location and size relative to the passenger station location. Train currents and voltages are considered, as was the case for the a.c. design procedure. Similarly, line data, substation data and substation loads are examined. De Koranyi gives a numerical example to highlight the design process. The results are based on a simple model, as is to be expected when attempting the analysis of a whole system. No reference is made to regenerative breaking which indicates that this paper predates the implementation of power electronic devices in more advanced circuit applications. However, silicon rectifiers are discussed in substation data. Lincoln [16] provides a summary of what he terms fringe areas affecting the power–supply engineering of traction systems. These include harmonic generation, interference and induced voltages.

By 1970, the use of regenerative breaking had become established, although Holden [17] pointed out that the practical application was unsatisfactory. This seemed to be because the rectifier substations of the day could not accept reverse power flow. Even with modern semiconductor devices, inverting substations are still often prohibited by cost, although not by technology. Holden provides a useful summary of the elements

that make up the electrical distribution and drive systems.

Suzuki [18] presents a more recent description of a d.c. power supply system for rapid transit operations. He discusses the principle of a reversible d.c. power supply and gives, as an example application, the Seishin Line of the Kobe Metro, Japan. Again, substation positions and ratings are considered together with control and operation of the substation inverter circuits. Mellitt et al. [19] also describe the merits of energy savings, when using chopper control on the Jubilee Line of the L.U. system in London, evaluated by simulation. Comparison between conventional equipment and that of a regenerative braking scheme is made. It is explained that three principal factors influence the reduction in energy demanded by the system:

- *The power losses associated with mechanical components.* The electrical losses of motors and conductor rails are reported as not being significant but mechanical losses provide some of the *electrical* braking effort. Hence, the energy delivered to power the train is usually less than that available for electrical braking.

- *The availability of load demand and the constraints on power transmission.* The periods of braking and motoring influence the energy demanded by the system. The paper describes this as the *coincidence* of these periods. It could also be thought of as an effective mark–to–space ratio. This ratio is affected by train headway and station waiting time. There is also the constraint of sectioning in the power supply system. Ideally, the whole system should be fully linked but limits of voltage at the train terminals, when braking, constrain the distance over which regenerated power can be transmitted.

- *The power rating of the electric brake.* Traditionally, low characteristic tractive–effort/speed curves are followed during powering of motors. This constrains the

regeneration capability. In addition, it is expected that non–motoring axles may have to take part in the braking so that traditional braking rates can be achieved without extensive mechanical braking.

After explaining how the calculations can be carried out, the paper concludes with numerical examples. Gondo [20] also discusses modern d.c. railway feeding systems and provides a description of modern substation design, capable of absorbing power.

A number of reports provide details of actual systems in operation. Examples of these are by Olsen [21] and Miller [22], which gives a general description of the B.A.R.T. (Bay Area Rapid Transit) (USA) electrical power distribution system. Emphasis is placed on the power distribution to the traction equipment. Lincoln [23], and later Prickett [24], give similar types of reports on the Tyne and Wear Metro (U.K.). Lincoln provides a good overview of the apparatus and Prickett offers descriptions of various constructional details together with more detail of the control of the system. Later papers [25, 26] provide reports of electrical power systems operating in Hong Kong and Dublin. A more recent paper by Buchanan [27] places more emphasis on the computer–based control of a power system. He describes the L.U. power network control strategy. This paper differs from earlier examples by reflecting the move to reliance of power system control on software.

2.1.3 Traction Drives

The development of traction drives has been briefly summarised in Chapter 1. Crawshaw [28] explains that the performance of the drive system is limited by the machine characteristics, power source and control method. The actual performance achievable may be a balance between the ideal and equipment cost, with the restriction of existing

infrastructure. Crawshaw also explains that traditionally it is thought that the d.c. motor is most suitable for traction use, as it is the easiest to control to give satisfactory performance. U.K. manufacturers have limited a.c. traction motor development to cage induction motors and Crawshaw provides a comparison between this system and the d.c. motor system. The paper reviews the early days of d.c. electric traction and then summarises the characteristics of the separately excited d.c. motor and the induction motor, together with more advanced methods of control.

Jager et al. [29] consider typical power electronic circuits used in traction systems for the control of d.c. motors. This paper indicates that the major advantages of using these circuits are

- Improved adhesion due to continuously variable control and selection of suitable tractive effort/speed characteristics.
- Automatic train running by use of computer control without human intervention.

However, the advantages must be considered together with the disadvantages. The main drawbacks are stated as

- Increased reactive and distortive loading of substations.
- Electromagnetic interference into other systems.

Jager et al. provide a basic analysis of phase control for the a.c. supplied system, further emphasising the problem of generated harmonics. They also discuss where these harmonics might cause problems in other systems. They then proceed to examine the use of filtering, more advanced circuits and switching methods to improve the situation. An example of the implementation of thyristor control is given, the Berne–Lotschberg–Simplon Railway. D.C. supplied systems are then considered and an examination of the

origins of harmonics, resulting from chopper circuits, is given. A similar discussion to that for a.c. supplied systems is provided.

Wagner [30] describes the continuing increase in the use of a.c. motors with power–electronic control. Wagner's paper provides practical circuits used by Siemens in a number of recent projects. He also explains that, up to that time, both current–fed and voltage–fed inverter circuits had been used in approximately equal number. However, with the development of the G.T.O. offering a simple power turn–off facility, combined with microprocessor control of gate signals, Wagner considers that voltage–fed inverters are the best candidate for further development. Since this publication, this has been confirmed to be the case. The advantages of the voltage–fed inverter with respect to the current–fed inverter are outlined by Lander [31]. He explains that the current–fed (or constant current) inverter suffers from torque pulsations at low speeds, the requirement for bulky capacitors and inductors with poor speed regulation at lower powers. In addition, Lander points out that P.W.M. (Pulse Width Modulation) methods have not been pursued with current–fed circuits; long commutation times would restrict the application to low output frequencies so that low–order harmonics could be eliminated. The main advantage of such circuits is that conventional thyristors can be used. Further publications [32, 33, 34, 35] specify particular algorithms and general considerations of P.W.M. to minimise harmonic interference into other systems. In some cases, detailed mathematical analysis is given.

An implementation of this is described by Fischer [36]. Although the supply is generated by an on–board diesel engine, the control principle is similar to an electrified supply system. An overall explanation of a particular locomotive application is given. At the same conference, Smith and Comer [37] presented the concept of a dual mode locomotive. For the particular application they described, the locomotive had to operate

as a diesel–powered, electric–motor driven vehicle with the option of being supplied from a third rail arrangement for tunnel operation.

As control methods develop, different techniques offer improved performance. In the last three years the move to field–oriented direct self control (vector control) has become prevalent in development and it is thought that this may replace P.W.M. Steimel [38] reviews the various control techniques available for traction applications and explains that field–oriented control uses simplified algorithms (compared to earlier techniques) allowing optimal switching of the inverter under all circumstances.

2.2 Train Signalling and Control Systems

As outlined in Chapter 1, the techniques and systems used to progress a train through a railway network can be thought of as a feedback control loop. The demand parameter or input to the control system is the time–table or desired operation. The forward path of the loop is the track–to–train signals (traditionally the line of sight of a driver to a wayside signal), with the feedback path representing the train detection method. This then leaves disruptions to the system as noise or disturbance inputs. The requirements of the electrical systems involved in train signalling and control in the form of forward and feedback paths of the control system are of particular importance in developing simulations of electrified track.

2.2.1 Train Detection – The Track Circuit

While several different methods of train detection exist, the method in widespread use on lines with moderate or heavy traffic is the track circuit[1]. The track circuit is a key subsystem which requires accurate modelling of the rail track itself to give full information concerning circuit performance and possible E.M.I. problems. Track circuit development has been the subject of many publications. Frielinghaus [39] and Hill [40] provide useful introductions to the subject, describing the basic track circuit operation. Both give brief historical reviews and indicate that d.c. track circuits were the first to be implemented. However, experience has shown that the necessary insulating block joints are a maintenance liability. In addition, since d.c. traction systems share the running rails as the same conduction path as the track circuit, the need for a.c. signalling methods becomes apparent.

Walter [41] describes developments occurring on the S.N.C.F. (Societe Nationale des Chemins de Fer) system during the 1960's with the advances in solid–state devices. He explains that, although of concern prior to this time, axle resistance was not a problem when used to shunt the track circuit. Wheel–rail contact was of concern, mainly due to rail oxidisation. A method of overcoming this problem is outlined: high–voltage d.c. pulses are used to overcome the oxidisation effect. Walter then continues by discussing track circuits at selected frequencies with insulated block joints. These are at the lower end of the audio frequency range but are limited in length for the applications considered. He also provides information relating to a.f. track circuit implementations without insulated block joints. Tuning and frequency separation are used to define the track circuit. The problem of inadequate train shunting, described by Walter, has

[1] Also axle counters are widely used on heavy traffic lines. On light traffic tracks, no train detection at all may be found.

been of concern continually throughout the evolution of track circuits. Nagase [42] also addresses the problem, presenting a practical method of measuring the shunting resistance and including example results.

The procedures involved in track circuit design have been the subject of a series of papers by Iancu [43, 44] and Iancu and Giuhat [45]. In the first of these papers, it is explained that determination of an optimum length and termination impedance may be treated as a non–linear programming problem. Two methods are suggested :–

- Fix a number of conditions and then optimise a simplified problem.
- Application of strict boundary conditions.

Iancu continues by identifying the critical parameters for the evaluation of terminal impedances. He then provides the algorithms for calculating optimum track circuit length and terminal impedances, concluding with numerical examples. The subsequent papers examine particular aspects of track circuit design. The influence of direct–coupled receivers is considered in detail as is the influence of track circuit parameters on maximum circuit length. Although the algorithms used are given in some detail in these papers, no experimental or practical confirmation of the method is provided.

Other papers covering similar material include published work by Frielinghaus[39] and Harmon [46]. Frielinghaus provides much practical data needed when establishing the maximum circuit length, for a.c. signals, while Harmon reviews problems that must be considered in circuit design.

A typical application is presented by Gaffney and Harris [47]. They give practical details of the signalling systems used on M.T.R.C. (Mass Transit Railway Corporation) in Hong Kong. The development of a number of signalling strategies is explained. The

improvement in technology and hence performance as the transit system expanded, is illustrated; future trends are suggested.

2.2.2 Train Control

Track circuits and other detection techniques provide train position data which allows control strategies to be carried out. However, to implement the controlling action, information must be transmitted to the train. Traditionally, this is achieved by setting signal aspects at the track–side for the driver to observe. Ogilvy [48] introduces this conventional control method, including A.W.S., and briefly introduces communication systems. However, to improve control and hence system performance, more reliable, faster methods must be used.

Track–to–train data transmission is generally recognised as being essential to modern train systems. Jeffries [49] explains how track circuits can also be developed into part of a track–to–train communications link. He initially reviews the historical progress of this idea and follows this by examining the basic principles. Included in this are the merits of various antenna positions, data transmission considerations, inherent properties of track circuits, attenuation compensation and limitations to the method. He then discusses what information should be included for transmission over this limited bandwidth channel. Hill [50] reviews the overall concept of A.T.O. Included in this overview are train detection and automatic signalling, track–to–train communication and computer–control supervision. A second paper [40] by Hill, also provides a detailed analysis of a specific transmission method using F.S.K. (Frequency Shift Keying) techniques and includes practical examples of F.S.K. transmission in a.f. track circuits.

Fricke [51] describes another technique which includes transposition of in–track con-

ductors for more refined train position and identification. A higher resolution of train control can be achieved and in this way it is possible to implement *moving block signalling.* He also considers that it is only by substituting *working by space intervals* with *working by time intervals* that cab signalling will offer very considerable advantages[2]. Considering this paper is dated 1964, it shows much forsight and imagination towards future trends, especially as computer technology was not well developed at that time.

In a paper by Gaffney and Harris [47] on signalling of the Hong Kong Mass Transit System, track design, vehicle and signal performance are considered, in practical terms, with respect to A.T.O., A.T.P. and A.T.S (or train regulation). This is a good illustration of future trends.

Most of the advanced signalling techniques are used in Mass Transit Systems. This is probably because the capital investment is less than would be required to implement such methods on main–line systems. However, main–line developments are often discussed and Alston and Birkby [52, 53] provide papers concerned with this. They describe developments in British Rail train control. It is explained that a number of systems are used to provide communication links to moving trains. These systems are similar to those described in the previous articles.

With modern computing facilities, together with the large capital costs involved in train signalling implementation, it is to be expected that C.A.D. (Computer Aided Design) methods should be developed. Ho et al. [54] provide a description of a simulator for modelling signalling in Rapid Transit systems. It appears that the application of A.I. (artifical intelligence) principles, in the form of expert systems could offer a powerful design aid.

[2]Working by space intervals is the traditional fixed track circuit (fixed block signalling) occupancy method.

2.3 Electromagnetic Interference and Compatibility in Railways

In order that E.M.C. can be achieved in any system, it is normally necessary to identify the sources of E.M.I. by measurement, analysis or modelling. It should be possible to predict problems that might occur during normal system operation and by careful design, eliminate such problems. This is particularly the case in railway systems and a general introduction has been given in Chapter 1. A typical selection of published studies are presented here.

2.3.1 Analysis of E.M.I. and E.M.C. Methods

In recent years, there have been two extensive studies of the problem of E.M.I. in railway signalling. Holmstrom [55, 56, 57, 58, 59, 60] published his findings, resulting from a study carried out on behalf of U.M.T.A. (Urban Mass Transit Administration – D.O.T. USA). In a series of volumes he examines the problem of E.M.I. in Rapid Transit Systems. An E.P.R.I. (Electric Power Research Institution) report [61] complements Holmstrom's work by describing track modelling using transmission line techniques. Both reports provide in–depth, detailed descriptions of the theory of and mechanisms by which interference occurs. Holmstrom clearly differentiates between inductive and conductive mechanisms. He also provides some novel experimental techniques for measuring the effects of rail impedance. The E.P.R.I. report follows a more conventional approach but provides extensive experimental results. Both reports offer an explanation of the problem, highlighting the difficulties in obtaining meaningful experimental and analytical results. For example, Holmstrom only measures changes in rail inductance, rather than internal inductance specifically, while the E.P.R.I. report uses some mea-

surement and some analytical techniques to provide results which have not been verified. The report is also limited to the case of two running rails only. In addition, it makes approximations concerning the earth reference point (or layer) in the track model and this puts the subsequent results in some doubt.

Frasco et al. [62] provide an overview of the effect of train–borne chopper circuits on a.f. track circuits. A more detailed study is given by Krempasky et al. [63] who describe a programme of testing and provide experimental results relating to E.M.I. in the W.M.A.T.A. (Washington Metropolitan Area Transit Authority) system. This study had been carried out because of the decision to use chopper–controlled d.c. traction drives in new rolling stock. They initially carried out laboratory tests, using tuned receiver circuits, to identify positions of maximum sensitivity and amplitudes relating to track circuit receiver operation. In addition, a tape–recording of the e.m. (electromagnetic) noise generated by chopper power–electronic control circuits was made and this was used for site testing. The recording was amplified and injected into the third rail system for testing purposes. The results of this program were then used to achieve compatibility between traction and signalling equipment. Smith [64] explains how this was achieved in a later paper and describes the spectrum management necessary to achieve E.M.C. He also includes other practical considerations.

The need for this type of study has been well understood for 20 years. A number of articles [65, 66, 67] briefly describe experiences where E.M.I. has been a problem. Abrahamsohn and White [68] and Abramson and Kapitonov [69] give more detail of the prediction and measurement of E.M.I. in situ. They also suggest methods of improving and controlling the problem.

2.3.2 Effects of Power Supply and Power Electronic Circuits on E.M.I.

Since a major generator of e.m. noise is the traction supply and power–electronic control equipment, many studies have examined the performance and design of these systems. Littler [70, 71] has considered the performance of a.c. electrified systems and latterly the performance of autotransformers at harmonic frequencies [72] . Mellitt et al. [73, 74, 75, 9] have published a series of papers describing how computer–aided design can analyse induced voltages from a.c. railways. Holtz and Klein [76] apply similar techniques to investigate the propagation of harmonic currents, generated by power electronic traction control circuitry.

Taufiq et al. [77] examine the compatibility between railway signalling and inverter–fed drives. The emphasis is placed on choosing methods of P.W.M. for the inverter such that harmonics are eliminated. Hill at al [78] describe the modelling of interference in d.c. fed rapid transit railways using chopper–controlled traction drives. Simulations of e.m. noise are compared with laboratory experimental measurements. Hill and Yu [79] further develop the technique to incorporate the idea of modal analysis of the track, to more easily simulate the mutual coupling between tracks. The theory is outlined and a number of graphical examples are given. The track impedance values are highlighted as being of critical importance to the propagation effect.

Studies relating to electrified railways and communication systems have also been reported. Cowdell [81], Mellitt et al. [82], and Manganella and Mario [83] examine the problem of acceptable levels of E.M.I. in telecommunication systems. Since telephone lines often follow the same route as the electrified track, this is of considerable importance. The methods of analysis given in these papers are used to provide examples of practical applications. Mellitt et al. make reference to the C.C.I.T.T. directives which

specify levels of induced noise permissible between these systems.

2.4 Evaluation of Track Parameters

As briefly discussed earlier, a number of papers [76, 2, 84] make use of assumed track parameter values. It is made clear in these papers that accurate values are required to achieve a useful numerical analysis.

Stanek et al. [85] explain that an accurate value of the impedance of a track/trolley system is important in the design of power systems in mines. The time constant of the electrical system must be known accurately to design fuse performance. The paper describes a simplified method of evaluating track impedance as the return path for the system. Then an analytical method is given for approximating the influence of the rail steel on the calculation. It should be noted that no attempt is made to evaluate the admittance of the track.

In an earlier paper by Mellitt [86], the loop electrical characteristics of a railway track are considered. This information is needed when considering track–to–train data transmission. Hence the characteristics have been evaluated for frequencies up to the audio range. In this case a single two–rail track has been evaluated; the characteristics include loop (circuit) series impedance together with shunt admittance. As explained earlier, a report from E.P.R.I. [61] covers measurement techniques for obtaining some of these parameters. Hill [40] also presents loop transmission line parameter data for varying conditions of track, applicable to data transmission.

Tylavsky [87] and Tylavsky and Kulkarmi [88] extent these ideas when working in a similar area to Stanek [85] i.e. mine track/trolley systems. In these later papers, the impedance is developed into a matrix, although it is not used in a true multiconductor

modal analysis. Tylavsky and Kulkarmi give a comparison of analytical and measured results but these are by no means conclusive.

2.4.1 Modal Analysis of Transmission Lines

To take full advantage of the matrix technique, developed by Tylavsky and Kulkarmi, a modal analysis of a multiconductor system using both impedance and admittance matrices of the track is required. The advantages of achieving this are that extensive studies have already been carried out in the power systems field; these well known methods and techniques could then be applied to electrified railway track. Development of this theory has been carried out over the past thirty years in power systems analysis and it is felt that this should be considered in some detail, so that it can be applied to rail track. Wedepohl [89] presented the basis of the method in 1963. He developed the multi–wire case by first considering a hypothetical single wire transmission line. This is extended to a simple two–wire case and then the general n–wire case is given in matrix form. In addition, Wedepohl shows that a special case of this, for a 3–wire geometrically symmetrical balanced line, leads to the well known symmetrical components formulation. Each symmetrical component is a mode in this particular case. The modal analysis is often termed the *concept of natural modes* and in a second paper, Wedepohl [90] presents further work for nonhomogeneous multiconductor systems. This forms a generalisation of the analysis given in the earlier paper.

In these papers it is seen that the earth resistivity may have considerable influence on the numerical evaluation of the system. Hence Wedepohl and Wasley [91] developed the principles to include a more realistic multilayer earth model. The inclusion of theory, developed independently by Carson [92] and Pollaczek [93] provides data for the completion of the impedance and admittance matrices. The theory as developed by

Carson is considered in a later section. The effectiveness of modal analysis is enhanced by further studies [94, 95, 96, 97] to include more practical features.

More recently Wedepohl and Efthymiadis [98, 99] have developed a more complete solution to determine the elements of the matrix. Many of the simplifications used earlier, which are inherent in Carson's work, have been removed. This is achieved by using an electromagnetic field solution. Although the elements of the impedance and admittance matrices are arrived at by a more accurate route, the application in terms of modal analysis is identical to earlier work. The impedance matrix elements are frequency dependent and a suitable time domain modelling method to allow for this is presented by Semlyen and Deri [100], for the three–phase case. Much effort is spent in achieving a fit between model and measured results and it is unlikely that the computational expense would be tolerated in a design aid simulator. More recently Arabi et al. [101] have carried out numerical methods of including frequency dependency in the impedance and admittance matrices, although the method is elaborate and limited in its applications.

2.4.2 Impedance and Admittance Matrix Elements

The impedance matrix for a multimode analysis is made up of self and mutual impedances; this is described in more detail in Chapter 3. The self impedance has two distinct parts which may be termed internal and external impedance. The internal impedance is made up of the conductor resistance and the internal inductance which is defined as the inductance due to flux inside the conductor. The external impedance is made up of a real part and an imaginary part also. The former is dependent on the power loss outside the conductor surface, including eddy currents in the track bed, while the inductive part is due to flux outside the conductor, generated by the conductor current itself rather than by currents in other conductors [102]. The definition of mutual inductance between two

conductors is described rigorously in terms of circuit effects [103, 104]. Also there may be mutual resistance between conductors depending on the surrounding environment.

The internal impedance of a steel rail is non–linear with temperature, frequency and current magnitude. This is due to the influence of the conductivity and permeability of the material. Techniques for conductivity modelling and evaluation are described in literature [105, 106]. The permeability of ferromagnetic materials with suitable methods for modelling also have been the subject of many publications. Only a selection can realistically be described here. One early and reasonably thorough set of definitions of permeability has been given by Von Hippel [107] [108]. These definitions have been adopted throughout this thesis since they appear to form the most complete description of permeability available. Many more modern methods of modelling hysteresis, and hence indirectly permeability, have been presented [109, 110, 111, 112, 113].

The majority of these methods are developed with application to numerical methods of solving e.m. problems. The most versatile of these methods, with non–linear permeability, is that of F.E.M. (Finite Element Method). The method has been shown capable of providing accurate values of resistance and inductance. An article by Luetke–Daldrup [114] compares the two–dimensional FE (finite element) solution for a non–linear eddy current problem with measurements and explains when favourable results can be expected. Further techniques for determining resistance and inductance in cables (as components of transmission lines) has also been presented [115]. Weiss and Csendes [116] use a "One–Step" F.E.M. for multiconductor skin effect problems but this requires specific algorithms which may not be available commercially. This is extended to a more general case by Chari and Csendes [117]. Nakata [118] explains how the principle can be widely used by describing the methods in terms of flux distributions (although in this case the application is one of electrical machines).

Many of the F.E.M. reports do not include hysteresis, but some particular studies by Nakata et al. [119], Del Vecchio [120] and Burais and Grellet [121] present varying techniques for including hysteresis in F.E.M. algorithms. The techniques are generally very application specific and are not easily introduced into commercial software. In addition, several attempts at simplified algebraic analyses, as an alternative to F.E.M, have been presented [122, 123, 124] but on examination it can be seen that the problems considered are of a particular specific nature. Hence on examination of the literature, it would seem that F.E.M. offers the most useful, general purpose method of evaluating the track impedance and admittance matrix elements.

The evaluation of self and mutual impedance of conductors above a conductive plane has been the subject of a number of papers. The basic approach is developed independently by Carson [92] and Pollaczek [93]. Carson develops the method further [125, 126] and many researchers have taken the analysis to a more complete form, especially with the advent of computer methods. Coleman [127] examines the case within a layered environment where each layer may have different conductivity. Wait, together with a number of colleagues [128, 129, 130], has written a number of papers describing a similar case of conductors above a conducting ground. Alvarado and Betancourt [131] further this investigation by presenting an approximate closed form of the original Carson equations but loose the generality of the original work. A comparison of Carson's work with image theory is also made for particular cases and this illustrates the areas where agreement is possible [132].

Using these developments, the principles also have been used to model impedances for conductors above a horizontally stratified, multilayer earth [133, 134, 135]. The method is summarised in a text [136]. Measurements are also available [137, 138] to indicate typical values for the impedances concerned. However, all the above papers are aimed at

either overhead lines or buried cables, which tend to be well insulated from the ground.

In a similar manner to the impedance matrix, the interconductor admittance matrix is made up of admittance elements dependent on ballast, soil and sleeper conductivity and permittivity. By analogy between electromagnetic and electrostatic analyses, it is possible to model inter–rail conductance and capacitance. However, the evaluation of conductivity and permittivity is a difficult problem. Starosol'skii [139] has presented results for the electrical resistance of ballast. Hill and Green [140] and Mayhan and Bailey [141] provide details of measuring soil permittivity and permeability but these are at radio frequencies rather than audio frequencies. Tables of resistivity and permittivity for various rock and soil types are provided by Keller and Frischknecht [142] although again these are at high frequencies. The influence of steel–reinforced concrete sleepers has been the subject of an investigation by Tso et al. [143]. However this again involves a simplified method of analysis and it would seem that an F.E.M. approach would yield a more accurate solution.

The evaluation of soil conductivity has been the subject of a number of studies. Initially the principle was developed by Langer [144, 145] and Slitcher [146]. Further theoretical and practical work by Blattner [147, 148] indicates that the technique is reliable. The evaluation of earth resistivity has also been considered by Meliopoulos et al. [149] and Baishiki et al. [150] but these authors do not extend the work of Blattner substantially. The method assumes that the ground is horizontally stratified and the ground conductivity can be determined by a four probe linear array. Telford et al. [151] describe a number of array techniques and Sunde [152] fully develops and collates the theoretical analysis.

2.5 Simulation Techniques

Although most of the work reported in this thesis is aimed at track modelling, the model results are used as data in a microsecond and millisecond timescale simulator intended for the study of E.M.I. in traction systems. In the development of this software simulator, two possible approaches were considered. The first of these was to develop the software from initial algorithms. An alternative approach to original source code development is to adopt an existing, more general commercial software package and modify the code where necessary. In electrified railway simulation, both types of software simulations have been used. Mellitt et al. [19, 9] and Ho et al. [54] have developed dedicated code to simulate various specialised aspects of traction and signalling problems. Others, such as Klauser et al. [153], have also developed specific programs for energy consumption investigations.

The adoption of commercial software has also been considered. Handel et al. [154] uses a common computer package (Lotus 123) to assist in the calculation of energy consumption of railway vehicles. This involved a single spread sheet approach. Hill and Yu [79] developed methods from Wedepohl's work, introduced earlier, such that matrices could be used to simulate both series impedance and parallel admittance of rail track. This was implemented by Hill et al. [155] using the S.P.I.C.E. software package and interference problems were considered. Wirth [156, 157] shows that a modal technique can be used for modelling p.c.b. tracks as transmission lines. However this must be carried out manually, causing considerable inconvenience and providing opportunity for additional error. Cesario et al. [13] also used a commercial package for traction power supply simulation. E.M.T.P. has been developed to simulate power systems and this paper shows that it is equally applicable to the special, single–phase case of traction supply. Wang and Mathur [158] show how the package can be modified to provide a

transmission line frequency response. Lin and Marti [159, 160] have illustrated how numerical oscillations, inherent in time stepping simulation software, can be eliminated by a technique of CDA (critical damping adjustment). A review of the E.M.T.P. simulation method is also given. The advantage of using commercial software and hence having extensive development and validation successfully completed, is indicated by Natarajan and Gentzler [161] who describe the problems of installing E.M.T.P. onto a personal computer system. In addition, a comparison between small and large computer system performance is given.

A very similar software package has also been subject to extensive validation and several papers describe this. Woodford et al. [162] describe how E.M.T.D.C. (Electromagnetic Transient D.C.) performs an analysis, and indicate methods of interfacing user–defined algorithms to the program. Subsystem models are described and the resulting output is given in a number of forms. Nyati et al. [163] provide examples of simulations and make comparisons between the results obtained and the actual power supply system installation. Nyati et al. [164], in a second paper, also compare the solution provided by an analogue simulator, E.M.T.D.C. and the actual installation. In all cases E.M.T.D.C. gives good agreement with measurements taken.

Chapter 3

The Use of Multimode Transmission Line Analysis in Simulation

Transmission lines may be represented using two main methods in simulation. One well known method is termed the *pi* line section representation. This technique couples a number of *pi* section networks together to make up any length of line. Since these networks are made up of lumped components, the method is most suitable for analogue simulation. Since every phase has to be connected to every other phase explicitly, the *pi* section network simulation becomes cumbersome and complicated when more than one or two phases are being considered. The second method was developed in the 1960's and is more suitable for digital computer simulation. A novel and complete solution to the problem of analysing a multiwire (or multiphase) transmission line, in the presence of a lossy ground, was first described by Wedepohl in 1963 [89]. He demonstrated how the performance of a transmission line can be predicted by developing the solution, in matrix form, of the distributed model using the principle of travelling waves. The solution of the n simultaneous equations, describing an n–phase line, is achieved by decoupling the phases into *modes*. The application of interest to Wedepohl was that of power system transmission and the problems of protection, fault location, switching of unloaded lines and calculation of recovery voltages on circuit breakers. It has now become a well known method for determining the characteristics of transmission lines in many types of systems, as shown in Chapter 2. Applications range from traditional power distribution systems, through telecommunications links, to printed circuit board

tracks coupling integrated circuits [156, 157]. The method has also been incorporated into a limited number of software packages based on work by Dommel and Meyer [165].

However the method has had limited application in rail track analysis. This is probably due to the fact that the assumptions made in many situations cannot be adopted in this case. A report by E.P.R.I. [61] considers the method but limits detailed investigation to a two rail track, with little consideration of the application of the results. The data is obtained by measurement or, where this was not possible, approximate analytical methods were used. Hill and Yu [79] use the method for a three rail system, but only estimate the data for the analysis. They show that the method could be used for simulation using the S.P.I.C.E. software package. In both cases, no attempts have been described which would validate the data or the analysis.

Since the principle of modal analysis of a transmission line is well understood, only a summary is given here, with further details in Appendix A.

3.1 Review of the Theory of Modal Transmission Lines

The objective of using the theory of modal (or eigenfunction) analysis is to determine the solution of coupled transmission line equations. This is achieved by decoupling the equations and solving each equation separately. It is most conveniently expressed in matrix form.

Consider a polyphase system of coupled transmission lines as shown in Figure 3.1. It is easily shown in Appendix A that the equations governing the electrical behaviour of a two wire system can be expressed as

$$\frac{dV_1}{dx} = -(Z_{11}I_1 + Z_{12}I_2) \tag{3.1}$$

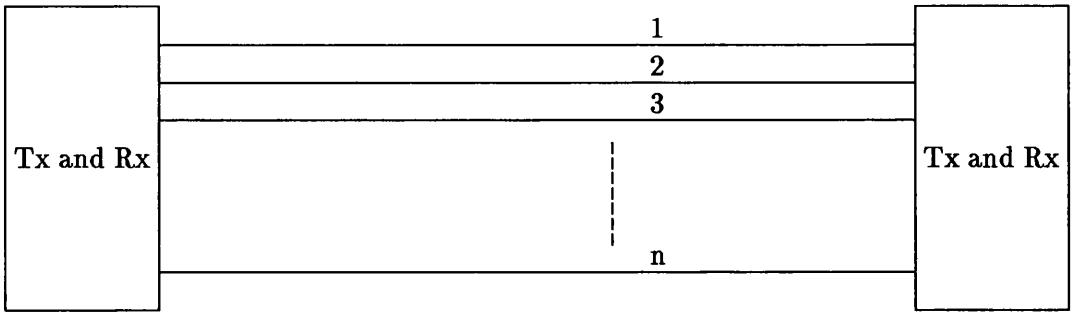

Figure 3.1: Multi–wire Transmission Line

and

$$\frac{dV_2}{dx} = -(Z_{12}I_1 + Z_{22}I_2) \tag{3.2}$$

where

V_n, I_n are the voltage and current in line n

Z_{nn} is the self impedance of line n (see Section 3.2.1)

Z_{nm} is the mutual impedance between lines n and m (see Section 3.2.1)

and

$$\frac{dI_1}{dx} = -(Y_{11}V_1 + Y_{12}V_2) \tag{3.3}$$

$$\frac{dI_2}{dx} = -(Y_{12}V_1 + Y_{22}V_2) \tag{3.4}$$

where

$Y_{nn} + Y_{nm}$ is the self admittance of line n (see Section 3.2.1)

$-Y_{nm}$ is the mutual admittance between lines n and m (see Section 3.2.1)

or in matrix form

$$\frac{d[\mathbf{V}]}{dx} = -[\mathbf{Z}].[\mathbf{I}] \tag{3.5}$$

and

$$\frac{d[I]}{dx} = -[\mathbf{Y}].[\mathbf{V}] \tag{3.6}$$

where

$[\mathbf{V}]$ is the vector of phase voltages

$[\mathbf{I}]$ is the vector of phase currents

$[\mathbf{Z}]$ is the matrix of phase impedances

$[\mathbf{Y}]$ is the matrix of phase admittances

The physical interpretation of the matrix elements, in the case of a rail track, is the subject of Section 3.2.1

It is easily shown that Equations 3.5 and 3.6 can be combined to give

$$\frac{d^2[\mathbf{V}]}{dx^2} = [\mathbf{A}]^T[\mathbf{V}] \tag{3.7}$$

and

$$\frac{d^2[\mathbf{I}]}{dx^2} = [\mathbf{A}][\mathbf{I}] \tag{3.8}$$

where

$[\mathbf{A}] = [\mathbf{Y}][\mathbf{Z}]$

$[\mathbf{M}]^T$ represents the transpose of matrix $\mathbf{M}$

The simultaneous Equations 3.7 and 3.8 are clearly coupled and represent the phase quantities of the polyphase system. To solve these Equations, the modal analysis method proceeds by decoupling them. This is achieved if

$$\frac{d^2[\mathbf{V}^m]}{dx^2} = [\mathbf{\Lambda}]^T[\mathbf{V}^m] = [\mathbf{\Lambda}][\mathbf{V}^m] \tag{3.9}$$

and

$$\frac{d^2[\mathbf{I}^m]}{dx^2} = [\mathbf{\Lambda}][\mathbf{I}^m] \tag{3.10}$$

where

superscript m indicates modal quantities

$[\mathbf{\Lambda}]$ is a diagonal matrix of modal (or eigen) values

Using the theory of similar matrices, a matrix operator $[\mathbf{T}]$ is introduced, which satisfies

$$[\mathbf{\Lambda}] = [\mathbf{T}]^T[\mathbf{A}][\mathbf{T}]^{T^{-1}} \tag{3.11}$$

where

$\mathbf{T}$ is the modal transformation matrix (further described in Appendix A)

$[\mathbf{M}]^{-1}$ represents the inverse of matrix $\mathbf{M}$

Hence Equations 3.9 and 3.10 provide decoupled forms of voltages and currents of the polyphase line[1] and may be solved in a straight forward manner. The solutions have the familiar form

$$V_n{}^m = V_n{}^{m+}e^{-\gamma_n x} + V_n{}^{m-}e^{\gamma_n x} \tag{3.12}$$

where

$V_n{}^{m+}$ is the forward travelling voltage component of mode n

$V_n{}^{m-}$ is the reverse travelling voltage component of mode n

γ_n is the propagation constant of mode n

The solution of $I_n{}^m$ has a similar form. These solutions can then be substituted back

[1] In general these decoupled equations cannot be related to the physical system.

into Equations 3.7 and 3.8 as shown in Appendix A since

$$[\mathbf{V}] = [\mathbf{T}][\mathbf{V}^m] \tag{3.13}$$

and

$$[\mathbf{I}] = [\mathbf{T}]^{T^{-1}}.[\mathbf{I}^m] \tag{3.14}$$

In a similar manner, the impedance and admittance matrices can be related between phase and mode by

$$[\mathbf{Z}] = [\mathbf{T}][\mathbf{Z}^m][\mathbf{T}]^T \tag{3.15}$$

and

$$[\mathbf{Y}] = [\mathbf{T}]^{T^{-1}}[\mathbf{Y}^m][\mathbf{T}]^{-1} \tag{3.16}$$

where

$\mathbf{Z}^m$ is the modal impedance matrix

$\mathbf{Y}^m$ is the modal admittance matrix

It is easily shown that from Equations 3.11, 3.15, and 3.16 that

$$[\mathbf{Y}^m][\mathbf{Z}^m] = [\mathbf{\Lambda}] \tag{3.17}$$

From two conductor transmission line analysis [61], it is usual to infer that the elements of the diagonal matrix $[\mathbf{\Lambda}]$ are the square of the modal propagation constants. Hence

$$[\mathbf{Y}^m][\mathbf{Z}^m] = [\gamma^2] \tag{3.18}$$

where $[\gamma^2]$ is a diagonal matrix of the square of the modal propagation constants

Hence each modal propagation constant is the square root of the eigenvalue $\gamma_i = \sqrt{\lambda_i}$. To decouple the transmission line equations and obtain solutions, provided the elements

of [Z] and [Y] are know, it is only necessary to determine the [Λ] and [T] matrices. The elements of the [Λ] matrix are eigenvalues of the system and can be obtained by rearranging Equations 3.11 as

$$[\mathbf{A}][\mathbf{T}]^{T^{-1}} = [\mathbf{T}]^{T^{-1}}[\mathbf{\Lambda}] \tag{3.19}$$

It is shown in Appendix A that this is satisfied if

$$|[\mathbf{A}] - \lambda_i[\mathbf{U}]| = 0 \tag{3.20}$$

where

$|\mathbf{M}|$ is the determinant of M

[U] is the unit matrix

λ_i are the eigenvalues of the system

The solution of Equation 3.20 yields the values $\lambda_i(i = 1..n)$ where n is the number of phases. This then permits the evaluation of the T matrix by standard numerical algorithms as described in Appendix H. This then yields

$$[\mathbf{A}][\mathbf{T}_i] = \lambda_i[\mathbf{T}_i] \tag{3.21}$$

where $\mathbf{T}_i$ is the ith column of the T matrix and is the eigenvector associated with the ith eigenvalue λ_i.

3.2 The Corollaries and Consequences of Using Modal Analysis

The main benefit of using modal analysis in the solution of the performance of a multi–wire transmission line is that each mode can be solved separately, as described in the

previous section. This avoids the problem of developing a complicated dense matrix formulation for the coupled physical system. The computational effort of solving the coupled line problem directly is far in excess of the modal method. This difference in computational effort increases as the number of lines increase.

It has been shown in Equation 3.17 and 3.18 that a direct result of determining the transformation matrices required to change from phase quantities to modal quantities is the evaluation of the eigenvalues and hence the modal propagation constants. These propagation constants indicate the behaviour of each mode in terms of attenuation and phase shift, along the line, in a similar way to classical transmission line theory. Apart from the special case of the symmetrical two wire and three wire systems, it is not apparent that these constants have physical significance, with respect to the phase quantities. To obtain physical meaning the propagation constants may be transposed back into the phase quantities. It should be noted that as the square of the propagation constants are the eigenvalues of the system, standard mathematical procedures can be used [168] for eigenvalue evaluation. Similar procedures can be used to determine the eigenvectors, which form the columns of the transformation matrices. These procedures are illustrated in Appendix H.

In association with the propagation constants are the modal characteristic impedances which are defined as

$$Z_{oi}^{m} = \sqrt{\frac{Z_{im}}{Y_{im}}} \tag{3.22}$$

where

Z_{im} is the element of the modal impedance matrix associated with the ith mode

Y_{im} is the element of the modal admittance matrix associated with the ith mode

Hence a set of modal characteristic impedances exist which form a diagonal modal characteristic impedance matrix $[\mathbf{Z}_{om}]$. This matrix is useful as it defines the current that would flow in an infinitely long mode, excited by a given modal voltage. It can also be expressed in terms of injected current and resultant potential difference along the line. For this reason it is utilised in software simulation. The phase characteristic impedance is the dual of the modal characteristic impedance and is defined as

$$[\mathbf{Z}_o] = [\mathbf{T}][\gamma]^{-1}[\mathbf{T}]^{-1}[\mathbf{Z}] \tag{3.23}$$

This has similar phase properties to the modal dual. However, in this case the matrix is not necessarily diagonal but does represent the physical system. That is, if the actual transmission line is terminated in a network represented by $[\mathbf{Z}_o]$, it appears as an infinitely long line.

The final property of interest is the reflection coefficient matrix defined by Wedepohl [89] as

$$[\mathbf{K}] = [\mathbf{Z} + \mathbf{Z}_o]^{-1}[\mathbf{Z} - \mathbf{Z}_o] \tag{3.24}$$

This can be used to determine the reverse voltage at the end of a line, subject to an incident (forward travelling) voltage. Since $[\mathbf{K}]$ is not necessarily diagonal, it is of interest to note that an incident voltage on one phase, may cause reflected voltages on other phases, which have not been excited.

3.2.1 Phase Admittance and Impedance Matrix Elements

The phase admittance and impedance matrices relating to the physical transmission line are given in Equations 3.1 to 3.4, together with Appendix A. Galloway et al [94] explain one method by which elements of these matrices may be calculated, for power

system overhead lines. This method incorporates the usual (and valid) approximation for power system transmission lines that, in the admittance matrix, conductance may be negligible with respect to the susceptance, $G << B$. That is the admittance matrix is made up of imaginary elements. This is not the case with rail track where the running rails are considered as separate conductors. Further, the method of evaluating susceptance assumes that the conductors are surrounded by a uniform medium of fixed permittivity. A uniform charge distribution may then be assumed, allowing the calculation of capacitance to be relatively straightforward. Again this is not the case for rail track; the rails lie on (or close to) a boundary between two substantially different media (i.e. air and the conductive track bed).

Galloway et al also describe a classical approach to evaluating the phase impedance matrix elements. It is stated that there are five components to each impedance element, i.e.

$$Z = R_c + R_e + j(X_g + X_c + X_e) \tag{3.25}$$

where

R_c, R_e are the resistance components due to the conductor and earth respectively.

X_g, X_c, X_e are the reactance components due to the geometry of the conductors, the conductor itself and the earth path respectively.

It should be noted that R_c and X_c are also known as internal resistance and reactance.

In his original paper, Carson [126] developed expressions for X_g, X_e and R_e, while Galloway et al. separate X_g from X_c, although the resulting numerical evaluations are the same. In subsequent developments of the so called "Carson Equations", it is usual to form an expression which combines X_g and X_e. This is the case in a useful summary

text by Bickford et al. [136]. The are no restrictions in the method used by Galloway et al. in determining the impedance elements, although the original "Carson Equations" do have some restrictions.

Considering the case of rail track specifically, the phase admittance matrix elements can be expected to be of a complex form. This is due to both capacitive and conductive components being present since the rails are in contact with the ground. The phase impedance matrix, for rail track, takes a similar form to that of the power system. However, the periodicity of the sleepers and the fact that the conductors are steel, with a varying value of relative permeability much greater than unity, creates addition non–linearities.

The physical significance of each phase element can be related to the track and track–bed structure. Within the impedance matrix of Equations 3.1 and 3.3, the diagonal elements, Z_{ii} $(i = 1 \ldots n)$ where n is the number of phases, are termed self–impedance and can be thought of as the impedance representing a single rail with earth return. This leaves the off–diagonal elements Z_{ij} $(j = 1 \ldots n)$ $i \neq j$, which can be considered to represent the mutual impedance between two rails with an earth plane present. The admittance matrix is less directly associated with the physical structure. The off–diagonal elements, Y_{ij}, represent the magnitude of the mutual admittance between rails but with a phase inversion, i.e.

$$Y_{ij} = -Y_{mij} \tag{3.26}$$

where Y_{mij} is the mutual admittance between two rails

The diagonal elements, Y_{ii} form part of the admittance from the rail to a remote ground,

Y_{ie}. The relationship is

$$Y_{ie} = Y_{ii} + \sum_{j}^{n} Y_{ij} \tag{3.27}$$

3.3 The Choice of Software Simulation Method

As indicated in Chapter 2, it may be considered that there are two methods for developing software simulators. One approach requires the development of the software from basic algorithms, whilst the alternative is to adopt existing simulation packages and make modifications to suit the particular application. Both methods have inherent advantages and disadvantages.

The former method requires the detailed development of original algorithms. By the nature of such work, the initial cost tends to be large since much validation and testing is required. Hence many man–years will be involved before the simulator can be used with a high degree of confidence in complicated analysis. In addition, code and user guide documentation must be prepared. The end product is usually a very powerful design aid. Such is the case with some existing simulation programs [9, 19, 54, 153]. The large number of man–years involved in these projects has resulted in successful products, although they are not all commercially available as packages. The main application of these packages is as part of a consultancy service, provided by the software originators i.e. the package is used for customer applications *in–house* rather than making the software directly available. Hence the majority of industrial users commission the software authors to provide simulation results.

The second approach has advantages in that commercial software will have had a satisfactory period of validation. In addition, documentation will be complete and previous user experience may be available. The obvious disadvantage is that there may be re-

strictions on certain applications since it is not dedicated to the specific problem.

In considering which of the two approaches should be used in this study, the main consideration was the requirement for robustness and minimisation of initial overheads. That is, the simulator should be developed to a useful working state in a relatively short period (less than three man–years). Hence the decision was taken to adopt commercial software and modify this where necessary.

To this end, suitable packages were considered. It was thought that three packages might be suitable, these being S.P.I.C.E, E.M.T.P, E.M.T.D.C. The latter, E.M.T.D.C., operates in a similar manner to E.M.T.P. but has special provision for d.c. power system links. The S.P.I.C.E. simulator is primarily used for discrete electronic component or integrated circuit simulation. It is not designed for power system applications and transmission lines must be modelled individually, especially when using modal transmission line techniques. Much of the sophistication of S.P.I.C.E. is in the modelling of semi–conductor components and it was thought that the modelling of power transformers and motors would be more difficult.

The similarities between E.M.T.P. and E.M.T.D.C. make the choice between the two packages difficult. Advice on the comparative strengths of the two programs was sought [166] which indicated that since d.c. traction systems were to be considered, then E.M.T.D.C. should be selected. The advantages of using E.M.T.D.C. apply equally to E.M.T.P. The versatility of E.M.T.P. has been indicated by reference to earlier work, as outlined in Chapter 2. This selection of the "D.C." version of the software is not thought to be irreversible. At any stage of development it is felt that E.M.T.P. could well by exchanged with E.M.T.D.C. as the algorithms are very similar. Further, it may well be that each package has relative strengths dependent on the application under consideration.

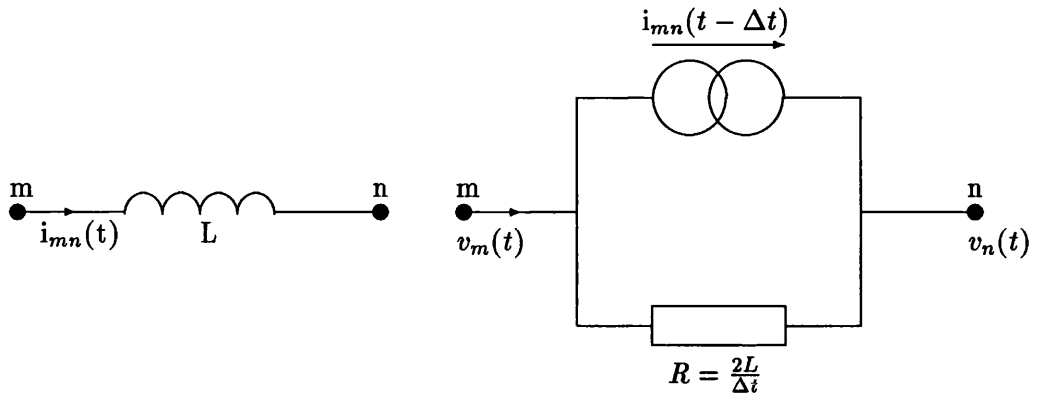

Figure 3.2: The Nodal Connections of the Inductor and its Computational Equivalent

3.3.1 The Time–Step Solution Method for Simulation

The theoretical basis of the solution method has been fully explained by Dommel and Meyer [165]. The principles can be easily explained if discrete passive components are considered. Using nodal analysis, a conductance matrix method can be used. *Lumped* resistors are modelled as resistive branches. Of course these are time invariant. However this is not the case with lumped inductors and capacitors. If the inductor, L, is considered, as shown in Figure 3.2

$$i_{mn}(t) = \frac{1}{L}\int (v_m(t) - v_n(t))\,dt \tag{3.28}$$

where

$i_{mn}(t)$ is the current in the branch between nodes m and n at time t

$v_k(t)$ is the voltage at node k at time t

Using the trapezoidal rule of integration

$$i_{mn}(t) = \frac{\Delta t}{2L}(v_m(t-\Delta t) - v_n(t-\Delta t)) + constant \tag{3.29}$$

where Δt is the time interval representing the time–step length of the simulation

The voltages $v_k(t-\Delta t)$ are used as these are known from the previous time step calculation. The constant provides a time history of the current through the branch i.e. a *memory function* relating to the current flowing up to time $(t-\Delta t)$. Dommel and Meyer define this constant as

$$I_{mn}(t-\Delta t) = i_{mn}(t-\Delta t) + \frac{\Delta t}{2L}(v_m(t-\Delta t) - v_n(t-\Delta t)) \tag{3.30}$$

which can be evaluated from the previous time step results. Defining

$$R_{eq} = \frac{2L}{\Delta t} \tag{3.31}$$

gives

$$i_{mn}(t) = \frac{1}{R_{eq}}(v_m(t-\Delta t) - v_n(t-\Delta t)) + I_{mn}(t-\Delta t) \tag{3.32}$$

The same equation holds for a capacitive branch (capacitance C) where

$$R_{eq} = \frac{\Delta t}{2C} \tag{3.33}$$

and

$$I_{mn}(t-\Delta t) = -i_{mn}(t-\Delta t) - \frac{2C}{\Delta t}(v_m(t-\Delta t) - v_n(t-\Delta t)) \tag{3.34}$$

The equivalent circuits for the inductor and capacitor are shown in Figures 3.2 and 3.3 respectively.

Since an equivalent resistance is obtained for each component, which is time invariant, this can be used as an element (or component of an element) in the conductance matrix.

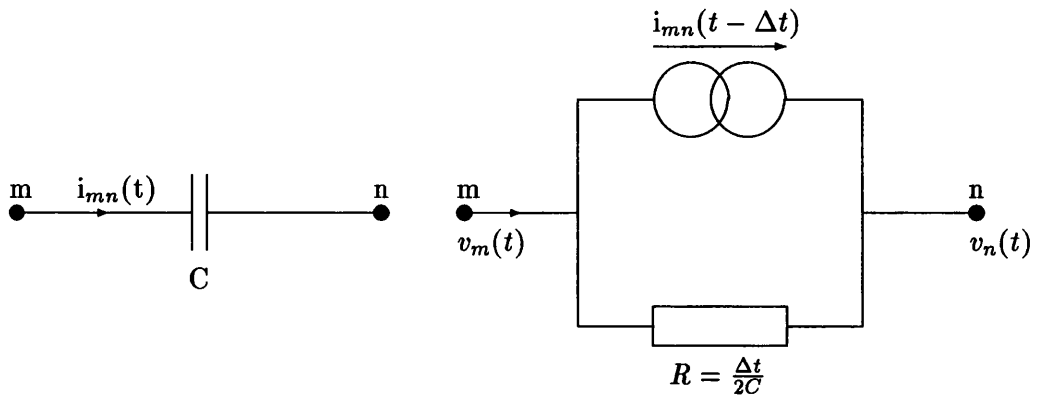

Figure 3.3: The Nodal Connections of the Capacitor and its Computational Equivalent

The whole of the conductance matrix is then time invariant. This procedure operates on the conductance matrix of equivalent resistances together with a current vector. The elements of the current vector are made up of the sum of the source currents at each node. The general principle is that at each time step

$$[\mathbf{G}_{node}].[\mathbf{V}_{node}] = [\mathbf{I}_{node}] \tag{3.35}$$

To solve for the voltages at each node, $[\mathbf{V}_{node}]$, then

$$[\mathbf{V}_{node}] = [\mathbf{G}_{node}]^{-1}[\mathbf{I}_{node}] \tag{3.36}$$

The method is computationally efficient as the conductance matrix need only be inverted at the start of the simulation, or when the circuit is changed (e.g. at times of switching). Mutually coupled branches can be incorporated into the conductance matrix in a similar manner [167]. The modelling of transmission lines is somewhat different and is the subject of the next section.

3.4 The Application of Modal Transmission Line Analysis in Simulation

As can be seen from Section 3.1 (in particular Equation 3.12), the modal analysis or distributed model operates by considering travelling waves along the transmission line. In E.M.T.D.C. the fundamental concept is that the transmission line acts as a delay function. That is, a voltage excitation at one end of the line will travel at the propagation velocity until it is reflected at the far end. The time taken for the wave to travel from one end to the other is the delay or travel time. Some distortion and interaction with termination networks is also likely to occur. As explained earlier, traditional simulation techniques used *pi* section lines. However, when using digital computer software, the main advantages of using a distributed line are

- the smaller computational time and smaller matrices
- the ease of modelling many multi–coupled lines
- the incorporation of frequency dependent attenuation of the travelling waves

To consider the basic principles used in implementation of the modal analysis in a digital simulation package, a simple case will be considered here with a more complicated situation discussed in Chapter 8. The single phase line is equivalent to a single mode line. In a power system model, it is assumed that the conductance to ground and between conductors is negligible. It is found that the travel time for such a line is

$$\tau = \sqrt{L.C}l \tag{3.37}$$

where

L is modal inductance per unit length

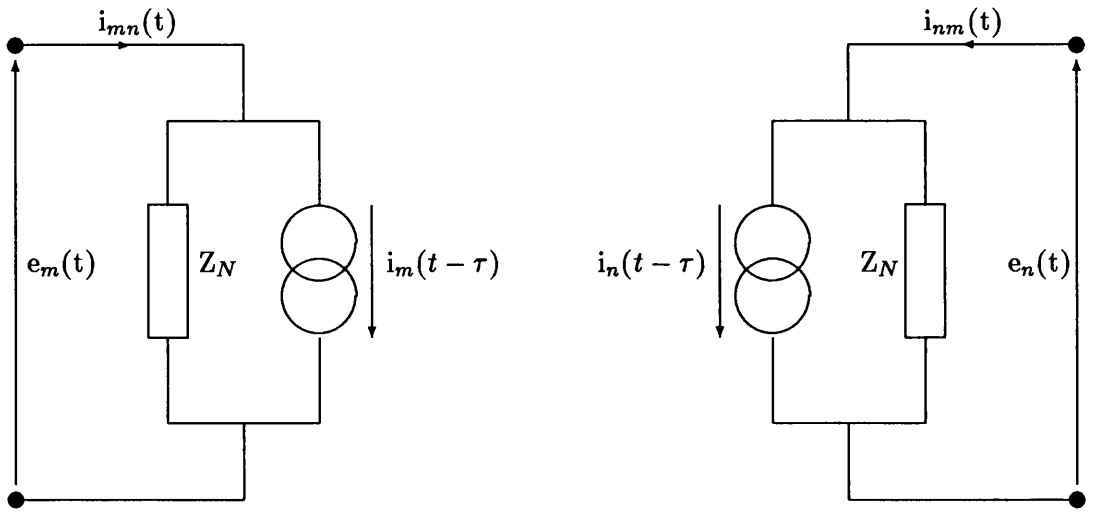

Figure 3.4: Transmission Line Interface

C is modal capacitance per unit length

l is the line length

The characteristic impedance of the line is then

$$Z_o = \sqrt{\frac{L}{C}} \tag{3.38}$$

The interface used in E.M.T.D.C. is shown in Figure 3.4. In this case the

Norton resistance in the Figure is

$$Z_N = Z_o + \frac{R}{4} \tag{3.39}$$

where R is the total series resistance of the line

Dommel and Meyer [165] have determined that the sending end Norton current source is given by

$$I_m(t-\tau) = \frac{1+h}{2}\left[\frac{-e_m(t-\tau)}{Z_N} - i_{mk}(t-\tau)\right] + \frac{1-h}{2}\left[\frac{-e_k(t-\tau)}{Z_N} - i_{km}(t-\tau)\right] \tag{3.40}$$

where $h = \frac{Z_N - \frac{R}{4}}{Z_N + \frac{R}{4}}$

$I_n(t-\tau)$ is determined in a similar manner by replacing the values above for those from the other end of the line. This approach inherently divides the line into two parts of equal length. $\frac{R}{2}$ is placed between the two lines i.e. the mid–point of the original line and $\frac{R}{4}$ is placed at each end of the line. To incorporate modal conductance, half the total conductance for the original line is place at either end of the line. If a more distributed effect for R and G is needed, the original line must be divided into a number of sections. Although this appears to create computational inefficiencies, it has certain advantages in that with shorter lines, the time step length can be reduced, allowing greater accuracy to be achieved. It should also be noted that there is a minimum line length that can be modelled. This is given by the travel time from one end to the other which has to be greater than the simulation time step.

Chapter 4

Material Properties of Rails and Track Bed

It will be shown in Chapter 5 and 6 that the material properties of the three rail track, i.e. the power and running rails, and the surrounding media, i.e. the ballast and soil, have a significant effect on the performance of the track as a transmission line. Hence it is necessary to determine accurately the electrical and magnetic properties of the materials involved.

In evaluating the material properties, it was decided that not only measurements should be made but also modelling techniques should be developed. In this way, the models of material properties could be used to evaluate the electrical performance of the system. By using this approach, once acceptable agreement between model and system measurement has been established, model validation is achieved. This allows the modelling method to be used when modified or new systems are examined and exhibit different properties.

4.1 Rail Material Properties

The material properties of the steel rails determine the internal impedance of the conductors of the transmission line. It will be shown in later chapters that the resistive part of the internal impedance dominates the series resistance of both the traction and

signalling circuits through the rails. It will also be shown that the inductive component of internal impedance is often a significant proportion of the total series inductance, depending on excitation conditions. To evaluate the internal impedance of the rails, electric and magnetic properties of the rail iron must be considered. There are two main parameters, these being conductivity and permeability. Conductivity (σ) of the rails is a microscopic effect and can be evaluated in a straightforward manner, by measurement. This is described in Section 4.1.3. Steel rails have magnetic properties which may be quantified by complete determination of the steel permeability. Permeability (μ) is the ratio of flux density (B) to magnetic field strength (H). However, permeability is found to be extremely non–linear and the B–H relationship exhibits hysteresis when the magnetic field strength excitation is bidirectional.

4.1.1 Measurement Technique for Permeability Evaluation

To evaluate permeability, in the absence of other effects, such as skin effects from eddy currents, careful consideration must be given to the experimental apparatus and dimensions of the specimen of material. It was decided to use equipment developed elsewhere [169] based on magnetisation of a filament of the test material with uniform longitudinal field. The method has been shown to reduce the effect of eddy currents on the measurements to a negligible level. The filament is subject to an alternating magnetic field of 0.33 Hz frequency in the direction of the long axis. For typical magnetic materials, of which rail steel is one, this creates a skin depth of many times greater than the width of the filament. Then, using a suitable search coil placed around the filament, the flux density can be measured.

Each of the three orthogonal orientations were measured for each type of rail material being tested. It was found that all rail steels under tests were isotropic. To obtain a

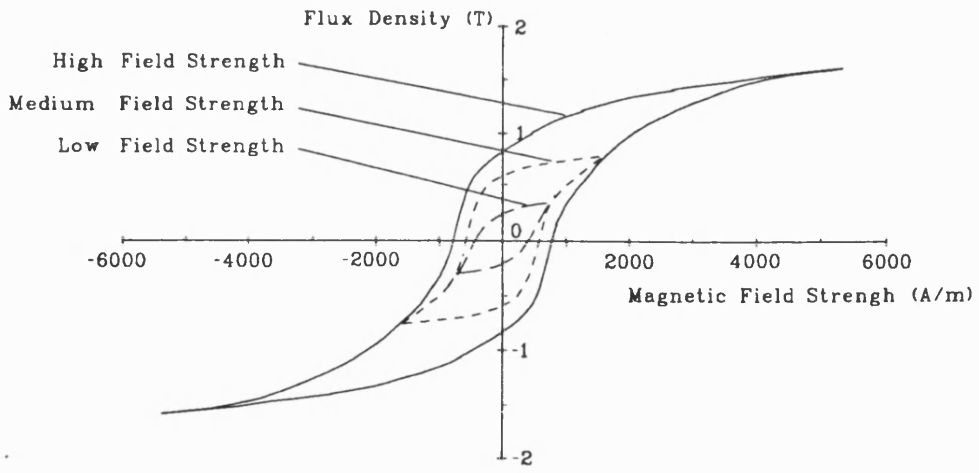

Figure 4.1: B–H Relationship for Flat–Bottom Rail Steel

range of curves, each material sample was subject to a number of different magnetic field strength magnitudes. The sample was demagnetised between tests.

Three rail types were examined for comparison purposes. Used rail has been chosen. This then includes any changes in magnetic properties due to operational "working". The types of rail examined were *flat–bottom* rail, *bull–head* rail and conductor (power) rail. The B–H relationships are shown in Figures 4.1 to 4.3 . There is some difference between the two running rail results but the most significant difference is seen when the conductor rail curve is examined. The B–H loop, for the conductor rail, is smaller in size. This is due to the different composition used to create a more conductive material. The rail also has less hysteresis loss.

This comparison can be seen quantitatively in Table 4.1. In addition to the three samples described above, the result for a typical mild steel sample is also given. The table shows the energy loss per cycle which is evaluated as $\int HdB$, the area of the B–H loop. In addition to skin effect, in some instances secondary effects may occur due to increase in frequency. One example of this is loop widening. However these tend to be negligible in comparison with hysteresis [112].

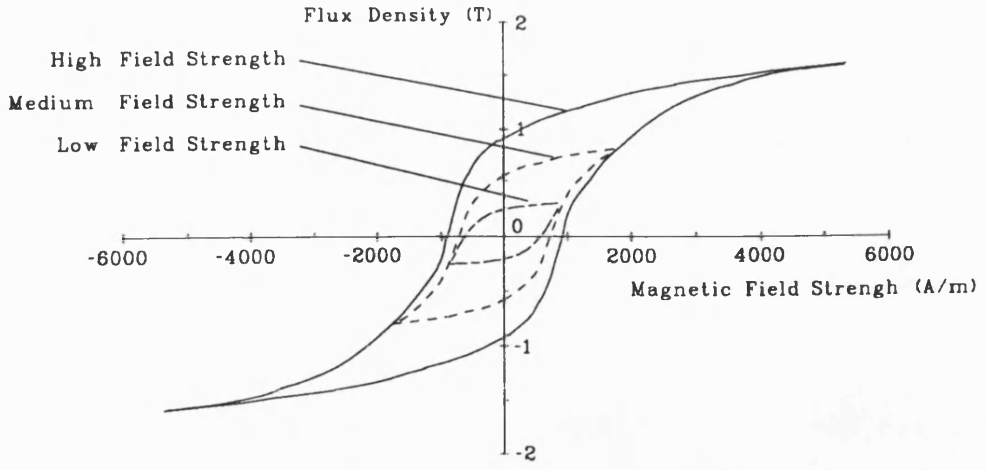

Figure 4.2: B–H Relationship for Bull–Head Rail Steel

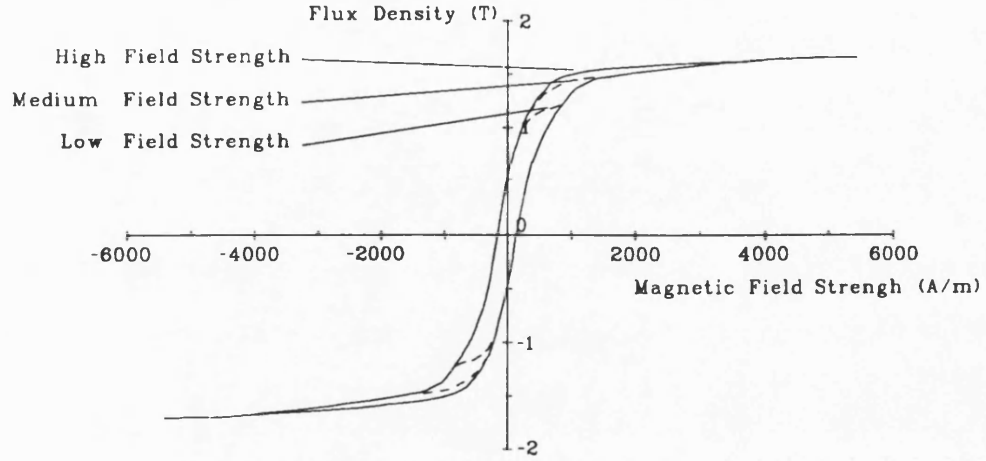

Figure 4.3: B–H Relationship for Conductor Rail Steel

Table 4.1: Energy per Cycle of Hysteresis Loops

Sample	Energy Loss Per Cycle (Jm^{-1})		
	H_{max} = 5600 Am^{-1}	H_{max} = 1700 Am^{-1}	H_{max} = 900 Am^{-1}
Mild Steel	1871	1318	680
Flat–Bottom Rail	3908	1805	506
Bull–Head Rail	3957	1704	461
Conductor Rail	844	650	432

4.1.2 Modelling Permeability for Rail Material

The data obtained above is required to determine the permeability function as the magnetic field strength varies sinusoidally. Permeability may be defined in a number of ways as illustrated in Figure 4.4. Von Hippel [108, 107] introduces a number of these and several further definitions have been included in the figure. All of those illustrated can be considered as instantaneous. That is, the value depends on the position, direction and peak value of the magnetic field strength. These are useful for a time and space numerical model where the permeability can be changed from one time step to the next and between spacial points. Such a model would be a full F.D.M. (Finite Difference Method) or a F.E.M. (Finite Element Method) with Finite Difference time steps.

For an analytical model, that is one in which a single effective value of permeability is required, it is necessary to develop the analysis further. A number of approaches have been considered for the evaluation of a single value of permeability.

If the expression for permeability is considered, then the hysteretic loss (i.e. the B–H loop area) can be approximated by a phase shift between the magnetic field strength and the flux density. This can be expressed as a complex permeability[1]

$$B = \mu^* H = (\mu' - j\mu'')H \tag{4.1}$$

The reactance due to the changing flux is proportional to

$$\frac{\Phi}{I} = \frac{\int B ds}{I} = \frac{\int (\mu' - j\mu'') H ds}{\int H dl} \tag{4.2}$$

For constant μ^*

$$\frac{\Phi}{I} = \frac{(\mu' - j\mu'') \int H ds}{\int H dl} = L - j\mu'' \frac{\int H ds}{\int H dl} \tag{4.3}$$

[1]Complex permeability is traditionally associated with molecular loss effects. However this alternative interpretation is dimensionally correct.

The rail internal impedance is then

$$\begin{aligned} Z_{rail} &= R(\sigma) + j\omega\frac{\Phi}{I} \\ &= R(\sigma) + j\omega L + \mu''\frac{\int H ds}{\int H dl} \\ &= R(\sigma) + R(\mu'') + j\omega L \end{aligned} \tag{4.4}$$

Here $R(\mu'')$ represents a resistance component of rail impedance due to the hysteresis losses.

As indicated earlier, a number of methods have been examined in an attempt to identify a suitably accurate procedure for evaluating permeability. These are described here.

- *Method 1 - Normal Permeability (μ_n).* In this method, the initial magnetisation curve is used to evaluate permeability by calculating the ratio of absolute flux density to magnetic field strength (B/H). This represents an approximate method since no allowance is made for hysteresis loss. However, nonlinearities are included. The method is graphical and is illustrated in Figure 4.5. This is the approach taken by many numerical methods (e.g. finite difference and finite element calculations). The method has been used on selected materials and an example, for flat–bottom rail with variation in magnetic field strength, is given in Figure 4.6.

- *Method 2 - Permeability from Fundamental Flux Density (μ_{B_o}).*

  Assuming a sinusoidal magnetic field strength (H), the resultant flux density (B) has been analysed by fourier transform. Using F.F.T. techniques [170] both fundamental and harmonic magnitudes together with phases have been evaluated, for all rails. An example, for flat–bottom rail with variation in magnetic field strength, is given in Figure 4.7. By considering only the fundamental flux density waveform, the measured hysteresis loop is represented by an ellipse, as shown in

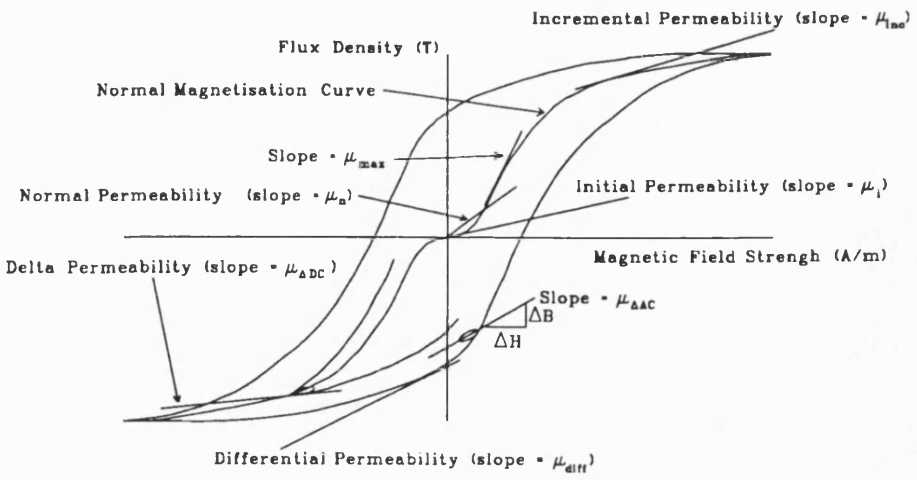

Figure 4.4: Definitions of Permeability

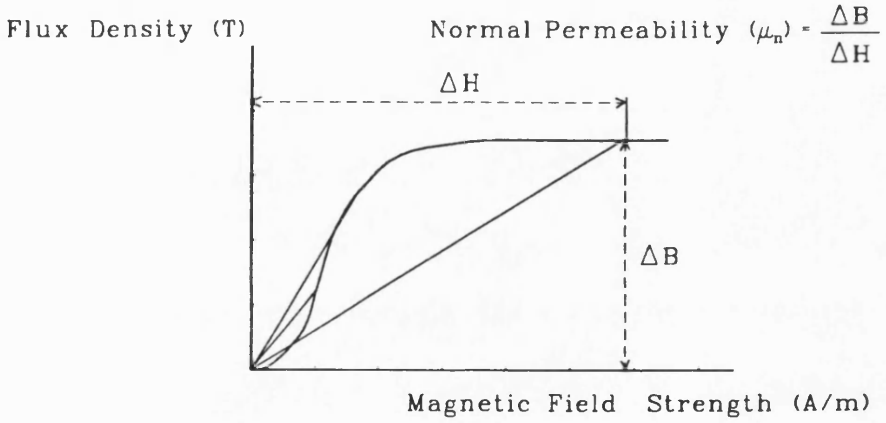

Figure 4.5: Graphical Evaluation of Normal Permeability

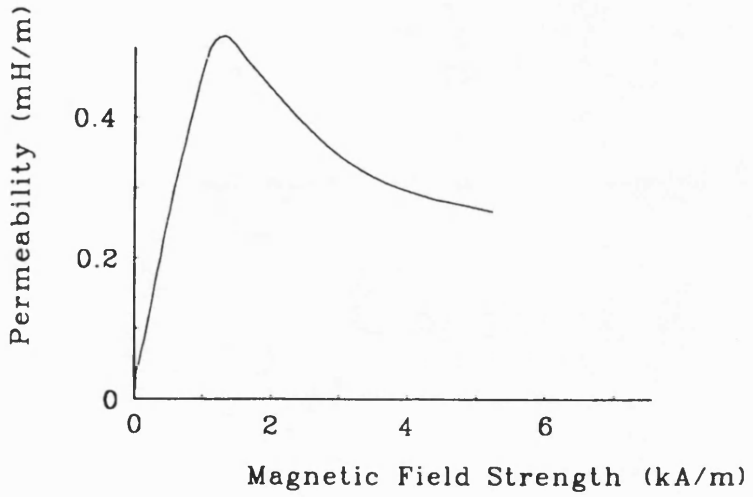

Figure 4.6: Normal Permeability against Magnetic Field Strength

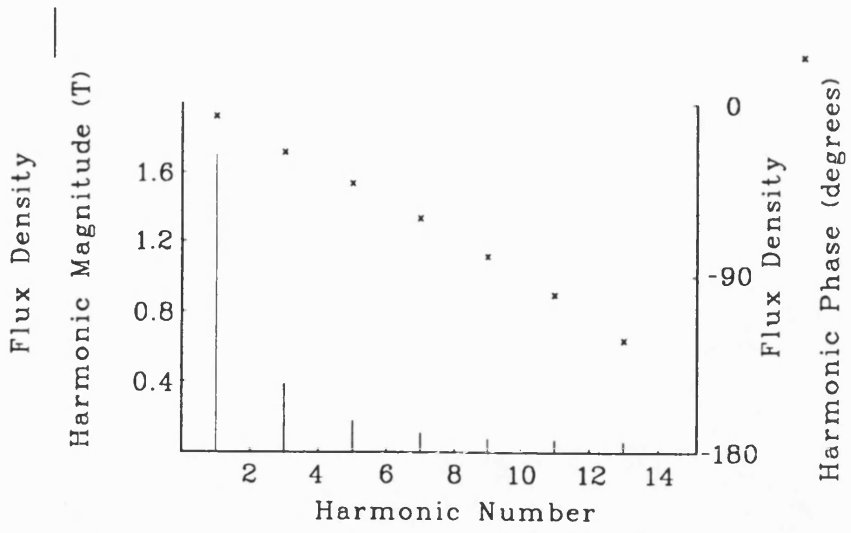

Figure 4.7: Fourier Transform of Flux Density for Flat–Bottom Rail Material

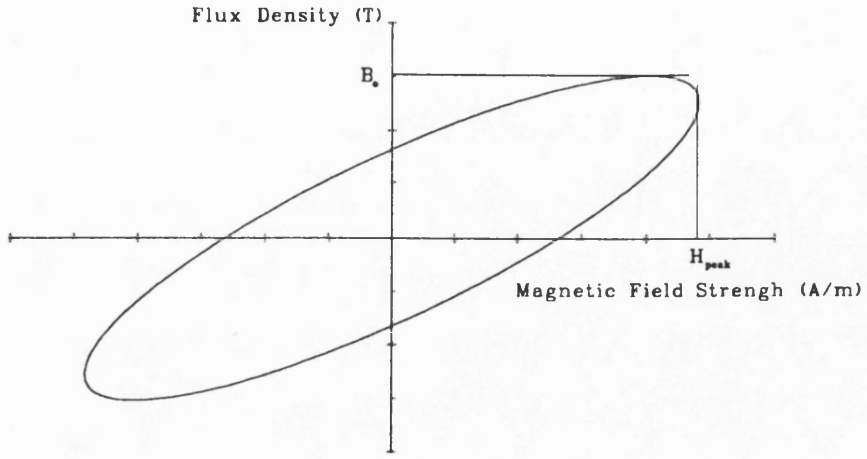

Figure 4.8: Relationship between Magnetic Field Strength and Fundamental Flux Density

Figure 4.8. This illustrates both the magnitude and phase relationships of the magnetic field strength and fundamental flux density waveform. Hysteresis loss is represented by the area of the ellipse (i.e. $\int BdH$) but will differ from the measured value due to the elimination of flux density harmonics. An example is given in Figure 4.9, which illustrates the variation with magnetic field strength.

- *Method 3 - Permeability from the B–H loop area (μ_{area}).*

  In this approach, the area of the hysteresis loop is equated to the area of an ellipse. The magnitude of losses due to hysteresis are represented completely by the

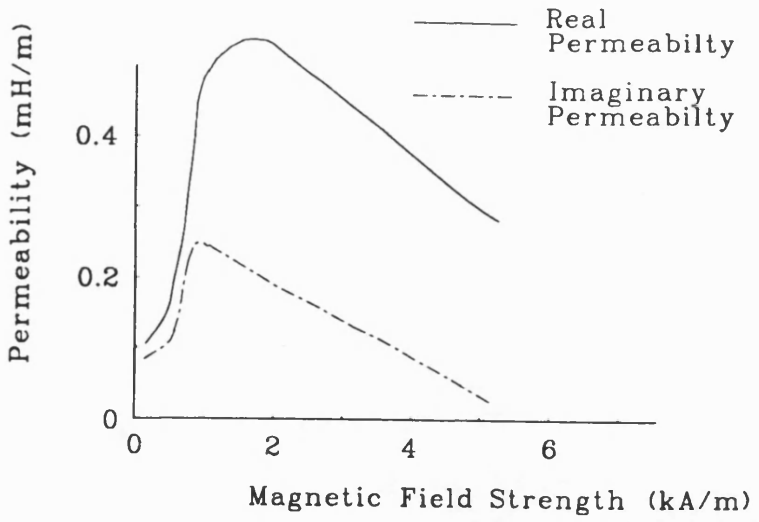

Figure 4.9: Complex Permeability – the B_o Model

ellipse area, including the non–linear (harmonic) losses. The form of the $B--H$ relationship is different since the harmonics of the flux density are eliminated and replaced by increasing the magnitude of fundamental. To obtain a unique orientation and unique major and minor semi–axes, the measured coercive force and remnant flux density are used in the elliptical model. This is illustrated in Figure 4.10. An example of this permeability, with variation in magnetic field strength, is given in Figure 4.11.

- *Method 4 – Incremental Permeability (μ_{inc}).*

  This method is used when the signal producing the magnetic field strength takes the form of a large d.c. offset with an small a.c. signal superimposed. The gradient of the $(B - H)$ loop (i.e. $\Delta B/\Delta H$) is evaluated at the operating (offset) point and negligible hysteresis loss is assumed. This is easily evaluated graphically. The method is illustrated in Figure 4.12. Incremental permeability has been evaluated for the materials of interest and an example is given in Figure 4.13, with variation in magnetic field strength.

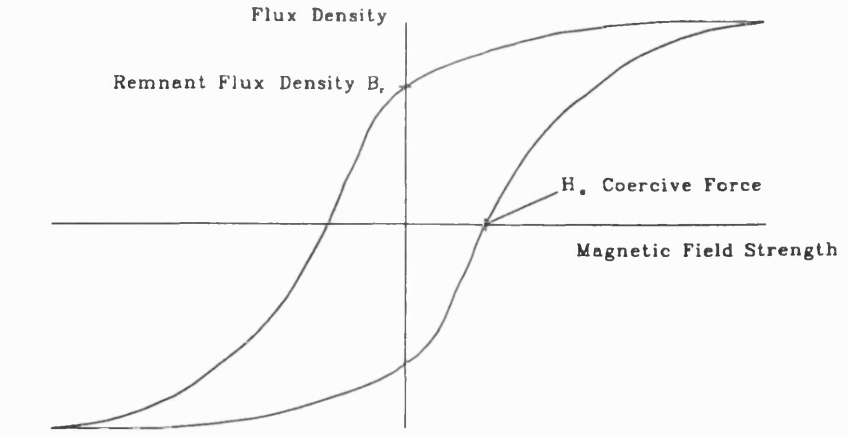

a) measured loop

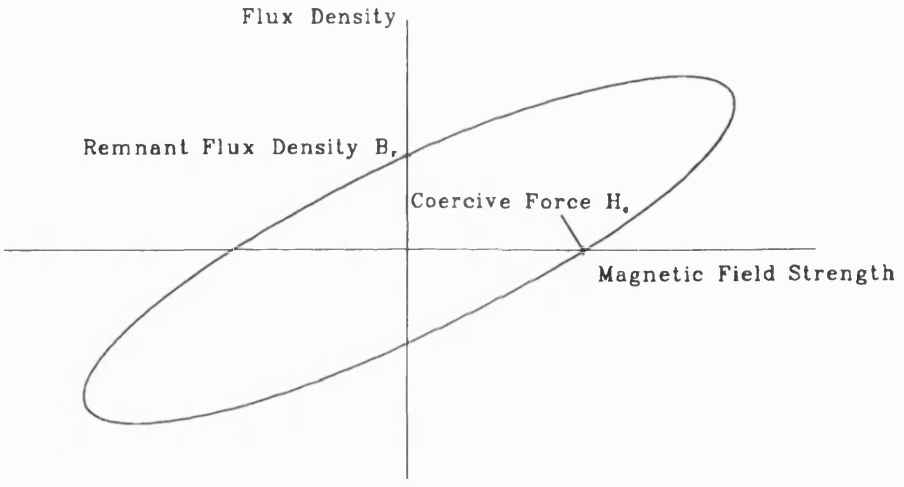

(b) elliptical model

Figure 4.10: Comparison of Measured Hysteresis Loop and Elliptical Model

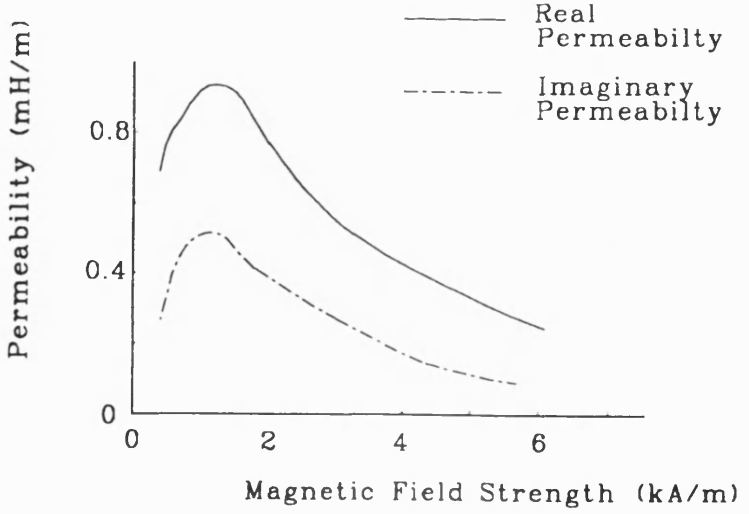

Figure 4.11: Complex Permeability – the Loop Area Model

- *Method 5 - Effective Permeability by F.D.M. Model*

In this approach, the magnetic field strength in the rail material is considered. In order that the effect of rail shape is eliminated, a semi–infinite slab model of the material is used. From Maxwell's equations, the magnetic field strength within the material is given by

$$\frac{\partial^2 H}{\partial y^2} = \sigma \frac{dB}{dH} \frac{\partial H}{\partial t} \tag{4.5}$$

It should be noted that in cases where the material is magnetic and non–linear, $\frac{dB}{dH}$ (i.e. permeability) will vary with the magnitude of H. Due to this non–linear variation, an analytical solution is not possible. Hence a finite difference technique has been used.

The Du Fort–Frankel Scheme [171] was chosen as it is an explicit equation which does not have stability restrictions. The basic difference equation is

$$H_{i,k+1} = r_{DF} H_{i+1,k} + (1 - 2r_{DF}) H_{i,k} + r_{DF} H_{i-1,k} \tag{4.6}$$

where

$r_{DF} = \frac{p}{\sigma \mu h_s^2}$

p is the time step length

h_s is the spacial step length

By substituting the average of the previous and next nodal values for the present nodal value into Equation 4.6, that is

$$H_{i,k} = \frac{1}{2}(H_{i,k+1} + H_{i,k-1}) \tag{4.7}$$

an explicit difference equation is formed.

$$H_{i,k+1} = H_{i,k-1} + \frac{2r_{DF}}{2r_{DF} + 1}(H_{i+1,k} - 2H_{i,k-1} + H_{i-1,k}) \tag{4.8}$$

By varying $H_{0,k}$ as a sine wave (i.e. the surface magnetic field strength) and observing the values of nodes into the material, then the distribution of the magnetic

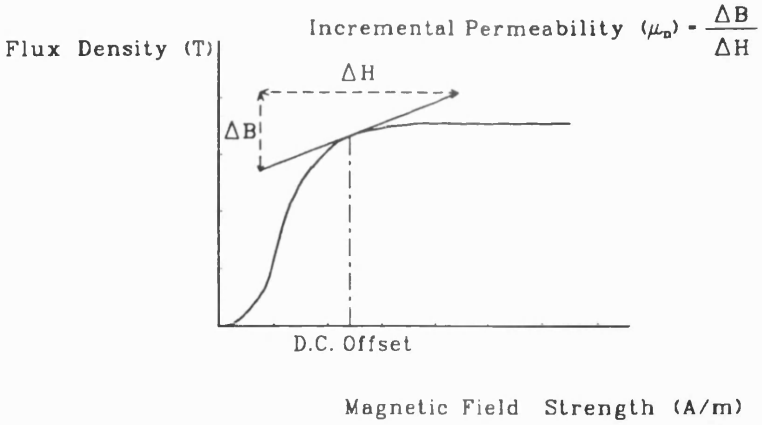

Figure 4.12: Evaluation of Incremental Permeability

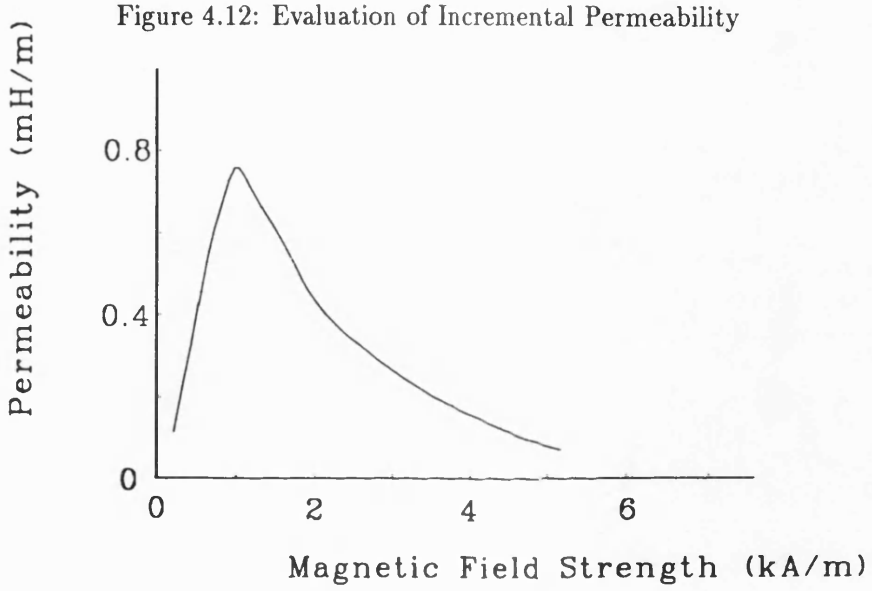

Figure 4.13: Incremental Permeability vs. Magnetic Field Strength

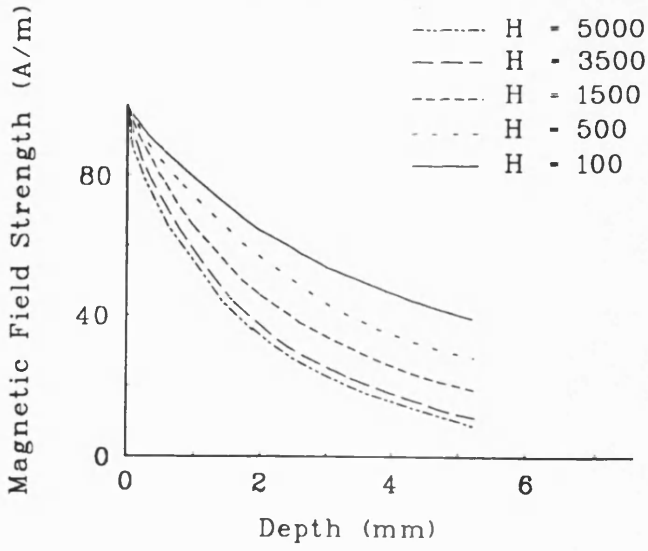

Figure 4.14: Finite Difference Model of Magnetic Field Strength Variation

field strength can be determined. The solution undergoes an initial transient period since the method is a time simulation (of discrete time step form). However, of most interest is the steady–state solution which follows this transient output. An example of the variation in time and space is given in Figure 4.14.

Examples of the steady–state results, for various Magnetic Field Strengths, are shown in Figure 4.15. It can be seen that although the decay of the magnetic field strength is not exponential, the shape is similar.

From this, it is possible to determine an effective skin depth directly from the resulting magnetic field distribution in the material. This may be expressed as

$$|\delta_{eff}| = \sqrt{\frac{2}{\omega\sigma\mu_{eff}}} \tag{4.9}$$

Hence the magnitude of an effective permeability can be obtained. The phase angle of the value of permeability is given by the angle determined in *Method 2* above. The results are illustrated in Figure 4.16.

4.1.3 Conductivity of Rail Material

The conductivity of a material is uniquely defined and will not be discussed here. The evaluation of the conductivity of the materials under investigation is described. The conductivity of filament samples where measured using the circuit shown in Figure 4.17. Temperature was also monitored so that a relationship between conductivity (σ) and temperature could be obtained. The measurements were carried out for each sample and repeated to obtain a suitable distribution of data.

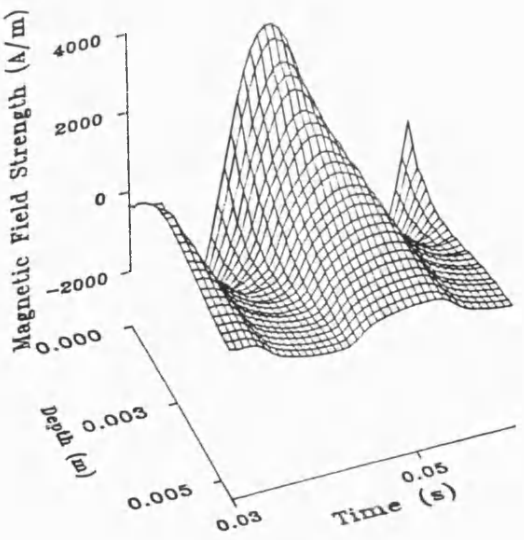

Figure 4.15: One–Dimensional Magnetic Field Distribution for Flat–Bottom Rail

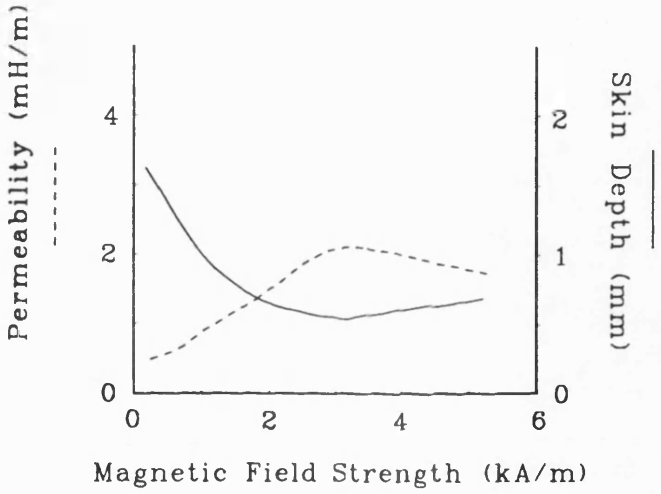

Figure 4.16: Effective Skin Depth and Permeability

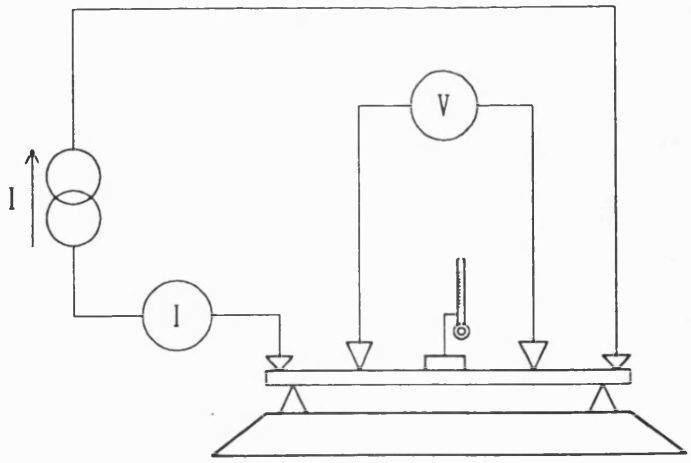

Figure 4.17: Conductivity Test Circuit

Table 4.2: Resistivity Results for Materials at 293 K

Sample	Resistivity ($\mu\Omega m$)	Temp. Coeff (K^{-1})
Mild Steel	0.159	0.004
Flat–Bottom Rail	0.225	0.0034
Bull–Head Rail	0.202	0.0031
Conductor Rail	0.113	0.008

Results.

The results are given in Table 4.2. They are of the form given by Equation 4.10 [105]

$$\rho = \rho_{20}(1 + \alpha T) \tag{4.10}$$

where

α is the temperature coefficient of resistivity (K^{-1}), assumed linear over the temperature range of interest

ρ is the material resistivity (Ωm^{-1})

T is the temperature (K)

4.1.4 Discussion on Rail Material Properties

It was necessary to determine the material properties experimentally. The design and construction of the experimental apparatus needed to determine the conductivity of the rail material proved to be straightforward. The temperature of the material was found to be the most critical variable. Care had to be taken to make measurements at specific temperatures. Samples of rail material were tested in each of the three orthogonal directions of the rail. No variation, with orientation, was found, within an acceptable

experimental error. The conduction process predicts that conductivity is constant with magnitude of current.

The experimental arrangements for determining the magnetic properties of the rail material were adapted from standard techniques [169]. Again the material was tested in the three orthogonal directions and again, no variation was found, to within experimental accuracy. The rail material was taken from "used" rails so that any effects due to mechanical working could be included. The experimental apparatus provided both an initial magnetisation curve and cyclic B–H loop data. Hence it was possible to use the data for d.c. excitation (with a.c. super–imposed) and for a.c. excitation.

Since the magnetic characteristics of the rails are extremely non–linear with magnetic field magnitude and hysteresis, it was decided that an analytical representation would be useful when describing the internal impedance of the rail. Although much work relating to the description of magnetic material characteristics has been published and some of the more relevant reports have been referenced in Chapter 2, the application to rail track has not been examined thoroughly or successfully. Hence, a number of magnetic material models have been developed to describe the phenomenon when applied to current carrying steel rails.

The incremental permeability model is directly applicable to the case of a rail excited by a large d.c. signal with a small a.c. signal superimposed. The effect of hysteresis, in this case, is negligible compared to the ohmic loss. The use of this model proved to give good agreement between experimental results and analytical methods for internal rail impedance evaluation when the rail is excited by this composite signal. This is seen later in Figures 5.2 to 5.5.

For the case of the rail excited by a large a.c. signal, three *direct* models for permeability

have been developed. They are termed *direct* since they have been evaluated directly from the B–H characteristic results. These have been termed :–

- *Normal Permeability* evaluated from the initial magnetization curve, with no allowance for hysteresis. The value is real, so there is no allowance for phase shift. Hence this method is limited to conditions where hysteresis effects are small. A comparison between experimental results and analytical modelling, using this method, is given later in Figures 5.10 and 5.11.

- *Permeability from Fundamental Flux Density* is based on the waveforms of the magnetic field strength and flux density. Assuming a sinusoidal magnetic field strength waveform, the Fourier transform of the resulting flux density waveform was evaluated. Taking the magnitude and phase of the fundamental of the flux density waveform, a value of complex permeability was calculated. This represents an elliptical B–H loop and so incorporates an allowance for hysteresis. The angle information proved to give good orientation agreement between the elliptical model and the measured B–H loop. However the magnitude of the permeability model only provided limited agreement with experimental evaluation of internal rail impedance, as can be seen later in Figures 5.10 and 5.11.

- *Permeability from B–H loop area* is a method which makes a complete allowance for the hysteresis loss by equating the true B–H loop area to that of the area of an ellipse. Both curves have the same coercive force and remnant flux values. Again only limited agreement was achieved between experimental results and analytical methods, using this model, as shown later in Figures 5.10 and 5.11.

A more sophisticated model was sought to provide more widespread agreement between experimental and analytical values.

- *Effective Permeability* is a model based on the phase shift information, adopted from the fundamental flux density method with the magnitude of the permeability model being determined from a F.D.M. model. To summarise the technique, the relationship between the flux density and magnetic field strength is modelled by finite differences in a one dimensional time varying model. From this an effective skin depth can be determined and hence an effective permeability magnitude. The results are shown later in Figures 5.6 to 5.9 with good agreement over a wide range of frequency and current.

4.2 Soil/Ballast Properties

The material properties of the track bed, i.e. sleepers and ballast material together with the soil composition, have a major influence on the admittance between rails of a track. The conductance component of the admittance is dominated by the conductivity of the track bed elements. The capacitance component of the admittance is determined by both the track bed permittivity and track geometry.

4.2.1 Ground Conductivity as a Function of Depth and Frequency

As outlined in Chapter 2, previous investigations into soil conductivity have made the assumption that the ground is horizontally stratified. This implies that the only variation in conductivity, within a limited area, is with depth. If the process of formation and the structure of ground at or near the surface of the earth is considered, this assumption would appear to be reasonable for short sections of track. Thus it has been adopted in this investigation.

An earlier investigation [172] made the assumption that the ground stratification could

be accounted for by using a two layer approximation. This was achieved by modelling the soil conductivity as two distinct values in two distinct layers[2] as shown in Figure 4.18. The method used to evaluate these conductivity values and the depth at which the interface between the two layers occurred was a four probe measurement technique. It follows the same method as outlined by earlier work [149, 150]. The probes were arranged in a Wenner array, also shown in Figure 4.18. By measuring the potential between the inner electrodes, due to current passing from one outer electrode to the other, an estimation of the conductivity of the two layers of earth and the interface depth can be obtained. The method follows that described for prospecting [151] and has only been reported for the d.c. excitation case.

It was felt that this two–layer model may not provide an accurate basis for determination of the conductance between rails, since it was restricted to two distinct values of conductivity. In addition, the method was restricted to d.c. excitation and thus would not provide frequency variations of conductivity. Hence a more rigorous and complete approach has been developed. The technique is based on work presented by Langer [144, 145] and Schliter [146], as outlined in Chapter 2. A summary of the theoretical arguments is given in a text by Sunde [152]. However, no experimental results were reported. Here the technique has been extended to provide frequency variation of conductivity, in addition to variation with depth. Practical details are given together with measured results and the process by which these results may be interpreted to give a complete function of conductivity.

[2]It should be noted that the two layer model is not intended to simulate the true conductivity depth profile, but only to approximate the current paths from the surface observations.

4.2.2 A Solution in Terms of the Electric Field Equation

Consider an isolated point current probe, at the surface of the earth, as shown in Figure 4.19. In general

$$\nabla \mathbf{J} = \nabla(\sigma \mathbf{E}) = 0 \tag{4.11}$$

and

$$\nabla(\sigma \mathbf{E}) = \sigma \nabla \mathbf{E} + \mathbf{E} \nabla \sigma = -\sigma \nabla^2 V - \nabla V . \nabla \sigma \tag{4.12}$$

Hence

$$\nabla^2 V + \frac{1}{\sigma} \nabla V . \nabla \sigma = 0 \tag{4.13}$$

Assuming σ is a function of depth (z) only, in cylindrical co–ordinates

$$\frac{\partial^2 V}{\partial r^2} + \frac{1}{r}\frac{\partial V}{\partial r} + \frac{\partial^2 V}{\partial z^2} + \frac{\partial V}{\partial z}\sigma'(z)\sigma(z) = 0 \tag{4.14}$$

where $\sigma' = \frac{d\sigma}{dz}$.

Following Slichter's approach and solving by separation of variables, where $V(r, z) = u(r)v(z)$, yields

$$\frac{d^2 u}{dr^2} + \frac{1}{r}\frac{du}{dr} + \lambda^2 u = 0 \tag{4.15}$$

$$\frac{d^2 v}{dz^2} + \frac{\sigma'}{\sigma}\frac{dv}{dz} - \lambda^2 v = 0 \tag{4.16}$$

Equation 4.15 is the Bessel Equation and Equation 4.16 is the Strum–Liouville Equation. While a solution to Equation 4.15 is given below, the solution to Equation 4.16 depends on conductivity and so is used, with the experimental results, to obtain the conductivity function. The solution of Equation 4.15 is

$$u(\lambda, r) = A_u J_0(\lambda r) + B_u Y_0(\lambda r) \tag{4.17}$$

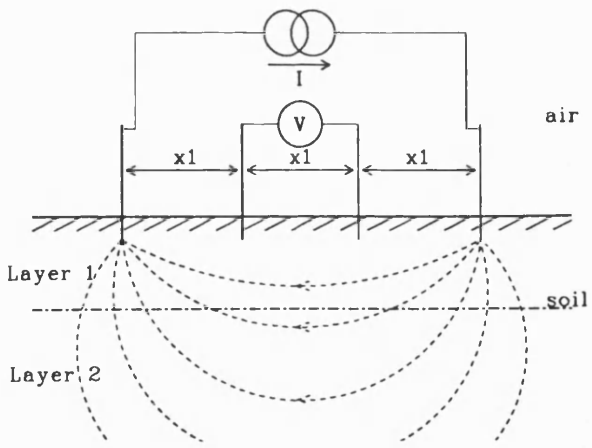

Figure 4.18: The Two–Layer Model with Wenner Array

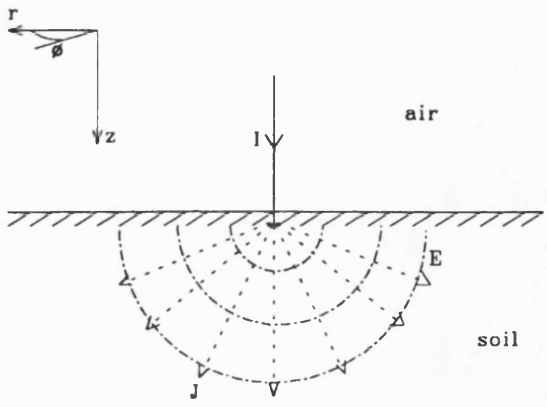

Figure 4.19: Isolated Current Probe at the Surface of the Earth

where

J_0 and Y_0 are Bessel Functions of the first and second kind respectively and of order zero

A_u and B_u are constants

When $r = 0$, $Y_0 \rightarrow \infty$, thus $B_u = 0$. This provides a general solution to Equation 4.14, which is dependent on the variation of potential with depth (due to the variation of

conductivity with depth), of the form

$$V = \int_0^\infty g(\lambda) J_0(\lambda r) v(\lambda, z) d\lambda \tag{4.18}$$

where $g(\lambda)$ is an arbitrary function of λ, chosen to suit the boundary conditions.

At the surface, since the current in the z direction is zero (except at the probe), the electric field must be zero. Hence $\frac{dV}{dz}\Big|_{z=0} = 0$. This gives

$$\frac{dV}{dz} = \int_0^\infty g(\lambda) J_0(\lambda r) v'(\lambda, z) d\lambda \Big|_{z=0} = 0 \tag{4.19}$$

where $v'(\lambda, z) = \frac{dv}{dz}$.

Slitcher shows that Equation 4.19 is satisfied by $g(\lambda) = \frac{A\lambda}{v'(\lambda,0)}$ and provides the potential solution

$$V = A \int_0^\infty J_0(\lambda r) k(\lambda, z) d\lambda \tag{4.20}$$

where

$$k(\lambda, z) = -\frac{\lambda v(\lambda, z)}{v'(\lambda, 0)} \tag{4.21}$$

and A is a constant.

4.2.3 Determining the Potential Equation Constant

Sunde provides a method of determining the constant A of Equation 4.20, which is outlined here. Since Equation 4.20 is a general solution, it must satisfy all cases, where the initial assumptions are valid. One such simple case is where $\sigma(z)$ is constant i.e. the earth has uniform conductivity. Equation 4.16 then has a solution

$$v = A_1 e^{\lambda z} + A_2 e^{-\lambda z} \tag{4.22}$$

and with $v \to 0$ as $z \to \infty$, $A_1 = 0$. This gives $k(\lambda, z) = e^{-\lambda z}$ and

$$V = A \int_0^\infty J_0(\lambda r) e^{-\lambda z} d\lambda = \frac{A}{\sqrt{r^2 + z^2}} \tag{4.23}$$

Now consider the physical significance of a uniform earth. If current I flows into the ground through a point electrode at the surface (see Figure 4.17), the current density will be radial with hemispherical equipotential surfaces. Hence the current density is $J = \frac{I}{2\pi s^2}$, where s is the radial distance from the point probe to the hemispherical surface. Since $E = \frac{J}{\sigma} = \frac{I}{2\pi\sigma s^2}$ then

$$V = -\int Eds = -\frac{I}{2\pi\sigma s^2} = -\frac{I}{2\pi\sigma\sqrt{r^2+z^2}} \tag{4.24}$$

which shows that

$$A = -\frac{I}{2\pi\sigma} \tag{4.25}$$

Equation 4.20 becomes

$$V = -\frac{I}{2\pi\sigma(0)}\int_0^\infty J_0(\lambda r)k(\lambda,z)d\lambda \tag{4.26}$$

4.2.4 An Expression for the Ground Conductivity

Both Langer and Slitcher briefly describe a method for the determination of the conductivity function. What follows is a full explanation of this approach.

The Kernel Function

Equation 4.26 can be written in terms of the mutual impedance

$$Q(r) = -\frac{V}{I} = \frac{1}{2\pi\sigma(0)}\int J_0(\lambda r)k(\lambda)d\lambda \tag{4.27}$$

where

$k(\lambda) = k(\lambda, 0)$

$\sigma(0)$ is the conductivity at the surface of the earth

The definition of the mutual impedance, $Q(r)$, is the ratio of the potential, V, at a distance r from the probe and the current in the probe. This is the current injected into the ground. The negative sign is due to the voltage being absolute (i.e. measured from $-\infty$).

Using the Inverse Hankel transform, this can be re–arranged to give

$$k(\lambda) = 2\pi\sigma(0)\lambda \int_0^\infty J_0(\lambda r)Q(r)rdr \tag{4.28}$$

$k(\lambda)$, the so called *kernel function*, can now be evaluated from experimental data. The resulting function can be used to determine the conductivity function, $\sigma(z)$.

4.2.5 Determining Ground Conductivity from the Kernel Function

It is now necessary to show how knowledge of the kernel function $k(\lambda)$ will provide a solution for ground conductivity, $\sigma(z)$. By substituting

$$\phi(\lambda, z) = -\frac{v(\lambda, z)}{v'(\lambda, z)} \tag{4.29}$$

then the Equation 4.16 becomes

$$\frac{\sigma'}{\sigma} = \frac{\phi' + 1}{\phi} - \lambda^2\phi \tag{4.30}$$

As $\lambda \to \infty$, Equation 4.16 can be approximated by

$$\frac{d^2v}{dz^2} - \lambda^2 v = 0 \tag{4.31}$$

and under these conditions $v \to B_1e^{\lambda z} + B_2e^{-\lambda z}$. However $v \to 0$ as $z \to \infty$ and so $B_1 = 0$. Hence $v \to B_2e^{-\lambda z}$.

From this result and Equation 4.29, $\phi \to \frac{1}{\lambda}$ as $\lambda \to \infty$. By Taylor's series

$$\phi = \frac{1}{\lambda + h} = \frac{1}{\lambda} + \frac{\alpha_1(z)}{\lambda^2} + \frac{\alpha_2(z)}{\lambda^3} + \ldots \tag{4.32}$$

where h is a small fraction of λ.

From Equation 4.21

$$k(\lambda) = -\lambda \frac{v}{v'}\Big|_{z=0} = \lambda\phi(\lambda,0)$$

$$= 1 + \frac{a_1}{\lambda} + \frac{a_2}{\lambda^2} + \frac{a_3}{\lambda^3} + \ldots \tag{4.33}$$

where

$a_n = \alpha_n(0)$

$\lambda \to \infty$

Substituting into Equation 4.30 and after some work

$$\frac{\sigma'}{\sigma} = -2\alpha_1 + \frac{1}{\lambda}\left\{\alpha' - 2\alpha_2 + {\alpha_1}^2\right\} + \frac{1}{\lambda^2}\left\{{\alpha_1}^3 + 2\alpha_1\alpha_2 - 2\alpha_3 - \alpha_1\alpha_1'\right\} + \ldots \tag{4.34}$$

For the ground conductivity not to be a function of λ, all but the first term must be zero. So

$$\alpha_1' = 2\alpha_2 - {\alpha_1}^2$$

$$\alpha_1'' = -2{\alpha_1}^3 + 4\alpha_3 - 4\alpha_1\alpha_2$$

$$\alpha_1''' = 2\left[8{\alpha_1}^2\alpha_2 - 3{\alpha_1}^4 - 4\alpha_1\alpha_3 - 2{\alpha_2}^2 + 4\alpha_4\right]$$

etc.

From Equation 4.34

$$\frac{\sigma'}{\sigma} = -2\alpha_1 \tag{4.35}$$

or

$$\frac{d\sigma}{dz} + 2\alpha_1\sigma = 0 \tag{4.36}$$

This has the solution

$$\sigma = Ce^{-2\int_0^z \alpha_1 dz} \tag{4.37}$$

and when $z = 0$, $\sigma = \sigma(0)$, giving $C = \sigma(0)$. Using MacLauren's series

$$\begin{aligned} \alpha_1(z) &= \alpha_1(0) + z\alpha_1'(0) + \tfrac{z^2}{2!}\alpha_2'(0) + \ldots \\ &= a_1 + (2a_2 - a_1^2)z + (-a_1^3 - 2a_1a_2 + 2a_3)z^2 + \ldots \end{aligned} \tag{4.38}$$

The final solution of the ground conductivity is then

$$\sigma(z) = \sigma(0)e^{-2\int_0^z \alpha_1 dz} \tag{4.39}$$

where

α_1 is determined from the coefficients of the series approximation for $k(\lambda)$.

4.2.6 Evaluation of Ground Conductivity from Experimental Results

To evaluate the Ground Conductivity as a function of depth, $\sigma(z)$, the kernel function has to be evaluated. This is achieved by using measured values of mutual impedance $Q(r)$ in Equation 4.27. Provided that the in–phase component of the signal is considered, $Q(r)$ reduces to a mutual *resistance.*

The experimental methods for obtaining practical values of $Q(r)$, which have been considered, are generally based on a four–probe technique.

Method of Analysis

The approach is somewhat novel as it is based on taking measurements which yield results directly applicable to Equation 4.27 and 4.28. Only a potential difference can

be measured so two sets of probe pairs must be used. This also allows for a practical current path. To keep the effective isolation between the current probes, the distance between the probe pairs, R_p, must satisfy

$$R_p \gg r_p \tag{4.40}$$

This is achieved as shown in Figure 4.20. In the diagram

$$V = (V_3(1) - V_3(2)) - (V_4(1) - V_4(2)) \tag{4.41}$$

where $V_n(m)$ is a potential on probe n due to current in probe m

However $V_3(1) \gg V_3(2)$ and $V_4(2) \gg V_4(1)$, hence

$$V \approx V_3(1) - V_4(2) = 2V_3(1) \tag{4.42}$$

Thus

$$2V_3(1) = -\frac{I}{2\pi\sigma(0)} \int_0^\infty J_0(\lambda r) k(\lambda) d\lambda \tag{4.43}$$

and so

$$Q(r) = \frac{1}{4\pi\sigma(0)} \int_0^\infty J_0(\lambda r) k(\lambda) d\lambda \tag{4.44}$$

Hence

$$k(\lambda) = 4\pi\sigma(0)\lambda \int_0^\infty J_0(\lambda r) Q(r) r dr \tag{4.45}$$

To determine an analytical function for $k(\lambda)$, the experimental data, $Q(r)$, must be approximated by an analytical function. In addition, this approximation must be of a form that allows Equation 4.45 to be evaluated. By using *least square error* curve fitting, the expression

$$Q_e(r) = a r^b e^{cr^2} \tag{4.46}$$

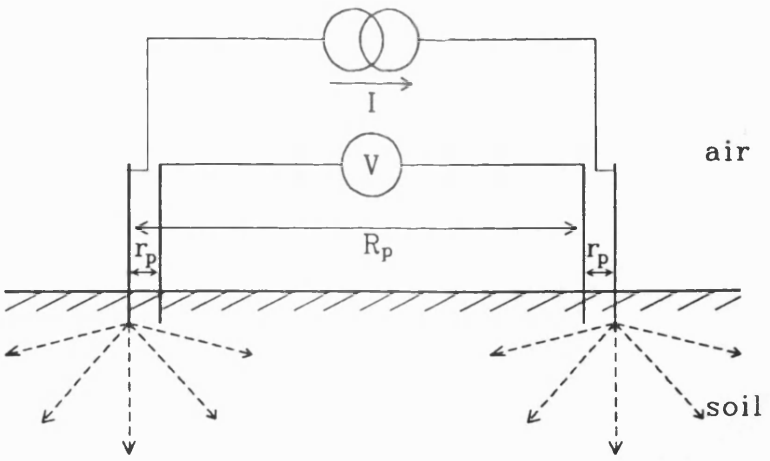

Figure 4.20: Practical Isolation between Probe Pairs

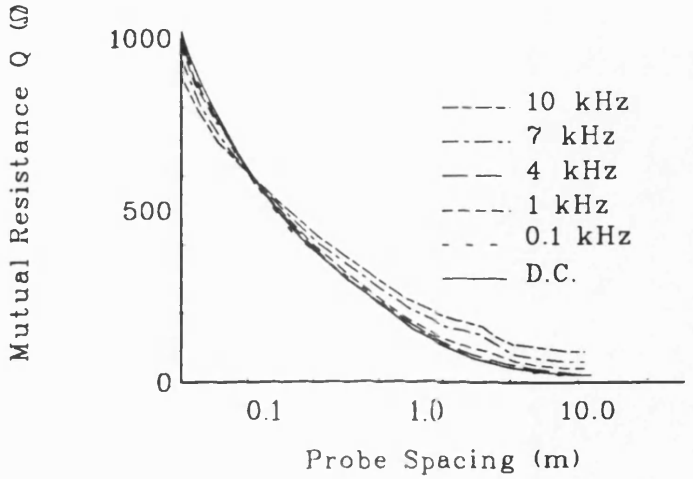

Figure 4.21: Experimental Results of Mutual Resistance with Frequency

gives a good approximation for $Q(r)$. The experimental results for Q(r) are shown in Figure 4.21, with a frequency variation, measured on site. The values of the constants to give a minimum error are shown in Table 4.3

It can be shown that [173]

$$\begin{aligned} k(\lambda) &= 4\pi\sigma(0)\int_0^\infty J_0(\lambda r)ar^{b+1}e^{cr^2}dr \\ &= 4\pi\sigma(0)\lambda a\frac{\Gamma\left(\frac{b+2}{2}\right)}{2(-c)^{\frac{b+2}{2}}}{}_1F_1\left(\frac{b+2}{2};1;\frac{\lambda^2}{4c}\right) \end{aligned} \tag{4.47}$$

where ${}_1F_1(x;y;z)$ is the degenerate hypergeometric function.

Table 4.3: Coefficients of Analytical Mutual Resistance Function

Frequency (kHz)	a	b	c
0.0	100	-0.753	0.006
0.1	95	-0.769	0.005
1.0	97	-0.755	0.002
4.0	126	-0.639	-0.003
7.0	160	-0.538	-0.005
10.0	185	-0.478	-0.005

Alternatively

$$k(\lambda) = \frac{4\pi\sigma(0)a\Gamma\left(\frac{b+2}{2}\right)e^{\frac{\lambda^2}{8c}}}{(-c)^{\frac{b+1}{2}}} M_{\frac{b+1}{2},0}\left(-\frac{\lambda^2}{4cc}\right) \tag{4.48}$$

where $M_{p,q}(z)$ is Whittaker's Function.

Using suitable (relatively large) values of λ in Equation 4.47 and evaluating the coefficients of Equation 4.33, the expression for ground conductivity as a function of depth is evaluated, by application of Equation 4.39. The function, with depth and frequency variation, is illustrated in Figure 4.22, together with the two layer model obtained in previous work. The agreement between methods at extreme points is good.

The agreement between the two layer model and the continuous model provides confidence in the results obtained. These results may now be used to obtain inter–rail and inter–track admittances, as described in Chapter 5.

4.2.7 Effective Permittivity of the Ground

A number of experimental techniques have been considered to directly determine the permittivity of the ground in the vicinity of track–bed. However, it was found that,

in the frequency range required for this study, the impedance (or admittance) that could be measured to provide a value of permittivity is dominated by the real, or resistive, part. It has been reported [174] that direct measurements of capacitance, for a known geometry, have been made at much higher frequencies (i.e. > 1 GHz) together with *in situ* measurements at similar frequencies. However, even at these frequencies, the variation of permittivity with depth is not determined. At these frequencies, it is possible to measure the effect of e.m. wave penetration, rather than provide direct excitation.

Under comparable circumstances, Mayhan and Bailey [141] have carried out an indirect experimental evaluation of an *effective permittivity.* Their experimental data are intended for the implementation of loop detectors for automobile transportation and therefore apply to road surfaces. They adopt a simple analytical model to explain the experimental results and hence deduce a permittivity which is constant over the whole ground substructure. Although this cannot represent the true variation of permittivity through the ground, because the main determinator of permittivity is moisture content, it does provide a value of permittivity which returns the correct value of susceptance between two conductors lying on the surface of the earth. This is the case since the conductors themselves have been used as the measurement probes.

In order to improve upon the method used by Mayhan and Bailey, it was decided to numerically model the susceptance between the running rails of a track and track bed structure. This model provides a solution that is a closer approximation to the practical structure. The dimensions of the track and bed are given in Appendix G. The numerical method chosen is a two–dimensional F.E.M. technique. Although F.E.M. is often presented as an electromagnetic analysis method, it is equally suited to electrostatic modelling. The general electromagnetic theory of F.E.M. is outlined in Appendix E,

together with the electrostatic duality required to model electrostatic fields with the packages used.

In addition to this modelling method, the susceptance between the (open circuit) running rails of rail–track has been measured. By comparing the measured results with those computed from the F.E.M. analysis, it is possible to arrive at a value of *effective permittivity*[3]. However, unlike the conductivity evaluation, it has not proved to be possible to provide an independent method of evaluation.

Mayhan and Bailey evaluate effective permittivity at a higher range of frequencies than are required for this study. It is worth noting that the values of effective permittivity obtained here compare favourable with the higher frequency values in that the two sets of data form one smooth curve. These results are illustrated in Figure 4.23. A typical F.E.M. model is shown in Figure 4.24, although the values of susceptance are fully reported in Chapter 5. It can be seen that the F.E.M. technique makes efficient use of any model symmetry.

4.2.8 Discussion on Soil Material Properties

The method developed to evaluate the ground conductivity is based on geological exploration techniques and may be applied to any site. The new implementation allows the technique to be applied to give a continuous model of conductivity with depth of soil instead of the standard one, two or, in exceptional cases, three layers of conductivity at discrete layers of soil. In addition, a frequency variation of the continuous model has been developed. This interpretation of the results is a new development which gives a function of conductivity with signal frequency as well as depth below the track. This

[3]This requires repeated iterations of the numerical modelling procedure to arrive at a coincident result.

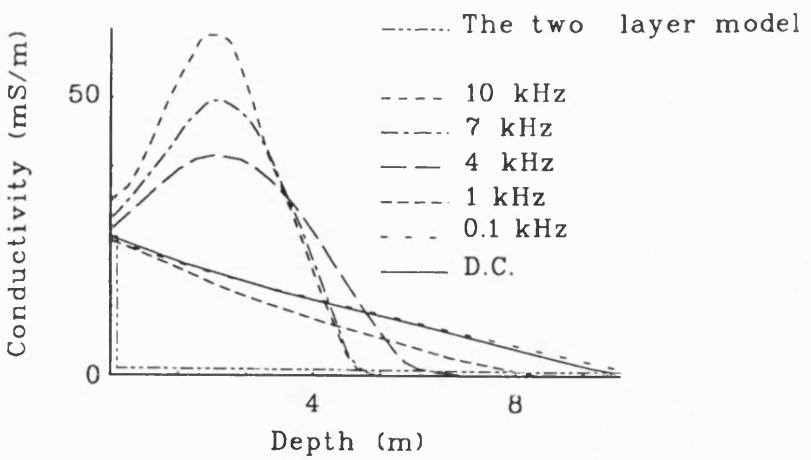

Figure 4.22: Soil Conductivity Model

function is readily applicable to numerical modelling and is used in later chapters as F.E.M. data. It was hoped to develop the technique further to obtain permittivity. However, since the ground conductance dominated all direct ground material measurements, this proved not to be the case, and an effective permittivity value had to be deduced from rail track experimental results. By comparing experimental and F.E.M. results for inter–rail capacitance, it was possible to determine a function of permittivity with frequency although the value was constant with depth. The results of this effective permittivity are consistent with previously published work although the latter was carried out at higher frequencies than are considered here, so the comparison was actually made by interpolation. However, the effective permittivity function reported here, at the frequencies relating to rail applications, have not been previously published.

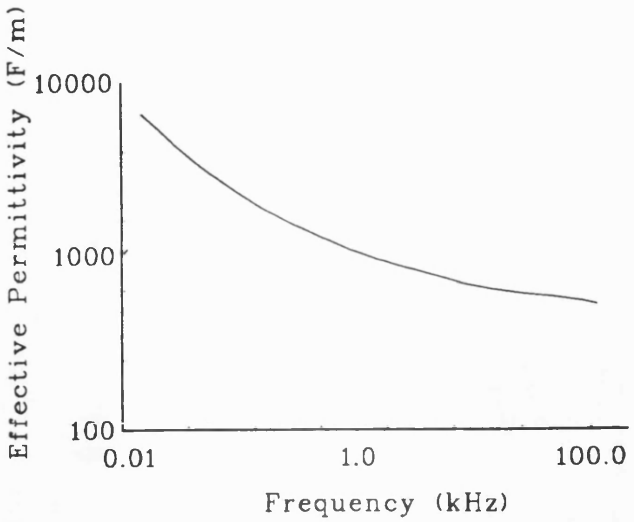

Figure 4.23: Effective Permittivity with Frequency Variation

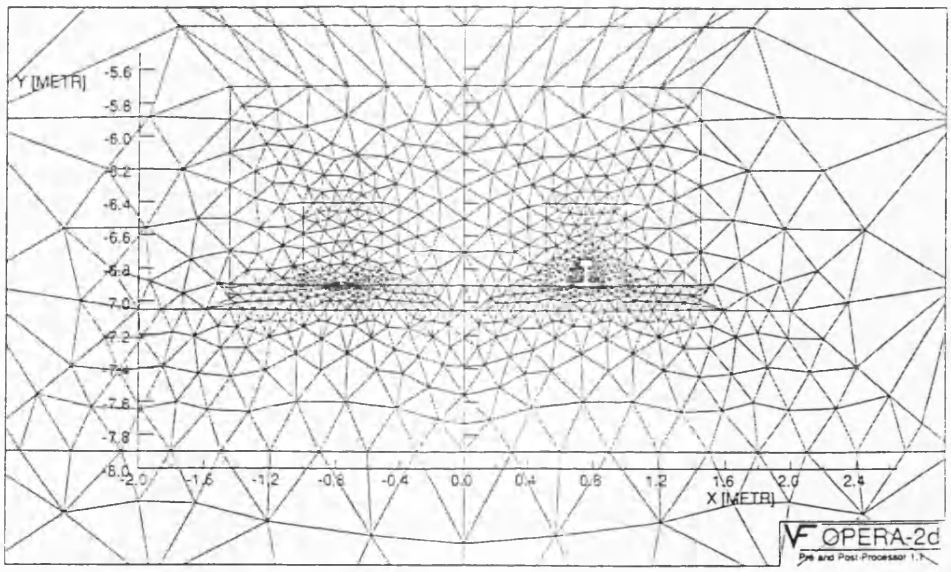

Figure 4.24: Finite Element Model of Track Running Rails

Chapter 5

Determination of Phase Impedance Matrix Elements of third rail Track

The impedance matrix elements introduced in Section 3.2.1 may be determined by experimental methods. These experimental methods provide information, in the form of measured impedances, which are then processed to provide the matrix element impedances. The values obtained by measurement are then compared with approximate analytical methods and numerical models. The tests, results and processed information are fully described in this chapter. The dimensions of the third rail Track is given in Appendix G.

The analytical and numerical techniques utilise the rail material data, i.e. conductivity and permeability. These values have been measured experimentally, modelled and the properties are fully described in Chapter 4. The results for impedance matrix elements are given in in–phase and quadrature component form.

A number of experimental methods are required to fully determine the components of the elements of the matrix. It is necessary to determine both internal and external self impedance of the rail, as defined in Chapter 3, using different techniques. This is because the material properties of the rail dominate the value of internal impedance while the external impedance depends on the track–bed structure. It should be noted that the rail shape influences both internal and external impedance.

5.1 Internal Impedance

A previously reported experimental technique (Holmstrom [55]), provided a method for measuring the difference in impedance between a length of rail and a conductor of standard geometry. This technique has been developed and extended to provide a comprehensive experimental method for the determination of absolute internal impedance for a length of rail. Further, a more comprehensive frequency and current range has been examined than had previously been reported. Alternative experimental techniques [175] [176] have attempted to use a *bifilar* winding method. However the results obtained, using these alternative methods, have not been confirmed by accurate analytical or modelling methods. It will be seen that the results obtained using the new approach and reported here compare favourably with both analytical approximations and numerical models.

The two major modes of excitation of a rail as a conductor are

- *Incremental a.c. excitation.* This is the case of a small signal a.c. excitation, superimposed on a large d.c. traction current. Typically, such a case is to be found in a metro system.
- *Large signal excitation.* This is the case of a large a.c. signal, typical of traction current. Main–line traction return circuits may be represented in this way.

A third case of a small a.c. signal superimposed on a large a.c. signal traction current has not been considered explicitly. This is because the results from the two cases above can be extrapolated to include this situation, provided that measurement and analysis of these cases are in agreement.

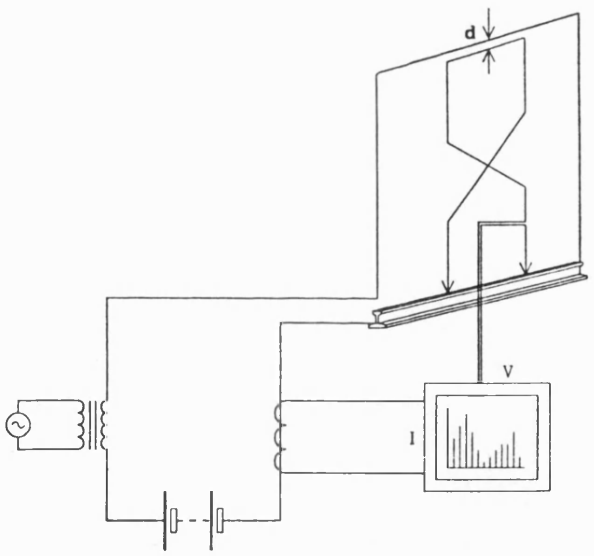

Figure 5.1: Experimental Apparatus and Circuit for Internal Impedance Measurement

5.1.1 Measurement of Rail Internal Impedance

The measurement of rail internal impedance has been made by conducting tests on an isolated length of rail. The apparatus and test circuit are illustrated in Figure 5.1. The same circuit is used for measurement with both *incremental a.c. excitation* and *large signal excitation.* In the former case, the a.c. signal is relatively small ($\sim 5A$ compared to a d.c. traction currents) and in the latter case, the d.c. signal is zero.

Initially, a reference conductor is placed in the test circuit. The reference conductor is a hollow copper conductor[1] having an identical shape to the rail under investigation. This *copper rail* has negligible internal impedance, especially at relatively high frequencies. By energising the circuit at the highest frequency of interest, not only does the copper rail have negligible internal impedance but all loop reactances are relatively large. The circuit is then adjusted (by varying distance "d", shown in Figure 5.1) such that the measurement has zero phase shift. This implies that the overall measurement circuit inductance is negligible. This is achieved because the two large measurement circuit loops have equal and opposite flux linkage. The in-phase quantity measured is the a.c.

[1]This has been termed the *copper rail* for brevity

resistance of the copper rail over the measurement distance of 1m.

The copper rail is then replaced by the length of rail under investigation. The measurement is repeated, with the circuit geometry left unchanged. The impedance measured is that due to the flux (and current) within the rail. The in–phase component of this impedance is the a.c. resistance of the rail between the measurement points. The quadrature component is the absolute internal impedance of the rail. All measurements have been processed using an on–line F.F.T. (Fast Fourier Transform) analyzer to provide good noise immunity and accurate phase and frequency evaluation.

Results of Rail Internal Impedance Measurements

Figures 5.2 to 5.5 show results of the incremental a.c. excitation tests with the impedance expressed as in–phase and quadrature components. Small signal a.c. internal impedance is illustrated with variation in frequency and d.c. offset current. It can be seen in Figures 5.4 and 5.5 that variation in inductance and resistance with d.c. offset is small for the range of measured results[2]. This implies that the variation due to permeability and the effect of hysteresis, for this measurement range, is less significant than that for frequency.

Figures 5.6 to 5.9 illustrate the results of the large signal a.c. excitation tests. Figure 5.6 and 5.7 show inductance and resistance variations with frequency for an excitation of 5 A. For this constant current, the inductance decreases and the resistance increases with frequency, as is to be expected, due to skin effect. In Figures 5.8 and 5.9 both inductance and resistance continually increase with increases in current magnitude, for a signal frequency of 50 Hz. This indicates that complete saturation has not been reached

[2]Modelled and theoretical results are also shown for comparison purposes in subsequent sections.

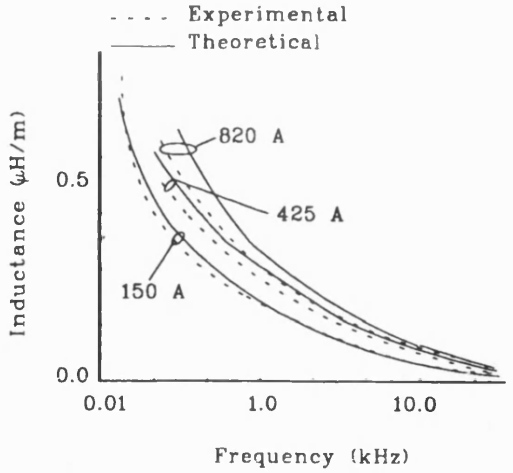

Figure 5.2: Rail Incremental A.C. Internal Inductance with Variation in Frequency

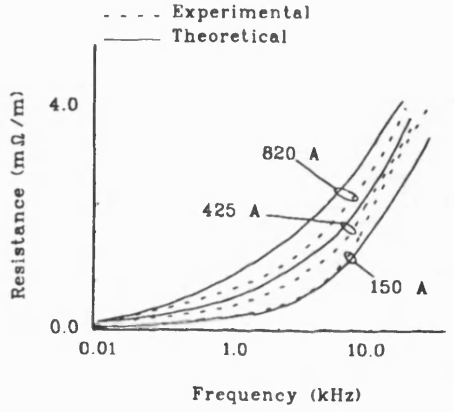

Figure 5.3: Rail Incremental A.C. Resistance with Variation in Frequency

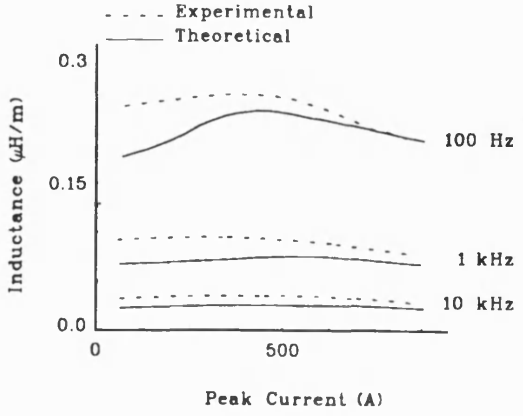

Figure 5.4: Rail Incremental A.C. Internal Inductance with Variation in D.C.

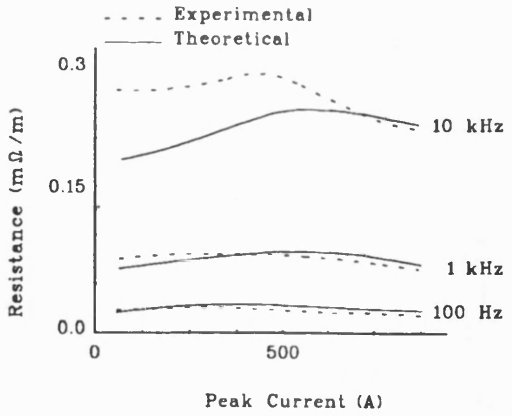

Figure 5.5: Rail Incremental A.C. Internal Resistance with Variation in D.C.

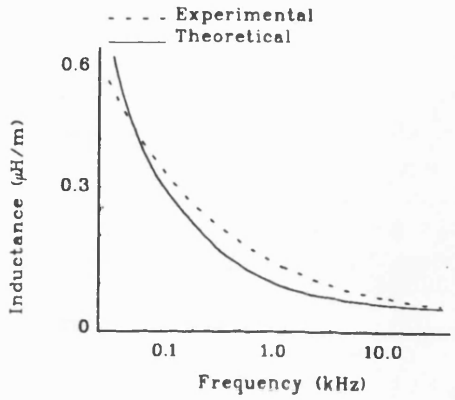

Figure 5.6: Rail Large Signal Internal Inductance with Variation in Frequency

in the measurement range. The tests for the large signal excitation case illustrate that variation with frequency is more significant than permeability, even though they appear with the same weighting in the skin depth equation, Equation 4.9.

5.1.2 Theoretical and Numerical Models of Rail Internal Impedance

An Approximate Theoretical Model

It is possible to develop an analytical expression that will provide an approximate value for the internal impedance of a conductor, if a simple cross-sectional geometry is as-

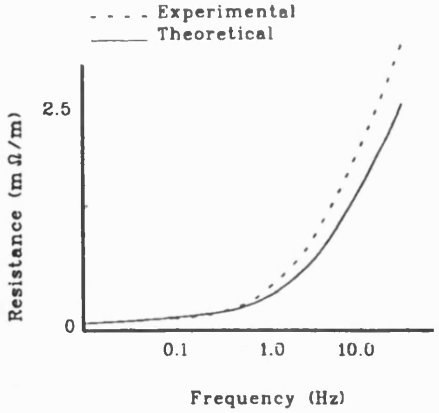

Figure 5.7: Rail Large Signal Internal Resistance with Variation in Frequency

sumed. It is shown in Appendix B that, for a conductor of circular cross–section, the internal impedance is given by

$$\begin{aligned} z_{circ} &= r_{circ} + j\omega l_{circ} \\ &= \frac{\alpha_{circ}}{2\pi a_{rad}\sigma} \frac{I_{oB}(\alpha_{circ} a_{rad})}{I_{1B}(\alpha_{circ} a_{rad})} \end{aligned} \tag{5.1}$$

where

$\alpha^2{}_{circ} = j\omega\sigma\mu^*$

a_{rad} is the conductor radius

I_{nB} is the modified bessel function of the nth order

l_{circ} is the internal inductance of the circular conductor

μ^* is the complex permeability as described in Chapter 4.

σ is the conductivity of the conductor material

It has been shown in Chapter 4 that it is relatively straightforward to obtain a value for the conductivity of a material. The other variables, i.e. radius and permeability, require further consideration.

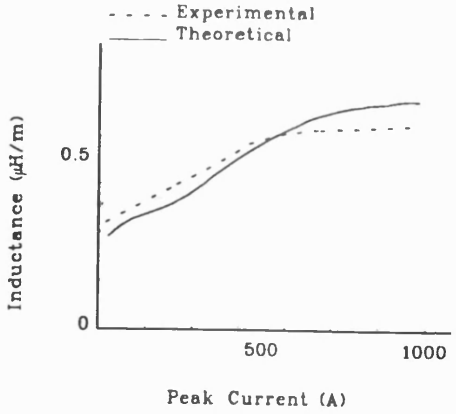

Figure 5.8: Rail Large Signal Internal Inductance with Variation in D.C.

Influence of Shape on Analytical Solution of Rail Internal Impedance

An equivalent radius, a_{eq}, must be determined such that the analytical solution is closely associated with the actual rail under consideration. It is assumed that at most frequencies in this study, the skin–effect is dominant, i.e. ($a_{eq} \gg \delta$) and the current is crowded near the outer surface of the cross–section of the conductor.

- *For resistance*, assuming the above condition is justified, then the circumference of the cross–section of the circular conductor is equated to the perimeter of the rail cross–section, i.e.

$$rail\ perimeter = 2\pi a_{eq} \tag{5.2}$$

This was evaluated for 56.4 kg/m flat–bottom rail and found to be 0.1m. At very low frequencies, which are below the measurement range of this study and where $a_{eq} \ll \delta$, then the cross–section of the rail and circular conductor can be equated, that is

$$rail\ section\ area = \pi a^2{}_{eq} \tag{5.3}$$

For 56.4 kg/m flat–bottom rail this was found to be 0.05 m.

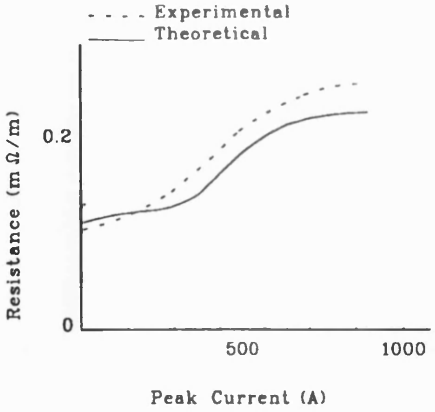

Figure 5.9: Rail Large Signal Internal Resistance with Variation in D.C.

- *For inductance*, it is known [177] that the G.M.D. (geometric mean distance)[3], of a conductor with an irregular shaped cross-section, from itself, interpreted as a circular conductor, is required so that the internal inductance may be evaluated. The method of evaluating the G.M.D. depends on whether the skin effect dominates, as described above. The general technique is described in Appendix C. For 56.4 kg/m Flat-Bottom Rail the GMD is 0.11m.

Permeability Evaluation for the Analytical Model

Section 4.1.2 describes a number of methods for evaluating real and complex permeability using several criteria for variable magnetic field strength. Methods 1 to 3 use relatively direct techniques that are most suitable for use in Equation 5.1. This is the evaluation of large signal internal impedance, making allowance for the effects of hysteresis. The evaluation is based on the peak-to-peak limits of the magnetic field strength. The values are shown in Figures 5.10 and 5.11 together with the measured results. It can be seen that each method might be used to provide agreement with certain parts of the of the measured curve but none of these methods model the whole

[3] Although this is strictly correct, some authors have termed this a geometric mean radius (G.M.R.).

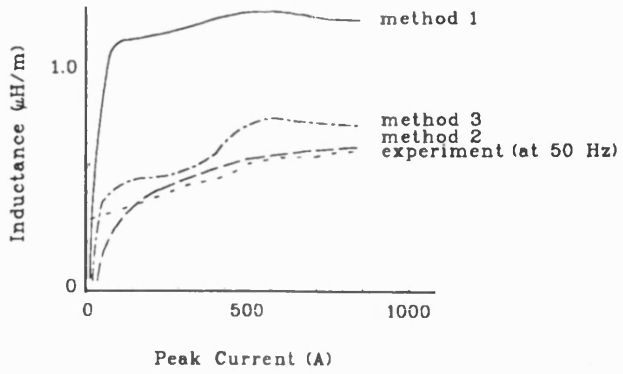

Figure 5.10: Simple Permeability Models and Measured Results for Inductance

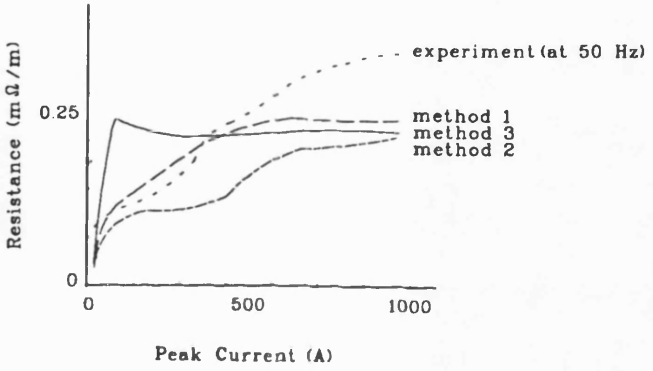

Figure 5.11: Simple Permeability Models and Measured Results for Resistance

measurement range. However, Method 5 of Section 4.1.2 describes a more complicated method of evaluating permeability. It has been termed effective permeability, μ_{eff}, and is illustrated in Figures 5.6 to 5.9. As can be seen from these graphs, this modelling method agrees more closely with the experimental results, for the large signal excitation cases.

For the incremental a.c. impedance cases of Figures 5.2 to 5.5, Equation 5.1 is also a valid approximation. The most suitable technique for evaluating permeability is that of Method 4 of Section 4.1.2. It should be noted that the influence of hysteresis on the value of incremental impedance is thought to be negligible compared to the resistive

losses. The analytical solutions are also given in Figures 5.2 to 5.5 for comparison with experimental results.

A Finite Element Model

Although the analytical model provides a closed form expression to approximate the internal impedance of the rail, it cannot accurately model the non–linear material behaviour variation through the material cross–section. It is expected that localised saturation, at sharp corners of the rail cross–section, occur when large signal excitation is used. That is, the complex geometry of the rail cross–section may have effects not modelled by the circular conductor analysis[4].

Hence a F.E.M. model has been used to obtain further confirmation that the experimental results are an accurate evaluation of the practical situation for the large signal case. This allows both shape and non–linear material behaviour to be included. The technique uses the minimisation of a magnetic vector potential functional which is associated with the energy of the system. A detailed description of the method is given in Appendix F. Since one dimension of the problem (along the rail length) has negligible variation in vector potential, it is possible to use a reduced formulation. This permits analysis in two dimensions only, reducing computational effort. The symmetry of the cross–section, in the vertical axis, is also used so that only half the rail section is modelled. This further reduces the problem size. Figure 5.12 illustrates the form of the model, with the problem area divide up into *finite elements.* It should be noted that smaller elements are used in regions of rapidly changing potential, to provide an accurate solution, especially where saturation and skin effects occur. Once a solution

[4]This is not of concern when incremental a.c. excitation is used, since the d.c. signal dominates the B–H characteristic

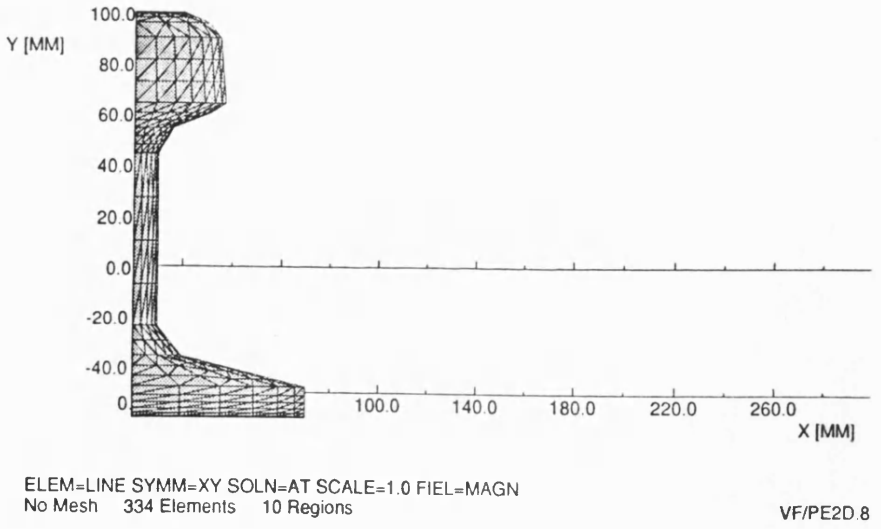

Figure 5.12: Finite Element Model For Internal Impedance Evaluation

to the vector potential distribution has been achieved, the evaluation of the internal inductance of the rail, per unit length (of the third dimension), is obtained from

$$l_{int-FEM} = \frac{2}{I^2_{int}} \sum_{A_{FEM}} H \delta B \tag{5.4}$$

where

I_{int} is the total rail current

H is the magnetic field strength

dB is the elemental flux density

A_{FEM} is the cross-sectional area of the rail

over the rail cross-section.

The a.c. resistance per unit length in the third dimension is given by

$$r_{int-FEM} = \frac{1}{I^2_{int}} \sum_{A_{FEM}} \left(\frac{J_s}{\sigma_{FEM}} \right) \delta A_{FEM} \tag{5.5}$$

where

J_s is the elemental current density

σ_{FEM} is the conductivity of the rail material

A limited set of results for this modelling technique is given in Table E2 of Appendix E. It can be seen that the method gives good agreement with the measured values, confirming the experimental technique and results.

5.1.3 Discussion on Rail Internal Impedance

The description of the phase impedance matrix elements clearly shows that the self impedance of the rails, that is the z_{ii} (diagonal) element, is made up of two components. One is due to the internal conductor magnetic field and conductivity and has been termed the internal impedance of the rail. The other is due to the geometric relationship of the rail to an ideal earth plane and is termed the external self–impedance. The off diagonal terms z_{ij} represent the mutual impedances between any two (i and j) conductors. This is dependent on the relative geometry of the two rails.

The internal self–impedance has been evaluated in detail since this was expected to show major nonlinear behaviour, due to material permeability and signal frequency effects. The evaluation has taken the form of experimental and theoretical calculations with some sample points being modelled by F.E.M. The limited F.E.M. evaluations have been used to confirm both the experimental results and the theoretical model. The F.E.M. modelling of nonlinear current–carrying ferromagnetic conductors requires a full–transient analysis to be performed for each case to be studied. This is expensive in computational effort and so only a limited number of studies have been carried out.

Figures 5.2 to 5.9 illustrate the results obtained. Two main cases have been examined:–

- Small signal a.c. excitation superimposed on a large d.c. signal, i.e. incremental a.c. impedance.

- Large signal a.c. excitation.

Incremental a.c. impedance has been evaluated over a suitable range of frequencies and d.c. currents. The a.c. current was set at 5 A, to represent a typical signalling current. Some typical results for variation in inductance and resistance with frequency are shown in Figures 5.2 and 5.3. Variations with d.c. current, for given frequencies are shown in Figures 5.4 and 5.5. The graphs illustrate the variation of impedance due to changes in permeability and frequency.

Theoretically, the incremental permeability will be (almost) constant, for a given d.c. current and so the characteristics are dominated by the frequency effects. This is clearly shown in Figures 5.4 and 5.5. This implies that the effects due to hysteresis and permeability are small, especially at low frequency. At higher frequencies, Figure 5.3 indicates that the experimental resistance values diverge from the theoretical case, indicating where hysteretic influences cannot be neglected. The main influences on the experimental results which have not been included in the theoretical model are:–

- Second order changes in incremental permeability with frequency
- Localised effects in rail shape i.e. narrowing of cross–section.
- Hysteresis losses at high frequencies
- Loop widening
- Experimental tolerance

Large signal a.c. impedance results are illustrated in Figures 5.2 to 5.9. Generally agreement is good. The experimental variations of internal resistance compared to the theoretical values, at high frequencies, may be explained by:–

- Hysteresis loss at high frequencies
- Loop widening
- Rail shape
- Experimental tolerance

The variation in agreement between the model and the experimental values of inductance are small and may be explained by:–

- Rail shape
- Experimental tolerance

For completeness, the simple models of permeability have been illustrated in Figures 5.10 and 5.11; these show comparison at different excitation values. These can be summarised as

- Normal permeability (method 1) provides the correct shape of curve but the magnitude is generally too large in terms of inductance. This is because the gradient of the B–H curve provided by this model gives a permeability value which is large compared to the practical value. For resistance, agreement only occurs at small values of current where the initial permeability agrees with the practical value.
- Permeability from the fundamental flux density (method 2) gives better agreement at higher current levels for inductance but only provides limited agreement for resistance at low excitation levels. This is due to the magnitude of permeability being in error at lower current levels compared with the practical value. The phase of the model appears to give good agreement.

- Permeability from the B–H loop area (method 3) has similar agreement to method 2 but tends to vary as the area of the practical B–H loop varies non–linearly.

5.2 External Self and Mutual Impedance

If the assumption that the series impedance of the track is much less than the parallel impedance, i.e. the admittance of the track, that is

$$z_{ij}.l \ll \frac{1}{y_{ij}.l} \tag{5.6}$$

then circuit impedance measurements, rather than transmission line tests, may be used to determine the impedance matrix elements.

There are two main considerations when experiments are to be devised to measure the external self and mutual impedances.

- The remote earth plane (or terminal) is inaccessible which means that absolute voltage measurements cannot be made.
- Differential measurements between track ends cannot be made, since additional (measuring equipment) loop inductances would be created.

This implies that only certain combinations of inductance matrix elements can be experimentally obtained. However by use of well established analytical methods, together with numerical techniques, the individual matrix elements can be determined.

5.2.1 Measurement of Track Impedance

One of the experimental configurations used to determine the external impedances of a 36 m length of track is shown in Figure 5.13. The particular configuration has the power

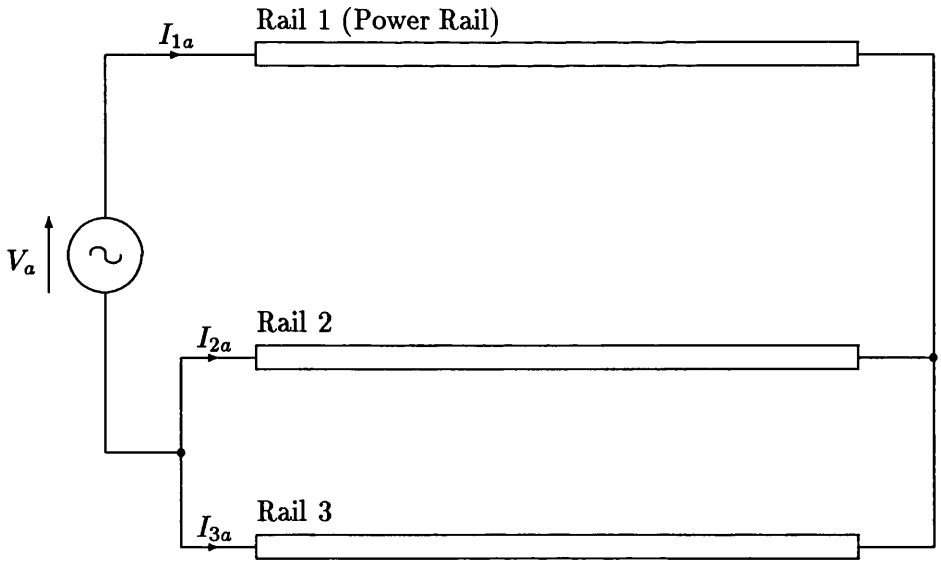

Figure 5.13: Experimental Configuration for the Triple Short Circuit Test

rail outside the running rails and in close proximity to one of them. The test procedure has been termed the *triple short-circuit test.* Since the track is long compared to the inter–rail distance, end effects have been assumed to be negligible. In this arrangement, the two running rails and the traction supply (third rail) are incorporated into one experiment. For Figure 5.13 the loop equations are given by

$$\begin{bmatrix} V_a \\ 0 \end{bmatrix} = \begin{bmatrix} (z_{11} - z_{12}) & (z_{12} - z_{22}) & (z_{13} - z_{23}) \\ (z_{13} - z_{12}) & (z_{23} - z_{22}) & (z_{33} - z_{23}) \end{bmatrix} \begin{bmatrix} I_{1a} \\ I_{2a} \\ I_{3a} \end{bmatrix} \tag{5.7}$$

since rails 2 and 3 are connected in parallel. The subscript notation follows that defined in Chapter 3, with the power rail identified by 1, the running rail nearest the power rail is identified by 2, leaving the second running rail to be identified by 3. By cycling round all three combinations of parallel rail pairs, two further equation sets can be derived.

These are

$$\begin{bmatrix} V_b \\ 0 \end{bmatrix} = \begin{bmatrix} (z_{12} - z_{13}) & (z_{22} - z_{23}) & (z_{23} - z_{33}) \\ (z_{11} - z_{13}) & (z_{12} - z_{23}) & (z_{13} - z_{33}) \end{bmatrix} \begin{bmatrix} I_{1b} \\ I_{2b} \\ I_{3b} \end{bmatrix} \tag{5.8}$$

$$\begin{bmatrix} V_c \\ 0 \end{bmatrix} = \begin{bmatrix} (z_{13} - z_{12}) & (z_{23} - z_{22}) & (z_{33} - z_{23}) \\ (z_{11} - z_{12}) & (z_{12} - z_{22}) & (z_{13} - z_{23}) \end{bmatrix} \begin{bmatrix} I_{1c} \\ I_{2c} \\ I_{3c} \end{bmatrix} \tag{5.9}$$

This provides three independent equations with six impedances to be found. The combinations of *impedance differences* of Equations 5.7 to 5.9 in practice cannot be separated. To evaluate these results, the self–impedance of each rail is determined by F.E.M. techniques and this is described below. This permits the evaluation of the mutual impedances which form the elements of the impedance matrix. These are given in Figures 5.14 and 5.15[5] as the in–phase and quadrature components.

5.2.2 Analytical Approximation for External Impedance

Carson [92] and Pollaczek [93] have independently derived solutions which predict the electromagnetic field distribution around conductors above a conducting ground plane with earth return. The resulting equations form the basis for many studies into the characteristics of ground return conductors. There has been much interest in these solutions with many applications of the equations demonstrated in the modelling of overhead electric power line behaviour.

[5]Also illustrated are analytical and numerical model results, discussed below, for comparison.

Self Impedance

Carson's formulae are not of a closed form, as several parts have to be evaluated as series. However these have been extended and modified in later developments [131] to give the impedance of a ground return conductor as

$$z_{ext-self} = j\omega\frac{\mu_o}{2\pi}\left(\frac{2h_t}{a_{rad}}\right) + j\omega\frac{\mu}{\pi}J_{xs} \tag{5.10}$$

where

$J_{xs} = \int_0^\infty \frac{e^{-2h\lambda}}{\lambda+\sqrt{\lambda^2+j\omega\mu_e\sigma_e}}d\lambda$

σ_e is the conductivity of the earth

μ_e is the permeability of the earth

μ_o is the permeability of free space

λ is the variable of integration

h_t is the height of the conductor above the earth

a_{rad} is the radius of the conductor

Equation 5.10 gives a complex impedance where the real part represents additional power loss due to the earth plane and the imaginary part represents the stored energy in the magnetic field of the air and ground. The assumption that the earth has a uniform conductivity is somewhat dubious and further studies [135] [178] have developed modified equations for horizontally stratified earth.

A better approximation has been found to give more realistic results and the applicable equations have been summarised by Bickford et al. [136] as

$$z_{ext-s} = j\omega\frac{\mu_1\mu_o}{2\pi}ln\left(\frac{2h_t}{a_{rad}}\right) + j\omega\frac{\mu_1\mu_o}{\pi}J_s \tag{5.11}$$

where

$J_s = \int_0^\infty \frac{\mu_2 e^{-2h\lambda}}{\mu_2\lambda+\mu_1 A(\lambda)}d\lambda$

$A(\lambda) = \gamma_{x2} \frac{\mu_3 \gamma_{x2} sinh(d_x \gamma_{x2}) + \mu_2 \gamma_{x3} cosh(d_x \gamma_{x2})}{\mu_3 \gamma_{x2} cosh(d_x \gamma_x 2) + \mu_2 \gamma_{x3} sinh(d_x \gamma_{x2})}$

$\gamma_{xn}{}^2 = \lambda^2 + j\omega\mu_n\mu_o\sigma_n$

subscripts 1,2,3 refer to air, upper ground layer and lower ground layer respectively.

d_x is the depth of the ground layer interface.

These equations have been used to approximate the self impedance of each of the three rails in an electrified third rail system. These are illustrated in Figures 5.16 and 5.17[6].

Mutual Impedance

In a similar manner to the external self impedance, the impedance between two (geometrically) parallel conductors above a ground plane can be developed from the Carson Equations. The corresponding equations to those for self impedance case, summarised by Bickford et al. [136], are

$$z_m = j\omega \frac{\mu_1\mu_o}{2\pi} ln \sqrt{\frac{(h_k + h_m)^2 + d_{rail}^2}{(h_k - h_m)^2 + d_{rail}^2}} + j\omega \frac{\mu_1\mu_o}{\pi} J_m \qquad (5.12)$$

where

$J_m = \int_0^\infty \frac{\mu_2 cos(\lambda(d_{rail}) e^{-\lambda(h_k + h_m)})}{\lambda + \sqrt{\lambda^2 + j\omega\mu_e\sigma_e}} d\lambda$

h_k, h_m are heights of the two conductors above the earth plane

d_{rail} is the horizontal separation between rails

These equations have been evaluated for the three rail system under study and results are given in Figures 5.14 and 5.15.

[6]F.E.M. results, for the same cases, are given for comparison purposes.

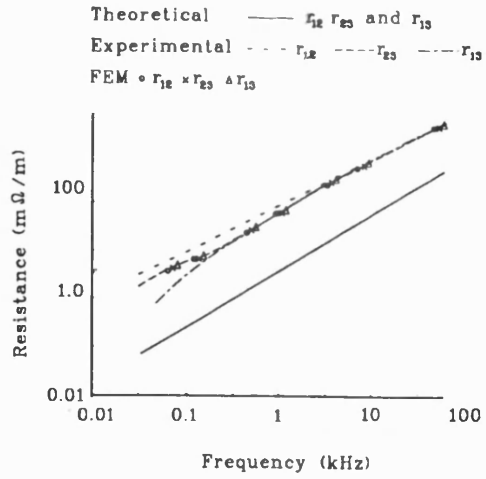

Figure 5.14: Mutual Resistance Matrix Element of Three Rail Track

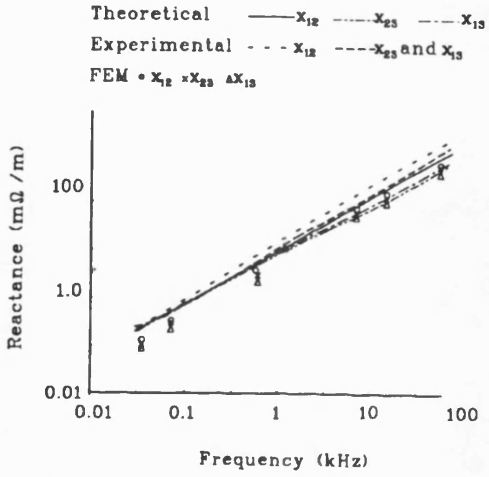

Figure 5.15: Mutual Reactance Matrix Element of Three Rail Track

5.2.3 Numerical Models for External Impedance

As explained in Section 5.2.1, it is necessary to determine the external self impedance of a rail with earth return by numerical or analytical methods. The technique chosen here is F.E.M. since it allows complex shapes and non-linear effects to be included. This is of major importance since the proximity of the ground means that the shape of the rail will be significant in determining the local field profile. This is because the size of some features of the rail are of the same order as the distance between rail and ground. The general method of electromagnetic analysis used by F.E.M. is given in Appendix E.

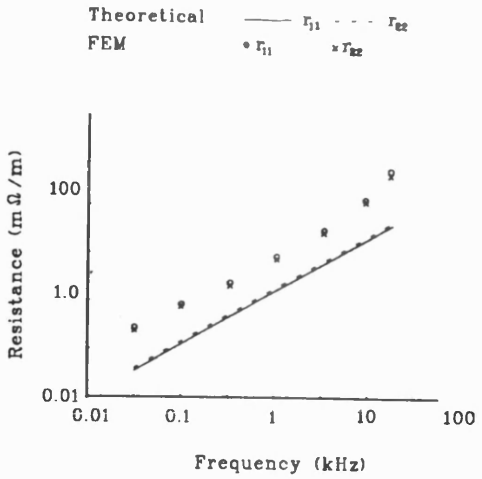

Figure 5.16: In-Phase Component of Self Impedance for a Three Rail System

Self Impedance

An element mesh around a single rail model, as used in a F.E.M. model, is shown in Figure 5.18. This illustrates the necessary size of the mesh used for a two dimensional study. The method is inherently more accurate in obtaining integrals of the field quantities than predicting individual field values [179]. This implies that the integrals used to determine the energy of the problem space provide realistic solutions, even when the field values at particular points contain significant errors. This is particularly useful at high frequencies where the field gradients in conductive and magnetic materials become large. It has been found to be unnecessary to modify the elemental mesh over the frequency range of this study.

The results for the self impedance of the running rails and power rail of a three rail electrified system are given in Figures 5.16 and 5.17. They are given as in-phase and quadrature components. Good agreement is achieved for the quadrature or reactive part but this is not the case for the in-phase (power dissipation) case. It is thought that the analytical model, for the in-phase case, does not provide realistic results. This is due to the model of the ground conductivity profile that had to be incorporated in

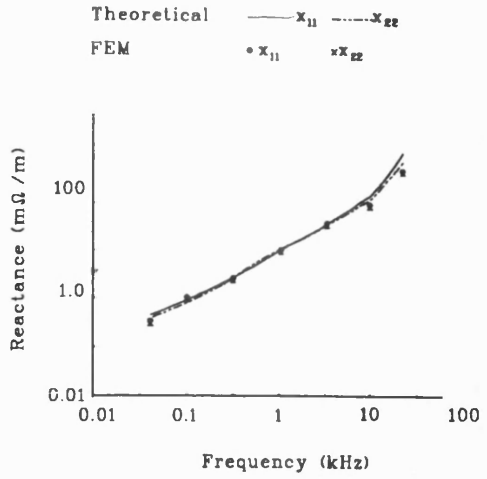

Figure 5.17: Quadrature Component of Self Impedance for a Three Rail System

the analytical equations. In particular, the adoption of a realistic multi–layer ground conductivity profile for F.E.M. allows the calculation of actual field distributions rather than the average value in the analytical model. The analytical expression is based on a two layer earth model and is not able to allow for the complex shapes of rail, sleeper etc. It produces an impedance that is insensitive to changes in soil conductivity.

Mutual Impedance

In a similar manner to the self impedance, the numerical modelling of mutual impedance has been carried out by F.E.M.. Figures 5.19 and 5.20 illustrate magnetic vector potential contours of the solutions obtained. The results are given in Figures 5.14 and 5.15. Again the quadrature components, i.e. the reactive parts, provide good agreement with both experimental results and theory. However, as for the self impedance, the resistive components do not agree well with the analytical results. It should be noted that the F.E.M. and experimental results for the resistive case are in good agreement. This confirms that the real part of the analytical expressions does not provide accurate data for a rail track system. In particular, the predicted value of mutual resistance is invariant with changes of soil conductivity. This is surprising from a physical understanding of

the modelled system since the mutual resistance is a measure of ground eddy current losses which should depend on conductivity. In circuit calculations this effect cancels with the self resistance of the conductors and this discrepancy is then not significant.

5.2.4 Discussion on External Self and Mutual Impedance

The impedances due to flux external to the conductors have been evaluated for the three rail configuration. Three distinct methods have been used:

1. Experimental measurement of the impedance differences of Equations 5.7 to 5.9. These impedance differences cannot be separated experimentally and so the technique must be used in conjunction with the second method.

2. Numerical evaluation of the self and mutual impedances using F.E.M. This method allows a single conductor to be connected to the earth return by a zero impedance bond. This is not possible in practice but the hypothetical situation allows return current to flow, giving a circuit impedance per unit length calculation. This permits evaluation of the individual impedance elements.

3. Analytical approximation based on well established techniques used in power system analysis and summarised previously.

The results of these different approaches are given in Figures 5.14 to 5.17 in terms of resistance and reactance values. Comparison between the results allow a number of observations to be made.

- Figure 5.14 compares values of mutual resistance. It can be seen that good agreement is found between the experimental and F.E.M. evaluations. This is not the

case with the theoretical approximation which consistently underestimates the resistive value of the mutual impedance.

- Figure 5.15 compares values of mutual reactance. Generally good agreement is found between all three methods. The differences may be attributed to experimental tolerances.

- Figure 5.16 compares values of self resistance determined by the analytical approximation and F.E.M.. As for Figure 5.14, the analytical result consistently shows a lower value than for the F.E.M.. The trends in both sets of results are similar.

- Figure 5.17 compares values of self reactance determined by the analytical approximation and F.E.M.. Good agreement is obtained over the whole frequency range considered.

Overall, the three methods give good agreement with the exception of the analytical approximation for resistance, which under estimates the value of resistance. Therefore the real part of the analytical approximation is unsuitable for rail track parameter evaluation. The reason is due to the treatment of the ground conductivity. Adopting a uniform value for conductivity is sufficient for lines suspended far above the earth, such as power lines, since it is possible to calculate an average field energy distribution near to actual conditions. When conductors are brought close to the earth surface, such as rails, the exact field distribution near the surface becomes important in determining energy distribution. The variation in conductivity with depth must be taken into account in calculating this field distribution because the field changes very close to the rail–ground surface. Example illustrations of the F.E.M. models and solutions have also been given and indicate the geometric complexity that can be incorporated in a numerical solution.

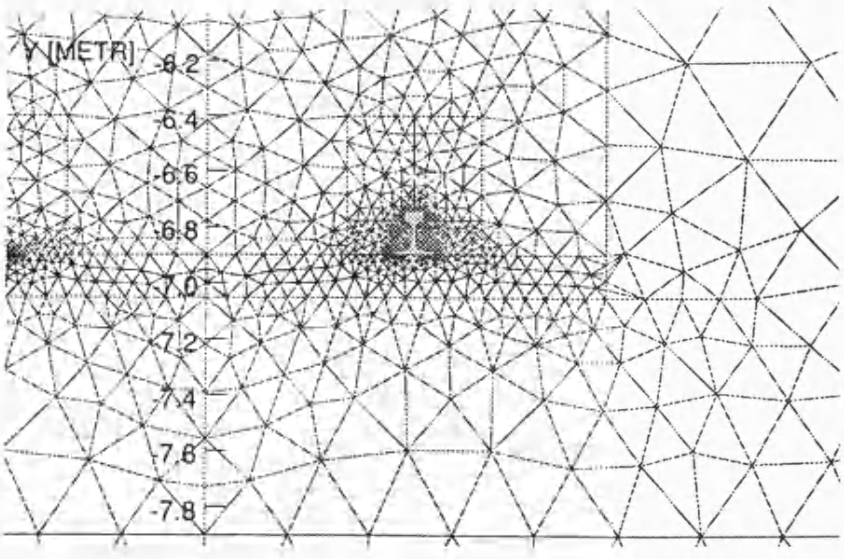

Figure 5.18: F.E.M. Model of Single Rail

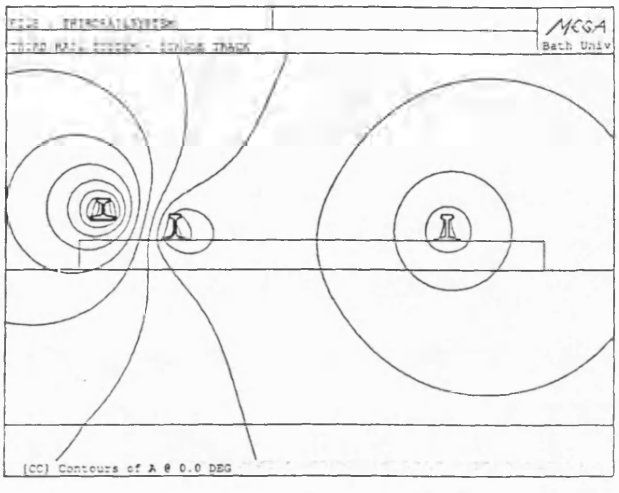

Figure 5.19: The F.E.M. model of Mutual Impedance Between Rails 1 and 2 with 3

The results presented here rely on the principle that the impedance between the rails is much greater than that of the rail series impedance, allowing the measurements to be carried out separately.

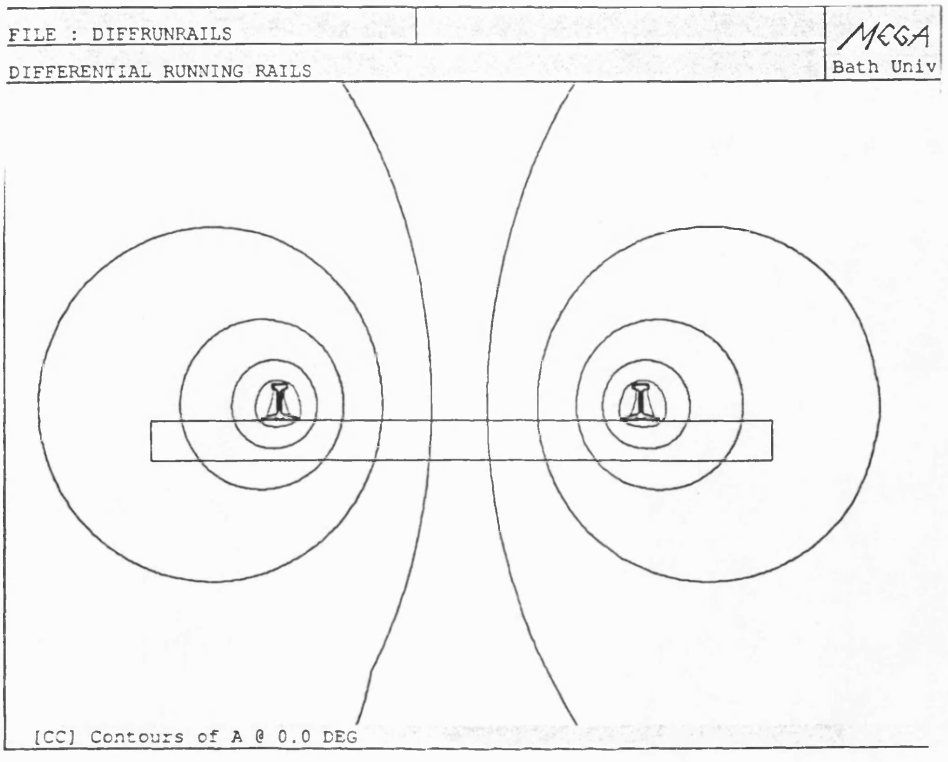

Figure 5.20: The F.E.M. model of Mutual Impedance Between Rails 2 and 3

Chapter 6

Determination of Phase Admittance Matrix Elements for Third Rail Track

A direct method of determining the elements of the Admittance Matrix introduced in Section 3.2.1 is to perform experimental measurements on the system under study. The various tests used are fully described in this chapter, together with the results obtained. The methods used to process these results, to evaluate the matrix elements and the element values themselves are also provided.

To confirm that the experimental measurements obtained describe the practical system, modelling techniques have also been used. The methods for, and the results from, the evaluation of electrical properties of the track–bed that influence inter–rail admittance have been described in the previous chapter. The dimensions of the track and bed are given in Appendix G. These properties are used to calculate the elements of the admittance matrix. The calculations are based on numerical models and this allows separation of the in–phase and quadrature components of admittance, provided that displacement currents are insignificant.

6.1 Admittance by Experiment

It is not possible to separate conductance and susceptance quantities in practical tests as is the case with the modelling methods. Hence it is necessary to measure complex

quantities. In other transmission line systems such as power networks and telecommunications lines, it is possible to make the assumption that the conductance is negligible compared to the susceptance, at the frequencies of interest that is

$$G \gg B \tag{6.1}$$

However, since the running rails are not normally insulated from the track–bed, this is not true for rail track. For this reason, it is not possible to use standard transmission line experimental techniques and analysis. This causes difficulties when *in situ* testing is to be carried out, as the earth–return paths have significant effects on both the in–phase and quadrature components of admittance. It is also necessary to perform the tests over a wide range of frequencies, suitable for both traction power transmission and train signalling transmission. For a two rail system (i.e. running rails only) what will be referred to as the *discontinuous rail test* is used to determine inter–rail admittance. When a third rail is introduced into the system, typical of an electrified power–rail fed system, an additional type of test is required, this being referred to as *inter–rail admittance test.* The results from these two different tests provide a complete set of data for admittance between rails of a three rail system. Inherent in this experimental technique is the assumption that the series impedance is small compared to the impedance between the rails. This assumption appears valid when the material properties of the rails and track bed are compared and when the measurement length is short.

6.1.1 Discontinuous Rail Test

The running rail self and mutual admittances, Y_{ie} and Y_{mij}, as defined in Chapter 3, have been evaluated for an isolated two (running) rail track. The frequencies cover the audio range of 15 Hz to 40 kHz with a track length of 36 m (l_r). The test requires that

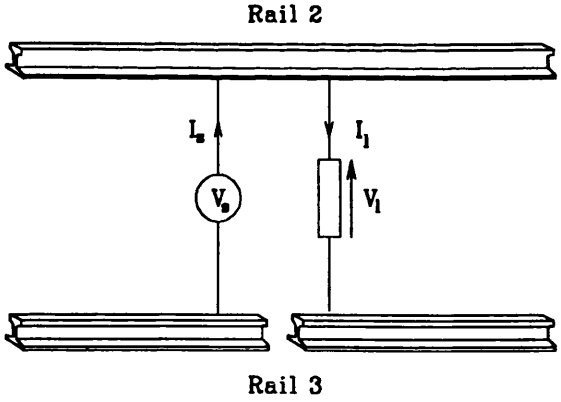

Figure 6.1: Discontinuous Rail Test Practical Circuit

a break is made at the centre of one of the running rail lengths, as shown in Figure 6.1[1]. The rail pair is then excited at one end, with a known load admittance, Y_l, connected across the other end. For ease of measurement and to provide good resolution, the load admittance must be of comparable value to the total inter–rail admittance for the line length used. The source voltage, source current and load current are then measured. The equivalent circuit of Figure 6.2 provides a set of loop equations which, together with current continuity, yields

$$\begin{bmatrix} V_s \\ 0 \\ 0 \\ 0 \\ I_s \end{bmatrix} = \begin{bmatrix} \frac{2}{Y_{m23}l_r} & 0 & 0 & 0 \\ \frac{2}{Y_{m23}l_r} & -(\frac{1}{Y_{2e}l_r} + \frac{2}{Y_{3e}l_r}) & -\frac{2}{Y_{3e}l_r} & -\frac{2}{Y_{3e}l_r} \\ 0 & \frac{1}{Y_{2e}l_r} & -2(\frac{1}{Y_{m23}l_r} + \frac{1}{Y_{3e}l_r}) & -\frac{2}{Y_{3e}l_r} \\ 0 & 0 & \frac{2}{Y_{m23}l_r} & -\frac{1}{Yl_r} \\ 1 & 1 & 1 & 1 \end{bmatrix} \begin{bmatrix} I_1 \\ I_2 \\ I_3 \\ I_4 \end{bmatrix} \quad (6.2)$$

From the symmetry of the track, it may be assumed that $Y_{2e} = Y_{3e}$. Equation 6.2 may be solved to give $Y_{2e} = Y_{3e}$, Y_{m23}, I_1, I_2 and I_3. Since the track length is large compared to the inter–rail distance, end effects are assumed to be negligible. Also, on

[1] Rail/conductor 1 is reserved for the power rail.

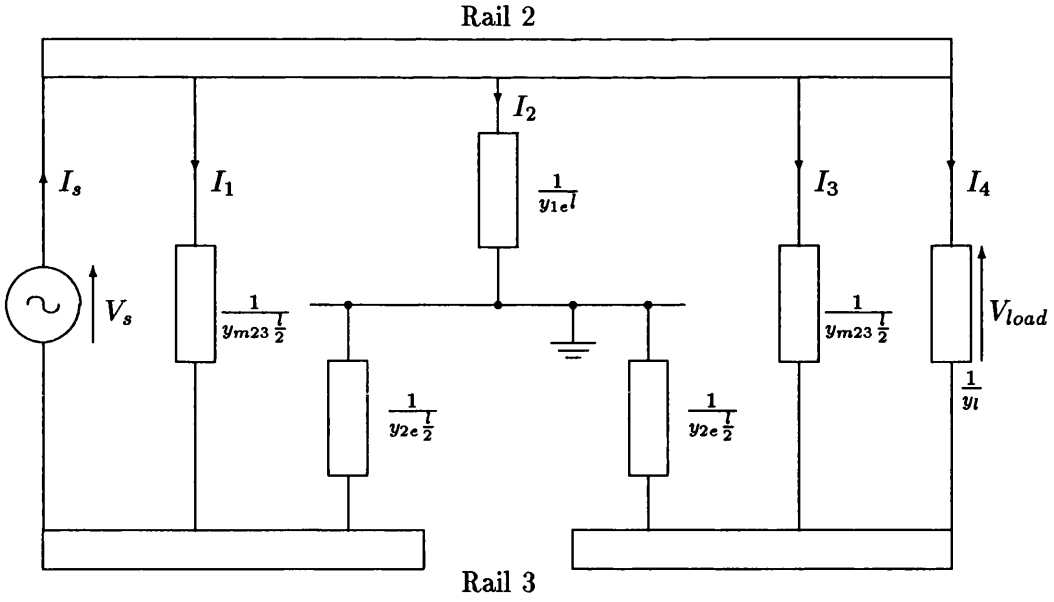

Figure 6.2: Discontinuous Rail Test Equivalent Circuit

the test track used the track bed had been newly laid which implies impurities are at a minimum. On working track, it would be expected that conductance values may be higher, due to increased impurities in the ballast.

The results for $Y_{2e}(= Y_{3e})$ with variation in frequency are shown in Figures 6.3 and 6.4. From Figure 6.2 it can also be seen that the effective inter–rail admittance is given by

$$Y_{eff} = \frac{Y_{2e}}{2} + Y_{m23} \tag{6.3}$$

The effective admittance results are also shown in Figures 6.3 and 6.4. It is possible to measure the inter–rail admittance (i.e. the effective admittance) directly. This has been termed Y_{meas} and these results are also shown in the figures, for comparison purposes.

It can be seen that the values are expressed in terms of in–phase (conductive) components and quadrature (susceptive) components. These experimental results are now used to evaluate the admittance matrix elements for a two rail system. As shown in

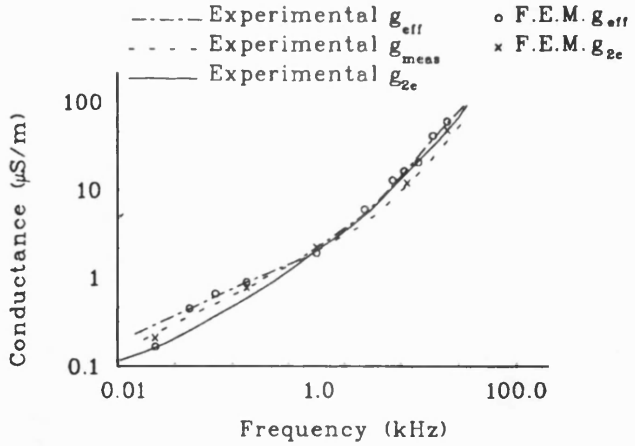

Figure 6.3: Variation of Running Rail Conductance with Frequency

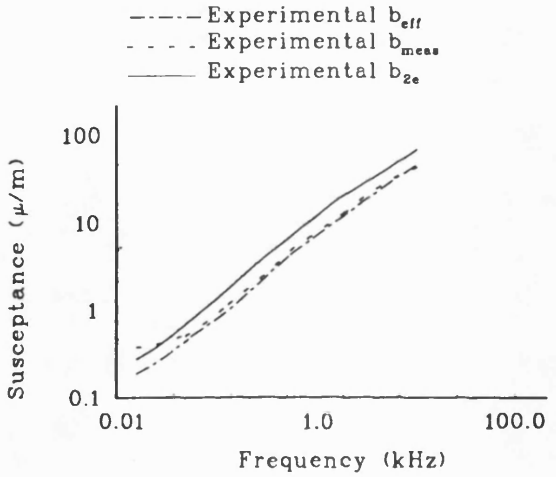

Figure 6.4: Variation of Running Rail Susceptance with Frequency

Chapter 3, using Equations 3.26 and 3.27 such that

$$Y_{23} = Y_{32} = -Y_{m23} \tag{6.4}$$

$$Y_{2e} = Y_{3e} = Y_{22} + Y_{23} \tag{6.5}$$

$$\tag{6.6}$$

a 2 × 2 admittance matrix is formed. These results are shown in Figure 6.5 and 6.6.

6.1.2 Inter–rail Admittance Test

In this experiment, the admittance for three circuit configurations of the three rail system are measured. The three configurations are illustrated in Figure 6.7

The configuration shown in Figure 6.7a indicates the arrangement for the measurement of the admittance, $Y_{meas:A}$ between the power rail and the far running rail. It can be shown that this admittance can be expressed as

$$Y_{meas:A} = Y_{m12} + \frac{Y_z Y_x}{Y_z + Y_x} \tag{6.7}$$

where

$Y_z = \frac{Y_x Y_{m13}}{Y_x + Y_{m13}} + \frac{Y_{1e} Y_y}{Y_{1e} + Y_y}$

$Y_x = \frac{Y_m Y_{2e}}{Y_m + Y_{2e}}$

$Y_y = \frac{{Y_{2e}}^2}{Y_m + 2Y_{2e}}$

In a similar manner, the admittance measured between the power rail and the near running rail, as illustrated in Figure 6.7b, is given by

$$Y_{meas:B} = Y_{m13} + \frac{Y_a Y_x}{Y_a + Y_x} \tag{6.8}$$

where $Y_a = \frac{Y_{m12} Y_x}{Y_{m12} + Y_x} + \frac{Y_{1e} Y_y}{Y_{1e} + Y_y}$

The final configuration provides a measurement of admittance between the power rail and the running rails in parallel, as illustrated in Figure 6.7c. It is given by

$$Y_{meas:C} = Y_{m13} + Y_{m12} + \frac{2Y_e Y_{1e}}{2Y_e + Y_{1e}} \tag{6.9}$$

Equations 6.7, 6.8 and 6.9 form a set of simultaneous equations which have been solved

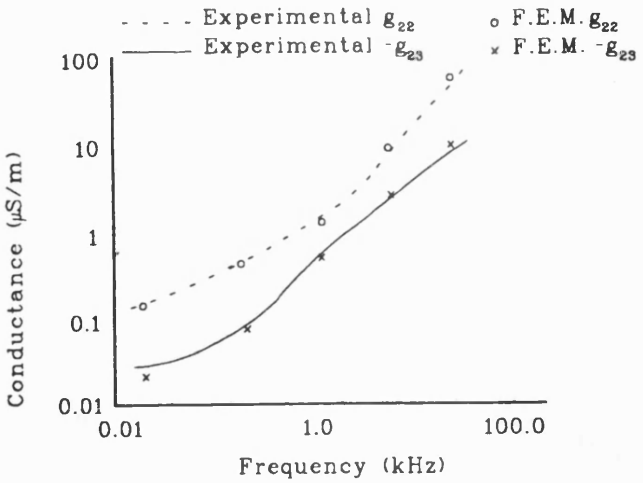

Figure 6.5: Conductance Elements of a Two Rail System

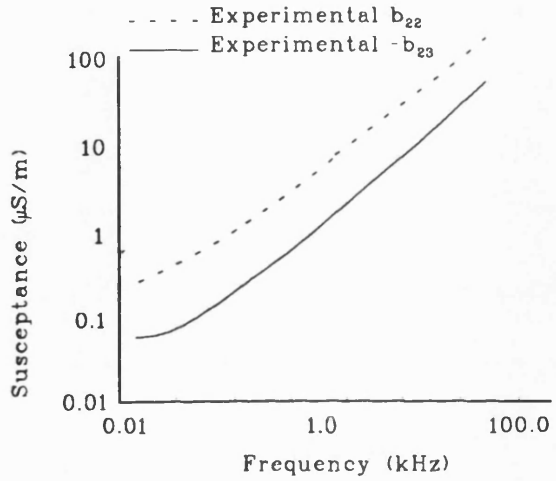

Figure 6.6: Susceptance Elements of a Two Rail System

numerically, for Y_{1e} Y_{m12} and Y_{m13} using a standard iterative Levenberg–Marquardt method [180].

The lower frequency measurement limit is approximately 400 Hz since the measured conductances associated with the power rail are negligible[2] over the whole frequency range and the small capacitance values provide only a small susceptance at low frequencies. Since the results are totally reactive, they are shown in Figure 6.8, expressed as capacitance. Again using Equations 3.26 and 3.27 the admittance matrix elements for the three rail system can be expressed as

[2]This is to be expected as the rail is mounted on insulators.

$$Y_{12} = -Y_{m12} \tag{6.10}$$

$$Y_{13} = -Y_{m13} \tag{6.11}$$

$$Y_{11} = Y_{1e} + Y_{m12} + Y_{m13} \tag{6.12}$$

These results are shown as in–phase and quadrature components with variation in frequency in Figures 6.9 and 6.10.

6.2 Numerical Modelling of Admittance

A numerical model is chosen to determine the conductance and susceptance components of the elements of the admittance matrix because the cross–section of the track and track bed is not composed of regular geometric shapes. The general principle used in F.E.M. analysis is outlined in Appendix E. As can been seen from this, the method is normally applied to electromagnetic problems, as is the case in Chapter 6. However, using the duals shown in Appendix E, it is possible to model rail–to–earth conductance and susceptance g_{ie} and b_{ie}, together with rail–to–rail conductance and susceptance, g_{mij} and b_{mij}.

Examples of the four models used are given in Figures 6.11 to 6.14. The contours of relevant equipotentials superimposed on the model outlines are illustrated. The frequency effects are included by varying the material properties as described in Chapter 4. Also care has been taken to ensure that the far field boundaries do not influence the solution. This has been achieved by modifying the boundaries and confirming that the solution does not vary by more than an acceptable error (i.e. $< 3\%$) which is small compared to experimental errors.

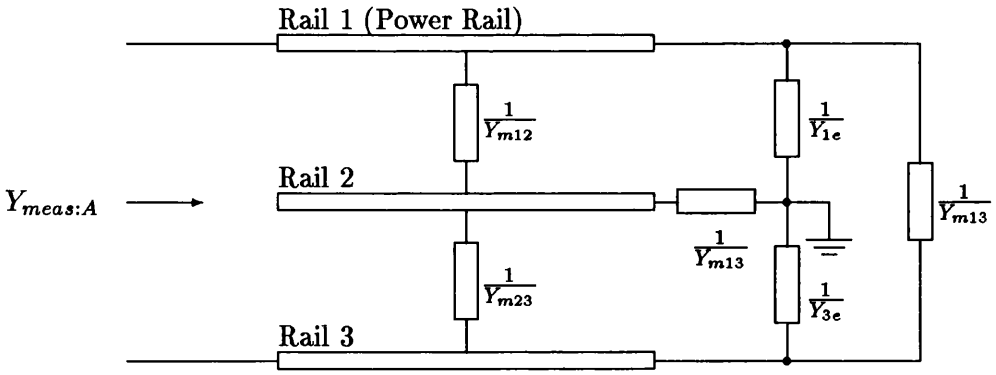

(a) Power Rail and Far Rail Admittance Measurement

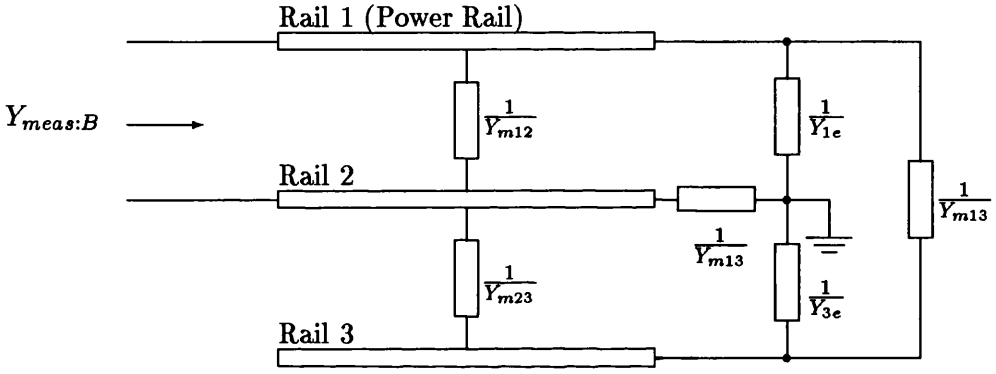

(b) Power Rail and Near Rail Admittance Measurement

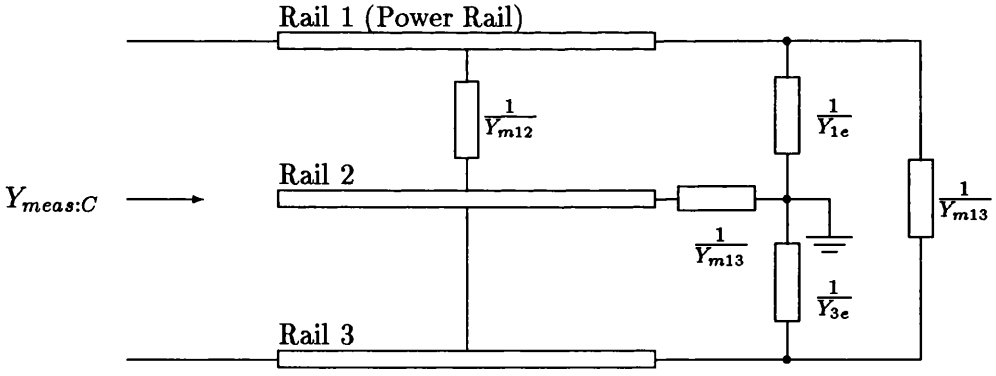

(c) Power Rail and Shorted Running Rails Admittance Measurement

Figure 6.7: Equivalent Circuits of an Inter–rail Admittance Test

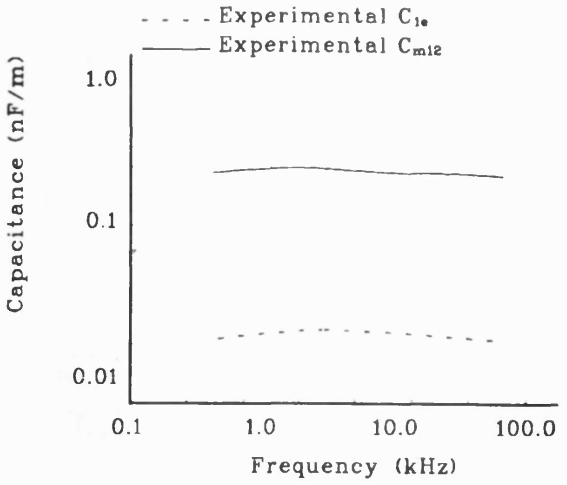

Figure 6.8: Experimental Capacitances of Power Rail Track Configuration

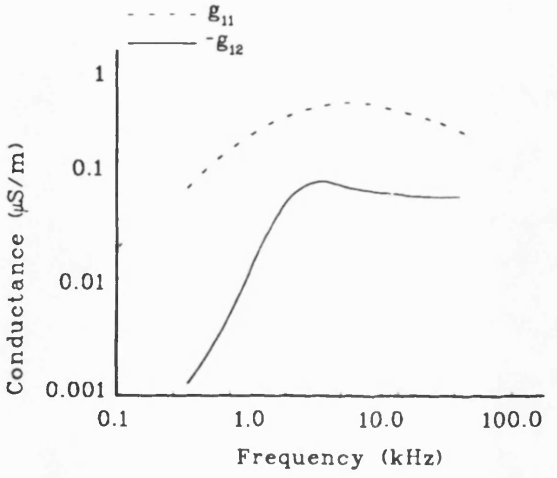

Figure 6.9: Conductance Elements of Third Rail of System Admittance Matrix

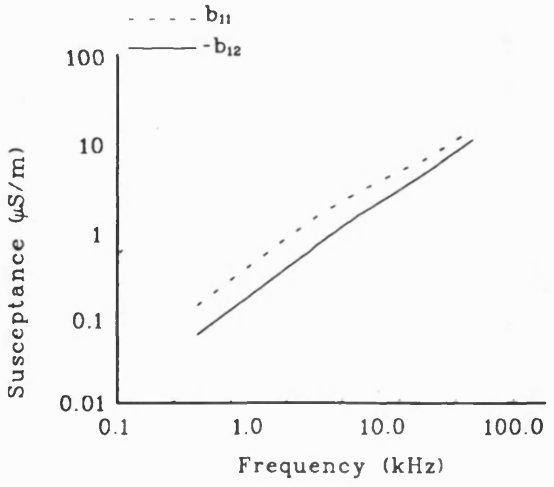

Figure 6.10: Susceptance Elements of Third Rail of System Admittance Matrix

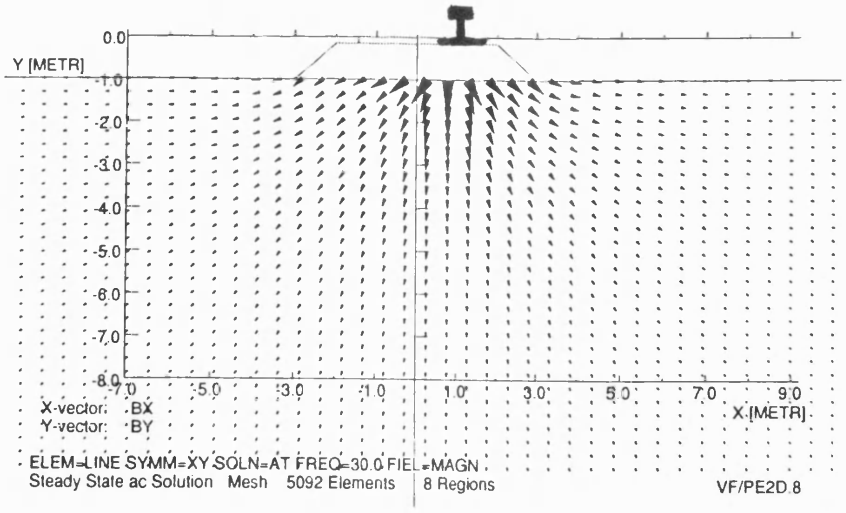

Figure 6.11: F.E.M. Solution of Rail–to–Ground Conductance Model

In the case of conductivity modelling, the appropriate conductivity profile, for given frequency, is chosen from those developed in Chapter 4. It is then discretised for use in the numerical model. The sleeper conductivity has been evaluated in earlier reports [181] as has the ballast conductivity [139]. In the air region the conductivity $\sigma = 0$ implies that the electromagnetic dual will have infinite permeability so $\mu \rightarrow \infty$. To account for this, the elements of the air are removed from the model.

For electrostatic modelling, for a good conductor is $\varepsilon = 0$, the electromagnetic dual will have $\mu \rightarrow \infty$. Again the elements of the conductors are removed in the models.

By determining the total dissipated or stored energy in the problem space, it is possible to evaluate the conductance and capacitance for each case considered with the exception of C_{ie}. This value cannot be obtained because the constant permeability model used implies that the stored energy is dependent on the distance between the single rail and boundary. Using Table E1 in Appendix E, the computed dissipated and stored energies of the regions of interest, together with specified potential differences, are used to obtain values of admittance for comparison with the experimental results described above. Again, these are evaluated in component form but may be combined to give Y_{ie} and Y_{eff}. Comparison between the experimental and model results are shown in

Figures 6.3, 6.4, 6.8 and 6.5. The modelled results are also processed to yield admittance matrix elements and these are shown in Figures 6.9 and 6.10.

6.3 Discussion on Phase Admittance Matrix Elements

By making the assumption that the series impedance is much less than the inter–rail impedance i.e.

$$z_{ij}l < \frac{1}{y_{ij}l} \tag{6.13}$$

where l is the measurement length

then it is possible to separate the experimental methods used to determine the phase admittance and impedance elements. Accepting that the admittance and impedance measurements may be decoupled, then circuit analysis can be used to interpret the experimental results.

The frequency response of the phase admittances for the two rail system, i.e. the running rail pair, are based on both measurements and modelling. These are shown in Figures 6.3 and 6.4. It can be seen that the model results show close agreement with the experimental results. From the running rail track conductance results, in Figure 6.3, it is clear that the g_{eff} values from modelled data and experimental measurements are in agreement with one another and with the experimental value of g_{meas}. In a similar manner, the modelled and experimental values of g_{2e} also give close agreement. The same is true for the experimental results for the b_{eff} and b_{meas} susceptances illustrated in Figure 6.4. This confirms that the circuit elements of y_{ie} and y_{mij} (which make up y_{eff}) give a good model of the physical system as measured directly by y_{meas} (see Equation 6.3).

The resultant phase conductance matrix elements, given in Figure 6.5, have been evaluated from the experimental results and F.E.M. models. Again, excellent agreement has been achieved, confirming that the modelling procedure closely describes the practical system. Since it has not been possible to evaluate the permittivity of the track bed, a similar comparison is not available for the susceptances.

In determining the phase admittance elements of the third rail of the three rail system, it was found that the conductance between this rail and the running rails is negligible. This is to be expected since it is mounted on insulators. This implies, in phase admittance terms that

$$y_{m1j} = jB_{m1j} \tag{6.14}$$

$$y_{1e} = jB_{1e} \tag{6.15}$$

$$g_{m1j} = g_{1e} = 0 \tag{6.16}$$

where j=2,3

Using the three configurations shown in Figure 6.7 and the phase admittances previously determined, it has been possible to deduce the phase capacitance values as illustrated in Figure 6.8. It is of interest that $C_{m12} = C_{m13}$ even though the geometric relationship between the power rail and each of the running rails is different. This is explained by the dominating influence of the track bed, acting as a conductor. Each of the running rails are conductively coupled to the track bed so that the capacitance between power rail and either running rail is equivalent to the power rail to track bed capacitance. This may be seen directly from the F.E.M. results illustrated in Figures 6.12 and 6.14.

Using the running rail phase admittance results, it is possible to determine the third rail phase admittance elements. These are shown in Figures 6.9 and 6.10 in both con-

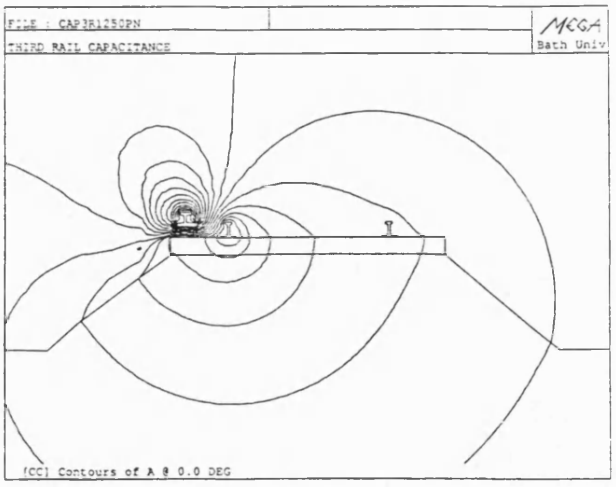

Figure 6.12: F.E.M. Solution of Rail–to–Ground Capacitance Model

ductance and susceptance component form. Although the numerical (or modelled) quantities are purely susceptive, when these values are combined into the phase matrix element form, using the Equations 6.7 to 6.12, the matrix elements contain conductive components. This is due to the non–physical nature of the matrix elements.

Example solutions of F.E.M. results are given in Figures 6.11 to 6.14. As has been noted earlier, these give excellent agreement with measured results. This close agreement is to be expected when the material properties have been well defined. This shows that the F.E.M. analysis is extremely dependent on material properties and characteristics but yields good results for well defined problems.

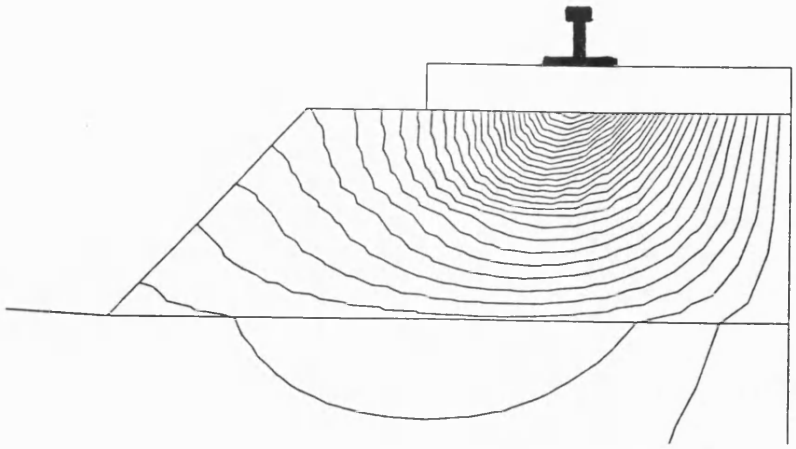

Figure 6.13: F.E.M. Solution of Rail–to–Rail Conductance Model

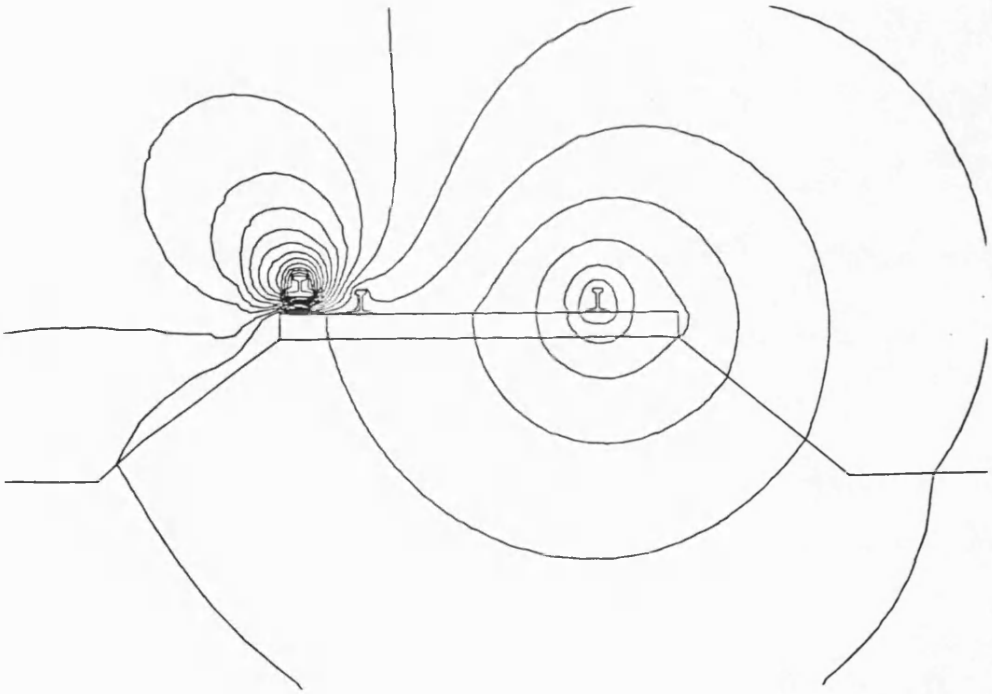

Figure 6.14: F.E.M. Solution of Power Rail–to–Running Rails Capacitance Model

Chapter 7

Composite Measurement of Track Parameters

The experimental methods described in Chapters 5 and 6 rely on the assumption that $z_{ij}l \ll \frac{1}{y_{ij}l}$. Although this would appear to be a reasonable physical assumption, an alternative method of admittance and impedance matrix element evaluation, which does not rely on the above assumption, has been examined. The method is described in this Chapter and the results presented.

The technique determines all the track parameters in a single set of tests. However, additional specific circuit elements and extreme measurement accuracy are required. These limitations have meant that the investigation has been restricted to a single power frequency. This requires only one suitably rated and stable supply to be available together with one set of external components. Also, the accuracy of the measuring equipment can be selected for the single frequency of concern. However these restrictions do not prevent the method from being fully exploited.

The method considers two rails at a time. The matrix elements relating to the two parallel running rails have been evaluated. This allows the symmetry of the geometry to be exploited in the expressions used.

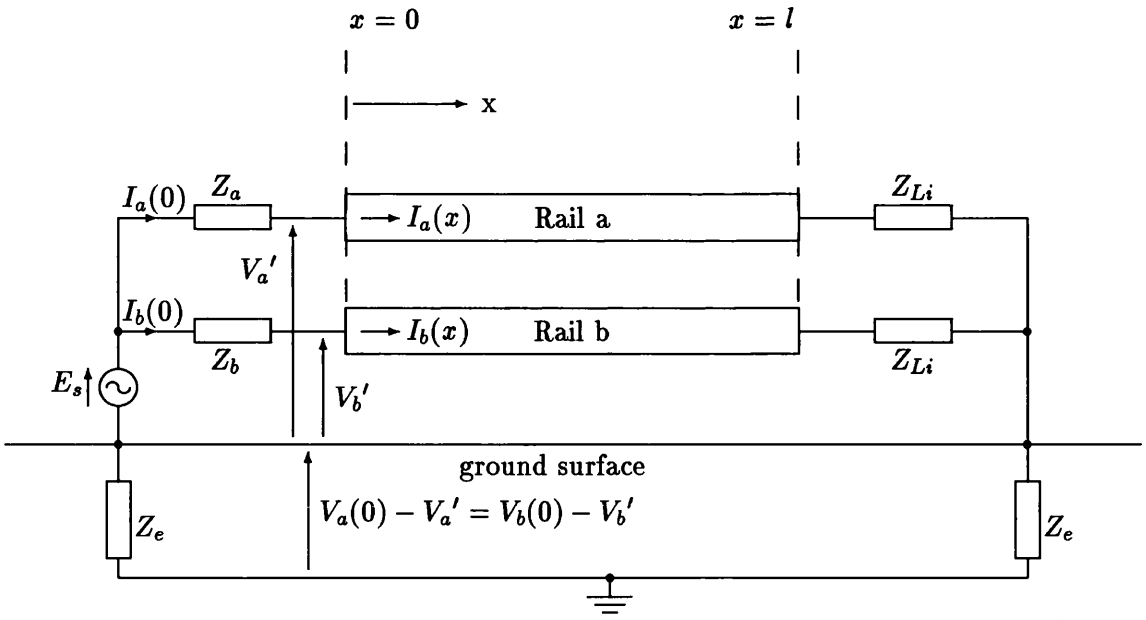

Figure 7.1: Rail–Pair Excitation Test Circuit

7.1 Matrix Elements from Rail–Pair Excitation

It is possible determine the matrix elements by considering two Rails A and B which are excited with voltages $V_a(x)$ and $V_b(x)$ and are carrying different currents $I_a(x)$ and $I_b(x)$ as shown in Figure 7.1. The two lines are loaded with equal impedances Z_{Li} but the source impedances are different i.e. Z_a and Z_b. The voltage source, E_s and load impedances Z_{Li} are both connected to a remote earth with impedance Z_E.

If the lines are homogeneous, the solution of Equation 3.7 is expressed in terms of exponential functions and is given by

$$\begin{bmatrix} V_a(x) \\ V_b(x) \end{bmatrix} = \begin{bmatrix} F_{aa} & F_{ab} \\ F_{ba} & F_{bb} \end{bmatrix} \begin{bmatrix} a_a' e^{-\gamma_a x} + b_a' e^{\gamma_a x} \\ c_b' e^{-\gamma_b x} + d_b' e^{\gamma_b x} \end{bmatrix} \tag{7.1}$$

where $F_{ij}, a_a', b_a' c_b'$ and d_b' are constants determined by the terminating conditions

The matrix [F] is evaluated using Equations 3.7 and 7.1 since

$$\begin{bmatrix} F_{aa} & F_{ab} \\ F_{ba} & F_{bb} \end{bmatrix} \begin{bmatrix} {\gamma_a}^2 & 0 \\ 0 & {\gamma_b}^2 \end{bmatrix} = \begin{bmatrix} A_{11} & A_{12} \\ A_{21} & A_{22} \end{bmatrix} \begin{bmatrix} F_{aa} & F_{ab} \\ F_{ba} & F_{bb} \end{bmatrix} \tag{7.2}$$

If the propagation constants are now examined, for a two rail system, it is possible to relate the modes of propagation to circuit configurations [167] [89]. These are

- *Common mode propagation* where the rails are connected in parallel with an earth return. Associated with this mode is a propagation constant, γ_{comm}.
- *Differential mode propagation* where the rails are connected as a go–and–return path (above a ground plane). This also has a propagation constant, γ_{diff}, associated with it.

Using the association

$$\gamma_{comm} \rightarrow \gamma_a \tag{7.3}$$

$$\gamma_{diff} \rightarrow \gamma_b \tag{7.4}$$

then in the differential mode case, from Equation 3.8 with the elements of the current matrix being related as $I_a = -I_b$, it follows that

$$F_{aa} = F_{ba} \tag{7.5}$$

In a similar manner, the common mode case gives

$$F_{ab} = -F_{bb} \tag{7.6}$$

From Equation 7.1, the line voltages can be expressed as

$$\begin{bmatrix} V_a(x) \\ V_b(x) \end{bmatrix} = \begin{bmatrix} F_{aa} & -F_{bb} \\ F_{aa} & F_{bb} \end{bmatrix} \begin{bmatrix} {a_a}' e^{-\gamma_a x} + {b_a}' e^{\gamma_a x} \\ {c_b}' e^{-\gamma_b x} + {d_b}' e^{\gamma_b x} \end{bmatrix} \tag{7.7}$$

$$= \begin{bmatrix} 1 & -1 \\ 1 & 1 \end{bmatrix} \begin{bmatrix} ae^{-\gamma_a x} + be^{\gamma_a x} \\ ce^{-\gamma_b x} + de^{\gamma_b x} \end{bmatrix} \tag{7.8}$$

where a, b, c and d are constants dependent on the terminating conditions

Similarly, the line currents are

$$\begin{bmatrix} I_a(x) \\ I_b(x) \end{bmatrix} = \begin{bmatrix} z_{aa} & z_{ab} \\ z_{ba} & z_{bb} \end{bmatrix}^{-1} \begin{bmatrix} \frac{dV_a}{dx} \\ \frac{dV_b}{dx} \end{bmatrix} \tag{7.9}$$

Assuming the lines are symmetric, $z_{aa} = z_{bb}$ and $z_{ba} = z_{ab}$ then

$$\begin{bmatrix} I_a(x) \\ I_b(x) \end{bmatrix} = k_1 \begin{bmatrix} -1 & 1 \\ -1 & 1 \end{bmatrix} \begin{bmatrix} ae^{-\gamma_a x} \\ be^{\gamma_a x} \end{bmatrix} + k_2 \begin{bmatrix} 1 & -1 \\ -1 & 1 \end{bmatrix} \begin{bmatrix} ce^{-\gamma_b x} \\ de^{\gamma_b x} \end{bmatrix} \tag{7.10}$$

where k_n is a constant dependent on track geometry

On substituting the differential of Equation 7.8 into Equation 7.9 the current vector becomes

$$\begin{bmatrix} I_a(x) \\ I_b(x) \end{bmatrix} = \begin{bmatrix} z_{aa} & z_{ab} \\ z_{ba} & z_{bb} \end{bmatrix}^{-1} \gamma_a \begin{bmatrix} -ae^{-\gamma_a x} + be^{\gamma_a x} \\ -ae^{-\gamma_a x} + be^{\gamma_a x} \end{bmatrix} \gamma_b \begin{bmatrix} +ce^{-\gamma_b x} - de^{\gamma_b x} \\ -ae^{-\gamma_b x} + de^{\gamma_b x} \end{bmatrix} \tag{7.11}$$

Equating 7.8 and 7.11 gives

$$\begin{bmatrix} k_1 & k_2 \\ k_1 & -k_2 \end{bmatrix} \gamma_a \begin{bmatrix} -ae^{-\gamma_a x} + be^{\gamma_a x} \\ ce^{-\gamma_b x} - de^{\gamma_b x} \end{bmatrix}$$

$$= \frac{1}{det[Z]} \begin{bmatrix} z_{aa} & -z_{ab} \\ -z_{ba} & z_{bb} \end{bmatrix} \begin{bmatrix} \gamma_a & \gamma_b \\ \gamma_a & \gamma_b \end{bmatrix} \begin{bmatrix} -ae^{-\gamma_a x} + be^{\gamma_a x} \\ ce^{-\gamma_a x} - de^{\gamma_a x} \end{bmatrix} \tag{7.12}$$

If the rows of Equation 7.12 are added, this gives

$$k_1 \left(-ae^{-\gamma_a x} + be^{\gamma_a x}\right) = \frac{\gamma_a}{det[Z]} \left[(z_{aa} - z_{ab}) \left(-ae^{-\gamma_a x} + +be^{\gamma_a x}\right)\right] \tag{7.13}$$

so that

$$k_1 = \frac{\gamma_a}{z_{aa} + z_{ab}} \tag{7.14}$$

By subtracting rows of Equation 7.12 a similar relationship is obtained, that is

$$k_2 = \frac{\gamma_b}{z_{aa} - z_{ab}} \tag{7.15}$$

By adding and subtracting Equations 7.14 and 7.15 the values of the impedance elements are obtained as

$$z_{aa} = \frac{1}{2}\left[\frac{\gamma_a}{k_1} + \frac{\gamma_b}{k_2}\right] \tag{7.16}$$

$$z_{ab} = \frac{1}{2}\left[\frac{\gamma_a}{k_1} - \frac{\gamma_b}{k_2}\right] \tag{7.17}$$

Similarly, using Equations 3.8, 7.16 and 7.17, together with the ideas of common and differential mode excitation, the admittance matrix elements are determined by

$$y_{aa} = \frac{(z_{aa} - z_{ab})\gamma_a{}^2 + (z_{aa} + z_{ab})\gamma_b{}^2}{det[Z]} \tag{7.18}$$

and

$$y_{ab} = \frac{(z_{aa} - z_{ab})\gamma_a{}^2 - (z_{aa} + z_{ab})\gamma_b{}^2}{det[Z]} \tag{7.19}$$

7.2 Application of Terminating Conditions

The constants a, b, c and d are found in terms of $k_1, k_2, \gamma_a, \gamma_b$ and Z_e by using the receiving end impedances. The voltages at the receiving end are given by

$$\begin{bmatrix} V_a(l) \\ V_b(l) \end{bmatrix} = \begin{bmatrix} (Z_{Li} + Z_e) & Z_e \\ Z_e & (Z_{Li} + Z_e) \end{bmatrix} \begin{bmatrix} I_a(l) \\ I_b(l) \end{bmatrix} \tag{7.20}$$

Alternatively the line voltages and currents at $x = l$ may be determined in terms of

$k_1, k_2, \gamma_a, \gamma_b, a, b, c$, and d. Also, at the sending end with $x = 0$, Equation 7.10 becomes

$$\begin{bmatrix} I_a(0) \\ I_b(0) \end{bmatrix} = k_1 \begin{bmatrix} -1 & 1 \\ -1 & 1 \end{bmatrix} \begin{bmatrix} a \\ b \end{bmatrix} + k_2 \begin{bmatrix} 1 & -1 \\ -1 & 1 \end{bmatrix} \begin{bmatrix} c \\ d \end{bmatrix} \tag{7.21}$$

This result, combined with Equation 7.10, with $x = l$, Equation 7.8 and 7.20 are solved to give values of a, b, c and d as functions of $Z_{Li}, Z_e, k_1, k_2, \gamma_a\gamma_b, I_a(0)$ and $I_b(0)$. These are given by

$$a = -\frac{I_a(0) + I_b(0)}{2k_1} \frac{[1 - k_1(Z_{Li} + 2Z_e)]}{[1 - k_1(Z_{Li} + 2Z_e)] + [1 + k_1(Z_{Li} + 2Z_e)]e^{-2\gamma_a l}} \tag{7.22}$$

$$b = \frac{I_a(0) + I_b(0)}{2k_1} \frac{[1 + k_1(Z_{Li} + 2Z_e)]}{[1 + k_1(Z_{Li} + 2Z_e)] + [1 - k_1(Z_{Li} + 2Z_e)]e^{2\gamma_a l}} \tag{7.23}$$

$$c = \frac{I_a(0) - I_b(0)}{2k_2} \frac{(1 - Z_{Li}k_2)}{[(1 - Z_{Li}k_2) + (1 + Z_{Li}k_2)]e^{-2\gamma_b l}} \tag{7.24}$$

$$d = \frac{-I_a(0) - I_b(0)}{2k_2} \frac{[1 + Z_{Li}k_2]}{[(1 + Z_{Li}k_2) + (1 - Z_{Li}k_2)]e^{2\gamma_b l}} \tag{7.25}$$

However the absolute values of $V_1(0)$ and $V_2(0)$ cannot be measured, since the true earth plane is subterranean, as depicted in Figure 7.1. To overcome this problem, the sending end conditions are used to obtain an expression so that the earth impedance, Z_e, can be evaluated (or eliminated). The test only permits the voltages V_a' and V_b' referenced to the source voltage, and currents $I_a(0)$ and $I_b(0)$ to be measured. As there are five unknown impedances ($z_{aa}, z_{ab}, y_{aa}, y_{ab}$ and Z_e) at least five independent equations must be available. Hence, three different load impedances are used to make three independent sets of measurements (providing six equations and some redundancy).

Assuming the lines are equally loaded with impedance Z_{Li} (i = 1 to 3), the sending

end voltages are related to the measured line voltages and currents by

$$\begin{bmatrix} V_{ai}'(0) \\ V_{bi}'(0) \end{bmatrix} = \begin{bmatrix} V_{ai}(0) \\ V_{bi}(0) \end{bmatrix} + Z_e \begin{bmatrix} 1 & 1 \\ 1 & 1 \end{bmatrix} \begin{bmatrix} I_{ai}(0) \\ I_{bi}(0) \end{bmatrix} \tag{7.26}$$

The solution technique is given in Appendix D. In brief, the method finds analytical expressions for the measured line voltages in terms of the basic unknowns Z_e, k_1, k_2, γ_a and γ_b using the constants a, b, c and d from Equations 7.22 to 7.23. The track matrix elements are then found from Equations 7.16 to 7.19.

7.3 Experimental Considerations and Results

The source voltage, series sending end impedances and load impedances are chosen such that the relative magnitudes of those impedances provide large enough signals for accurate measurement. Practical restrictions which must be considered include

- The relationship between the series impedance and shunt admittance of the rail and track bed structure i.e. $z_{series} \ll \frac{1}{y_{shunt}}$.
- The earth impedance cannot be reduced below a certain value because of the contact resistance and finite ground conductivity.

In the test circuit, this causes most of the series voltage drop to occur across the earth impedances, rather than to appear as a line potential difference, which is required to facilitate measurement. The line excitation is chosen to produce a high potential difference between the two rails, creating an appreciable shunt current flow through the track bed. Also high currents are required through the rails to create a longitudinal potential difference which is large enough to be measured. These conditions are most closely satisfied by choosing the series sending end impedances so that the test circuit is

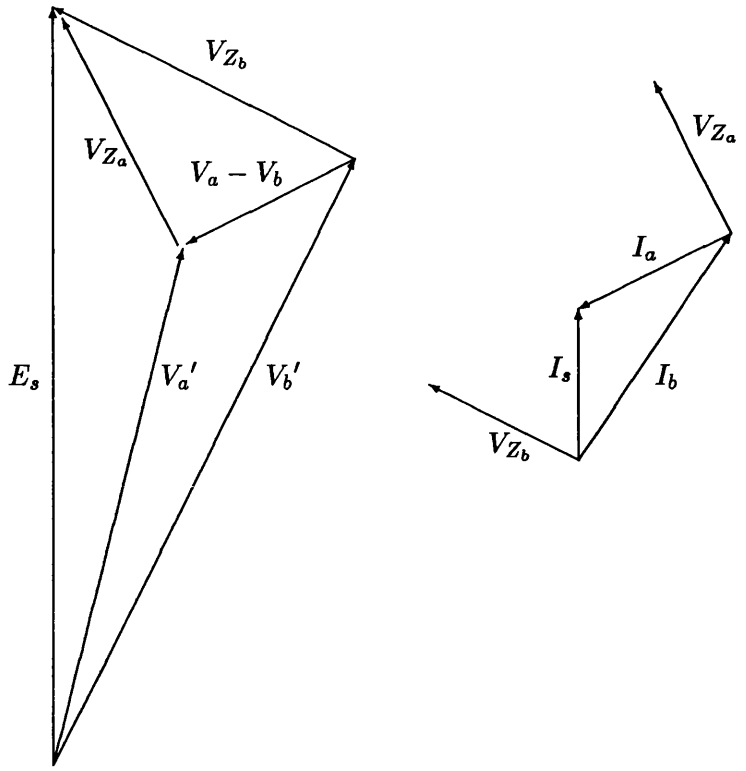

Figure 7.2: Phasor Relationship for the Test Circuit (Not to Scale)

in series resonance. Also, the source and load impedances are comparable in magnitude to the line impedances. Figure 7.2 shows the phasor relationship of the test circuit signals.

Measurements have been made on a 36 m isolated track length, with 56.4 kg/m Flat-bottom Rail layed on concrete sleepers, at a frequency of 50 Hz. The source voltages, currents, load impedances, sending end voltages and sending end currents are given in Table 7.1. The results for the primary constants of line self and mutual impedances and admittances, together with the ground impedance, are given in Table 7.2. The results for the secondary constants of characteristic impedance and propagation constants are given in Table 7.3.

Table 7.1: Experimental Parameters of Test Circuit

Parameter			
Test Number	1	2	3
Source Voltage $E_s(V)$	243.9 + j0	243.5 + j0	240.9 + j0
Rail Voltage $V_{ai}'(V)$	243.4 - j 8.5	243.0 - j8.5	241.3 - j6.7
Rail Voltage $V_{bi}'(V)$	242.7 - j8.5	241.5 - j8.4	239.2 - j6.7
Source Current $I_{si}(A)$	3.84 - j0.317	3.83 - j0.32	3.80 - j0.27
Rail a Current $I_{ai}(0)(A)$	2.01 - j0.16	2.23 - j0.17	2.54 - j0.15
Rail b Current $I_{bi}(0)(A)$	1.83 - j0.16	1.60 - j0.15	1.26 - j1.34
Load Impedance $Z_{Li}(\Omega)$	0.099 + j0	0.198 + j0	0.298 + j0
Sending End Series Impedance $Z_a(\Omega)$	0.12 - j4.21		
Sending End Series Impedance $Z_b(\Omega)$	0.27 + j4.65		

Table 7.2: Primary Constant Results

Parameter	Value
Self Impedance $z_{aa}(m\Omega/m)$	0.55 + j0.49
Mutual Impedance $z_{ab}(\Omega/m)$	0.51 + j0.31
Self Admittance $y_{aa}(\mu S/m)$	0.38 + j0.93
Mutual Admittance $y_{ab}(\mu S/m)$	0.048 + j 0.061
Ground Impedance $Z_e(\Omega)$	63.0 + j3.7

Table 7.3: Secondary Constant Results

Parameter	Propagation Constant γ (Napier/m) $\times 10^{-5}$	Characteristic Impedance $Z_o(\Omega)$
Single Rail	2.34 + j2.98	33.91 - j8.96
Differential Mode	3.77 + j1.25	14.04 + j1.03
Common Mode	1.57 + j2.22	26.38 - j6.11

Table 7.4: Comparison of Track Parameters at 50 Hz

Source	Z_{aa} $(m\Omega/m)$	Z_{ab} $(m\Omega/m)$	Y_{aa} $(\mu S/m)$	Y_ab $(\mu S/m)$
In situ tests	0.55 + j0.49	0.51 + j0.31	0.38 + j 0.93	0.048 + j0.061
FEM	0.53 + j0.51	0.50 + j0.29	-	-
Circuit tests	-	0.48 + j0.30	0.37 + j0.90	0.51 + j0.063
Theoretical	0.05 + j0.39	0.05 + j0.35	-	-

7.4 Discussion on Composite Measurements of Track Parameters

The results at 50 Hz are consistent with impedance and admittance values at that frequency found by other techniques and reported in Chapters 5 and 6. The exception is shown to be the theoretical expressions, as noted earlier. Table 7.4 gives a detailed comparison.

The technique described in this chapter was developed to provide an independent method of obtaining track impedance and admittance values to support the models

described in Chapters 5 and 6. The transmission line expression is exploited and by applying various termination configurations, it has been possible to obtain the impedance and admittance matrix elements for the two (running) rail system. However, the method inherently relies on comparing the series impedances and shunt impedances; these values are orders of magnitudes different and the resulting equations are ill–conditioned. Also, signals used in the test have to be large enough for measurements to be made, especially in the case of series rail potential differences, which tend to be small. Generally these restrictions cause experimental errors to be relatively large and sensitive to the values of external circuit components. Hence only a limited set of results have been presented in Chapter 7. However they do confirm the results reported in Chapters 5 and 6.

It should be noted that some practical difficulties apply when using the method described in this chapter:–

- Since successive approximation is used to solve the equations, an approximate value of Z_e is needed initially so that the algorithm has a starting point. This implies the solution may not be unique.
- The experimental method requires a large power supply at 50Hz e.g. 3 kW so that signals may be measured above noise.
- Frequency dependency is also difficult since high power sources will be required.

Chapter 8

Determination of Modal Matrix Elements of Third Rail System and Application to Simulation

As introduced earlier, one of the major subsystems necessary to simulate signal and power propagation along an electrified railway, is the rail track and track bed structure. As explained in Chapter 3, the approach chosen for the simulation of this subsystem, is that of *modal transmission line theory*, with the implementation achieved using digital computer algorithms.

To achieve this, admittance and impedance matrix elements have been determined using the methods described in Chapters 5, 6 and 7. The results, for a particular configuration, have also been presented, together with verification by analytical and numerical techniques. In this chapter, using the methods outlined in Chapter 3, these matrices are transformed such that the modal propagation constant matrix is determined. This matrix represents the (mathematical) decoupled modes of the transmission line. Hence the matrix is diagonal. The matrix provides information from which the modal impedance and admittance matrices, together with the modal characteristic impedance matrix, may be formed. These matrices are useful as they indicate the behaviour of the individual modes. The modal matrices are processed further to provide data for the simulation program. It should be noted that the values of the elements of the matrices are frequency and current magnitude dependent. The simulation data are then applied

to a number of example studies. This illustrates the applicability of the data and the simulation method chosen to the practical situation.

8.1 Development of Modal Matrices

The technique used is outlined in Chapter 3. From Equation 3.7 and 3.8, the **A** matrix is determined from the phase matrices evaluated in Chapters 5 and 6, i.e.

$$[\mathbf{A}] = [\mathbf{Y}][\mathbf{Z}] \tag{8.1}$$

The eigenvalues are determined using Equation 3.20. Equations 3.11, 8.1 and 3.18 show that the eigenvalues λ_i are the square of the modal propagation constants, that is

$$\gamma_i = \pm\sqrt{\lambda_i} \tag{8.2}$$

For the configuration analysed in Chapters 5 and 6 (the two and three rail systems) the results of modal propagation constants, with variation in frequency, are illustrated in Figures 8.1 and 8.2. It can be seen that the two rail common mode propagation constant approaches mode 1 of the three rail system. The propagation constants of modes 2 and 3 of the three rail system are equally reduced from the differential mode of the two rail system.

The eigenvectors corresponding to the eigenvalues λ_i are determined from Equation 3.21 and Appendix H. These form the columns of the **T** matrix of Chapter 3.

This then allows the modal admittance and impedance matrices to be evaluated, using Equations 3.13 and 3.14. These are illustrated in Figures 8.3 to 8.6. From Equations 3.22, it is possible to develop a modal characteristic impedance, as explained in Section 3.2. These have been evaluated from the modal values shown in Figures 8.1 to 8.6 and the results are given in Figures 8.7 and 8.8.

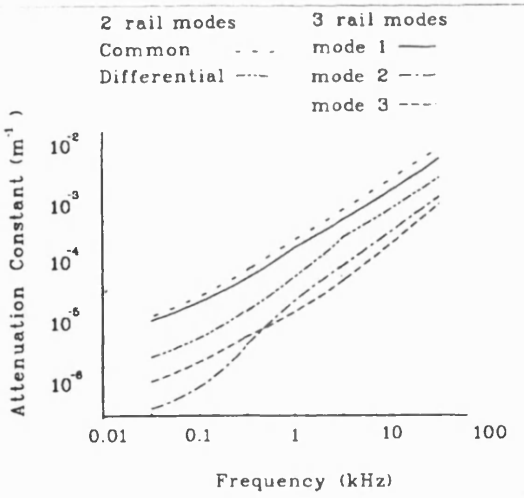

Figure 8.1: Variation in Modal Attenuation Constants with Frequency

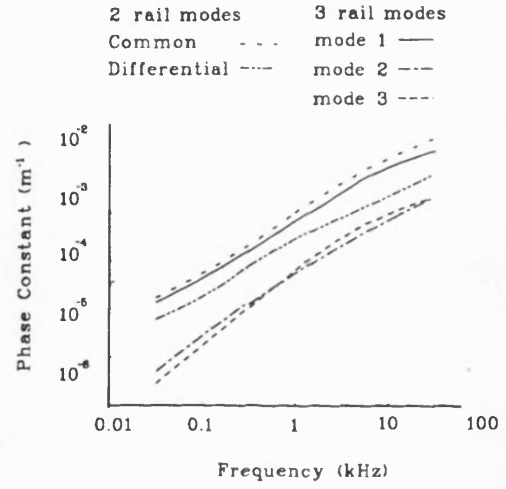

Figure 8.2: Variation in Modal Phase Constants with Frequency

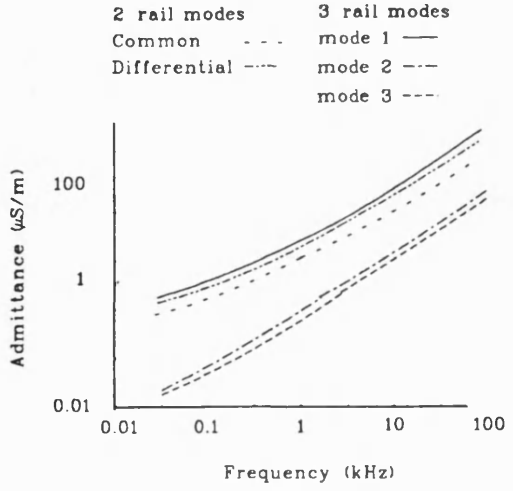

Figure 8.3: Variation in Modal Admittance Magnitude with Frequency

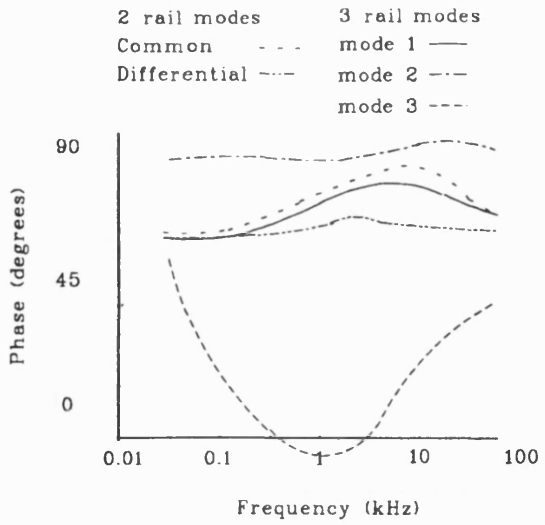

Figure 8.4: Variation in Modal Admittance Phase with Frequency

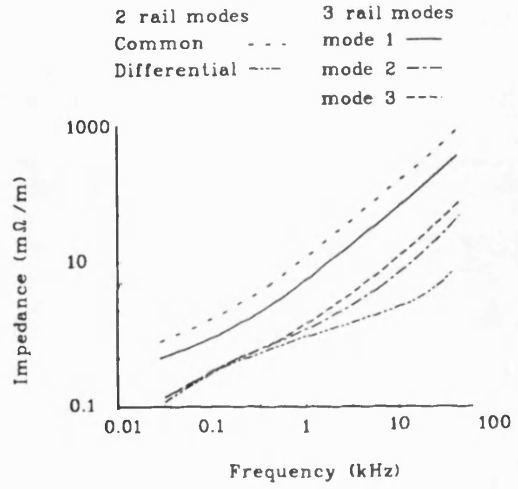

Figure 8.5: Variation in Modal Impedance Magnitude with Frequency

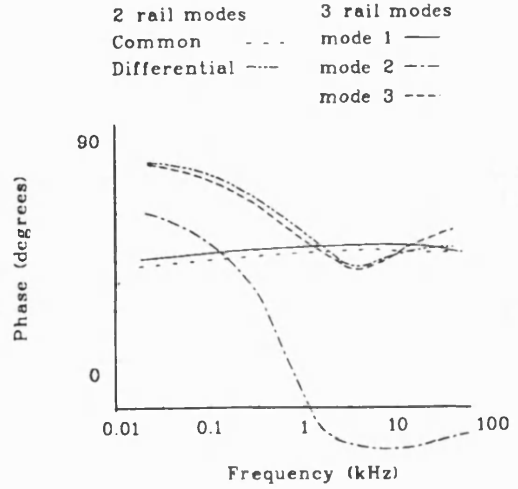

Figure 8.6: Variation in Modal Impedance Phase with Frequency

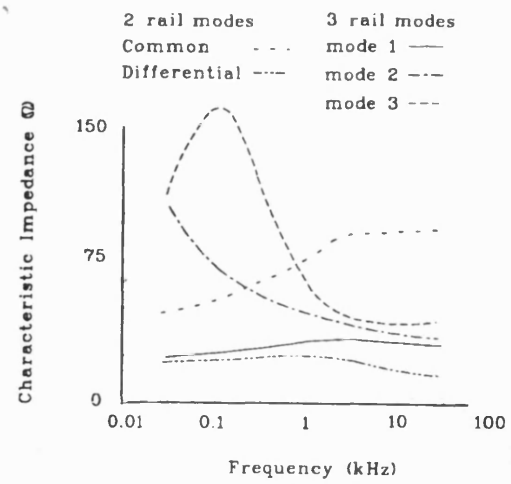

Figure 8.7: Variation in Magnitude of Modal Characteristic Impedance with Frequency

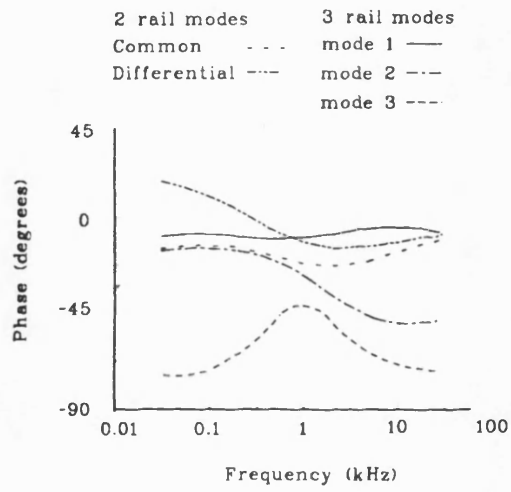

Figure 8.8: Variation in Phase of Modal Characteristic Impedance with Frequency

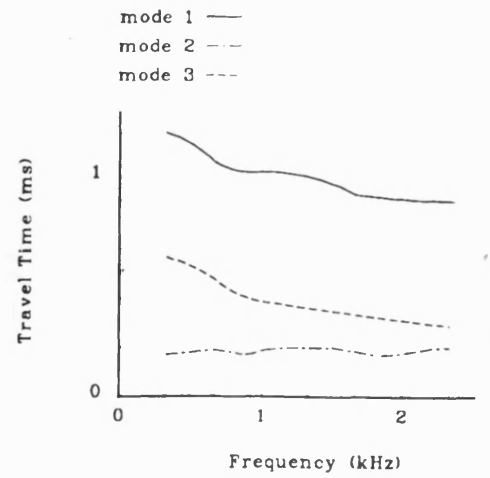

Figure 8.9: Modal Travel Time – Phase variation with Frequency for Three Rail System

8.2 Determination of Simulation Data

As has been explained in Chapter 3, the digital computer implementation of the modal analysis for general transmission lines is carried out in the time domain. It operates on a *travel time* τ, as defined by Equation 3.37. This is evaluated from the information in the preceeding section and the results are shown, with variation in frequency, for each mode of the three rail systems, over a selected frequency range in Figure 8.9. A tabulated format of all the information required to simulate a transmission line is given in Appendix F, together with an example set of data.

The relationship between transmission line length, travel time and simulation (calculation) time–step length has been carefully chosen. The calculation time–step length must be selected small enough to ensure reasonable accuracy of results[1]. The size of this time–step dictates the upper and lower limits of the transmission line length sections. The minimum length of a transmission line section must result in a travel time greater than 1 calculation time–step. The maximum length of a transmission line is constrained to have a travel time less than 200 calculation time–step lengths[2].

8.3 Discussion on Modal Matrix Elements and Parameters

In this chapter, the modal matrix elements and modal parameters have been evaluated for the two and three rail systems described earlier. These data are obtained from the

[1] Although a small simulation time–step is desirable, computation errors due to rounding errors and stability can be encountered. Additionally small time–step lengths lead to excessive computational time.

[2] Although the latter may be increased by recompiling the program, a substantial increase in computer memory is then required with the associated additional computational time requirements.

processing of the phase quantities, evaluated in Chapters 5 and 6. Equation 8.1 and 8.2 briefly summarise the relationship between phase admittance and impedance matrix elements and the modal propagation constant.

The propagation constants for the two and three rail systems are shown in Figures 8.1 and 8.2. It can be seen that the change in modal attenuation constant of the two rail system when a third rail is added does not affect the ground modes greatly. The metallic modes are more significantly affected. This indicates that there is a significant correspondence between the phase (physical system) quantities and the metallic modal quantities. This and the physical significance of a two conductor system is discussed briefly in the EMTDC manual [167]. The common mode attenuation constant of the two rail system is closely associated with that of mode 1 of the three rail system. The attenuation constant of the differential mode of the two rail system appears to be subdivided between the attenuation constants of modes 2 and 3 of the three rail system. The modal phase constants confirm this relationship but also show that the propagation constant of the differential mode of the two rail system is closely associated with the attenuation constants of modes 2 and 3 of the three rail system.

The eigenvectors of the system have been determined from these propagation constants (the square of which is the eigenvalues of the system). By using these in Equations 3.13 and 3.14, the modal admittance and impedance matrix elements have been determined. These results, shown in Figures 8.3 to 8.6, confirm the trends found in the propagation results, that is

- The common mode of the two rail system is associated with mode 1 of the three rail system.
- The differential mode of the two rail system is associated with modes 2 and 3 of

the three rail system.

- The variations between the associated modes is due to the addition of the third rail.

These observations are further emphasised by the modal characteristic impedance results given in Figures 8.7 and 8.8. Also the travel times for the three rail system have been evaluated and are shown in Figure 8.9. This together with the modal resistance and characteristic impedance show that the ground or zero sequence mode is mode 1 of the three rail system and hence the common mode of the two rail system[3].

8.4 Example Applications of Simulation Method

8.4.1 Track Circuit Simulation

The circuit details of a Westinghouse FS 2500 AF track circuit, having a carrier frequency of 4080 Hz, have been supplied by the manufacturers[4]. This allows a number of simulations to be performed to model the operation of the circuit with the measured track data shown earlier. These data refer to the two (running) rail system. The track circuit not only detects the presence of trains but can be used to provide information relating to a *broken rail*[5] condition. To separate adjacent track circuits, a tuned area is fitted at either end of the circuit [182].

The overall model is illustrated in Figure 8.10, showing how the presence of a train axle

[3]The ground or zero sequence mode is identified by having higher modal resistance, characteristic impedance and travel time.

[4]Where exact details have not been supplied, tests have been carried out on track circuit equipment supplied by Westinghouse.

[5]A break in the rail is detected when the signal is removed from the track circuit receiver.

can be simulated, as well as the occurrence of a broken rail. The ends of the rail section are terminated with the characteristic impedance, implying that the total length of the track is very large compared to the track–circuit length. The total track circuit length was set at 400 m with 7 m tuned areas.

The output condition of the track circuit is the receiver signal, determined by the voltage at the receiver terminals. Depending on the transmitted signal (i.e. *the input*), the receiver terminal voltage magnitude (*the output*) indicates the track circuit condition. Hence the simulation results, for train axle detection with variation in axle position, are given as a ratio of transmitted voltage magnitude to received voltage magnitude, as shown in Figures 8.11 and 8.12.

The function of the track circuit is dependent on the tuned area operation. Hence a more detailed study of the tuned area has been carried out. Again, the ratio of received voltage to transmitted voltage, with axle position, has been simulated. The results are given in Figure 8.13

8.4.2 Simulation of Electrified Three Rail Track

Although it is possible to simulate a d.c. power rail fed electrified traction track with complete track circuit signalling, only a subset of the system has been selected so that the features of the simulation are clear. The simplified system was chosen to test the modal method rather than provide a full simulation of a realistic case. In this study the power circuit has been simulated since examples of a signalling circuit have been examined earlier. This allows the salient features of coupling between rails of the track due to the power supply and traction drive signals to be examined. These signals include harmonic frequencies generated by substation ripple and train borne power electronic

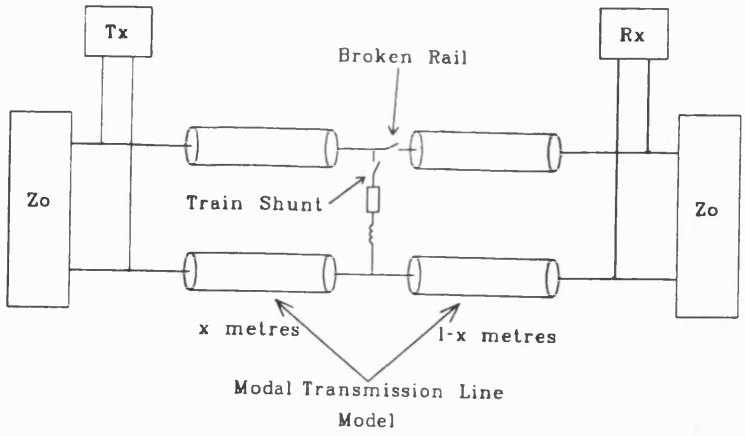

Figure 8.10: The Overall Model for Track Circuit Simulation Study

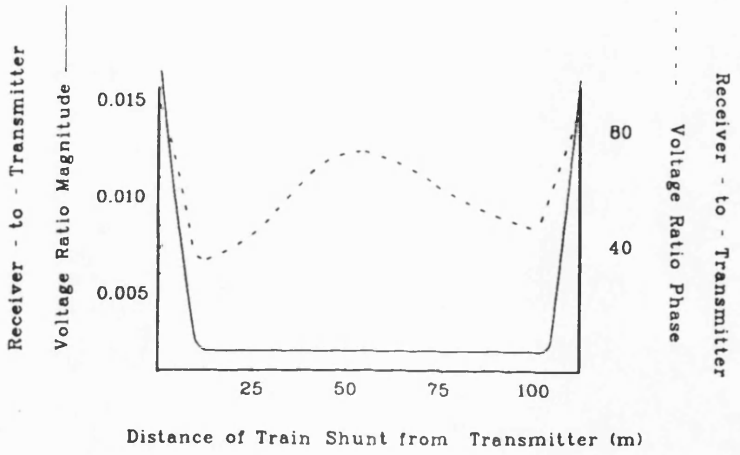

Figure 8.11: Results from Simulated Track Circuit Operation for Train Detection

drive circuits.

The track data have been taken from that evaluated for the three rail configuration, described earlier. The geometric arrangement is one in which the power rail lies outside the two running rails (but in close proximity to one). A track length of 24 km has been simulated, although by terminating in the characteristic impedance, the track appears to be infinitely long.

Two simulation studies have been carried out, in order that the influence of coupling between tracks can be examined. To achieve this, substation ripple has been examined

separately from chopper circuit noise. The substation–to–train distance is 4 km and the circuit response has been examined at a number of points along the track. The overall simulation arrangement is shown in Figure 8.14.

Substation Ripple Harmonics

The substation model is of an uncontrolled 12–pulse, balanced rectifier with a nominal rating of 600 V d.c. The a.c. ripple components are represented by the Fourier series [183]

$$V = \frac{3\sqrt{3}V_{pk}}{2\pi}\left(\sum_{n=1}^{\infty}\left[\frac{1}{(12n-1)^2}+\frac{1}{(12n+1)^2}-\frac{2}{(12n-1)(12n+1)}\right]^{\frac{1}{2}} \times sin\left[12\times 2\pi f+\left(\frac{\pi}{4}-\frac{n\pi}{2}\right)\right]\right) \quad (8.3)$$

Further simulation data, adopted from earlier reported work [155], are :–

Train Converter Power	240 W
Train Axle Shunt Impedance	0.2 Ω
Impedance Bond	1.0 mΩ, 3.18 μH
Substation Impedance	0.2 Ω

The simulation results are given in Figure 8.15. The Thevenin equivalent circuit voltage and Norton equivalent circuit current are given at 1, 2 and 3 km from the substation, for rectifier ripple frequencies of 600, 1200, 1800 and 2400 Hz.

Chopper Traction Harmonics

The circuit modelled had the same characteristics and values as for the substation ripple harmonic model. However the harmonics generated by the traction equipment

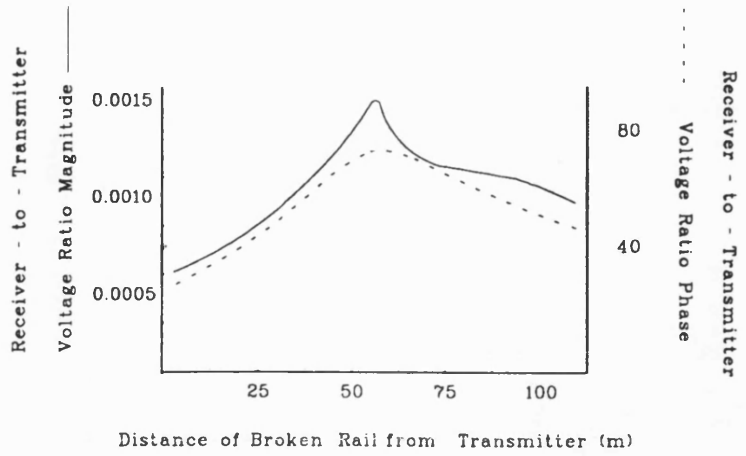

Figure 8.12: Results from Simulated Track Circuit Operation for Broken Rail Detection

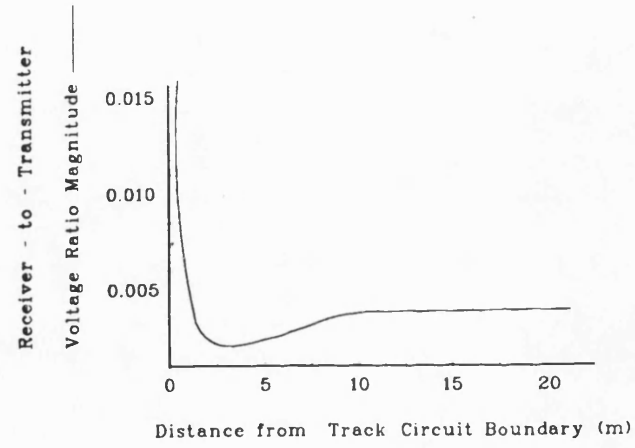

Figure 8.13: Results from Simulated Track Circuit Tuned Area

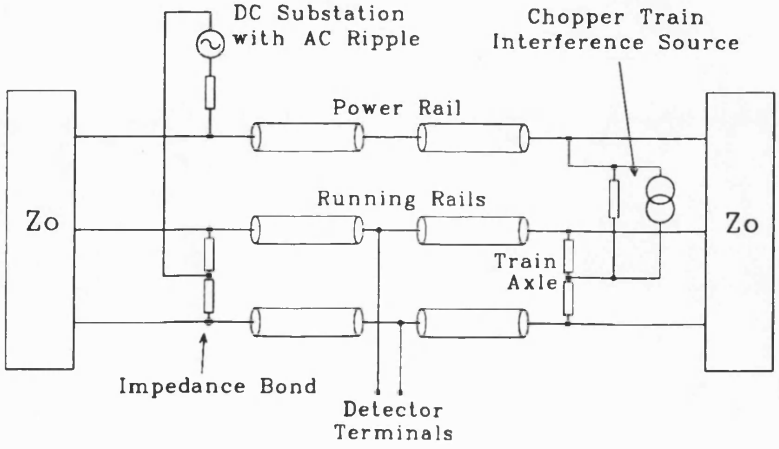

Figure 8.14: The Simulation Model for Third Rail Fed Electrified Track

are assumed to have a resistive path through the substation [184]. The chopper is a 280 Hz single–phase converter with average train power of 240 kW and is supplied through a line filter of [155]:–

Resistance	0.047 Ω
Inductance	13.8 mΩ
Capacitance	7.5 mF

The harmonic components of the chopper, prior to filtering, have been modelled by a current source which can be represented by the Fourier series

$$I = I_{pk}\left[1 + \frac{2}{\pi}\sum_{n=1}^{\infty}\frac{1}{2n-1}sin(n\omega t)\right] \tag{8.4}$$

giving a worst case condition of a square current waveform.

Again the Thevenin and Norton equivalent voltages and currents are given in Figure 8.16 for 1, 2 and 3 km from the substation, at frequencies of 280, 560, 840 and 1020 Hz.

8.5 Discussion on Example Applications

The example applications are intended to illustrate how the modal parameters derived in this thesis may be used in simulation studies. Two examples are given, a practical example of a.f. track circuit operation and a hypothetical example of the propagation of harmonic interference along a coupled line. The latter is based on signalling circuit operation and harmonic analysis of traction circuits.

Signal Circuit Simulation

The signalling circuits were modelled using the data derived earlier and additional circuit information supplied by Westinghouse Brakes and Signal Limited. The circuit simulations have examined the performance of the Westinghouse FS 2500 AF track circuit. The main functions of this system are train detection and broken rail detection, although a capability exists to provide track–train data transmission.

The results obtained from the simulation are in agreement with the practical track circuit operation, given that the track bed measurements have been performed on a "new" track structure. The effect of this is that the inter–rail impedance is high and the train detection characteristics, given in Figure 8.11, has been found to be excellent. For a more practical track bed, the performance may well be degraded.

Similar observations may be made for broken rail detection. The characteristics are shown in Figure 8.12. Again a near ideal performance has been found, over the whole length of the track circuit. In a similar way to the train detection results, if the conductance of the track bed became higher, this characteristic may well be degraded.

A further area of importance, in track circuit design, is in the region of track circuit boundaries (known as the tuned areas). This section of the circuit has been modelled

in more detail and the characteristics have been determined. The simulation is dependent on accurate circuit data. In this case the additional track side circuit elements are particularly significant. As much of this information has been supplied by the manufacturers, the simulation results are dependent on the accuracy of this information. The results shown in Figure 8.13, for the track circuit tuned area indicate system operation is as described in the manufacturers specifications.

Traction Circuit Harmonics

As has been introduced in the early chapters of this thesis, the influence of traction circuit harmonics on signalling systems is of much concern in electrified rail systems. To illustrate how the simulator may be applied to such studies, a simulation involving substation and traction drive harmonics has been carried out. The aim of the study has been to examine the effect of typical harmonics on inter–rail voltages and currents. The results, shown in Figures 8.15 and 8.16, indicate a significant frequency dependency which is not simply explained by standard circuit analysis. It is a result of the frequency response of the track seen through the models implemented by modal techniques. The results may be further developed in practical cases to predict the effect of harmonics on track circuit receivers. They have been expressed in terms of Thevenin and Norton Equivalent sources as a standard representation.

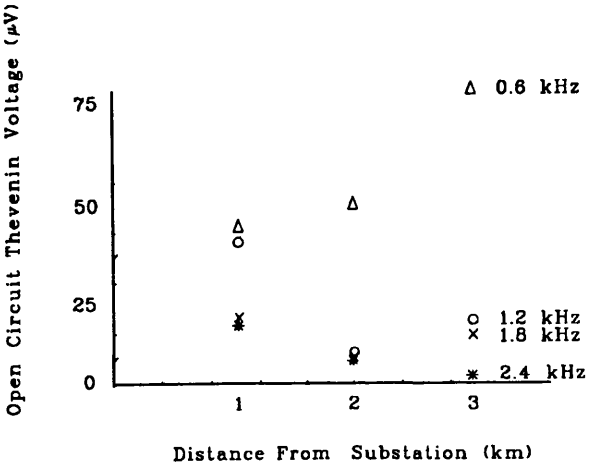

(a) Thevenin Voltage Sources

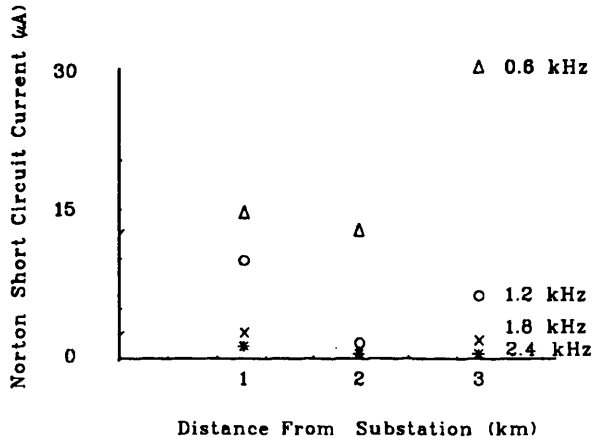

(b) Norton Current Sources

Figure 8.15: Equivalent Circuit Thevenin Voltages and Norton Currents for the Substation Ripple Simulation

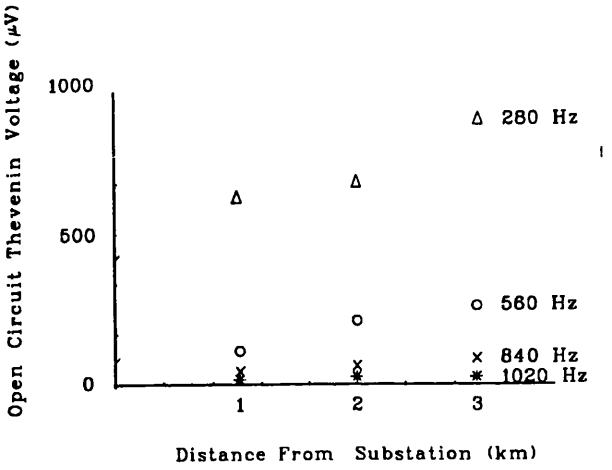

(a) Thevenin Voltage Sources

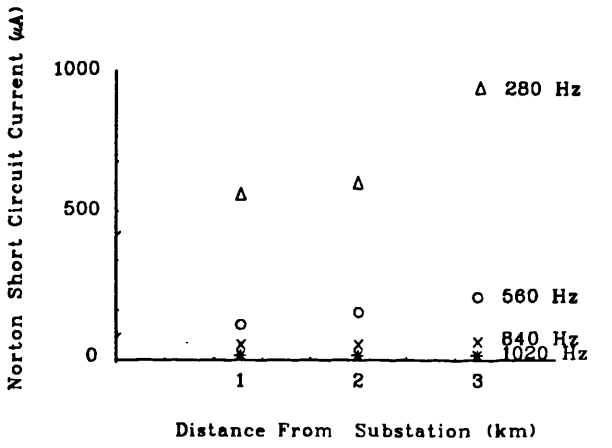

(b) Norton Current Sources

Figure 8.16: Thevenin and Norton Equivalent Sources for the Chopper Harmonic Simulation

Chapter 9

Simulation Data for a Catenary System

In Chapters 3 to 8, it has been shown that it is possible to apply transmission line modal analysis to an electrified, three rail system. The earlier chapters describe approximate theoretical and accurate numerical analyses that have been used to determine the electrical characteristics of the track. These methods have been confirmed by measurements. Chapters 3 and 8 also describe the technique used to apply these electrical characteristics in modal analysis for circuit simulation.

In this chapter, the numerical methods developed earlier are applied to an alternative electrified track configuration. The characteristics of a catenary fed electrified track have been determined and these values have been applied to the modal transmission line analysis. The dimensions of this configuration are given in Appendix G. This analysis is used to examine the system performance, contrast the results to the third rail case and compare the F.E.M. phase impedances and admittances to those published elsewhere [185] [189].

9.1 Track Phase Characteristics

The model described here is intended to represent the track in the vicinity of a train where return current flows along the rails and ground rather than through a return conductor. Thus it models both D.C. catenary directly and A.C. simple feeding (without booster or autotransformers which modify the current path). Even so, some notable

differences exist between the third rail and catenary system models. In the catenary feed, two conductors supply current in parallel. The contact wire is suspended vertically below the actual catenary wire. The three rail feed system has only one conductor (the third rail) supplying the power current. In addition, the contact wire is not ferromagnetic.

Since the published measurements [185] have only included a single value of ground conductivity, with depth and frequency, this simple approach has been adopted here. The effect of this is considered at the end of the chapter, although it is of interest that this is closer to the analytical model assumptions, considered earlier.

The phase impedance matrix element values are illustrated in Figures 9.1 and 9.2, for two values of conductivity, 0.0033 S/m and 0.077 S/m, which were chosen to correspond to actual low and high [185] measured values. The elements for both impedance and admittance matrices have been evaluated, using the Finite Element Technique. The definition for these matrix elements, and the matrices themselves, have been described in Chapter 3.

The impedance results are expressed in terms of magnitude and phase. Conductor 1 refers to the catenary and 2,3 refer to the running rails. The self impedance values of z_{11} and $z_{22} = z_{33}$ are similar since the return path in each case is through the earth. The earth has a significant influence on the values z_{ii}, in terms of both resistance and reactance and the values of ground conductivity thus have a predictable if moderate effect on the impedance matrix element values, i.e. the impedance increases with decrease in conductivity.

The phase admittance matrix element values are also illustrated in Figures 9.3 and 9.4 in the same form as the impedance values. It can be seen that an increase in conductivity causes an increase in admittance, as is to be expected. Since the catenary is insulated

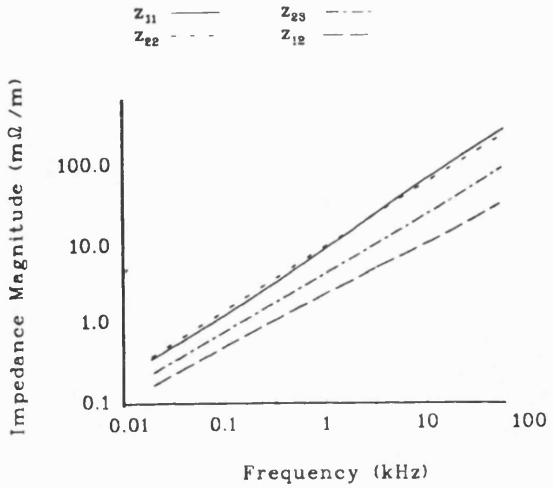

a) Impedance Magnitude

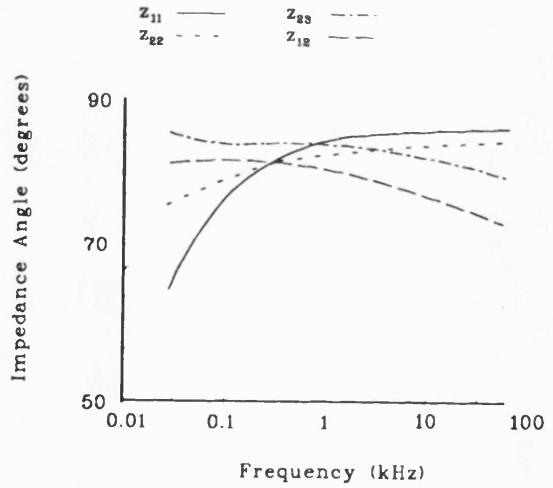

b) Impedance Phase

Figure 9.1: Catenary Phase Impedance Matrix Elements ($\sigma_{gnd} = 0.076923 S/m$)

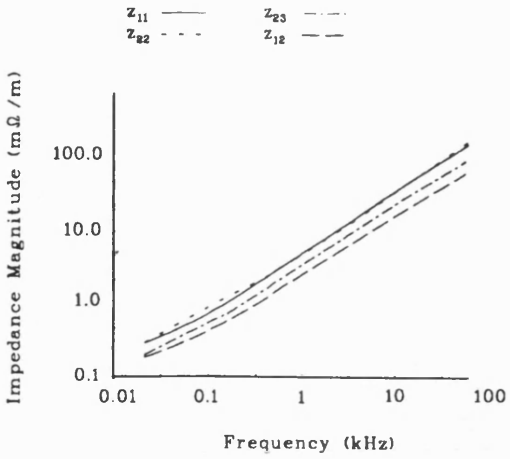

a) Impedance Magnitude

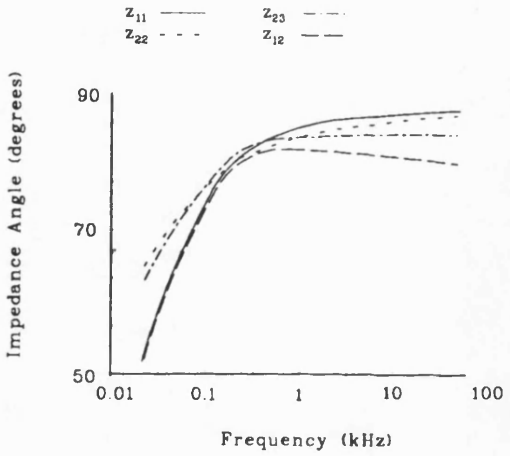

b) Impedance Phase

Figure 9.2: Catenary Phase Impedance Matrix Elements ($\sigma_{gnd} = 0.00333 S/m$)

from ground, the admittance matrix element values y_{11} and y_{12} are reactive in nature. In contrast, the element values associated with the running rails are dominated by the conductive component. It should be noted that the catenary capacitance and inductance are constant with frequency and in agreement with other published results [185] [189].

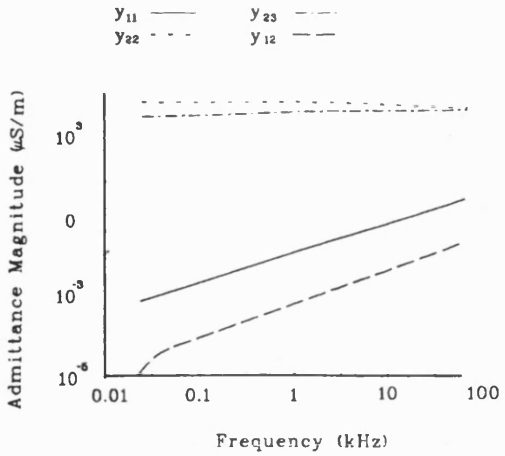

a) Admittance Magnitude

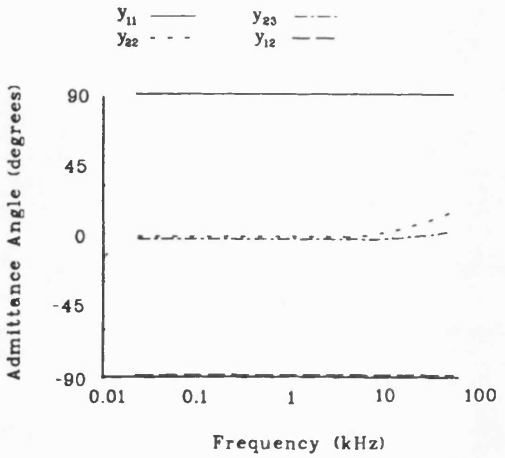

b) Admittance Phase

Figure 9.3: Catenary Phase Admittance Matrix Elements ($\sigma_{gnd} = 0.076923 S/m$)

9.2 Modal Characteristics

It has been described, in Chapter 3, that the modal propagation constants may be determined from the phase matrix elements. These constants have been evaluated from the phase values shown in Figures 9.1 to 9.4. The results are illustrated in Figures 9.5 and 9.6 in terms of attenuation and phase constant (i.e. real and imaginary parts), for the two values of ground conductivity.

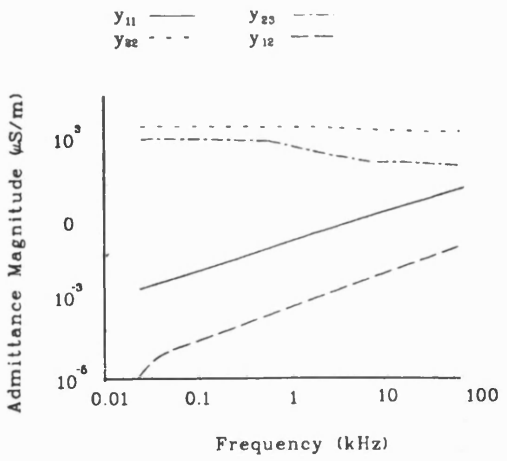

a) Admittance Magnitude

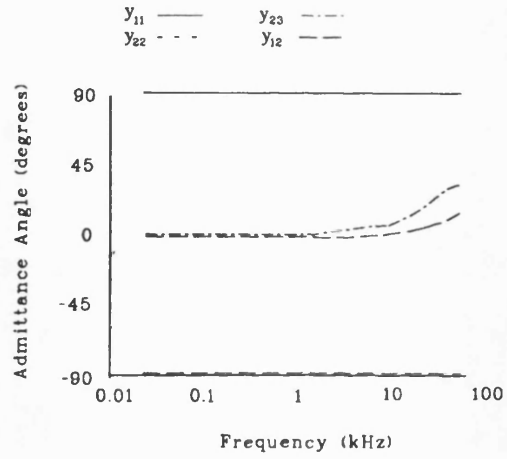

b) Admittance Phase

Figure 9.4: Catenary Phase Admittance Matrix Elements ($\sigma_{gnd} = 0.00333 S/m$)

As with the three rail system, it can be seen that two of the modal propagation constants are close together, with the third significantly lower in value. Although direct physical significance cannot easily be associated with the modes, the symmetry of the system, together with some similar features, cause the analysis to produce similar results. The influence of the ground conductivity is only of minor significance here.

The modal impedance and admittance matrix elements have also been evaluated and are illustrated in Figure 9.7 to 9.10 in magnitude and phase form.

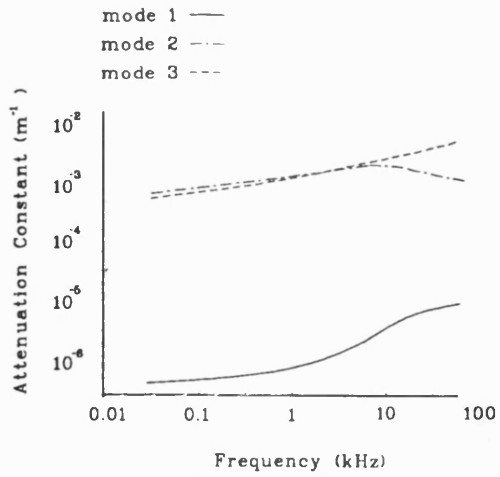

a) Attenuation Constant

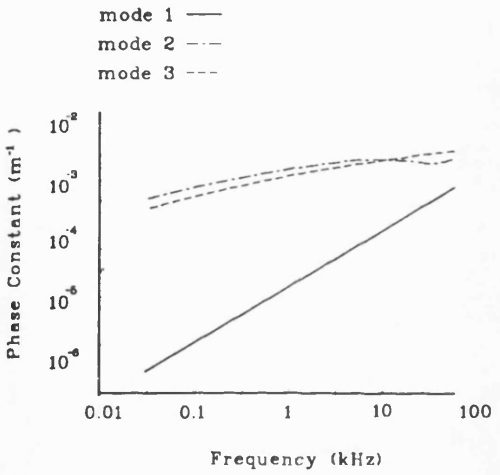

b) Phase Constant

Figure 9.5: Catenary Modal Propagation Constant ($\sigma_{gnd} = 0.076923 S/m$)

Mode 2 is often termed the "ground" or "common" mode. This is significant when ground currents flow and is identified by the larger characteristic impedance. The other two modes are termed metallic modes and are significant when circuit currents are present. The significance of the variation in ground conductivity is only small.

9.3 The Influence of the Ground Conductivity Model

For the three rail system, it has been shown earlier that the ground conductivity has

been evaluated as a continuous function with depth and frequency. In the case described in this chapter, since it was intended to compare the measurements with published work, so the ground conductivity was assumed uniform and constant. The agreement between these numerical analyses and the published measured results for catenary inductance and capacitance was good. Good agreement was also found between these methods and the approximate analytical techniques based on Carson's equations [92] as implemented by Bickford et al. [136] described earlier. This was to be expected since the analytical methods also assume constant ground conductivity with frequency (but may include a two layer model as in the approach by Bickford et al.). This is in contrast to the ground conductivity model which varies with depth and frequency (i.e. the three rail system model). In this case the approximate analytical method did not give good agreement for the real part of the impedance matrix elements, although values from numerical methods and measurements did agree.

The influence of the insulated catenary can be seen in the modal admittance matrix element values, since one mode is purely reactive in nature (as has been found for the phase matrix elements).

The modal characteristic impedances are also illustrated in Figures 9.11 and 9.12.

9.4 Discussion on Modelling of Catenary Systems

To illustrate that the techniques used to determine the electrical characteristics of the three rail system are applicable to any rail track configuration, a catenary electrified rail track has also been examined. The fundamental measurement data had been published elsewhere [185] for the Skawina–Chabowka Railway line in Poland. These were used to provide dimensional information and ground conductivity data for modelling of the track

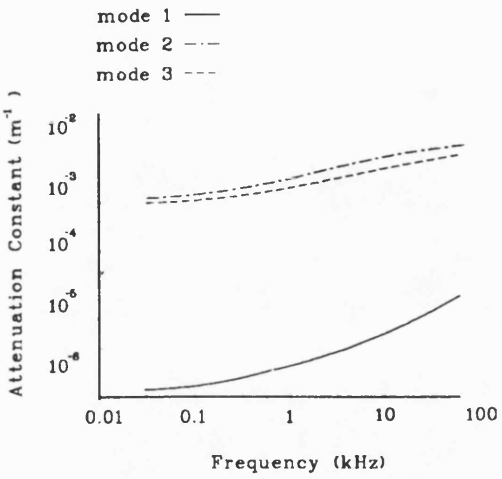

a) Attenuation Constant

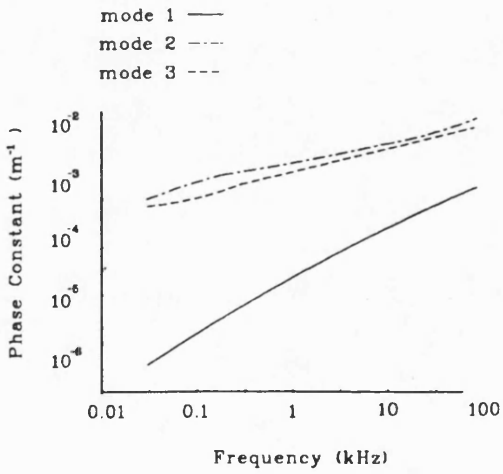

b) Phase Constant

Figure 9.6: Catenary Modal Propagation Constant ($\sigma_{gnd} = 0.00333 S/m$)

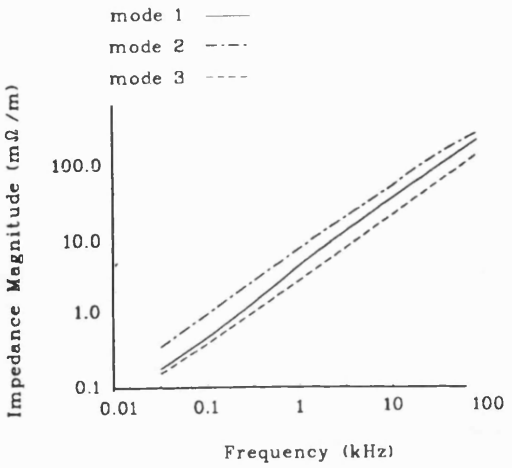

a) Impedance Magnitude

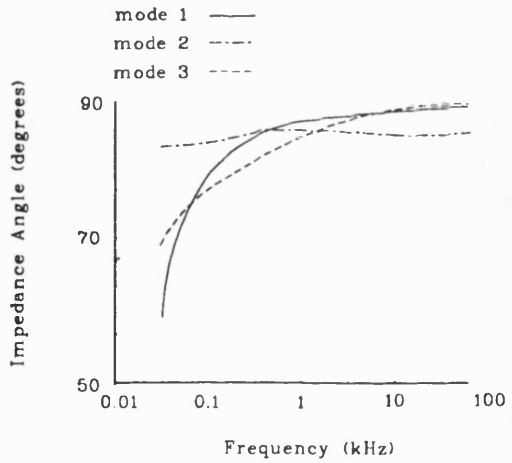

b) Impedance Phase

Figure 9.7: Catenary Modal Impedance Matrix Elements ($\sigma_{gnd} = 0.076923 S/m$)

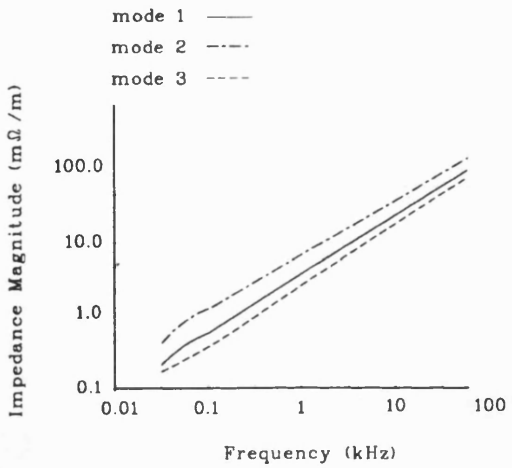

a) Impedance Magnitude

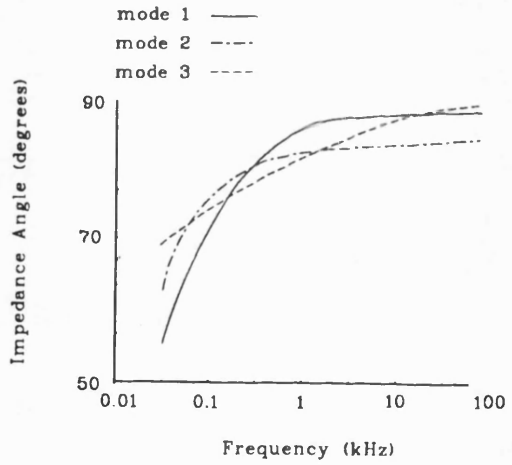

b) Impedance Phase

Figure 9.8: Catenary Modal Impedance Matrix Elements ($\sigma_{gnd} = 0.00333 S/m$)

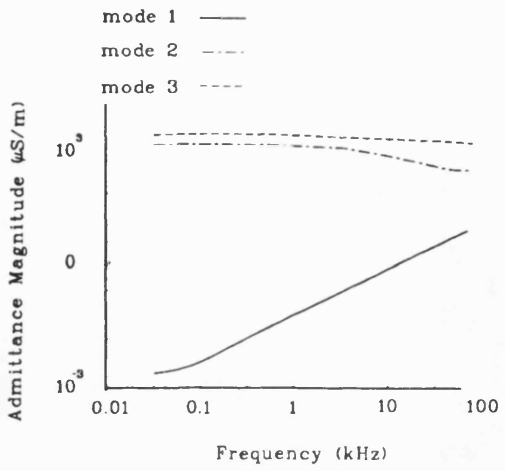

a) Admittance Magnitude

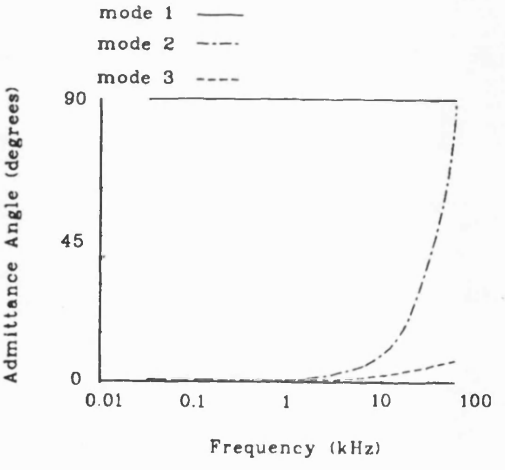

b) Admittance Phase

Figure 9.9: Catenary Modal Admittance Matrix Elements ($\sigma_{gnd} = 0.076923 S/m$)

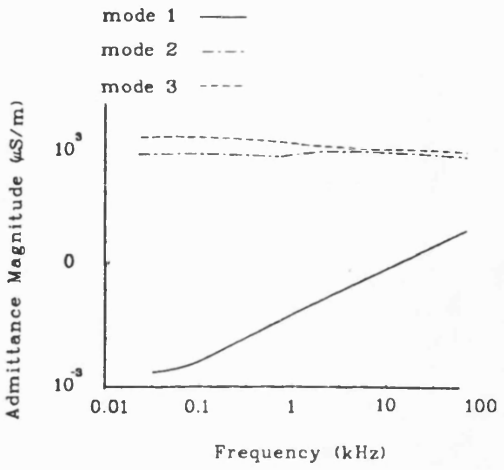

a) Admittance Magnitude

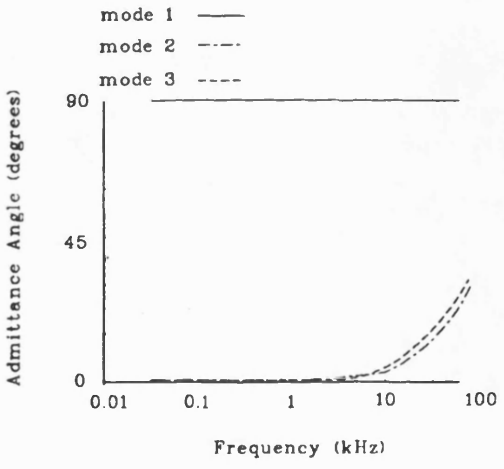

b) Admittance Phase

Figure 9.10: Catenary Modal Admittance Matrix Elements ($\sigma_{gnd} = 0.00333 S/m$)

system, allowing the track characteristics to be evaluated and certain results compared with published measurements.

The phase characteristics have been determined for two values of (constant) ground conductivity. These values represent the maximum and minimum values found on the Skawina–Chabowka Railway line. Hence upper and lower bounds have been established for the track characteristics. The results of the numerical modelling have been presented in Figures 9.1 to 9.4. They are in the form of magnitude and phase since some of the catenary to rail admittances are reactive only. This representation clearly indicates this feature. The catenary capacitance is approximately 11 nF/km and the catenary–to–rails inductance is approximately 1.4 mH/km which are in agreement with the published work [189].

As is to be expected, the results show similar features to the three rail system in that the impedance magnitudes are comparable. The rail–to–rail admittances are also very similar to the three rail case. Differences in these results for the two track configurations (i.e. three rail and catenary systems) is accounted for by the method of modelling the ground conductivity and the values of ground conductivity used. In the catenary case, the model for ground conductivity is uniform (following the published data) and the values are taken for the Skawina–Chabowka Railway.

A major deviation between the two systems occurs with the power feed conductor. The power rail has approximately comparable characteristics to the two running rails, as described earlier. In this chapter, for the catenary system it has been shown that the admittance is not only smaller than for the rails but is almost completely reactive in nature. As stated above, this is in full agreement with the characteristics of the practical circuit.

The modal data for the catenary system have also been evaluated and are given in Figures 9.5 to 9.12. It can be seen that the differences in the phase data cause marked changes in the modal information. The variations in range of the individual propagation constants (Figure 9.5 to 9.6) is smaller when compared with the three rail system and the separation between mode 1 and modes 2 and 3 is larger. This feature is not clearly seen in the modal impedance matrix element values but is a dominant feature of the modal admittance matrix elements. This is carried over to the characteristic impedance matrix elements in Figures 9.11 and 9.12.

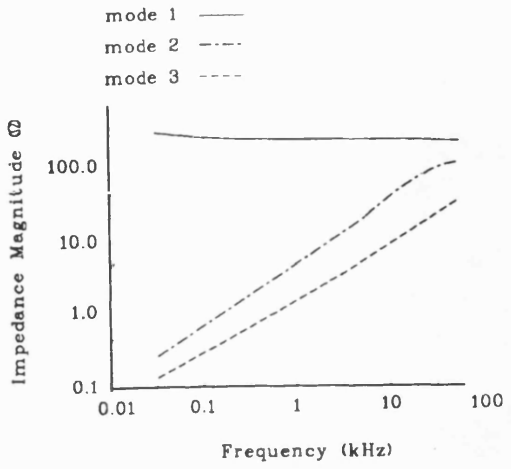

a) Impedance Magnitude

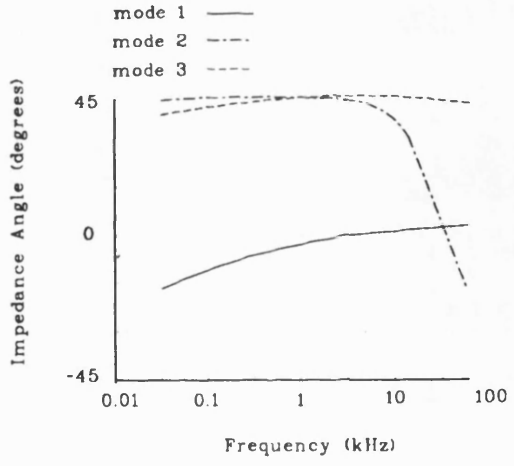

b) Impedance Phase

Figure 9.11: Catenary Characteristic Impedance Matrix Elements ($\sigma_{gnd} = 0.076923 S/m$)

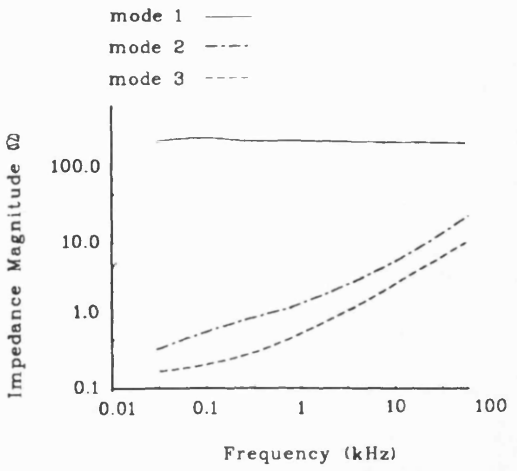

a) Impedance Magnitude

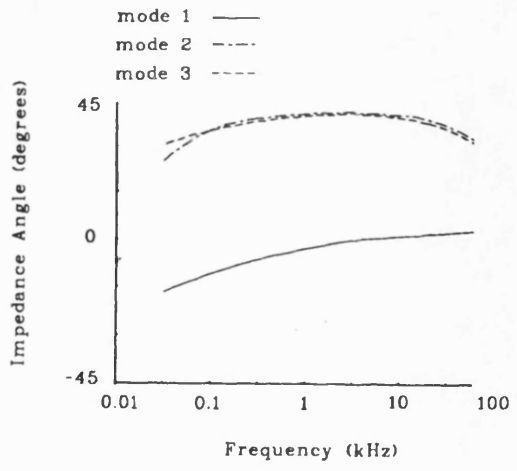

b) Impedance Phase

Figure 9.12: Catenary Characteristic Impedance Matrix Elements ($\sigma_{gnd} = 0.00333 S/m$)

Chapter 10

Discussions, Conclusions and Further Work

10.1 Summary and Scope of Thesis

This thesis has outlined the need for numerical simulation of electrified rail track. A review of the basic operation of traction power feed systems and drives, together with signalling and control techniques commonly used has been provided. An important application of the work is the problem of E.M.I. between track signalling, power supply and traction systems.

A brief comparison between circuit representation methods for the rail track was made and a multimode transmission line analysis was chosen as a suitable approach. A detailed examination of the necessary simulation technique and selection of a suitable solution method has been given. The main benefits of the modal approach are

- For systems with parallel electric tracks, simulation with coupled transmission lines is advantageous. The use of modal analysis allows each transmission line to be decoupled from the others. This implies less computational effort is necessary to calculate system performance than for a fully coupled circuit in the time domain, especially when considering mutual impedance and admittance coupling between all rails of all tracks.

- The use of modal analysis involves the simulation package constructing equivalent

single phase lines and assigning to each a specific travel time delay. A conventional lumped representation would require many transmission line 'T' and 'PI' sections to suitably represent long multiconductor lines. This would involve the setting up of very large conductance matrices with significant penalties in computational effort required for inversion and storage.

- An extra overhead when using the multi–mode method is the transformation between phase and modal quantities. However, this is achieved by a once-only domain transformation which requires limited computational effort. Appendix H illustrates the code used to produce all the required output for the simulation using the *Mathematica* mathematical analysis package [192].

For an accurate track simulation, precise evaluation of the electrical track parameters is essential. The starting point is the track phase impedances and admittances; considerable effort was expended in deriving these values. A significant part of this thesis has been the identification of suitable methods for the evaluation of track electrical parameters, so a review of measurement methods, together with the numerical and analytical techniques required to implement and extend them, was made. A full understanding of physical processes determining both the phase and modal values has been obtained. Their expression as matrix elements is convenient since transformation between phase and modal domains is then straightforward.

Several complementary techniques have been used to determine these phase quantities. As part of a practical approach to the parameter identification, a series of experimental methods have been developed. In summary these are:–

- Discontinuous rail measurements to directly determine the phase admittance matrix elements for a two (running) rail system.

- Inter–rail admittance measurements (for a three rail configuration), the results of which yield the phase admittance of the power conductor (after some processing).
- Isolated rail measurements, developed so that internal impedance of traction rail can be determined directly. This has included a.c. signals and small signals superimposed on d.c.
- The use of triple short–circuit rail measurements to provide phase impedance matrix element values (after some processing).

One of the main complications of the determination of the phase matrix elements is that the true system earth plane is remote and so not available for inclusion in the test procedure. The techniques shown above have been developed such that the elements can be determined without connection to this earth plane.

To ensure that the experimental results provide accurate data, the results have been compared with analytical and numerical methods. These methods rely on accurate material properties and these have been determined for both conductors and track bed. Hence further experimental techniques have been used to identify these material data. In summary:–

- Measurement of rail magnetic material to obtain values of permeability as a function of current and frequency.
- Measurement of rail conductivity
- Development of test procedures and subsequent data analysis methods to determine the conductivity of the track bed as a function of frequency and depth.

These material data have then allowed analytical and numerical methods to be used for validation of the experimental results.

The analytical approach, based on the Carson–Pollaczek equations, provide reasonable agreement for many cases of series impedance matrix elements. However it has been shown that in certain circumstances agreement is not good. This is due to a number of reasons. Since the conductor shape is not accounted for, the series resistance tends to be inaccurate at high frequencies. Also the equations have been developed for power system analysis and do not cope with conductors having leakage to ground. Hence in some cases the analytical methods show divergence from experimental results. As this did not occur with the numerical methods, the analytical techniques are considered to be unreliable for certain conditions.

As a third approach to parameter evaluation, the F.E.M. analysis of the rail track system, in two dimensions, has been fully analysed. It has been shown that this numerical method provides a consistent accurate technique for track electrical parameter calculation. This offers a very cost effective means of providing phase matrix data compared with extensive experimental testing. These data are then processed into modal matrix information for simulation studies.

Since the processing of phase data to modal information has been shown to be achievable at moderate computational cost, the modal transmission line analysis provides an efficient method of multi–track simulation. The computational cost diminishes, as the number of tracks (or rails) increases when compared to traditional "PI" or "T" circuit analysis methods.

The application of the F.E.M. technique for phase analysis combined with the modal transmission line simulation offers signalling and traction engineers a powerful set of computational tools for system design. This is especially the case when the simulator permits external circuit elements to be added to the model.

10.2 Main Achievements

The novel aspects reported in the thesis are concerned with the evaluation of rail track impedance and admittance together with the use of the data within circuit simulation. The main areas of novelty have been (or are in the process of being) published[1] and are:–

- Development of a practical model to account for hysteresis in rail steel using a complex permeability approach, including a supporting measurement technique. The model has been successfully applied to internal rail impedance which is non-linear with frequency and current. Papers 2,3,4,7 and 9 in Appendix I have been published on this topic.

- A method to measure soil conductivity as a function of depth and frequency has been developed, together with a method to obtain track self and mutual conductance from the results. Paper 15 has been accepted for publication on the topic and the results of the method have been used in papers 1, 5, 6, 10, 13 and 14 in Appendix I.

- F.E.M. modelling of rail track admittance and impedance, using software packages with confirmation of the results experimentally and/or from analytical theory. F.E.M. is the subject of papers 6, 10, 11, 13 and 14 in Appendix I.

- A contribution to the development of an in situ measurement technique for track impedance and admittance using a transmission line approach. Paper 12 in Appendix I has been published on this topic.

[1] Papers 1 to 12 in Appendix I have been published and papers 13 to 16 have been accepted for publication.

- Use of the impedance and admittance values in a modal transformation to derive modal data. Included here is a demonstration of how the modal results can be used in a circuit simulation package to model track circuit operation and further applications in modelling E.M.I. propagation between signalling, power supply and traction systems has been given. Paper 8 in Appendix I has been published on this topic.

10.3 Further Work

Although the project described in this thesis has successfully demonstrated methods of obtaining accurate modal data from electrified rail track simulation, several avenues of further work have been identified.

- An independent method of evaluating ground permittivity would further confirm that the F.E.M. models provide accurate data for the reactive part of the admittance matrix elements. Although some time and effort has been expended in attempting this, the conductivity of the ground has always dominated the measurements in the frequency range of interest.

- Examination of multi–track simulation would be of further interest as a development (rather than a research topic). Comparison with practical data, i.e. experimental results or system performance criteria, would give further confirmation of the accuracy of track data and simulation method.

- A full study of the flat bottom rail (as a conductor) has been given in this thesis. However many more recent rapid transit systems use novel and varied rails, track bed configurations and power feed conductor types. These variants could form the

basis of a further study to examine the influence of such modifications on system performance.

- A large variety of traction drives and control circuits should be examined to gain a wider appreciation of their influences in the problem of EMI into signalling circuits. This should be coupled with the simulation of active power supply systems to allow regenerative breaking schemes to be simulated.

- Following the experiences of using power system software for electrical track simulation, it is felt that more efficient algorithms could be developed. This implies that there is a requirement for writing original software, dedicated to rail–track performance simulation. This would be a longer term aim in the category of further work.

Bibliography

[1] Sykes W.J.A. "The Bournemouth Electrification". Journal of the Institution of Locomotive Engineers, 1968–1969, Volume 58, Part 5, Paper 710, pp. 445–488.

[2] Glover J.D, Kusko A, Peeran S.M. "Train Voltage Analysis for A.C. Railroad Electrification". Conference Record of the Industry Applications Society IEEE–IAS–1982, Annual Meeting, San Francisco, CA, 4–7 October 1982, pp. 207–216. (New York : IEEE 1982).

[3] Suddards A.D. "Electrification Systems". Rail Engineering – The Way Ahead, Volume 1, Institution of Mechanical Engineering, September 1975, pp. 279–293.

[4] Spenny C, Kusko A. "Survey of Worldwide Railroad Electrification". First Rail Systems Technology and Operations Symposium. Jointly sponsored by Carnegie–Mellon University and the Federal Railroad Administration, Pittsburgh, PA, December 2, 1980.

[5] Cole A.H, Roper H, Whittaker F. "Development of Power Supply and Supervisory Equipment for British Railways 50 Hz A.C. Electrification". Proceedings IEE, Volume 119, Number 2, February 1972, pp.189–199.

[6] Kneschke T. "Electrical Power Supply Configurations on 10,000 Miles of U.S. Railroads". Department of Transportation (USA) Contract No. DTRS–57–80–C–00042 (prepared by Electrak Inc.).

[7] Howard N. "System of Electrical Power Supply for 25 kV A.C. Electrification on British Rail". Elektr Bahnen, Volume 78, Number 8, August 1980, pp. 198–202.

[8] Bozkaya H, Shao Z.Y, Allan J, Mellitt B, Goodman C.J. "A Comparison Between Autotransformers and Booster Transformers for A.C. Traction Supply".

International Conference on Electric Railway Systems for a New Century (Conf. Publication No. 279) London, 22–25 September 1987, pp. 114–118. (London : IEE 1987).

[9] Mellitt B, Allan J, Shao Z.Y, Johnston W.B, Goodman C.J. "Computer–Based Methods for Induced–Voltage Calculations in A.C. Railways". Proceedings IEE, Volume 135, Part B, Number 1, January 1990, pp. 59–72.

[10] Machczynski W. "Currents and Potentials in Earth–Return Circuits Exposed to Alternating Current Electric Railways". Proceedings IEE, Volume 129, Part B, Number 5, September 1982, pp. 279–288.

[11] Kneschke T.A. "Substation Spacing for A.C. Electrified Railroads — Some Influencing FActors". Proceedings ASME/IEEE Railroad Conference, Eire, PA, 19–22 April 1982, pp. 23–29.

[12] Kneschke T.A. "Simple Method for Determination of Substation Spacing for A.C. and D.C. Electrification". Conference Record : 1985 IEEE Industry Applications Society Annual Meeting. (Cat. No. 85CH2207–9) Toronto, Ontario, Canada, 6–11 October 1985 (New York : IEEE 1985) pp. 274–284.

[13] Cesario P, Passalacqua R, Pozzobon P, Sciutto G. "Analysis and Design of Electric Traction Systems : Performing Digital Simulation by E.M.T.P.". Second International Conference on Computer Aided Design, Manufacture and Operation in the Railway and Other Advanced Mass Transit Systems : Comprail 90, Rome, Volume 2 : Computer Applications in Railway Operations, 27–29 March 1990.

[14] Harprecht W, Seifert R, Kiessling F. "Tractive Power Supply at German Federal Railway's 400 km/h–Runs". 1989 IEEE/ASME Joint Railroad Conference, Philadelphia, PA, April 25–27, 1989, pp. 23–32

[15] De Koranyi L. "Design of D.C. Power Supply for Rapid Transit Systems". IEEE Transactions on Industry and General Applications, Volume 1, Number 2, March/April 1965, pp. 123–130.

[16] Lincoln H.S. "Power–Supply Engineering for D.C. Traction Schemes". Rail Engineering International, November/December 1975, Volume 5, Number 8, pp. 335–336.

[17] Holden W.H.T. "Electrical Systems for Rapid Transit Railroads". IEEE Transactions on Industry and General Applications, Volume 7, Number 5, September/October 1971, pp. 580–587.

[18] Suzuki T. "D.C. Power–Supply System with Inverting Substations for Traction Systems using Regenerative Brakes". IEE Proceedings, January 1982, Volume 129, Part B, Number 1, pp. 18–26.

[19] Mellitt B, Goodman C.J., Arthurton R.I.M. "Simulation Studies of Energy Saving with Chopper Control on the Jubilee Line". Proceedings IEE, 1978, Volume 125, Number 4, April 1978, pp. 304–310.

[20] Gondo T. "D.C. Railway Feeding System". Meiden Review (International Edition), Number 2, 1988, pp. 14–16.

[21] Olsen C.K. "Propulsion–Power Supply System for San Francisco Bay Area Rapid Transit". 1966 Joint ASME/IEEE Railroad Conference, San Francisco, CA, May 1966, (IEEE Paper Number 34 CP 66–205), pp. 1–13. (New York : IEEE 1966).

[22] Miller R.H. "The Design and Operation of the BART Power System". IEE Transactions on Industry Applications, Volume 10, Number 5, September/October 1974, pp. 560–566.

[23] Lincoln H. "Providing the 1500 V D.C. Supply for the New Tyne and Wear Metro". Electrical Times, 11 August 1978, Number 4486, pp. 12–13.

[24] Prickett B.R. "Electrification of the Tyne and Wear Metro". IEE Proceedings, Volume 128, Part B, Number 2, March 1981, pp. 81–91.

[25] Lawton P, Murphy F.J. "Hong Kong Mass Transit Railway Power Supply System". IEE Proceedings, Volume 133, Part C, Number 7, November 1986, pp. 462–468.

[26] Water C.D, Farrell M, Grainger R.P, Leahy P.J, Mellitt B. "Dublin Area Rapid Transit". IEE Proceedings, Volume 135, Part B, Number 3, May 1988, pp. 134–150.

[27] Buchanan I.D. "Computer–Based Control of London Underground's Power Network". Power Engineering Journal, July 1990, pp. 159–163. (London : IEE 1990).

[28] Crawshaw G. "Machine Control". D.C. Versus A.C. Traction Drives, Railway Division, I.Mech.E, London, 15th March 1988.

[29] Jager A, Baechler U, Brom B. "Measures for Improving the Grid response of Thyristor Controlled Traction Vehicles". Brown Boveri Review, Volume 60, Number 12, December 1973, pp. 501–525.

[30] Wagner R. "A.C. Drive Technology for Locomotives". 1989 IEEE/ASME Joint Railroad Conference, Philadelphia, P.A, April 25–27, 1989, pp. 1–5.

[31] Lander C.W. "Power Electronics". Second Edition, McGraw–Hill : London 1987.

[32] Crawshaw G. "System Design of Voltage Fed Inverter Drives with Minimisation of Signalling Interference". International Conference on Electric Railway Systems for a New Century (Conf. Publication No. 279) London, 22–25 September 1987, pp. 68–72. (London : IEE 1987).

[33] Taufiq J.A, Mellitt B, Goodman C.J. "Novel Algorithm for Generating Near Optimal P.W.M. Waveforms for A.C. Traction Drives". IEE Proceedings, Volume 133, Part B, Number 2, March 1986, pp. 85–94.

[34] Taufiq J.A, Chance R.J, Goodman C.J. "On–line Implementation of Optimised P.W.M. Schemes for Traction Inverter Drives". International Conference on Electric Railway Systems for a New Century (Conf. Publication No. 279) London, 22–25 September 1987, pp. 63–67. (London : IEE 1987).

[35] Cardwell B.J. "Torque Control of A.C. Induction Motor Traction Drives". International Conference on Electric Railway Systems for a New Century (Conf. Publication No. 279) London, 22–25 September 1987, pp. 73–77. (London : IEE 1987).

[36] Fischer J.F. "A.C. Three–Phase Power Transmission for AMTRAK's New Locomotive F69PH–AC". 1989 IEEE/ASME Joint Railroad Conference, Philadelphia, PA, April 25–27, 1989, pp. 7–11.

[37] Smith C.M, Comer D.E. "Dual Mode Locomotive". 1989 IEEE/ASME Joint Railroad Conference, Philadelphia, PA, April 25–27, 1989, pp. 13–22. (New York : IEEE).

[38] Steimel A. "High Power Traction Converters". Draft of paper as part of private communication with R.J. Hill – University of Bath.

[39] Frielinghaus K.H. "Contingencies in the Design of the Audio Track–Circuit". Rail Engineering International, May 1974, pp. 182–188.

[40] Hill R.J. "Train Position Detection and Track–Train Data Transmission using Audio Frequency Track Circuits". Journal of Electrical and Electronic Engineering,

Australia – IE Aust. and IREE Aust, Volume 5, Number 4, December 1985, pp. 267–277.

[41] Walter M. "Recent Improvements to Track Circuits". Revue Generale des Chemins de Fer, August/September 1965, pp. 376–388.

[42] Nagase K. "An Investigation into Inadequate Train Shunting Sensitivity of Track Circuit to Running Trains". Quarterly Reports of the Railway Technical Research Institute, Volume 23, Number 4, December 1982, pp. 166–170.

[43] Iancu O.D. "Computer–Aided Design of Non–Insulated Track Circuits". Rail International, January 1974, pp. 421–436.

[44] Iancu O.D. "The Influence of Track Circuit Parameter Variation on Maximum Permissible Length". Rail International, June 1976, pp. 39–43.

[45] Iancu O.D, Giuhat R. "Non–insulated Track Circuits with Direct Coupled Receiver : Analysis Relations, Methods of Calculations". Rail International, November 1976, pp. 638–645.

[46] Harmon R.E. "Problems and Techniques in the Use of Audio Frequency Track Circuits". Railway System Controls, Volume 6, Number 1, May 1975, pp. 22–25.

[47] Gaffney P, Harris F.W. "Signalling for Mass Transit Railway – the Hong Kong Experience". Institution of Railway Signal Engineers, London, October 1988, pp. 1–19.

[48] Ogilvy H.H. "Automatic Train Control". Cybernetics and Electronics on Railways, Bulletin : International Railway Congress Association, Volume 4, Number 2, 1967, pp. 81–94.

[49] Jeffries A.E.H. "Track Circuits – Another Role". Proceedings of the Institution of Railway Signal Engineers (G.B.), 5th December 1973, (1973–1974), pp. 46–67.

[50] Hill R.J. "The Automation of Railways". Physics Technology, Volume 14, 1983, pp. 37–47.

[51] Fricke H. "Running Under Electrical Control Through the Identification of the Position of Trains Using Selective Systems of Signalling". Cybernetics and Electronics on Railways, Bulletin : International Railway Congress Association, Volume 1, Number 5, July 1964, pp. 302–307.

[52] Alston L.L, Birkby J.W. "Developments in Train Control on British Railways". Presented at Technical Meeting of the Institution. IEE, Wednesday, October 13, 1971, pp. 24–56.

[53] Alston L.L, Birkby J.W. "B.R. Train Control Developments for Main Lines". Rail Engineering International, November 1971, pp. 266–273.

[54] Ho T.K, Allan J, Digby G, Goodman C.J. "Modelling of Signalling for an Interactive On–Line Rapid Transit Railway Simulator". Second International Conference on Software Engineering for Real Time Systems. (IEE : Conf Pub No. 309)

[55] Holmstrom F.R. "Conductive Interference in Rapid Transit Signaling Systems – Volume I: Theory and Data". Final Report, November 1985, UMTA–MA–06–0153–85–5, DOT–TSC–UMTA–85–21.

[56] Holmstrom F.R. "Conductive Interference in Rapid Transit Signaling Systems – Volume II: Suggested Test Procedures". Final Report, UMTA–MA–06–0153–85–6, DOT–TSC–UMTA–86–7.

[57] Holmstrom F.R. "Laboratory and Field Testing of NYCTA Power Frequency Track Circuits". Final Report, February 1986, UMTA–MA–06–0153–85–12, DOT–

TSC–UMTA–85–26.

[58] Holmstrom F.R. "Inductive Interference in Rapid Transit Signaling Systems – Volume I: Theory and Data". Final Report, May 1986, UMTA–MA–06–0153–85–7, DOT–TSC–UMTA–86–2.

[59] Holmstrom F.R. "Inductive Interference in Rapid Transit Signaling Systems – Volume II: Suggested Test Procedures". Final Report, March 1987, UMTA–MA–06–0153–85–8, DOT–TSC–UMTA–86–6.

[60] Holmstrom F.R. "Inductive Interference in Rapid Transit Signaling Systems – Volume III: Data and Test Results". Final Report, November 1986, UMTA–MA–06–0153–85–9, DOT–TSC–UMTA–86–11.

[61] "Mutual Design of Overhead Transmission Lines and Railroad Communications and Signal Systems". EPRI EL–3301, Volume 1 and 2, Project 1902–1, Final Report, October 1983, (prepared by IIT Research Institute, Chicago, Il).

[62] Frasco L.A, Gagnon R, Holmstrom F.R. "Choppers Affect Operation of A.F. Track Circuits". Railway Gazette International, April 1980, pp. 291–294.

[63] Krempasky J.F, Clark G.E, Frasco L.A. "EMI/EMC Rail Testing Program at WMATA". APTA Rail Conference, Cleveland, OH, June 1982.

[64] Smith J.H. "Electromagnetic Compatibility (E.M.C.) Between Chopper Controlled Vehicles and Existing Train Control Systems". 1985 APTA Rapid Transit Conference on Power Signals and Communications Workshop, Atlanta, GE.

[65] Pace N.C. "Electrical Interference Impacts on Railways". Railway System Controls, Volume 3, Number 6, June 1972, pp. 14–17.

[66] Kendall H.C. "Electrification has Impact on Signals". Railway Systems Control, Volume 4, Number 5, May 1973, pp.28–31.

[67] Editorial. "Third Rail Gives Off Magnetic Smog". Railway Gazette International, Volume 136, Number 5, May 1980, pp. 427.

[68] Abrahamsohn G, White D.R.G. "EMI Prediction and Control in an Automated Rapid Transit System". Electromagnetic Compatibility 1975, Montreux, 20–22 May, pp. 396–401. (New York : IEEE 1975).

[69] Abramson Y.M, Kapitonov V.V. "Electromagnetic Environment on the Routes of Electric Transport and the Problems of Its Improvement". Second Symposium and Technical Exhibition on Electromagnetic Compatibility, Montreux, 28–30 June 1977. (New York : IEEE 1977).

[70] Littler G.E. "The Performance of an Electrified Railway System at Harmonic Frequencies". Electrical Engineering Transactions of IEAust, Volume EE16, Number 4, December 1980, pp. 184–189.

[71] Littler G.E. "The Harmonic Performance of a High Voltage A.C. Electrified Railway System with Single and Multiple Train Loading". International Conference on Railways in the Electronic Age, London, 17–20 November 1981, pp. 105–110. (London : IEE 1981).

[72] Littler G.E. "Harmonic Performance of an Autotransformer Type High Voltage A.C. Railway Electrification System". Electric Energy Conference 1986, Brisbane, 20–22 October 1986, pp. 85–90.

[73] Mellitt B, Allan J, Shao Z.Y, Bozkayah H, Johnston W.B. "CAD Techniques for Power System Studies and Electromagnetic Screening Calculations in A.C. Railways". First International Conference on Computer Aided Design, Manufacture

and Operation in the Railway and Other Advanced Mass Transit Systems, Frankfurt, 7–9 July 1987, pp. 145–172.

[74] Mellitt B, Allan J, Shao Z.Y, Johnston W.B. "Software Modelling for Induced Voltage Calculations in A.C. Railways". Conference on Railway Engineering, Perth, 14–16 September 1987, pp. 234–239.

[75] Mellitt B, Goodman C.J, Shao Z.Y, Johnston W.B. "Induced Noise Calculations in A.C. Railways Using CAD Techniques". International Conference on Electric Railway Systems for a New Century (Conf. Publication No. 279) London, 22–25 September 1987, pp. 22–25. (London : IEE 1987).

[76] Holtz J, Klein H.J. "The Propagation of Harmonic Currents Generated by Inverter–Fed Locomotives in the Distributed Overhead Supply System". IEEE Transactions on Power Electronics, Volume 4, Number 2, April 1989, pp. 168–174.

[77] Taufiq J.A, Goodman C.J, Mellitt B. "Railway Signalling Compatibility of Inverter Fed Induction Motor Drives for Rapid Transit". IEE Proceedings, Volume 133, Part B, Number 2, March 1986, pp. 71–84.

[78] Hill R.J, Yu S.L, Dunn N.J. "Chopper Traction Interference Modelling in D.C.–Fed Rapid Transit Railways". 1988 Joint ASME/IEEE Railroad Conference, Pittsburgh, PA, 13–14 April 1988, pp. 163–170. (New York : ASME 1988).

[79] Hill R.J, Yu S.L. "Computer Modelling Techniques for Railway Signalling Interference". International Journal of Modelling and Simulation, Volume 9, Number 1, 1989, pp. 8–13.

[80] Krittian F. "Contribution to Calculations of Interference by Thyristorized Units to Cables alongside a Railway Line." Rail International, Volume 12, 1981, pp.

245–256.

[81] Cowdell R.B. "Communication System Design in a High Level EMI Environment". International Symposium on EMC (23rd), Boulder, CO, 18–20 August 1981, pp. 187–193. (New York : IEEE 1981).

[82] Mellitt B, Allan J, Shao Z.Y, Johnston W.B. "Screening Requirements for Telecommunication Cables in A.C. Railways". Sixth International Conference on Electromagnetic Compatibility, York, 12–15 September 1988, (Publ. No. 81), pp. 233–243. (London : IEE 1988).

[83] Manganella L, Mario P.R. "New Proposals for Calculating Interference Between Electrified Railway Lines and Signalling and Communications Circuits". Second International Conference on Computer Aided Design, Manufacture and Operation in the Railway and Other Advanced Mass Transit Systems : Comprail 90, Rome, Volume 2 : Computer Applications in Railway Operations, 27–29 March 1990.

[84] Brown J.C, Allan J, Mellitt B. "Calculation of Remote Distance Short Circuit Fault Currents using an Inverse Fourier Transform Technique". Second International Conference on Computer Aided Design, Manufacture and Operation in the Railway and Other Advanced Mass Transit Systems : Comprail 90, Rome, Volume 2 : Computer Applications in Railway Operations, 27–29 March 1990.

[85] Stanek E.K, Cataltepe T, Wiitanen D.O. "Phenomena that Affect the Calculation of Inductance and Resistance of Mine Track/Trolley Systems". Industry Applications Society, IEEE–IAS–1984 Annual Meeting, Chicago, Il, 30 September–4 October 1984, pp.100–106.

[86] Mellitt B. "Data–Transmission Characteristics of Railway Track". Electronics Letters, 15 November 1973, Volume 9, Number 23, pp. 550–551.

[87] Tylavsky D.J. "Impedance of Track (Trolley Haulage Systems)". Industry Applications Society, IEEE–IAS–1985, Annual Meeting, Toronto 6–11 October 1985, pp. 206–212.

[88] Tylavsky D.J, Kulkarmi A.Y. "Inductance Calculations for Earth–Return Trolley Systems". Conference Record, Industry Applications Society, Annual Meeting (IEEE CAT No. 88CH2565–0), Volume 2, Pittsburgh, PA, 2–7 October 1988, pp. 1216–1223. (New York : IEEE 1988).

[89] Wedepohl L.M. "Application of Matrix Methods to the Solution of Travelling–Wave Phenomena in Polyphase Systems". Proceedings IEE, Volume 110, Number 12, December 1963, pp. 2200–2212.

[90] Wedepohl L.M. "Wave Propagation in Nonhomogeneous Multiconductor Systems using the Concept of Natural Modes". Proceedings IEE, Volume 113, Number 4, April 1966, pp. 622–626.

[91] Wedepohl L.M, Wasley R.G. "Wave Propagation in Multiconductor Overhead Lines. Calculation of Series Impedance for Multilayer Earth". Proceedings IEE, Volume 113, Number 4, April 1966, pp. 627–632.

[92] Carson J.R. "Wave Propagation in Overhead Wires with Ground Return". Bell System Technical Journal, 1926, Number 5, pp. 539–554.

[93] Pollaczek Von F. "The Field of a Single–Phase Alternating–Current Line". Elektrische Nachrichten–Tecknik, 1926, Volume 3, pp. 339–359.

[94] Galloway R.H, Shorrocks W.B, Wedepohl L.M. "Calculation of Electrical Parameters for Short and Long Polyphase Transmission Lines". Proceedings IEE, Volume 111, Number 12, December 1964, pp. 2051–2059.

[95] Wedepohl L.M, Wasley R.G. "Wave Propagation in Polyphase Transmission Systems Resonance Effects due to Discrete Bonded Earth Wires". Proceedings IEE, Volume 112, Number 11, December 1965, pp. 2113–2119.

[96] Wedepohl L.M. "Electrical Characteristics of Polyphase Transmission Systems with Special Reference to Boundary–Value Calculations at Power–Line Carrier Frequencies". Proceedings IEE, Volume 112, Number 11, December 1965, pp. 2103–2112.

[97] Clayton R.P. "Solution of the Transmission–Line Equations for Lossy Conductors and Imperfect Ground". Proceedings IEE, Volume 122, Number 2, February 1975, pp.177–182.

[98] Wedepohl L.M, Efthymiadis A.E. "Wave propagation in Transmission Lines over Lossy Ground – A New Complete Field Solution". Proceedings IEE, June 1978, Volume 125, Number 6, pp. 505–510.

[99] Efthymiadis A.E, Wedepohl L.M. "Propagation Characteristics of Infinitely–Long Single–Conductor Lines by the Complete Solution Method". Proceedings IEE, June 1978, Volume 125, Number 6, pp. 511–517.

[100] Semlyen A, Deri A. "Time Domain Modelling of Frequency Dependent Three Phase Transmission Line Impedance". IEEE Transactions on Power Apparatus and Systems, Volume 104, Number 6, June 1985, pp 1549–1555.

[101] Arabi T.R, Sarkar T.K, Djordjevic A.R. "Time and Frequency Domain Characterization of Multiconductor Transmission Lines". Electromagnetics, Volume 9, Number 1, 1989, pp. 85–112.

[102] Stratton J.A. "Electromagnetic Theory". McGraw–Hill : New York 1941.

[103] Hammond P. "Applied Electromagnetism". Pergamon Press : Oxford 1971.

[104] Carter G.W. "The Electromagnetic Field in Engineering Aspects". Longmans : London 1954.

[105] Pascoe K.J. "Properties of Materials for Electrical Engineers". John Wiley : Chichester 1973.

[106] Anderson J.C, Leader K.D, Alexander J.M, Rawlings R.D. "Material Science". Thomas Nelson : London 1974.

[107] Von Hippel A.R. "Dielectric Materials and Applications". Section : Permeability (by Epstein D.J.). John Wiley : New York 1954.

[108] Von Hippel A.R. "Dielectrics and Waves". John Wiley : New York 1954.

[109] Lin C.E, Wei J–B, Huang C.L, Huang C–J. "A New Model for Transformer Saturation Characteristics by Including Hysteresis Loops". IEEE Transactions on Magnetics, Volume 25, Number 3, May 1989, pp. 2706–2712.

[110] Ostiguy J.F, Silvester P.P. "Magnetic Field Computation in Hysteretic Media by Finite Element Method, Using the Preisach Model". Journal Applied Physics, Volume 57, Number 1, 15 April 1985, pp. 3833–3855.

[111] Mayergoyz I.D, Friedman G. "Generalized Preisach Model of Hysteresis". IEEE Transactions on Magnetics, Volume 24, Number 1, January 1988, pp. 212–218.

[112] Martinez M.C, Munoz V, Such V. "The Influence of Magnetic Characteristic Type in the Calculated Electromagnetic Field in Solid Steel Plates". EDF Bulletin de la Direction des Etudes et Recherches – Serie B Reseaux Electriques Materiels Electriques, Number 1, 1987, pp. 5–24.

[113] Hogdon M.L. "Applications of a Theory of Ferromagnetic Hysteresis". IEEE Transactions on Magnetics, Volume 24, Number 1, January 1988, pp. 218–221.

[114] Luetke–Daldrup B. "Comparison of Exact and Approximate Finite–Element Solution of the Two–Dimensional Non–Linear Eddy–Current Problem with Measurement". IEEE Transactions on Magnetics, Volume 20, Number 5, September 1984, pp. 1936–1938.

[115] Lucas R, Talukdar S. "Advances in Finite Element Techniques for Calculating Cable Resistances and Inductances". IEEE Transactions on Power Apparatus and Systems, Volume 97, Number 3, May/June 1978, pp. 875–883.

[116] Weiss J, Csendes Z.J. "A One–Step Finite Element Method for Multiconductor Skin Effect Problems". IEEE Transactions on Power Apparatus and Systems, Volume 101, Number 10, October 1982, pp. 3796–3803.

[117] Chari M.V.K, Csendes Z.J. "Finite Element Analysis of the Skin Effect in Current Carrying Conductors". IEEE Transactions on Magnetics, Volume 13, Number 5, September 1977, pp. 1125–1127.

[118] Nakata T. "Numerical Analysis of Flux and Loss Distributions in Electrical Machinery (invited)". IEEE Transactions on Magnetics, Volume 20, Number 5, September 1984, pp. 1750–1755.

[119] Nakata T, Takahashi N, Kawase Y. "Finite Element Analysis of Magnetic Fields Taking into Account Hysteresis Characteristics". IEEE Transactions on Magnetics, Volume 21, Number 5, September 1985, pp. 1856–1858.

[120] Del Vecchio R.M. "The Inclusion of Hysteresis Processes in a Special Class of Electromagnetic Finite Element Calculations". IEEE Transactions on Magnetics, Volume 18, Number 1, January 1982, pp. 275–284.

[121] Burais N, Grellet G. "Numerical Modelling of Iron Losses in Ferromagnetic Steel Plate". IEEE Transactions on Magnetics, Volume 18, Number 2, March 1982, pp. 558–562.

[122] Silvester P. "Eddy Current Modes in Linear Solid–Iron Bars". Proceedings IEE, Volume 112, Number 8, August 1965, pp. 1589–1594.

[123] Labrides D, Dokopoulos P. "Calculation of Eddy Current Losses in Nonlinear Ferromagnetic Materials". IEEE Transactions on Magnetics, Volume 25, Number 3, May 1989, pp. 2665–2669.

[124] Hsu J.S, Woodson H.H, Liou S.S.P. "Experimental Study of Harmonic–Flux Effects in Ferromagnetic Materials". IEEE Transactions on Magnetics, Volume 25, Number 3, May 1989, pp. 2678–2685.

[125] Carson J.R. "The Rigorous and Approximate Theories of Electrical Transmission Along Wires". Bell System Technical Journal, January 1928, Volume 7, pp. 11–25.

[126] Carson J.R. "Wave Propagation over Parallel Wires : The Proximity Effect". Philosophical Magazine, April 1921, pp. 607–663.

[127] Coleman B.L. "Propagation of Electromagnetic Disturbances Along a Thin Wire in a Horizontally Stratified Medium". Philosophical Magazine, Series 7, Volume 41, 1950, pp. 276–288.

[128] Wait J.R. "Theory of Wave Propagation Along a Thin Wire Parallel to an Interface". Radio Science, Volume 7, Number 6, June 1972, pp. 675–679.

[129] Wait J.R, Spies K.P. "On the Image Representation of the Quasi–Static Fields of a Line Current Source Above the Ground". Canadian Journal of Physics, Volume 47, 1969, pp. 2731–2733.

[130] Chang D.C, Wait J.R. "Extremely Low Frequency (ELF) Propagation Along a Horizontal Wire Located Above or Buried in the Earth". IEEE Transactions on Communications, Volume 22, Number 4, April 1974, pp. 421–427.

[131] Alvarado F.L, Betancourt R. "An Accurate Closed Form Approximation for Ground Return Impedance Calculations". Proceedings IEEE, Volume 71, Number 2, February 1983, pp. 279–280.

[132] Olsen R.G, Pankaskie T.A. "On the Exact Carson and Image Theories for Wires at or Above the Earth's Interface". IEEE Transactions on Power Apparatus and Systems, Volume 102, Number 4, April 1983, pp. 769–778.

[133] Kuester E.F, Chang D.C. "Electromagnetic Wave Propagation Along Horizontal Wire Systems in or Near a Layered Earth". Electromagnetics, Volume 1, July–September 1981, pp. 243–266.

[134] Deri A, Tevan G, Semlyen A, Castanheira A. "The Complex Ground Return Plane – A Simplified Model for Homogeneous and Multilayer Earth Return". IEEE Transactions on Power Apparatus and Systems, Volume 100, Number 8, August 1981, pp. 3686–3693.

[135] Nakagawa M, Iwamoto K. "Earth–Return Impedance for the Multi–Layer Case". IEEE Transactions on Power Apparatus and Systems, Volume 95, Number 2, March/April 1976, pp. 671–676.

[136] Bickford J.P, Mullineux N, Reed J.R. "Computation of Power System Transients". Peter Peregrinus : London 1976.

[137] Bowen A.E, Gilkeson C.L. "Mutual Impedances of Ground–Return Circuits – Some Experimental Studies". Bell System Technical Journal, October 1930, Volume 9, pp. 628–651.

[138] Collard J. "Measurement of the Mutual Impedance of Circuits with Earth Return". Journal IEE, Volume 71, Number 430, October 1932, pp. 674–682.

[139] Starosel'skii A. "Electrical Resistance of Ballast". Railway Research and Engineering News, Section E, 1979, RT 48955, 10, pp.1–3.

[140] Hill P.N, Green H.E. "In Situ Measurements of Soil Permittivity and Permeability". Journal of Electrical and Electronics Engineering Australia, IE Aust. and IREE Aust, Volume 2, Number 4, December 1982, pp. 202–208.

[141] Mayhan R.J, Bailey R.E. "An Indirect Measurement of the Effect Dielectric Constant and Loss Tangent of Typical Concrete Roadways". IEEE Transactions on Antennas and Propagation, July 1975, pp. 565–569.

[142] Keller G.V, Frischknecht F.C. "Electrical Methods in Geophysical Prospecting". Pergamon Press : Oxford 1966.

[143] Tso S.K, Lam F.K, Chan F.H.Y, Edgley R.K. "Attenuation Effects of Under–Track Reinforcing on Automatic Train Protection Signalling Systems". IEE Proceedings, Volume 128, Part B, Number 2, March 1981, pp. 92–100.

[144] Langer R.E. "An Inverse Problem in Differential Equations". Bulletin of the American Mathematical Society, Volume 39, 1933, pp. 814–820.

[145] Langer R.E. "On the Determination of Earth Conductivity from Observer Surface Potentials". Bulletin of the American Mathematical Society, Volume 42, 1936, pp. 747–754.

[146] Slitcher L.B. "The Interpretation of the Resistivity Prospecting Method for Horizontal Structures". Physics, Volume 4, 1933, pp. 307–322.

[147] Blattner C.J. "Prediction of Soil Resistivity and Ground Rod Resistance for Deep Ground Electrodes". IEEE Transactions on Power Apparatus and Systems, Volume 99, Number 5, September/October 1980, pp. 1758–1763.

[148] Blattner C.J. "Study of Driven Ground Rods and Four Point Soil Resistivity Tests". IEEE Transactions on Power Apparatus and Systems, Volume 101, Number 8, August 1982, pp. 2837–2843.

[149] Meliopoulos A.P, Papalexopoulos A.D, Webb R.P. "Estimation of Soil Parameters from Driven Rod Measurements". IEEE Transactions on Power Apparatus and Systems, Volume 103, Number 9, September 1984, pp. 2579–2585.

[150] Baishiki R.S, Osterberg C.K, Dawalibi F. "Earth Resistivity Measurements Using Cylindrical Electrodes at Short Spacings". IEEE Transactions on Power Delivery, Volume 2, Number 1, January 1987, pp.64–71.

[151] Telford W.M, Geldart L.P, Sheriff R.E, Keys D.A. "Applied Physics". Cambridge University Press : Cambridge 1976.

[152] Sunde E.D. "Earth Conduction Effects in Transmission Systems". Dover Publications : New York 1968.

[153] Klauser P.E, Mattoon D.W, Singh S.P, Ahmad O.K. "The Train Energy and Operation Simulator (TOES) : A New Approach to Train Simulation". 1986 ASME Winter Annual Meeting, Anaheim, CA, 7–12 December 1986.

[154] Handel S, Law E.H, Figliola R.S. "Simplified Methods for Calculating Energy Consumption of Railway Vehicles Using Lotus 1–2–3". Proceedings of 1987 IEEE/ASME Joint Railroad Conference, Toronto, Ontario, Canada, 21–23 April, (Cat No. 87CH23399 4, EEA 87 79079), pp. 31–38. (New York : IEEE 1982).

[155] Hill R.J, Yu S.L, Dunn N.J. "Rail transit Chopper Traction Interference Modelling Using the SPICE Circuit Simulation Package". IEEE Transactions on Vehicular Technology, Volume 38, Number 4, November 1989, pp. 237–246.

[156] Wirth K.–H. "New Model for Time Domain Simulation of Lossy Coupled Lines". Electronics Letters, Volume 26, Number 20, 27 September 1990, pp. 1723–1725.

[157] Wirth K.–H. "A Network Model for Time–Domain Simulation of Lossy Transmission Lines". Frequenz 1989, Volume 43, pp. 258–262.

[158] Wang X, Mathur R.M. "Real–Time Digital Simulator of the Electromagnetic Transients of Transmission Lines with Frequency Dependence". IEEE Transactions on Power Delivery, Volume 4, Number 4, October 1989, pp. 2249–225.

[159] Lin J, Marti J.R. "Implementation of the CDA Procedure in the E.M.T.P.". IEEE Transactions on Power Systems, Volume 5, Number 2, May 1990, pp. 394–402.

[160] Marti J.R, Lin J. "Suppression of Numerical Oscillations in the E.M.T.P.". IEEE Transactions on Power Systems, Volume 4, Number 2, May 1989, pp. 739–747.

[161] Natarajan R, Gentzler D.B. "Adoption of Electromagnetic Transients Program (E.M.T.P.) on Personal Computers". IEEE Transactions on Power Systems, Volume 4, Number 4, October 1989, pp. 1550–1556.

[162] Woodford D.A, Gole A.M, Menzies R.W. "Digital Simulation of D.C. Links and A.C. Machines". IEEE Transactions on Power Apparatus and Systems, Volume 102, Number 6, June 1983, pp. 1616–1623.

[163] Nyati S, Gueth G, Mathur R.M, Koschik V. "Investigation of HVDC Inverter with Series Compensation on Analogue Simulator". IEEE Transactions on Power Delivery, Volume 5, Number 2, April 1990, pp. 668–675.

[164] Nyati S, Atmuri S.R, Gordon D, Koschik V, Mathur R.M. "Comparison of Voltage Control Devices at HVDC Converter Stations Connected to weak A.C. Systems". IEEE Transactions on Power Delivery, Volume 3, Number 2, April 1988, pp. 684–693.

[165] Dommel H.W, Meyer W.S. "Computation of Electromagnetic Transients". Proceedings IEEE, Volume 62, Number 7, July 1974, pp 983–993.

[166] Private communication with Professor P. MacLaren of University of Manitoba, Manitoba, Canada.

[167] "EMTDC User's Manual". Manitoba HVDC Research Centre, Manitoba, Canada.

[168] "Routine F02AKF – Eigenvalues and Eigenvectors". NAGFLIB : 981/625 : Mk5:Aug75.

[169] Private communication with Mr. R. Hill–Cottingham of University of Bath, England. Experimental apparatus description to be published.

[170] Brigham E.O. "The Fast Fourier Transform." Prentice–0–Hall : New York 1973.

[171] Du Fort E.C, Frankel S.P. "Stability Conditions in the Numerical Treatment of Parabolic Differential Equations". Mathematical Tables and Aids Computation, Volume 7, 1953, pp. 135–52.

[172] Hill R.J, Carpenter D.C, Tasar T. "Railway Track Admittance, Earth–Leakage Effects and Track Circuit Operation". 1989 IEEE/ASME Railroad Conference, Philadelphia, 25–27 April 1989 (New York: IEEE 1989), pp. 55–62

[173] Gradshteyn I.S, Ryzhik I.M. "Table of Integrals, Series and Products". Academic Press : Orlando, Fl, 1965.

[174] Lytle R.J. "Measurement of Earth Medium Electrical Characteristics: Techniques, Results and Applications". IEEE Trans on Geoscience and Remote Sensing, 1974, pp. 81–101.

[175] Brown J.C. "An Investigation into Short Circuit Faults on the Power Supply of D.C. Traction Systems". Ph.D. Thesis, Birmingham University, UK, August 1988.

[176] Trueblood H.M, Wascheck G. "Investigation of Rail Impedance". Electrical Engineering, December 1933, pp. 898–907.

[177] Grover F.W. "Inductance Calculations". Dover Publications : New York 1945.

[178] Ametani A. "Stratified Earth Effects on Wave Propagation – Frequency Dependent Parameters". IEEE PES Winter Meeting, New York, 27 January – 1 February 1974, pp. 1233–1239, (New York : IEEE 1974).

[179] Crutzen Y.R, Molinari G, Rubinacci G. "Industrial Application of Electromagnetic Computer Codes". Kluwer Academic Publishers : Dordecht 1990.

[180] More J.J, Garbow B.S, Hillstrom K.E. "User's Guide to MINPACK I". Argonne National Laboratory publication ANL–80–74, 1980

[181] Brileev A, Kravtzov U, Shishlakov A. "Theory, Design and Operation of Track Circuits". Transport : Moscow, USSR 1978 (In Russian).

[182] "Metro Jointless Track Circuit FS 2500 – JTC". Westinghouse Signals Ltd, UK 1985.

[183] Pelly B.R. "Thyristor Phase–Controlled Converters and Cycloconverters – Operation, Control and Performance". John Wiley : New York 1971

[184] Kemp R.J. "Introduction of Chopper Controlled Trains on Established D.C. Railways". GEC Review, Volume 2, Number 2, 1986, pp. 89–96

[185] "Experimental Study of Induced Noise Voltages in Telecommunications Line along the 3kV Electrified Single–Track Skawina–Chabowka Railway Line." O.R.E. Technical Document DT 73 (A 122), Utrecht, October 1980 pp.51.

[186] Silvester P.P, Ferrari R.L. "Finite Elements For Electrical Engineers". Cambridge University Press : Cambridge 1983.

[187] Sadiku M.N.O. "A Further Introduction to Finite Element Analysis of Electromagnetic Problems". IEEE Transactions on Education, Volume 34, Number 4, November 1991, pp. 322–329.

[188] Sadiku M.N.O. "A Simple Introduction to Finite Element Analysis of Electromagnetic Problems". IEEE Transactions on Education, Volume 32, Number 2, May 1989, pp. 85–93.

[189] Morrison R.E, Corcoran J.C.W. "Specification of an Overvoltage Damping Filter for the National Railways of Zimbabwe". IEE Proceedings, Volume 136, Part B, Number 6, November 1989, pp. 249–256.

[190] Numerical Algorithms Group 1981. Fortran Library Manual Mark 8, Volume 1.

[191] Greenough C. Robinson K. "Finite Element Library. Level 1 Documentation." SERC Rutherford Appelton Laboratories 1981.

[192] Wolfram S. "Mathematica. A System for Doing Mathematics by Computer." Addison–Wesley : California 1991.

Appendix A

Modal Analysis of a Multi–wire System

For a two wire system with remote (or common) ground, where each wire (i) has a self impedance per unit length of Z_{ii} and a mutual impedance per unit length between wires of Z_{ij}, as shown in Figure A.1, it is usual to express the voltage relationship in terms of the distributed components as

$$\delta V_i = -(Z_{ii} I_i \delta x + Z_{ij} I_j \delta x) \tag{A.1}$$

where

I_i and I_j are the currents in wires i and j.

In the limit, as $\delta x \rightarrow 0$

$$\frac{\delta V_i}{\delta x} \rightarrow \frac{dV_i}{dx} = -(Z_{ii} I_i + Z_{ij} I_j) \tag{A.2}$$

In matrix form

$$\frac{d[\mathbf{V}]}{dx} = -[\mathbf{Z}][\mathbf{I}] \tag{A.3}$$

where, for a two wire system

$$[\mathbf{Z}] = \begin{bmatrix} Z_{11} & Z_{21} \\ Z_{12} & Z_{22} \end{bmatrix}$$

$$[\mathbf{V}] = \begin{bmatrix} V_1 \\ V_2 \end{bmatrix}$$

$$[\mathbf{I}] = \begin{bmatrix} I_1 \\ \\ I_2 \end{bmatrix}$$

In a similar manner, the currents in each conductor (i) are related by

$$\frac{d[\mathbf{I}]}{dx} = -[\mathbf{Y}][\mathbf{V}] \tag{A.4}$$

where

$$[\mathbf{Y}] = \begin{bmatrix} Y_{11} & Y_{21} \\ \\ Y_{12} & Y_{22} \end{bmatrix}$$

$Y_{ie} = Y_{i1} + Y_{i2}$

$Y_m = -Y_{12}$

Y_{ie} is the admittance per unit length to ground of conductor i.

Y_m is the mutual admittance between conductors.

The quantities in these equations relate directly to the physical system and are called the phase values. Similarly the expressions are termed the phase equations.

Substituting Equation A.4 into A.3 gives

$$\frac{d^2}{dx^2}\begin{bmatrix} V_1 \\ \\ V_2 \end{bmatrix} = \begin{bmatrix} Z_{11} & Z_{21} \\ \\ Z_{12} & Z_{22} \end{bmatrix}\begin{bmatrix} Y_{11} & Y_{21} \\ \\ Y_{12} & Y_{22} \end{bmatrix}\begin{bmatrix} V_1 \\ \\ V_2 \end{bmatrix} \tag{A.5}$$

Substituting Equation A.3 into A.4 gives

$$\frac{d^2}{dx^2}\begin{bmatrix} I_1 \\ \\ I_2 \end{bmatrix} = \begin{bmatrix} Y_{11} & Y_{21} \\ \\ Y_{12} & Y_{22} \end{bmatrix}\begin{bmatrix} Z_{11} & Z_{21} \\ \\ Z_{12} & Z_{22} \end{bmatrix}\begin{bmatrix} I_1 \\ \\ I_2 \end{bmatrix} \tag{A.6}$$

If $[\mathbf{A}] = [\mathbf{Y}].[\mathbf{Z}]$ then, in matrix form

$$\frac{d^2}{dx^2}[\mathbf{V}] = [\mathbf{A}]^T.[\mathbf{V}] \tag{A.7}$$

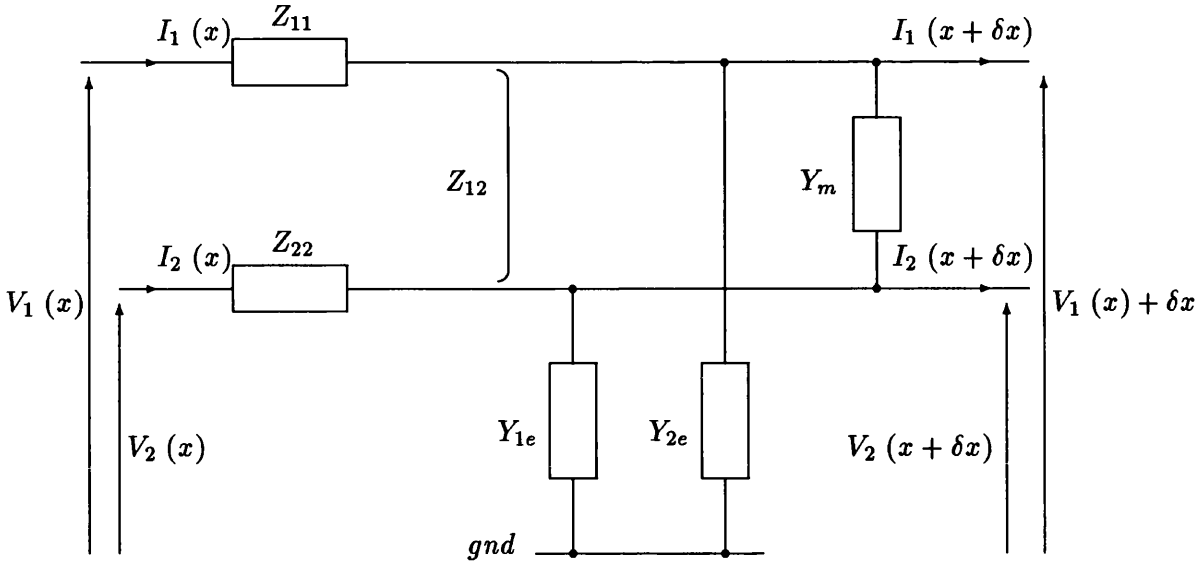

Figure A.1: Distributed Circuit Representation of a Two Wire Line

and

$$\frac{d^2}{dx^2}[\mathbf{I}] = [\mathbf{A}].[\mathbf{I}] \tag{A.8}$$

Since $[\mathbf{A}] = [\mathbf{Y}][\mathbf{Z}]$, it is unlikely to be a diagonal matrix. Hence the currents and voltages in any conductor are dependent on the currents and voltages in any other conductor. For efficient computation, it is beneficial to decouple the equations. Using the theorem of *Similar Transforms*, it is possible to develop a diagonal matrix Λ such that

$$[\mathbf{A}] = [\mathbf{Y}][\mathbf{Z}] = [\mathbf{T}]^{T^{-1}}[\Lambda][\mathbf{T}]^T \tag{A.9}$$

where

$\mathbf{\Lambda}$ is a diagonal matrix of eigenvalues or modes i.e. $\begin{bmatrix} \lambda_1 & & 0 \\ & \lambda_2 & \\ & \ddots & \\ 0 & & \lambda_m \end{bmatrix}$

$\lambda_n = \gamma_n{}^2$, the propagation constant of node n.

$\mathbf{T}$ is an eigen or modal transformation matrix given by $\mathbf{T} = [\mathbf{T_1 T_2} \ldots \mathbf{T_n} \ldots \mathbf{T_m}]$

and $\mathbf{T_n} = \begin{bmatrix} T_{n1} \\ T_{n2} \\ \vdots \\ T_{nm} \end{bmatrix}$

Hence

$$[\mathbf{\Lambda}] = [\mathbf{T}]^T[\mathbf{A}][\mathbf{T}]^{T^{-1}} = [\mathbf{T}^T][\mathbf{Y}][\mathbf{Z}][\mathbf{T}]^{T^{-1}} \tag{A.10}$$

To use this decoupled matrix, the transmission line equations are written in terms of modal quantities

$$\frac{d}{dx}[\mathbf{V}^m] = [\mathbf{Z}^m][\mathbf{I}^m] \tag{A.11}$$

and

$$\frac{d}{dx}[\mathbf{I}^m] = [\mathbf{Y}^m][\mathbf{V}^m] \tag{A.12}$$

where the superscript m indicates the modal quantities. This gives

$$\frac{d^2}{dx^2}[\mathbf{V}^m] = [\mathbf{Z}^m][\mathbf{Y}^m][\mathbf{V}^m] = [\mathbf{\Lambda}][\mathbf{V}^m] \tag{A.13}$$

and

$$\frac{d^2}{dx^2}[\mathbf{I}^m] = [\mathbf{Y}^m][\mathbf{Z}^m][\mathbf{I}^m] = [\mathbf{\Lambda}][\mathbf{I}^m] \tag{A.14}$$

This shows that

$$[\mathbf{Y}^m][\mathbf{Z}^m] = [\mathbf{A}] = [\mathbf{T}]^{-1}[\mathbf{A}][\mathbf{T}]^{T^{-1}} = [\mathbf{T}]^T[\mathbf{Y}][\mathbf{Z}][\mathbf{T}]^{T^{-1}} \tag{A.15}$$

To decouple the phase matrices, it can be seen that

$$[\mathbf{Y}^m][\mathbf{Z}^m] = [\mathbf{T}]^T[\mathbf{Y}][\mathbf{T}][\mathbf{T}]^{-1}[\mathbf{Z}][\mathbf{T}]^{T-1} \tag{A.16}$$

giving

$$[\mathbf{Y}^m] = [\mathbf{T}]^T[\mathbf{Y}][\mathbf{T}] \tag{A.17}$$

$$[\mathbf{Z}^m] = [\mathbf{T}]^{-1}[\mathbf{Z}][\mathbf{T}]^{T^{-1}} \tag{A.18}$$

$$[\mathbf{I}^m] = [\mathbf{T}]^T[\mathbf{I}] \tag{A.19}$$

$$[\mathbf{V}^m] = [\mathbf{T}]^{-1}[\mathbf{V}] \tag{A.20}$$

From the definition of the eigenvalue equation

$$\left([\mathbf{Y}][\mathbf{Z}] - \gamma_i{}^2[\mathbf{U}]\right)\mathbf{T}_i = 0 \tag{A.21}$$

The non–trivial solution of this exists only if

$$|[\mathbf{Y}][\mathbf{Z}] - \lambda_i[\mathbf{U}]| = 0 \tag{A.22}$$

or

$$|[\mathbf{A}] - \lambda_i[\mathbf{U}]| = 0 \tag{A.23}$$

Appendix B

Theoretical Calculation Of Internal Impedance

The theoretical approach to the calculation of internal impedance is based on the assumption that the conductor is circular. It is then possible to develop an expression for impedance per unit length of an isolated conductor. This is termed the *internal impedance.* The analysis also assumes that no saturation occurs.

Figure B.1 shows an isolated conductor, of circular cross–section, in which the current flows in the z direction, along the axis of symmetry of the conductor. Hence the magnetic field strength is in the ϕ direction.

At radius r

$$2\pi r H_\phi = \int_0^r 2\pi r J_z \tag{B.1}$$

Differentiating with respect to r gives

$$\frac{dH}{dr} + \frac{H}{r} = J_z \tag{B.2}$$

Differentiating again

$$\frac{dH^2}{dr^2} + \frac{1}{r}.\frac{dH}{dr} = \frac{dJ_z}{dr} \tag{B.3}$$

The e.m.f. induced at r by flux inside conductor is given by the difference between the resistance drops at r and a.

$$\frac{1}{\sigma}(J_z - J_{zo}) = -\frac{d}{dt}\int_r^a \mu^* H_\phi dr \tag{B.4}$$

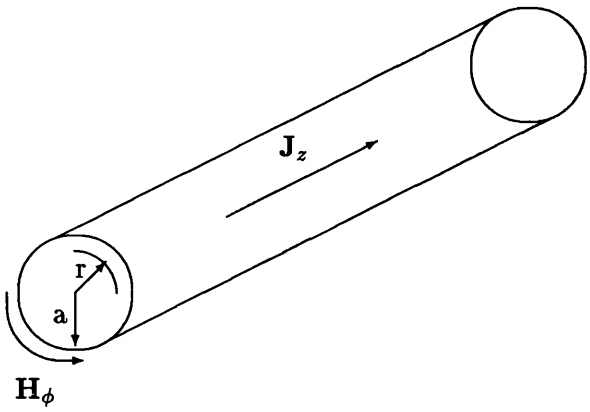

Figure B.1: Current and Magnetic Field of Isolated Conductor

where J_{zo} is the current density at the surface.

$$\frac{1}{\sigma}\frac{dJ_z}{dr} = \mu^* \frac{dH_\phi}{dt} \tag{B.5}$$

Assuming sinusoidal signals

$$\frac{1}{\sigma}\frac{dJ_z}{dr} = j\omega\sigma\mu^* H \tag{B.6}$$

From Equation 4.3

$$\frac{d^2H}{dr^2} + \frac{1}{r}\frac{dH}{dr} - (\alpha_{circ}^2 + \frac{1}{r})H = 0 \tag{B.7}$$

where $\alpha_{circ}^2 = j\omega\sigma\mu^*$

Hence

$$H = AI_{1B}(\alpha_{circ}r) + BK_{1B}(\alpha_{circ}r) \tag{B.8}$$

At $r = 0$, H must be finite, thus $B = 0$

At $r = a$, $H_o = \frac{I}{2\pi a}$ thus $A = \frac{I}{2\pi a}\frac{1}{I_{1B}(\alpha_{circ}a)}$

where I is the total current in the conductor.

Hence

$$H = \frac{I}{2\pi a}\frac{I_{1B}(\alpha_{circ}r)}{I_{1B}(\alpha_{circ}a)} \tag{B.9}$$

and from Equation (4.2)

$$J_z = \frac{I}{2\pi a}\frac{1}{I_{1B}(\alpha_{circ}a)}\left[\frac{dI_{1B}(\alpha_{circ}r)}{dr} + \frac{1}{r}I_{1B}(\alpha_{circ}r)\right] \tag{B.10}$$

$$\frac{dI_{1B}(\alpha_{circ}r)}{dr} = \alpha_{circ}\frac{dI_{1B}(\alpha_{circ}r)}{d(\alpha_{circ}r)} \tag{B.11}$$

$$= \alpha_{circ}\left[\frac{-1}{\alpha_{circ}r}[I_{1B}(\alpha_{circ}r)] + I_{0B}(\alpha_{circ}r)\right] \tag{B.12}$$

Thus

$$J_z = \frac{\alpha_{circ}I}{2\pi a}\frac{I_{0B}(\alpha_{circ}r)}{I_{1B}(\alpha_{circ}r)} \tag{B.13}$$

and with $J_z = \sigma E$, we have

$$R + jX = \frac{E|_{r=a}}{I} = \frac{\alpha_{circ}}{2\pi a\sigma}\frac{I_{0B}(\alpha_{circ}a)}{I_{1B}(\alpha_{circ}a)} \tag{B.14}$$

Since $\alpha_{circ}^2 \propto \mu^*$ and μ^* is a function of H then $\alpha_{circ} = f(I)$. To evaluate μ^* and hence α_{circ}, the values obtained from the material tests are used. The conductivity values obtained in Section 3.1 are also used here.

Hence

$$z_{circ} = f(\omega, \sigma, \mu^*, a) \tag{B.15}$$

and

$$\mu^* = f(H) = f(I) \tag{B.16}$$

The particular value of permeability varies through the material (with magnetic field strength) and a mean value is chosen as described in Section 4.2. For any particular

rail, a suitable equivalent radius a_{eq} must be obtained, in order to evaluate z_{circ}. At very low frequencies, the cross–sectional area of the rail can be used, that is

$$rail\ cross\ section = \pi {a_{eq}}^2 \tag{B.17}$$

However, for the majority of cases (see Section 6) where the frequency is above approximately 20 Hz, the skin effect due to the eddy currents limits the main current path to the perimeter of the rail cross–section. Hence the perimeter may be used to evaluate an equivalent radius by

$$rail\ perimeter = 2\pi a_{eq} \tag{B.18}$$

For any particular rail

$$z_{circ} = f(\omega, I) \tag{B.19}$$

Both ω and I may vary due to signal modulation and E.M.I. Thus the impedance varies with both for any particular study. This implies a continuous range of values of z_{circ} is required.

Appendix C

Geometric Mean Distances and Inductance

As described by Grover [177], when calculating the mutual inductance of two parallel conductors with large separation distance compared to their cross–section dimensions, it is possible to replace the actual conductors with filaments for calculation purposes. The computed result will have small errors. These are associated with the relative sizes of separation and cross–section dimensions. The distance between filaments for this calculation is the *Geometric Mean Distance* of all points in the cross–section of one of the conductors to those points in the other conductor.

Grover also discusses the same principle applied to self inductance of a long straight conductor. It is equal to the sum of the mutual inductances of all pairs of filaments making up the cross–section. From this argument, it can be seen that the self inductance of a rail is equivalent to the mutual inductance of two straight filaments, spaced at the geometric mean distance of all the cross–section points from each other. The cross–section must be interpreted from the actual section taking part in conduction. Allowance must be made for skin effect.

Evaluation has been carried out using computer methods as the algorithm inherently requires repeated calculations of separate points. Grover states that the mutual inductance of two filaments is given by:–

$$M = 0.002 l_t \left[log_e \frac{2l_t}{R_{GMD}} - 1 + \frac{R_{GMD}}{l_t} - \frac{1}{4} \frac{{R_{GMD}}^2}{l_t^2} + \ldots \right] \qquad \text{(C.1)}$$

where

l_t is the filament length

R_{GMD} is the GMD of the conductor

Appendix D

The Solution of the Composite Measurement Technique in Terms of Measured Line Voltages and Currents

The solution referred to in Chapter 7 is developed by combining Equation 7.8 and 7.21 to give

$$\begin{bmatrix} V_{ai}'(0) \\ V_{bi}'(0) \end{bmatrix} = \begin{bmatrix} 1 & -1 \\ 1 & 1 \end{bmatrix} \begin{bmatrix} ae^{-\gamma_a x} + be^{\gamma_a x} \\ ce^{-\gamma_b x} + de^{\gamma_b x} \end{bmatrix} + Z_e \begin{bmatrix} 1 & 1 \\ 1 & 1 \end{bmatrix} \begin{bmatrix} I_{ai}(0) \\ I_{bi}(0) \end{bmatrix} \tag{D.1}$$

Using Equations 7.22 to 7.25 and rearranging,

$$e^{2\gamma_a L} = \frac{[1 + k_1(Z_{Li} + 2Z_e)](1 - 2k_1 Z_{ABi})}{[1 - k_1(Z_{Li} + 2Z_e)](1 + 2k_1 Z_{ABi})} \tag{D.2}$$

and

$$e^{2\gamma_b L} = \frac{(1 + Z_{Li}k_2)(1 - 2k_2 Z_{CDi})}{(1 - Z_{Li}k_1)(1 + 2k_2 Z_{CDi})} \tag{D.3}$$

where

$Z_{ABi} = \frac{V_{ai}'(0) + V_{bi}'(0)}{2[I_a(0) + I_b(0)]} - Z_e$

$Z_{CDi} = \frac{V_{ai}'(0) - V_{bi}'(0)}{2[I_a(0) - I_b(0)]}$

Equation D.3 may be solved for k_2 by equating the value of $e^{2\gamma_b L}$ for two values of load ($i = 1, 2$). The result is

$$k_2 = \pm \frac{(Z_{L2} - Z_{L1}) + 2(Z_{CD1} - Z_{CD2})}{2[Z_{L1}Z_{L2}(Z_{CD1} - Z_{CD2}) + 2Z_{CD1}Z_{CD2}(Z_{L2} - Z_{L1})]} \tag{D.4}$$

Substituting k_2 into Equation D.3 then gives γ_b. By similar substitution of $i = 1, j$ into Equation D.2, the value of k_1 becomes

$$k_1 = \pm \frac{(Z_{Lj} - Z_{L1}) + 2(Z_{AB1} - Z_{ABj})}{2[(Z_{L1} + 2Z_e)(Z_{Lj} + 2Z_e)(Z_{AB1} - Z_{ABj}) + 2Z_{AB1}Z_{ABj}(Z_{Lj} - Z_{L1})]} \quad \text{(D.5)}$$

By setting $j = 2, 3$, the resulting solutions for k_1 may be equated, yielding

$$Z_e = -\frac{G \pm \sqrt{(G^2 - 4FH)}}{2F} \quad \text{(D.6)}$$

where

$F = 2(2Z_{p2}\delta Z_3 - 2Z_{p3}\delta Z_2 + Z_{p2}\delta Z_{L3} - Z_{p3}\delta Z_{L2})$

$G = 2[Z_{p2}(Z_{L3}+Z_{L1})\delta Z_3 - Z_{p2}\delta Z_{L3}(Z_{q1}+Z_{q3}) - Z_{p3}(Z_{L2}+Z_{L1})\delta Z_2 + Z_{p3}\delta Z_{L2}(Z_{q1}+Z_{q2})]$

$H = Z_{L1}(Z_{p2}Z_{L3}\delta Z_3 - Z_{p3}Z_{L2}\delta Z_2) + 2Z_{q1}(Z_{q3}Z_{p2}\delta Z_{L3} - Z_{q2}Z_{p3}\delta Z_{L2})$

$Z_{Pj} = \delta Z_{Lj} + 2\delta Z_j \ (j = 2, 3)$

$\delta Z_{Lj} = Z_{Lj} - Z_{L1} \ (j = 2, 3)$

$\delta Z_j = Z_{AB1} - Z_{ABj} \ (j = 2, 3)$

$Z_{qi} = \frac{V_{ai}'(0)+V_{bi}'(0)}{2[I_1(0)+I_2(0)]} \ (i = 1, 2, 3)$

Appendix E

The Use of F.E.M. in Rail Track Electromagnetic Analysis

The application of an F.E.M. package to the analysis of the electromagnetic properties of a system is well–known and well documented. Only example references are cited here [186], [179], [187], [188]. Hence only a summary of the processes involved are given here, with specific reference to rail–track where applicable.

The Equations to be Solved

The field equations to be solved may be summarised as :–

$$\nabla.\mathbf{D} = \rho \tag{E.1}$$

$$\nabla.\mathbf{B} = 0 \tag{E.2}$$

$$\nabla \times \mathbf{E} = -\frac{\partial \mathbf{B}}{\partial t} \tag{E.3}$$

$$\nabla \times \mathbf{H} = \mathbf{J} \tag{E.4}$$

where $\mathbf{J}$ is made up of source currents ($\mathbf{J_s}$) and eddy currents ($\sigma\mathbf{E}$)

with the material properties being defined as

$$\mathbf{D} = \epsilon\mathbf{E} \tag{E.5}$$

$$\mathbf{B} = \mu\mathbf{H} \tag{E.6}$$

In the electrostatics case, it is less complicated to solve for a scalar potential V rather

than a vector potential **E**. From

$$\mathbf{E} = -\nabla V \tag{E.7}$$

then it follows that the equation to be solved is

$$-\nabla.\epsilon\nabla V = \rho \tag{E.8}$$

Although the magnetostatics case can be developed in the same way, in order that dynamic solutions can be obtained, i.e. including eddy currents, a continuous vector potential is required. The magnetostatic solution is then simply a special case of the electromagnetic problem.

In the electromagnetic case the vector potential is defined as

$$\nabla \times \mathbf{A} = \mathbf{B} \tag{E.9}$$

since

$$\nabla \times \mathbf{H} = \mathbf{J_s} + \sigma\mathbf{E} \tag{E.10}$$

$$= \mathbf{J_s} - \sigma\frac{\partial \mathbf{A}}{\partial t} \tag{E.11}$$

then the equation to solve is

$$\nabla \times \frac{1}{\mu}(\nabla \times \mathbf{A}) = \mathbf{J_s} - \sigma\frac{\partial \mathbf{A}}{\partial t} \tag{E.12}$$

Fortunately, in two dimensions, only the z–component of **A** is required, as the other two components are assumed to be constant in the model space. This simplifies the implementation procedure.

Building the Models

The process of modelling a physical system using the Finite Element Method, may be considered as series of conceptual modelling steps:–

1. Determination of the physical model requires the relevant features of the physical system to be identified. These would include the geometry, material properties and excitation of the actual system. Dimensions, permeabilities, permittivities, conductivities, conductor (source) current densities and driving voltage magnitudes and waveforms must be known.

2. This information, contained in the physical model, is refined to what is often termed the geometric model. This is a simplification process where only the features, relevant to the particular analysis, are included. For example, in an inductance calculation, permittivity is not required (or it is assumed to be unity). Alternatively, to determine the capacitance between two rails, the permeability is of no interest.

   Other considerations include boundary conditions. The boundaries must be chosen to provide a suitable shape, function condition and distance so that a meaningful and accurate solution is obtained. To ensure that the far field boundaries are a sufficient distance away from the rail track, two different boundary conditions have been used, know as the Neumann and Dirichlet conditions. The former, also known as the natural F.E.M. condition, sets the normal derivative of the potential to zero; the later sets the potential to zero. If the solutions from the two conditions provide results which agree with each other, to within an acceptable error, the boundary is deemed to be an acceptable distance from the track[1].

3. The geometric model may still contain redundant information, especially in the case of the problem symmetry. Hence a mathematical model is constructed which may not obviously relate to the physical system. Here, use is made of symmetry in the system geometry. For example, when analysing a single rail, only half

[1]The true solution lies somewhere between these two extreme solutions

the cross–section needs to be modelled i.e. the geometry has a vertical line of symmetry.

Other examples of redundant information include conductors, in electrostatic analysis. Since permittivity, $\epsilon \rightarrow \infty$ in conductors, they are omitted from the mathematical model (although their outline is required).

Other mathematical considerations are also included here. Since the potential is related to the field by:–

$$\mathbf{B} = \nabla \times \mathbf{A} \tag{E.13}$$

the potential does not have an inherently unique value. Hence the potential must be set at a minimum of one point one point in the model, e.g. on a boundary.

4. Once the mathematical model is formed, it is discretised into a numerical model. The number of elements which can be used is limited by a practical limitation in computational effort. Hence more sophisticated models may be used when computer power is increased. To obtain a suitably accurate result, more elements are required in regions of rapidly changing fields. The error of the solution is proportional to h^2 where h is the largest dimension of the element. In addition, the elemental interpolation method may be improved by changing from linear to quadratic, although the computational effort will increase.

   To illustrate this in a simple form, consider the process for a one dimensional case. A function Φ, shown in Figure E.1, is to be approximated by a polynomial.

   Let the polynomial be first order i.e.

$$\Phi = a + bs \tag{E.14}$$

   where a, b are coefficients; higher order polynomials can be used. In local coordi-

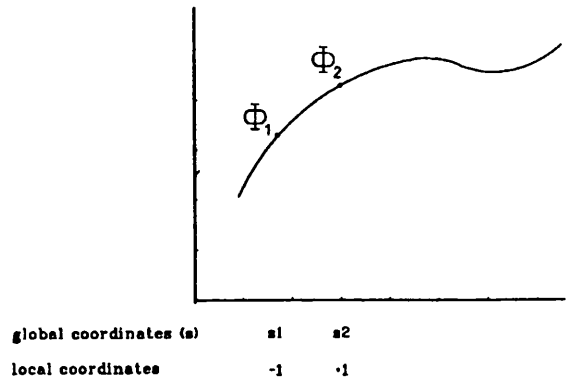

Figure E.1: A 1–D Function

nates

$$\Phi_1 = a - b \tag{E.15}$$

$$\Phi_2 = a + b \tag{E.16}$$

This gives

$$a = f_1(\Phi_1, \Phi_2) \tag{E.17}$$

$$b = f_2(\Phi_1, \Phi_2) \tag{E.18}$$

In this case

$$a = \tfrac{1}{2}(\Phi_1 + \Phi_2) \tag{E.19}$$

$$b = -\tfrac{1}{2}(\Phi_1 - \Phi_2) \tag{E.20}$$

Between Φ_1 and Φ_2 the function is approximated by

$$\Phi = f_1(\Phi_1, \Phi_2) + f_2(\Phi_1, \Phi_2) \tag{E.21}$$

which can be rewritten as

$$\Phi = N_1\Phi_1 + N_2\Phi_2 \tag{E.22}$$

where N_i are the shape functions

$$N_1 = \alpha + \beta s \tag{E.23}$$

$$N_2 = \gamma + \lambda s \tag{E.24}$$

At a discretised point (node i),

$$N_i = 1 \tag{E.25}$$

$$N_j = 0 \tag{E.26}$$

$$j \neq i \tag{E.27}$$

So the finite element method is a linear (or higher order) approximation of Φ as it varies with s. To maintain good accuracy, in regions of rapidly changing fields, discretisation should be greater (see Figure E.2-a) and quadratic approximation may be used (see Figure E.2-b). Both techniques will require additional computational effort.

In the 2–D case, the same principles are used as for the 1–D case. Global and local coordinates are set up. This is illustrated in Figure E.3, for element number 6.

The function is now approximated by a linear interpolation in two dimensions

$$\Psi = a + bx + cy \tag{E.28}$$

In local coordinate notation, it can be seen that the function at each vertex is

$$\Psi_1 = a + bx_1 + cy_1 \tag{E.29}$$

$$\Psi_2 = a + bx_2 + cy_2 \tag{E.30}$$

$$\Psi_3 = a + bx_3 + cy_3 \tag{E.31}$$

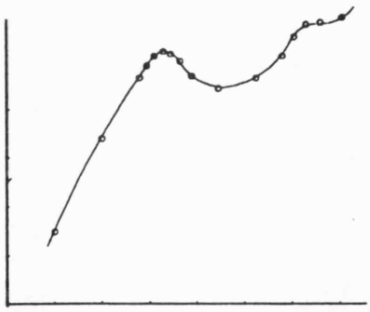

(a) Selective Increase Discretisation

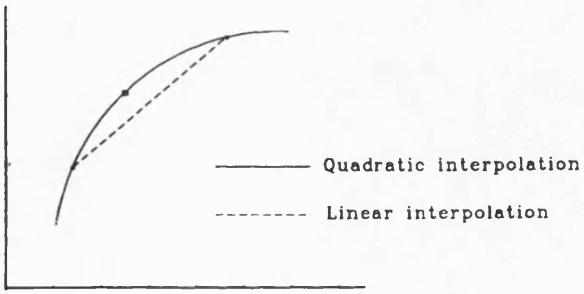

(b) Quadratic Interpolation

Figure E.2: Consideration of Rapidly Changing Fields

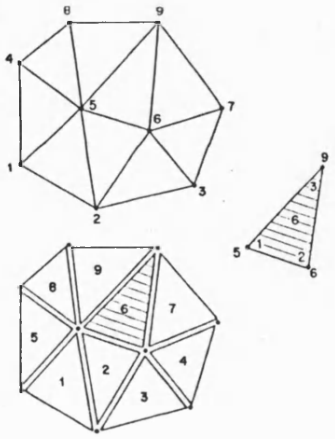

Figure E.3: Discretisation of 2-D Problem Space

which may be solved to give

$$a = f_1(\Psi_1, \Psi_2, \Psi_3) \tag{E.32}$$

$$b = f_2(\Psi_1, \Psi_2, \Psi_3) \tag{E.33}$$

$$c = f_3(\Psi_1, \Psi_2, \Psi_3) \tag{E.34}$$

As with the 1 – D case, shape functions may be used

$$\Psi = N_1\Psi_1 + N_2\Psi_2 + N_3\Psi_3 = \sum_1^3 N_i\Psi_i \tag{E.35}$$

where generally

$$N_i = v_i + \eta_i x + \zeta_i y \tag{E.36}$$

Again, at node 1, $N_1 = 1$ with $N_2 = N_3 = 0$

5. Finally the functions approximating each discretised element of the model are brought together and a series of matrix equations are formed. The structure of these matrices is such that elements sharing vertices are related. The solution of the problem is now reduced to the solution of these large sparse matrices. The exact method chosen to solve these equations differs from package to package. However, the methods are well known and well documented in standard mathematical texts on the subject. Typical references are given here [190], [191]

It is usual to use the F.E.M. packages commercially available to model the electromagnetic (including magnetostatic) and electrostatic cases. However, the physical process of conduction is mathematically similar to these. This has allowed the F.E.M. software to be used to not only determine the series rail impedance and inter–rail capacitance but also the inter–rail conductance. The basic duals of the equations are given in Table E.1.

Table E.1: Finite Element Duality Equations in Two Dimensions

Electromagnetic	Conductivity	Electrostatic	Comment
$\nabla H = 0$	$\nabla J = 0$	$\nabla D = 0$	Divergence Constraint
$H = \mu B$	$J = \sigma E$	$D = \varepsilon E$	Material Properties Relationship
$B = \nabla \times A$	$E = -\nabla V$	$E = -\nabla V$	Potential Relationship
$\frac{1}{\mu}$	σ	ε	Material Properties
$\int HBds$	$\int EJds$	$\int EDds$	Energy/Power Integral
$= \frac{1}{2}LI^2$	$= GV^2$	$= \frac{1}{2}CV^2$	
$\nabla(\frac{1}{\mu}\nabla A) = 0$	$-\nabla\sigma\nabla V = 0$	$-\nabla\varepsilon\nabla V = 0$	Static Governing Equations
$\nabla(\frac{1}{\mu}\nabla A) = J_z - \sigma\frac{\partial A_z}{\partial t}$	$-\nabla\sigma\nabla V = -\mu\frac{\partial H_z}{\partial t}$		Dynamic Governing Equations

Table E.2: Sample Results for Internal Rail Impedance at 50 Hz

Excitation	F.E.M.		Analytical		Experimental	
Current (A)	L (μH/m)	R (mΩ/m)	L (μH/m)	R (mΩ /m)	L (μH/m)	R (mΩ/m)
800	0.672	0.231	0.670	0.220	0.635	0.252
900	0.647	0.233	0.705	0.228	0.641	0.259
1000	0.615	0.235	0.719	0.233	0.644	0.263

Appendix F

E.M.T.D.C. Transmission Line Data

The data format for the transmission line model used in E.M.T.D.C. starts with a line:–

```
Np Nl SSN RSN fp fs L
```

and n lines in the following format (where n is the number of phases)

```
Ntx Nrx tc Zmo Rp Rs [Tim] [Tvm]
```

where

Np is the number of phases

Nl is the transmission line label

SSN is the Sending end subsystem number

RSN is the receiving end subsystem number

fp is the power frequency

fs is the signaling frequency

L is the transmission line length

Ntx is the sending end node number

Nrx is the receiving end node number

tc = τ is the travel time (ms)

Zmo is the modal characteristic impedance

Rp power resistance

Rs signalling resistance

[Tim] Row of current modal transformation matrix

[Tvm] Row of voltage modal transformation matrix

As an example consider a third rail electrified line for a frequency of 1800 Hz

```
3 0 1 2 50 1800 20 /
1 1 0.8618 60.0 0.9938  25.0 0.001 -0.510 -0.085 /
2 2 0.2055 36.0 0.0494 -0.5  0.707  0.815 -0.660 /
3 3 0.3492 17.0 0.0273  2.3  0.710 -0.240  0.740 /
```

Appendix G

The Dimensions of the Third Rail and Catenary Systems used in Analysis

The dimensions used for the analytical and numerical analyses are given in the following diagrams.

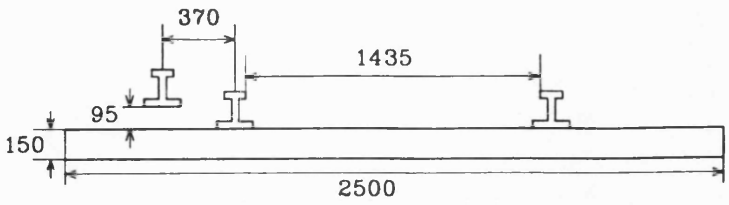

Dimensions in mm

Figure G.1: Third Rail System Dimensions

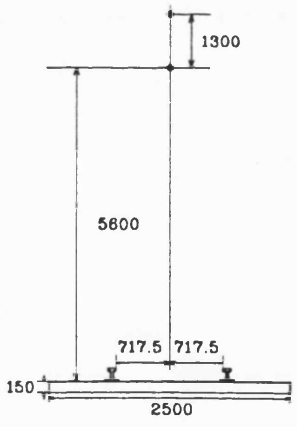

Dimensions in mm

Figure G.2: Catenary System Dimensions

Appendix H

Methods of Phase Parameter Analysis

There are a number of approaches to performing the analysis on the phase matrix elements to determine the modal quantities for simulation studies. The main task is to calculate the eigenvalues and vectors of the phase matrices from which the modal data is obtained. In this study two standard numerical algorithms have been used. The NAG library of mathematical subroutines had been used initially. However a more modern software package – "MATHEMATICA" – was adopted later.

Sample results from each were compared as a validation of accuracy between the two sets of software. There was found to be negligible difference in the results. However, the use of MATHEMATICA has been found to be far less time consuming, and has been used for most of the analysis required.

A sample algorithm is given below and it can be seen that the code is easily extendable to a larger number of conductors (rails, catenary etc.). In addition, the computational effort required is also negligible compared to simulation time.

```
<<Algebra/ReIm.m
zdata=OpenRead["zvals.hi"]
znrows=Read[zdata, Number]
zncols=Read[zdata, Number]
zimax=(zncols-1)/2
Do[zfreq[j]=Read[zdata, Number];
zz=Table[z[i]=Read[zdata, Number] +
Read[zdata, Number] I, {i, zimax}];
zp[j]={{z[1], z[2], z[2]}, {z[2], z[3], z[4]}, {z[2], z[4], z[3]}},
{j,znrows}]
Close[zdata]
ydata=OpenRead["yvals.hi"]
ynrows=Read[ydata, Number]
yncols=Read[ydata, Number]
yimax=(yncols-1)/2
Do[yfreq[j]=Read[ydata, Number];
yy=Table[y[i]=Read[ydata, Number] +
Read[ydata, Number] I, {i, yimax}];
```

```
yp[j]={{y[1], y[4], y[4]}, {y[4], y[2], y[3]}, {y[4], y[3], y[2]}},
{j,ynrows}]
Close[ydata]
Do[a[i]=yp[i] . zp[i];
{vals[i],vecs}=Eigensystem[a[i]];
T1=vecs[[1]];
T2=vecs[[2]];
T3=vecs[[3]];
If[Abs[T1[[1]]] > Abs[T1[[2]]], T1max = T1[[1]], T1max = T1[[2]]];
If[Abs[T1max] > Abs[T1[[3]]], dummy = T1max, T1max = T1[[3]]];
If[Abs[T2[[1]]] > Abs[T2[[2]]], T2max = T2[[1]], T2max = T2[[2]]];
If[Abs[T2max] > Abs[T2[[3]]], dummy = T2max, T2max = T2[[3]]];
If[Abs[T3[[1]]] > Abs[T3[[2]]], T3max = T3[[1]], T3max = T3[[2]]];
If[Abs[T3max] > Abs[T3[[3]]], dummy = T3max, T3max = T3[[3]]];
T1mod = Conjugate[T1max] T1;
T2mod = Conjugate[T2max] T2;
T3mod = Conjugate[T3max] T3;
T1m = Transpose[T1mod] . Conjugate[T1mod];
T2m = Transpose[T2mod] . Conjugate[T2mod];
T3m = Transpose[T3mod] . Conjugate[T3mod];
T1mat = (1/Sqrt[T1m]) T1mod;
T2mat = (1/Sqrt[T2m]) T2mod;
T3mat = (1/Sqrt[T3m]) T3mod;
TT[i] = {T1mat, T2mat, T3mat};
T[i] = Transpose[TT[i]];
ym[i] = Inverse[T[i]] . yp[i] . Inverse[Transpose[T[i]]];
zm[i] = Transpose[T[i]] . zp[i] . T[i];
zo1 = Sqrt[zm[i][[1,1]]/(ym[i][[1,1]] 10^-3)];
zo2 = Sqrt[zm[i][[2,2]]/(ym[i][[2,2]] 10^-3)];
zo3 = Sqrt[zm[i][[3,3]]/(ym[i][[3,3]] 10^-3)];
zo[i] = {{zo1}, {zo2}, {zo3}};
zoalt[i] = {{Abs[zo1], (Arg[zo1] N[180/Pi])},
{Abs[zo2], (Arg[zo2] N[180/Pi])}, {Abs[zo3], (Arg[zo3] N[180/Pi])}}
, {i, znrows}]
results = OpenWrite["modal.hi.res", FormatType -> OutputForm]
WriteString[results, "Eigenvalues/vectors of Catenary (Conductivity = 0.076923 S/m) \n"]
WriteString[results, " \n"]
Do[WriteString[results, "freq (Hz) ="];
Write[results, zfreq[i]];
WriteString[results, " \n"];
WriteString[results, " \n"];
WriteString[results, " \n"];
WriteString[results,"Eigenvalues \n"];
WriteString[results, " \n"];
Write[results,SetAccuracy[MatrixForm[vals[i]], 5]];
WriteString[results, " \n"];
WriteString[results, " \n"];
WriteString[results, " \n"];
WriteString[results,"Eigenvectors\n"];
WriteString[results," \n"];
Write[results,SetAccuracy[MatrixForm[T[i]], 5]];
WriteString[results," \n"];
WriteString[results," \n"];
WriteString[results," \n"];
WriteString[results,"Modal Admittance Matrix\n"];
WriteString[results," \n"];
Write[results,SetAccuracy[MatrixForm[ym[i]], 5]];
WriteString[results," \n"];
WriteString[results," \n"];
WriteString[results," \n"];
WriteString[results,"Modal Impedance Matrix\n"];
WriteString[results," \n"];
Write[results,SetAccuracy[MatrixForm[zm[i]], 5]];
WriteString[results," \n"];
WriteString[results," \n"];
WriteString[results," \n"];
WriteString[results," \n"];
WriteString[results,"Modal Characteristic Impedance Matrix (Conductivity = 0.076923 S/m) \n"];
WriteString[results," \n"];
Write[results,SetAccuracy[MatrixForm[zo[i]], 5]];
WriteString[results," \n"];
WriteString[results," \n"];
```

```
WriteString[results," \n"];
WriteString[results," \n"];
Write[results,SetAccuracy[MatrixForm[zoalt[i]], 5]];
WriteString[results, " \n"];
WriteString[results, " \n"];
WriteString[results, " \n"];
WriteString[results, " \n"];
WriteString[results, " \n"];
, {i, znrows}]
Close[results]
Do[vals[i] = vals[i]*10;
gammaA[i] = {{zfreq[i], Abs[Sqrt[vals[i][[1]]]],
Arg[Sqrt[vals[i][[1]]]]/N[Degree],
Abs[Sqrt[vals[i][[2]]]], Arg[Sqrt[vals[i][[2]]]]/N[Degree],
Abs[Sqrt[vals[i][[3]]]],
Arg[Sqrt[vals[i][[3]]]]/N[Degree]}};
gammaB[i] = {{Sqrt[vals[i][[1]]],
Sqrt[vals[i][[2]]],Sqrt[vals[i][[3]]]}},
{i, znrows}]
propcon= OpenWrite["propcon.hi.res", FormatType -> OutputForm]
Write[propcon,"Propagation Constants (Conductivity = 0.076923 S/m)\n"]
WriteString[propcon," \n"]
WriteString[propcon,"freq (Hz)              gamma (per m 10^-5)\n"]
WriteString[propcon," \n"]
Do[Write[propcon, MatrixForm[gammaA[i]]], {i, znrows}]
WriteString[propcon," \n"]
Do[Write[propcon, MatrixForm[gammaB[i]]], {i, znrows}]
Close[propcon]
Do[
zmoutA[i] = {{zfreq[i], Abs[zm[i][[1,1]]],
Arg[zm[i][[1,1]]]/N[Degree],
Abs[zm[i][[2,2]]], Arg[zm[i][[2,2]]]/N[Degree],
Abs[zm[i][[3,3]]],
Arg[zm[i][[3,3]]]/N[Degree]}},
{i, znrows}]
zmodal= OpenWrite["zmodal.hi.res", FormatType -> OutputForm]
Write[zmodal,"Modal Impedance Matrix Elements (Conductivity = 0.076923 S/m)\n"]
WriteString[zmodal," \n"]
WriteString[zmodal,"freq (Hz)              Impedance (ohms/m)\n"]
WriteString[zmodal," \n"]
Do[Write[zmodal, SetAccuracy[MatrixForm[zmoutA[i]], 3]], {i, znrows}]
Close[zmodal]
Do[
ymoutA[i] = {{zfreq[i], Abs[ym[i][[1,1]]],
Arg[ym[i][[1,1]]]/N[Degree],
Abs[ym[i][[2,2]]], Arg[ym[i][[2,2]]]/N[Degree],
Abs[ym[i][[3,3]]],
Arg[ym[i][[3,3]]]/N[Degree]}},
{i, znrows}]
ymodal= OpenWrite["ymodal.hi.res", FormatType -> OutputForm]
Write[ymodal,"Modal Admittance Matrix Elements (Conductivity = 0.076923 S/m)\n"]
WriteString[ymodal," \n"]
WriteString[ymodal,"freq (Hz)              Admittance (micro-siemens/m)\n"]
WriteString[ymodal," \n"]
Do[Write[ymodal, SetAccuracy[MatrixForm[ymoutA[i]], 3]], {i, znrows}]
Close[ymodal]
Do[
zoaltA[i] = {{zfreq[i], zoalt[i][[1,1]],
zoalt[i][[1,2]],
zoalt[i][[2,1]],
zoalt[i][[2,2]],
zoalt[i][[3,1]],
zoalt[i][[3,2]]}}, {i, znrows}]
zmo = OpenWrite["zmo.hi.res", FormatType -> OutputForm]
Write[zmo,"Modal Characteristic Impedances (Conductivity = 0.076923 S/m)\n"]
WriteString[zmo," \n"]
WriteString[zmo,"freq (Hz)              Impedance (ohms/m)\n"]
WriteString[zmo," \n"]
Do[Write[zmo, SetAccuracy[MatrixForm[zoaltA[i]], 4]], {i, znrows}]
Close[zmo]
Do[
zpoA[i] = {{zfreq[i], Abs[Sqrt[zp[i][[1,1]]/(yp[i][[1,1]] 10^-3)]],
```

```
Arg[zp[i][[1,1]]/(2 yp[i][[1,1]])]/N[Degree],
Abs[Sqrt[zp[i][[2,2]]/(yp[i][[2,2]] 10^-3)]],
Arg[zp[i][[2,2]]/(2 yp[i][[2,2]])]/N[Degree],
Abs[Sqrt[zp[i][[3,3]]/(yp[i][[3,3]] 10^-3)]],
Arg[zp[i][[3,3]]/(2 yp[i][[3,3]])]/N[Degree]}}, {i, znrows}]
zpo= OpenWrite["zpo.hi.res", FormatType -> OutputForm]
Write[zpo,"Phase Characteristic Impedances (Conductivity = 0.076923 S/m)\n"]
WriteString[zpo," \n"]
WriteString[zpo,"freq (Hz)              Impedance (ohms/m)\n"]
WriteString[zpo," \n"]
Do[Write[zpo, SetAccuracy[MatrixForm[zpoA[i]], 4]], {i, znrows}]
Close[zpo]
Do[
ppoA[i] = {{zfreq[i], Re[Sqrt[zp[i][[1,1]] (yp[i][[1,1]] 10^-3)]],
Im[Sqrt[zp[i][[1,1]] (yp[i][[1,1]] 10^-3)]],
Re[Sqrt[zp[i][[2,2]] (yp[i][[2,2]] 10^-3)]],
Im[Sqrt[zp[i][[2,2]] (yp[i][[2,2]] 10^-3)]],
Re[Sqrt[zp[i][[3,3]] (yp[i][[3,3]] 10^-3)]],
Im[Sqrt[zp[i][[3,3]] (yp[i][[3,3]] 10^-3)]]
}}, {i, znrows}]
ppo= OpenWrite["ppo.hi.res", FormatType -> OutputForm]
Write[ppo,"Phase Propagation Constants (Conductivity = 0.076923 S/m)\n"]
WriteString[ppo," \n"]
WriteString[ppo,"freq (Hz)              Propagation Constant x 10^-3 (per m) \n"]
WriteString[ppo," \n"]
Do[Write[ppo, SetAccuracy[MatrixForm[ppoA[i]], 5]], {i, znrows}]
Close[ppo]
```

Appendix I

List of Publications

1. "Railway Track Admittance, Earth-Leakage Effects and Track Circuit Operation". 1989 IEEE/ASME Joint Railroad Conference, Philadelphia, USA, April 1989, pp. 55-62 (with R.J. Hill and T. Tasar).

2. "The Effects of Magnetic Saturation, Hysteresis and Eddy Currents on Rail Track Impedance". 1989 IEEE/ASME Joint Railroad Conference, Philadelphia, USA, April 1989, pp. 73-79 (with R.J. Hill).

3. "Rail Impedance Modelling for D.C.-Fed Railway Traction Simulation". Int. Sym. Applied Modelling and Simulation, Lugano, Switzerland, June 1990, pp. 105-108 (with R.J. Hill).

4. "Modelling of Nonlinear Rail Impedance in A.C. Traction Power Systems". 4th Int. Conf. Harmonics in Power Systems (ICHPS IV), Budapest, Hungary, October 1990, pp. 268-274 (with R.J. Hill).

5. "Rail Track Modelling for Signalling and Electrification System Simulation Studies". Rail Engineering International, Vol. 19, No. 4, December 1990, pp. 16-20 (with R.J. Hill).

6. "FEM Applied to Railroad Track Electrical Impedance and Adjacent Track Crosstalk Modelling". 1991 Joint IEEE/ASME Railroad Conference, St. Louis, USA, May 1991, pp.87-95 (with R.J. Hill)

7. "'Using the Circuit Simulation Package EMTDC for Audio Frequency Track Circuit Design". Int. Conf. Automation Signalling Performance Equipment Control Telecommunications, ASPECT '91, London, UK, October 1991, pp.456-469 (with R.J. Hill, M.L. Berova, G.J.W. Meecham).

8. "Modelling of Nonlinear Rail Impedance in A.C. Traction Power Systems". IEEE Transactions on Power Delivery, Vol. 6, No. 4, October 1991, pp. 1755-1761 (with R.J. Hill).

9. "Determination of Rail Internal Impedance for Electric Railway Traction System Simulation". IEE Proceedings Part B: Electric Power Applications, Vol. 138, No. 6, November 1991, pp. 311-321 (with R.J. Hill).

10. 'Electromagnetic Field Modelling of Rail Track using the Finite Element Method". Rail Engineering International, Vol. 20, No. 4, December 1991, pp. 17-20 (with R.J. Hill).

11. "Finite Element Method Modelling of Overhead Catenary Rail Track Impedance and Admittance". Computers in Railways, volume 2: Technology. Proceedings of the Third International Conference on Computer Aided Design, Manufacture and Operation in the Railway and other Advanced Mass Transit Systems (COMPRAIL 92), Washington DC, USA, October 1992, pp.403-416. (with R.J. Hill).

12. "In-Situ Determination of Rail Track Electrical Impedance and Admittance Matrix Elements". IEEE Transactions on Instrumentation and Measurement, Vol. 41, No. 5, October 1992, pp. 666-673. (with R.J. Hill)

13. Accepted – December 1992

    "Rail Track Transmission Line Distributed Impedance and Admittance: Theoretical Modelling and Experimental Results". IEEE Transactions on Vehicular Technology (with R.J. Hill)

14. Under final review – January 1993

    "Railroad Track Electrical Impedance and Adjacent Track Crosstalk Modelling Using the Finite–Element Method of Electromagnetic Systems Analysis". IEEE Transactions on Vehicular Technology. (with R.J. Hill)

15. Accepted – March 1993

    "A Continuous-Function Ground Conductivity Model for the Determination of Electric Railway Earth Conductance". IEEE Transactions on Geoscience and Remote Sensing (with R.J. Hill).

16. Accepted – February 1993

    "Signal Propagation Characteristics of Electrified Railway Track". ITTG 93, Technological Innovation in Guided Transports, Lille, September 1993, France. (with R.J. Hill)

RAILWAY TRACK ADMITTANCE, EARTH-LEAKAGE EFFECTS AND TRACK CIRCUIT OPERATION

R. J. Hill, D. C. Carpenter and T. Tasar

School of Electrical Engineering, University of Bath,
Claverton Down, Bath BA2 7AY, UK

Abstract - Railway track acts as a pair of leaky ground-return conductors for propulsion current in the immediate vicinity of trains, and as an imperfectly insulated conductor pair for double-rail track circuits. This paper considers the effect of ground admittance and leakage conditions from both the traction and signalling viewpoints. Problems concerning rail voltage safety level, earth leakage currents and rail current distribution are considered. Capacitive compensation is evaluated as a means of improving the shunting sensitivity of track circuits with high ballast conductivity.

INTRODUCTION

Electric railway propulsion return current flows along the running rails in the immediate vicinity of trains. The rails act as leaky ground conductors in returning the current to the substation. If the running rails also carry track signalling current, the inter-rail electrical admittance causes shunting of part of the track circuit current. The connection of structures to the rails, for safety or other reasons, modifies this grounding impedance and can cause safety problems when rails are used for the return of propulsion current. It can also interfere with the correct operation of track circuits.

Determining the flow of propulsion and signalling currents, and the associated potentials, through the ground in an electrified railway is important for a number of reasons. Excitation of nearby earth return circuits can result in interference, corrosion problems and danger to personnel. The calculation of currents and potentials in nearby underground conductors such as cables and pipes requires knowledge of the electrical properties of the earth, in particular the resistivity of the local soil.

The traction engineer is interested in current propagation to determine the network impedances and track-ground voltages. The ground return current problem can be analysed by considering the distribution of track voltages and currents. This problem was apparent in early electric railways. For example, Riordan [1] considered current propagation along rail tracks and their associated conductors, and Sunde [2] derived general formulae for currents and voltages along straight, uniform wires laid on the surface of the earth, making various assumptions about earthing and excitation conditions.

Currents and potentials in telecommunications cables due to harmonic components of traction current are a major problem, and Rosen's [3] early analytic methods have been the subject of recent computer modelling by Mellitt et al [4].

For DC-fed railroads and rail transit systems, electrolytic corrosion may occur if substantial current escapes to ground from track components and materials. This corrosion can be a particular problem for nearby metal gas and water pipes, and cables. Corrosion problems have been considered by several authors. Takihara [5], for example, evaluated rail-to-earth voltage and rail current and gave estimates of rail leakage resistance. Kneschke [6] and Shaffer [7] propose design solutions for particular problems arising from stray current effects.

Safety is also a problem, since hazardous step and touch voltages may be present on the rails. Jacimovic [8] has evaluated safety voltage levels and related the results to practical situations.

TRACK ELECTRICAL CIRCUIT AND TRANSMISSION LINE MODELLING

Transmission line equation of propagation

Currents and voltages along the balanced conductor pair represented by the running rails and shown in Figure 1 are determined by standard transmission line analysis in terms of exponential, trigonometric or hyperbolic functions. In exponential form, the line voltage and current are:

$$V(x) = \frac{V_L}{1+\mu}\left[e^{\gamma x} + \mu e^{-\gamma x}\right] \qquad (1)$$

and

$$I(x) = \frac{I_L}{1-\mu}\left[e^{\gamma x} - \mu e^{-\gamma x}\right]. \qquad (2)$$

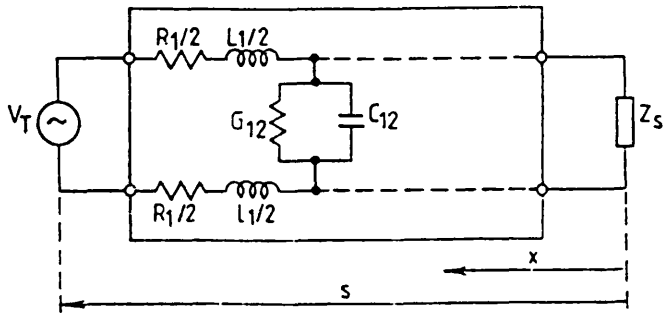

Figure 1: Rail track balanced transmission line model

The distance x along the line is measured from the load L and γ and μ are the propagation constant and reflection factor defined by

$$\gamma = \sqrt{(R_1 + j\omega L_1)(G_{12} + j\omega C_{12})} \quad (3)$$

and $$\mu = (Z_L - Z_{01})/(Z_L + Z_{01}), \quad (4)$$

with line characteristic impedance

$$Z_{01} = \sqrt{(R_1 + j\omega L_1)/(G_{12} + j\omega C_{12})}. \quad (5)$$

This form of analysis is useful for considering track circuit operation. The earth admittance appears in the propagation constant as leakage conductance G_{12} and capacitance C_{12}. Symmetric conditions apply where the earth admittance of each line is the same. In cases where asymmetric earthing conditions occur, the line is no longer balanced and there can be several signal propagation modes.

The Heaviside condition for distortionless transmission of signals along the line and minimum attenuation relates the line constants according to

$$R_1 C_{12} = L_1 G_{12}, \quad (6)$$

so in this case the propagation constant becomes

$$\gamma = \sqrt{(R_1 G_{12})} + j\omega L_1 \sqrt{(G_{12}/R_1)}. \quad (7)$$

Leaky ground-return conductor theory

The basic electric railway catenary circuit with rail/earth return exhibits rail currents and voltages to earth determined from the distributed nature of the circuit. Normally, both rails are used for current return and the two-rail system may be considered as an equivalent single rail with earth leakage admittance. The equivalent circuit, as shown in Figure 2, demonstrates the presence of both inductive and conductive coupling between catenary and rail. The solution for rail current I, earth current i and rail-to-earth voltage V may be obtained by superimposing these two components - the conductive part injected into the track at train and substation terminals, with exponential propagation with distance, and the inductive part due to catenary-rail mutual coupling.

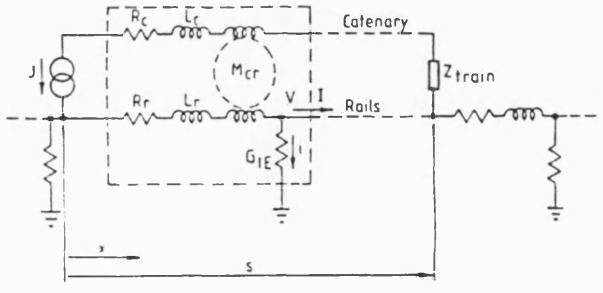

Figure 2: Rail track as leaky ground-return conductor

For the single-rail feeding system of Figure 2, the currents flow beyond the ends of the energized section, and track currents and voltages may be derived using the differential equations of propagation. Riordan [1] gives the solution as:

$x < 0$ $$I(x) = 0.5\,(1-\eta)\,(1 - e^{-\Gamma s})e^{-\Gamma|x|}J \quad (8)$$

$$i(x) = -I(x) \quad (9)$$

$$V(x) = 0.5\,Z_{02}\,(1-\eta)(1 - e^{-\Gamma s})e^{-\Gamma|x|}J \quad (10)$$

$s > x > 0$ $$I(x) = \eta J + 0.5(1-\eta)(e^{-\Gamma x} + e^{-\Gamma(s-x)})J \quad (11)$$

$$i(x) = J - I(x) \quad (12)$$

$$V(x) = 0.5\,Z_{02}\,(1-\eta)(e^{-\Gamma x} - e^{-\Gamma(s-x)})J \quad (13)$$

$x > s$ $$I(x) = -0.5\,(1-\eta)(1-e^{-\Gamma s})\,e^{-\Gamma(x-s)}J \quad (14)$$

$$I(x) = -I(x) \quad (15)$$

$$V(x) = -0.5\,Z_{02}\,(1-\eta)(1 - e^{-\Gamma s})e^{-\Gamma(x-s)}J \quad (16)$$

In these equations, J is the catenary current, η is the ratio of catenary-track mutual impedance with earth return, to the track earth-return series impedance

$$\eta = z_{ct}/z_t, \quad (17)$$

Γ is the propagation constant,

$$\Gamma = \sqrt{(z_t\,g)} = \sqrt{[(R_S + j\omega L_S)G_{1E}]}, \quad (18)$$

Z_{02} is the characteristic impedance

$$Z_{02} = \sqrt{(z_t/g)} = \sqrt{[(R_S + j\omega L_S)/G_{1E}]} \quad (19)$$

and s is the line length.

Ground admittance modelling

The practical application of the above equations depends on realistic modelling, verified by measurement of the ground admittance. The difficulty in modelling ground admittance (conductance and susceptance) is that it is critically dependent upon local topsoil, substrata and environmental conditions. Therefore the track admittance is dependent on these factors as well as the physical position of the rails relative to the ground.

In the literature, studies of ground electrical properties have been reported for applications ranging from power frequency transmission line grounding to microwave frequency radio propagation. The results indicate that the ground conductivity and permittivity scalar functions are generally both anisotropic and inhomogeneous. Except in ferrous regions, the ground relative permeability may be taken as unity, so the susceptance is capacitive.

Ground conductance

In low frequency earth-return circuit studies, suitable assumptions relating to isotropy and homogenity of the conductivity function are generally made, with depth dependency determined by approximations of uniform, homogeneous horizontal layers. Machczynski [9], for example, has calculated the excitation of underground conductors assuming a uniform conductivity function with depth, whereas Wedepohl [10] considers upper and lower strata for power line studies.

In the electric railway application, inter-rail leakage current flows close to the surface, whereas longitudinal propulsion current may flow at a deeper level. Therefore, a single-layer earth conductance function is inappropriate, and either a two-layer or continuous function conductivity model must be considered to give reasonable correlation with physical conditions.

Resistivity, rather than electromagnetic, experimental techniques are suitable for electric railway grounding studies, since the linear right of way conveniently defines a range of suitable electrode positions. The basic principle of galvanic ground conductivity measurements is well known from geophysical prospecting techniques [11,12]. A current

is introduced into the ground through point or contact electrodes, and other electrodes sense potentials in the vicinity of the current flow. The ratio of voltage to current is the apparent resistance

$$R = \frac{\Delta V}{I}. \qquad (20)$$

The dimensions of the electrode array – shape, depth and spacing – then enable calculation of conductivity (or resistivity) with depth according to the model adopted.

The theoretical problem is to relate the apparent resistance measurements (a function of horizontal distance over the ground surface), to the determination of best fit values for conductivity as a function of depth. This is done by applying Laplace's equation for the potential throughout the medium. The spread of current from the electrodes dictates the use of spherical coordinates so Laplace's equation becomes

$$\nabla^2 V = \frac{d^2V}{dr^2} + \left[\frac{2}{r}\right]\frac{dV}{dr} = 0 \qquad (21)$$

The solution is dependent upon the configuration of the electrode array in conjunction with appropriate boundary conditions at regions of different conductivity.

For the four-probe measurement technique (Figure 3), the apparent resistance is

$$\frac{\Delta V}{I} = \frac{[(1/r_1 - 1/r_2) - (1/r_3 - 1/r_4)]\,\rho_a}{2\pi} \qquad (22)$$

where ρ_a is the apparent resistivity. For any medium other than the uniform, homogenous, isotropic case, the measured value of ρ_a will vary with electrode spacing. For the Wenner array, the electrodes are equally spaced and collinear, i.e.

$$r_1 = a, \quad i = 1\text{–}4, \qquad (23)$$

so

$$\rho_a = \frac{2\pi a\,\Delta V}{I}. \qquad (24)$$

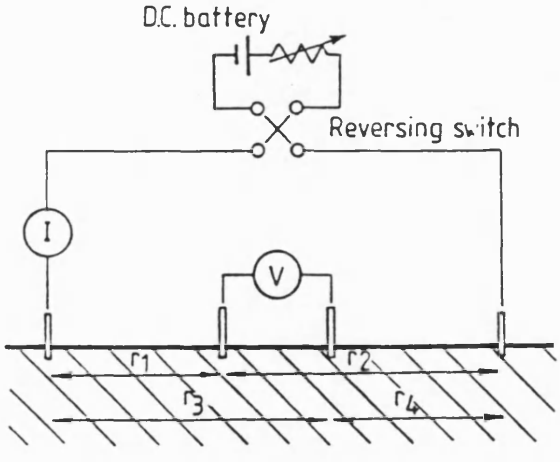

Figure 3: Four-probe measurement of ground resistivity

To model the earth as a two-layer homogenous, isotropic medium, the surface potential difference between the sensing electrodes is measured as a function of current and electrode spacing. At small electrode spacings, the apparent resistivity is $\rho_a = \rho_1$, the upper layer resistivity, and at large spacings it is ρ_2, the lower layer resistivity. It can be shown [11] that the apparent resistivity can be theoretically expressed in the form

$$\frac{\rho_a}{\rho_1} = 1 + \sum_{m=1}^{\infty} \frac{4k^m}{\sqrt{[1+(2mz/a)^2]}} - \sum_{m=1}^{\infty} \frac{4k^m}{\sqrt{[4+(2mz/a)^2]}} \qquad (25)$$

where k is a reflection coefficient defined by

$$k = \frac{\rho_2 - \rho_1}{\rho_2 + \rho_1} \qquad (26)$$

and z is the depth of the surface layer ρ_1.

Extraction of best fit ρ_1, ρ_2 and z values from the measurements may be carried out by a number of methods, the most appropriate of which depends on the exact site conditions. The experimental curve will be a smooth transition between ρ_1 and ρ_2 and one common interpretive method relies on the comparison of the experimental field profiles with standard characteristic curves of ρ_a/ρ_1 versus a/z with ρ_2/ρ_1 as parameter.

A more accurate technique, the Tagg method, uses the analytical solution of Equation 25 directly. A set of theoretical curves $\rho_a/\rho_1 = f(a/z)$, with k parameter, is calculated. Then from the experimental points, ρ_a/ρ_1 for each value of a is superimposed as horizontal lines. At each curve intersection, values of z (from a/z) and k are extracted. A further graph of k vs z, with parameter a, then gives a single intersection, hence determining best fit k and z (the layer depth), and thus defining the optimum ρ_1, ρ_2 and z combination.

The interpretation of the experimental ground conductivity results depends on obtaining an accurate value of ρ_1 from the short-distance measurements. The disadvantage of the Wenner array in this respect is its inherent inaccuracy for small probe spacings, because it assumes point sources for the electrodes. Baishiki [13] considered this problem, producing an alternative formula taking account of the cylindrical electrode shape. The apparent upper layer resistivity for the Wenner array

$$\rho_a = \left[\frac{4\pi a}{1 + \frac{2a}{\sqrt{(a^2+4b^2)}} - \frac{2a}{\sqrt{(a^2+b^2)}}}\right] R \qquad (27)$$

of which Equation 23 is an approximation for large electrode spacings, is replaced by a new formula

$$\rho_a = \left[\frac{2\pi L}{1 + 2\ln\frac{2+E}{1+F} + 2F - E - \frac{a}{L}}\right] R \qquad (28)$$

where L is the electrode length and

$$E = \sqrt{[4 + (a/L)^2]} \qquad (29)$$

and

$$F = \sqrt{[1 + (a/L)^2]}. \qquad (30)$$

The aim of the conductivity modelling process is to estimate values of track (inter-rail) conductance and rail (single-

rail to earth) conductance for insertion into the propagation constant equations 3 and 18. The ballast conductance is that between two parallel wires in continuous contact with the earth [11]

$$G_{12} = \frac{\pi}{\rho_1} \qquad (31)$$

and the maximum rail leakage conductance [2] is

$$G_{1E} = \frac{0.34}{\rho_2} \text{ to } \frac{0.66}{\rho_2} . \qquad (32)$$

Inter-rail capacitance

The measurement of ground susceptance, via the scalar permittivity function, has been successfully carried out at radio and microwave frequencies using electromagnetic sensing techniques. In general the variation of permittivity is dependent on frequency as well as environment, soil and substrata conditions. At low and power frequencies, the ground admittance is dominated by the conductive component, and measurements of capacitance or permittivity, either electromagnetically or by direct sensing, are difficult.

For rail track, it is necessary to know the inter-rail capacitance and an approximate model may be created by considering the track as two parallel cylindrical conductors, of effective diameter D and separation S, laid on the surface of a homogenous, isotropic ground of relative permittivity ε_r. The inter-rail capacitance is

$$C_{12} = \frac{2\pi \varepsilon_0 \varepsilon_r}{(1 + \varepsilon_r) \ln[(S-D)/D]} . \qquad (33)$$

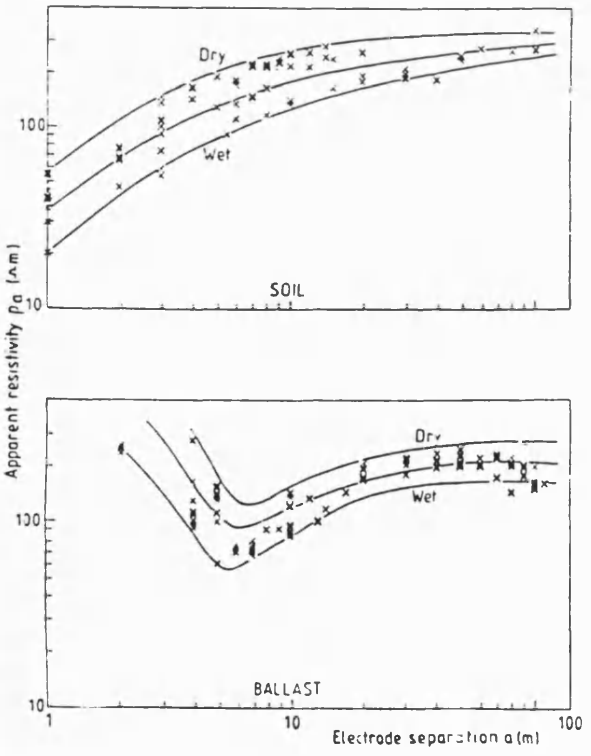

Figure 4: Experimental measurements of apparent resistance for a, soil; and b, ballast bed

Measurement of C_{12} as a function of frequency then gives an estimate of $\varepsilon_r(f)$. The relative permittivity may be assumed constant over the region of interest since the inter-track spacing is small. The ballast condition (grade, wetness) is the most important factor in the determination of the relative permittivity and track capacitance.

EXPERIMENTAL DATA

Practical measurements were made on and near a short length of rail track. This track consisted of 44 kg m^{-1} rail laid on wooden sleepers with good quality limestone ballast of depth 30 mm below the sleepers. The ground beneath the track was on a bed of sand over a geotextile membrane.

Ground conductance

Ground conductivity measurements along the length of a test railway track were made using a Wenner array. Readings of apparent resistance for electrode spacings from 0.1 to 10 m were recorded using a 50V DC source and reversing switch (Figure 3). The raw measurements for both track ballast and nearby ground are shown in Figure 4. These results were interpreted by the Tagg method by plotting curves of k as a function of z for each electrode spacing (Figure 5). For greater accuracy at small probe spacings (less than 0.4 m), the Baishiki correction using Equation 28 was made.

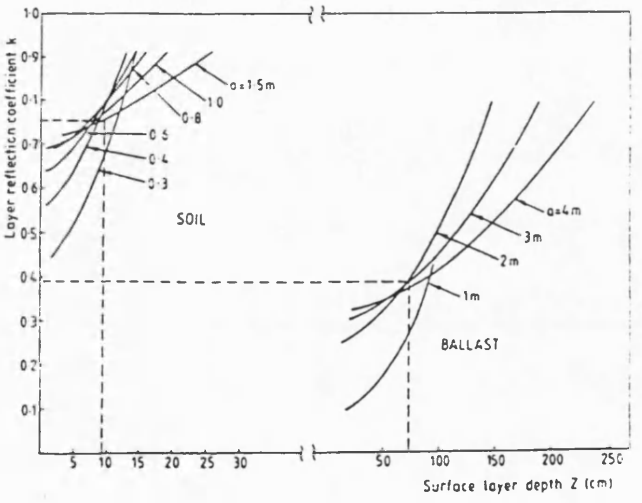

Figure 5: Surface layer depth as a function of ground reflection coefficient for resistivity measurements

Table 1 shows the final values of ρ_1, ρ_2 and z for ballast and soil for wet and dry conditions, together with derived values of inter-rail conductance G_{12} and track conductance G_{1r}. The dominant geological construction in the test area was Jurassic limestone.

Track electrical parameters

The track impedance and admittance were measured using conventional short-circuit and open-circuit transmission line tests. The impedance Z and admittance Y per unit length are derived from the short-circuit impedance Z_{sc} and open-circuit impedance Z_{oc} via the characteristic

	ρ_1 (Ω m)	ρ_2 (Ω m)	z (cm)	G_{12} (S m^{-1})	G_{1E} (S m^{-1})
Dry soil	56	338	10	0.056	0.00147
Wet soil	20	262	10	0.157	0.0019
Av. soil	40	280	10	0.078	0.00179
Dry ballast	150	260	80	0.021	0.0019
Wet ballast	60	180	80	0.052	0.0028
Av. ballast	110	257	80	0.028	0.00195

Table 1: Experimentally-derived upper and lower level conductivities, layer depth and track and rail-rail conductivities

impedance Z_0 and propagation constant γ using the equations:

$$Z_0 = \sqrt{(Z_{sc} Z_{oc})} = \sqrt{(Z/Y)} \quad (34)$$

and $$\tanh \gamma l = \sqrt{(Z_{sc}/Z_{oc})} \quad (35)$$

with $$\gamma = \sqrt{(ZY)}. \quad (36)$$

The experimental results for the test track are shown in Figure 6. The conductance measurements represent good, dry ballast and are much lower than the highest permissible value specified by railway signal engineers (e.g. 0.5 mS m^{-1} in Britain).

The inter-rail conductance agrees well with values calculated from the ground conductivity measurements (Table 1), if the upper layer (ballast) conductance is taken as data. The value of rail leakage conductance for longitudinal propulsion current leakage studies, however, cannot be directly measured and must be estimated from the lower level resistivity ρ_2.

The experimentally derived values for characteristic impedance and the propagation constants are given in Table 2.

MODELLING AC-SUPPLY PROPULSION CURRENT LEAKAGE EFFECTS

Rail-to-earth voltage and rail current

In high-voltage electric railways, it is important to maintain rail-to-earth voltages within specific safety limits. In the USA, for example, rail voltages which exceed 300 V are classified as hazardous [8]. Using the data of the previous section and the supply conditions of Figure 2, calculations of rail-to-earth voltage have been made over a track length of 12 km, of which the central 3 km represent the train - feeder transformer section. In order to determine the effect of variable ground conductivity, only conductive rail excitation is simulated. The supply voltage is 25 kV and the traction load is nominally 6.25 MW. The results of Figure 7 are with the ground conductance at the previously determined value given in Table 1 (curve A), and at a value a factor of 10 smaller (curve B). The latter case could occur, for example, in dry regions with limestones from the precambrian geological age [14]. Clearly, under

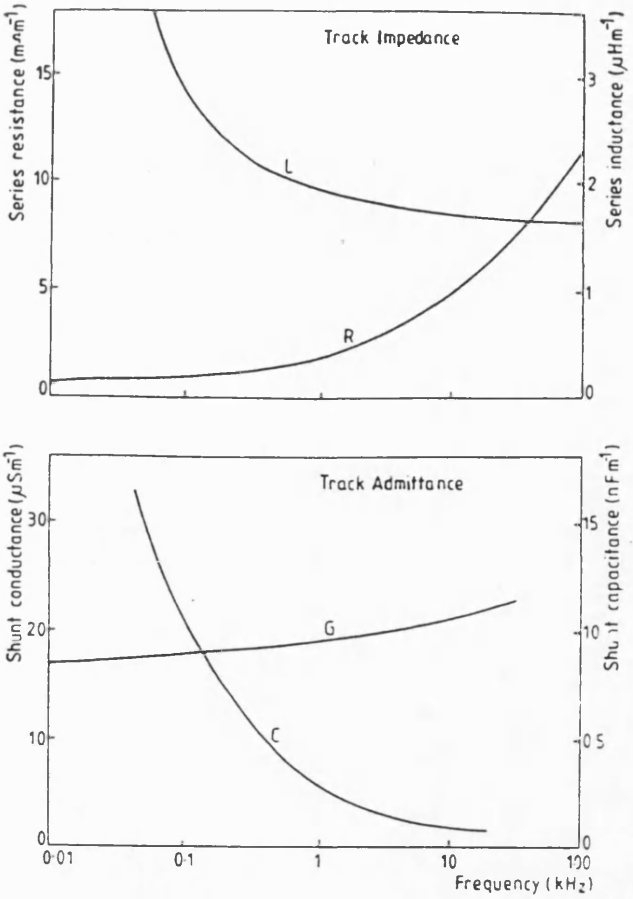

Figure 6: Experimental measurements of track impedance and admittance

	Z_0 (Ω)	γ (2 kHz)	Γ (50 Hz)	λ (km)
Balanced track transmission line	27.0 + j21.8	(4.64 + j4.70)10^{-4}	-	13.4 km
Compensated track transmission line	11.0 + j 0	(2.07 + j20.8)10^{-4}	-	3.03 km
Track as leaky ground conductor	0.389 j0.035	-	0.732 + j0.136	46 km

Table 2: Transmission line characteristics for 50 Hz power frequency and 2 kHz track signalling frequency

low ground conductivity conditions, the rail voltage can be appreciable, so additional rail earthing measures should be considered for safety assurance.

Figure 8 shows the corresponding rail current distribution. Although the section is single-end fed, the rail current flows in both directions from the locomotive due to the continuous track-earth impedance. Evidently, the condition of low ground conductance encourages uniformity of rail current over the section.

In a catenary- or trolley-fed electrified railway, the masts, if made of steel, are normally connected to the nearest running rail to provide a secure earth path for fault

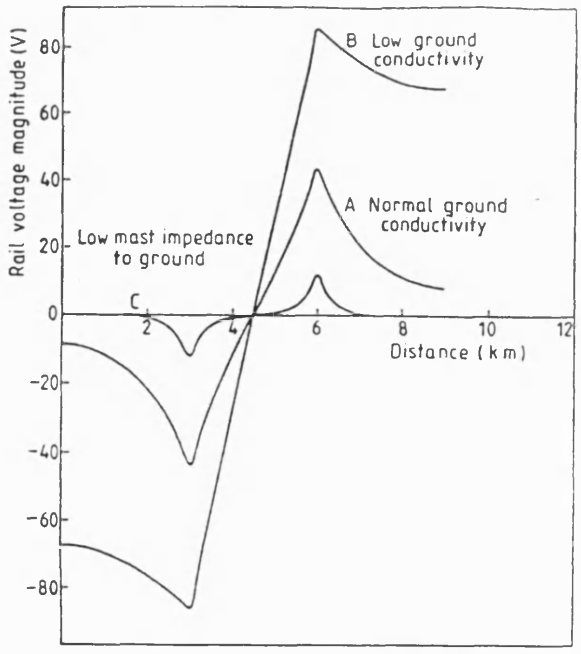

Figure 7: Rail-to-earth voltage in 25 kV AC railway for normal and low track conductivity and low mast impedance to ground

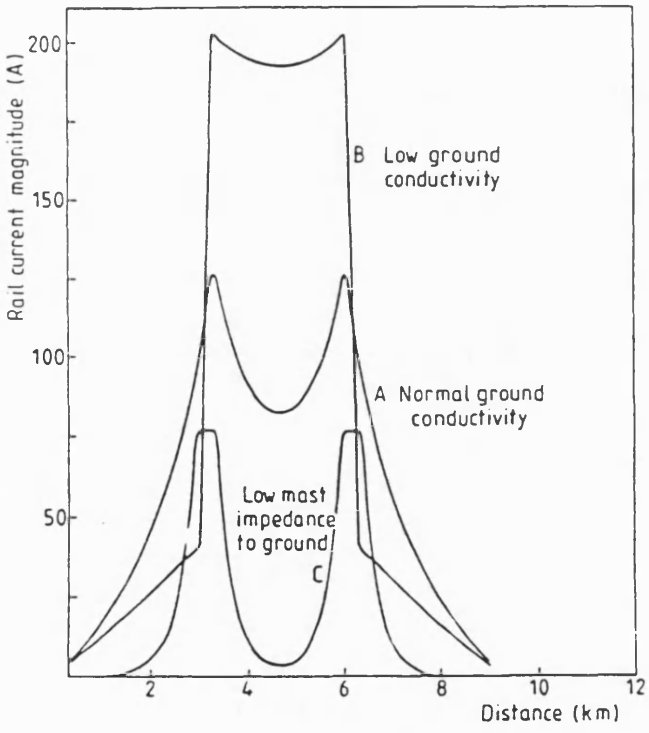

Figure 8: Rail current in 25 kV AC railway for normal and low track conductivity and low mast impedance to ground

currents. This connection has the effect of reducing the overall track-earth conductance, whilst also introducing a differential voltage between the rails. Curves C in Figures 7 and 8 show the effect of such catenary mast earthing. The masts are connected at 50 m intervals to one rail and it is assumed that their bases are also almost perfectly earthed via their foundations. With a normal traction current load, the inter-rail voltage would be almost the same as the rail-to-earth voltage, perhaps indicating a need for additional traction current equalization bonds.

Earth currents

Limitation of earth currents is important for energy management and other reasons. Figure 9 shows earth current distribution along the same section of AC railway as before, with normal and low ballast conductance and with metal catenary mast connection to the nearest rail. The simulation shows that earth currents with appreciable magnitudes can exist under low mast earth impedance conditions (curve C).

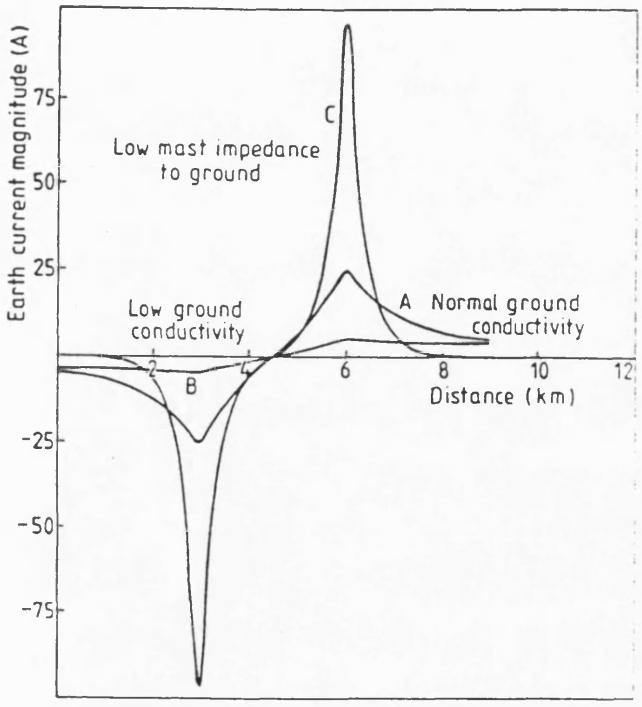

Figure 9: Earth current distribution in 25 kV AC railway for normal and low track conductivity and low mast impedance to ground

Rail and earth currents in DC-supplied railways are usually larger than those in AC railways since there is no mutual inductance effect for ing the return traction current to flow in the rails, the catenary current is higher and the rail impedance is lower. Moreover, earth current limitation is especially important on DC-fed railways because of the corrosion problem to adjacent structures, cables and pipes. For example, Shaffer [7] quotes a specification for the Miami Metro of 1 mA/m stray current. Clearly, with high ballast conductance and mast earthing, additional stray current mitigation bonds may be required for low voltage DC rail transit systems.

MODELLING AUDIO FREQUENCY TRACK CIRCUIT OPERATION

Blockjointless audio frequency (AF) track circuits are attractive for AC electrified railways since they may be used in conjunction with continuously-welded rail to eliminate blockjoint maintenance. On main lines, the need is to increase the track circuit length towards the optimum

signal block length. To improve the resolution of AF track circuits, control of the permitted ballast conductance variation is necessary. Curve A in Figure 10 shows the inherent track attenuation as a function of rail-rail conductance along a 500 m track section, corresponding to the track circuit model of Figure 1, at a frequency of 2 kHz. Rail impedance and capacitance data were taken from Figure 6. Curve B shows the case of minimum attenuation, according the the Heaviside criterion, achieved by connecting variable capacitors across the rails, and curve C shows a practical case, with compensation calculated at the maximum permitted ballast conductance of 0.5 mS/m. Because the line is less than a quarter wavelength long (the wavelength is 13.4 km for the unbalanced case, and 3.0 km for the compensated line), this capacitance need not be uniformly distributed. The results show how the data transmission characteristics of rail track may be easily varied, although it should be remembered that connection of low impedances across the rails, such as track signalling apparatus, would itself modify the track transmission characteristics.

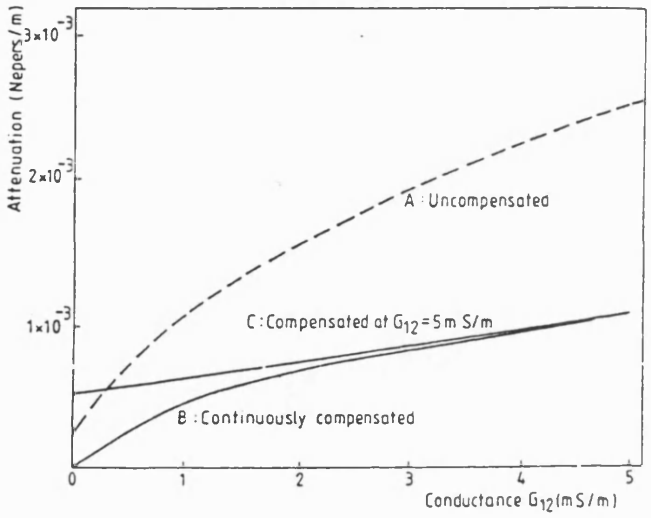

Figure 10: Track circuit attenuation as a function of ballast conductance, showing effect of capacitive line compensation

Structure bonding effects

On overhead catenary fed electrified lines, the electrification masts may be connected to the rails at periodic intervals along the track for safety or other reasons. If the mast foundations have a high impedance to ground, then the track circuit operation will be unaffected, but if one or more masts have a low impedance to ground, it is possible that the track circuit receiver, normally energized with no train shunt on the section, will falsely energize with the train shunt in the track circuit. To simulate this condition, the mast conductance to earth must be combined with the inter-rail conductance. This is not straightforward because the conductance to earth from the center of the equivalent inter-rail admittance is undefined.

Figure 11 shows the results of a simulation in which masts near the track circuit transmitter and receiver are assumed to have 1 S earth conductance. The track circuit length and frequency are as before, the receiver resistance is 1 Ω and the train shunt resistance is 0.2 Ω. The curves show the ratio of the track occupied to unoccupied receiver voltage, for a nominal 1 V transmitter voltage, as the vehicle moves along the track circuit. Both normal track (ballast) conductance (curve A) and high track conductance (curve B) are considered, together with the situation when the masts nearest the track circuit transmitter and receiver have a very low impedance to ground (curve C). Although in this case there is no danger of the track circuit receiver becoming de-energized with the train in the section, the receiver voltage does increase, thus lowering the margin between the track clear and track occupied receiver threshold.

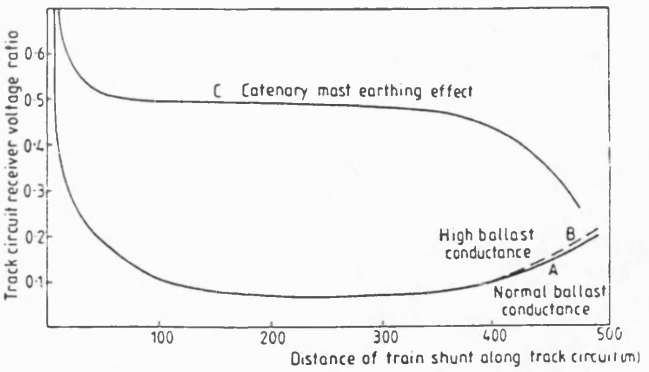

Figure 11: Track circuit receiver voltage ratio as a function of train shunt position for normal operation, high ballast conductivity and low mast ground impedance

DISCUSSION AND CONCLUSIONS

Knowledge of track admittance is important for both longitudinal propulsion current return and track circuit operation studies. The track-grounding model is complex, and the short distance rail-to-rail conductance is not generally the same as the ground conductance of a single rail over long distances. Representation of the ground with a two-layer homogenous, isotropic conductivity function gives reasonable correlation with experimental measurements. The upper layer is associated with inter-rail, and the lower layer with rail-earth conductance. The exact magnitude of the conductivity function depends on environment, soil and underlying strata type and cannot easily be quantified.

At low and audio frequencies ground admittance is dominated by its conductance. In long-distance ground-return conductor studies at power frequencies, the susceptance may be neglected in the calculation of the propagation constant. For rail-rail admittance calculations, the capacitance should be considered at higher audio frequencies. Here, direct measurements of capacitance can be made to estimate the ground relative permittivity. The moisture content of the ground is its largest determinator.

The rail-to-earth voltage, rail and earth current simulations for the propulsion current return studies demonstrate the design difficulties that exist in satisfying both safety voltage and stray current limits. The simulations show only normal (no fault) operating conditions. Fault currents of several orders of magnitude higher than propulsion levels may appear under some conditions, thus introducing the possibility of raising voltages above prescribed safety limits. There is, unfortunately, a direct trade-off between the reduction of earth currents and the maintenance of rail voltages below specified safety levels. Indeed, it is often desirable to

control, rather than eliminate, stray current levels for this reason [6].

The application of the Heaviside criterion to maintain track circuit shunting sensitivity with high ballast and structure-ground conductance is a possible approach to optimization of data transmission characteristics of railway track. However choosing the optimum value of added capacitance is not straightforward, due to the variability of ground admittance with soil and environmental conditions.

ACKNOWLEDGEMENTS

This research was performed with financial assistance from the Science and Engineering Research Council, UK. Mr Tasar acknowledges the Turkish government for the provision of a research studentship.

REFERENCES

[1] J. Riordan, "Current propagation in electric railway propulsion systems," *Transactions AIEE,* vol. 51, pp. 1011-1019, December 1932.

[2] E. D. Sunde, "Currents and potentials along leaky ground-return conductors," *Electrical Engineering,* vol. 55, pp. 1338-1346, 1936.

[3] A. Rosen, "Interference in railway lineside telephone cable circuits from 25 kV 50 Hz traction systems," *Institution of Railway Signalling Engineers Proceedings,* pp. 55-79, 1958.

[4] B. Mellitt, C. J. Goodman, Z. Y. Shao and W. B. Johnston, "Induced noise calculations in AC railways using CAD techniques," *Proceedings International Conference on Electric Railway Systems for a new Century,* London, 22-25 September 1987, pp. 126-131.

[5] M. Takihara, "On stray-current corrosion," *Quarterly Reports of the Railway Technical Research Institute,* vol. 12, no. 2, pp. 61-67, June 1971.

[6] T. A. Kneschke, "Design considerations for the DART traction electrification system," *Proceedings 1987 Joint IEEE/ASME Railroad Conference,* Toronto, 21-23 April 1987, pp. 1-11.

[7] R. E. Shaffer and S. I. Venugopalan, "Stray current control in Dade County 'Metrorail' system," *Proceedings 1980 IEEE-IAS Annual Meeting,* Cincinnati OH, 28 Sept - 3 Oct 1980, pp. 285-291.

[8] S. D. Jacimovic, "Maximum permissible values of step and touch voltages with special consideration to electrified railroads," *IEEE Transactions on Industry Applications,* vol. IA-20, no. 4, pp. 935-941, July/August 1984.

[9] W. Machczynski, "Currents and potentials in earth-return circuits exposed to alternating current electric railways," *IEE Proceedings,* vol. 129, part B, no. 5, pp. 279-288, September 1982.

[10] L. M. Wedepohl, "Wave propagation in multiconductor overhead lines," *IEE Proceedings,* vol. 113, no. 4, pp. 627-32, April 1966.

[11] W. M. Telford, L. P. Geldart, R. E. Sheriff and D. A. Keys, *Applied Geophysics.* Cambridge UK: CUP 1976.

[12] E. D. Sunde, *Earth conduction effects in transmission systems.* New York: Dover 1968.

[13] R. S. Baishiki, C. K. Osterberg and F. Dawalibi, "Earth resistivity measurements using cylindrical electrodes at short spacings," *IEEE Transactions on Power Delivery,* vol. PWRD-2, no. 1, pp. 64-71, January 1987.

[14] G. V. Keller, "Electrical properties of rocks and minerals." In: *Handbook of Physical Constants* (Editor: S. P. Clark). New York: Geological Society of America 1966.

The Effects of Magnetic Saturation, Hysteresis and Eddy Currents on Rail Track Impedance

D. C. Carpenter and R. J. Hill

University Of Bath, Bath, BA2 7AY, England

ABSTRACT

Knowledge of the transfer function of rail track is required for both electric railway return current studies and track signalling equipment design. The most significant component of the transfer function is the series impedance, which is a function of current, frequency and rail composition. The accurate modelling of series impedance requires information about of how eddy current and hysteresis losses affect the resistance and internal inductance. Once the track transfer function is known, propagation and mixing of signals along the track can be simulated for track signalling, power current and electromagnetic interference studies.

Introduction

The development of thyristor-controlled rail traction drives and the adoption of computer-based train control systems has resulted in modern, economic and safe railroad and rail transit systems. In order to manufacture and operate these systems with high reliability, safety and availability levels, the design process must be based on detailed research and development. The use of electrical circuit simulation packages in recent years has accelerated equipment development, whilst also emphasizing the need for accurate data. The design of track signalling systems and the prediction of their behaviour with electromagnetic interference requires knowledge of the electrical impedance characteristics of traction rails. In this paper, the series impedance of rail track is considered in detail.

Various values of series rail track impedance have been reported in electric railway return current propagation studies. In an early paper, Trueblood and Wascheck [1] introduce the concepts of internal and external rail reactance and equivalent circular conductors, reporting experimental measurements, for rail of irregular shape. Their technique was later refined by Holmstrom [2] who reported measurements of A.C. rail impedance with a superimposed D.C. current. Further studies of rail impedance have been made for automatic train protection safety assurance [3] and mine traction systems [4,5].

The use of running rails for traction current return and for signalling current requires accurate knowledge of rail electrical and magnetic properties over a range of current and frequency. The nonlinear magnetic properties of iron mean that eddy current (and hence skin effect), magnetic saturation and hysteresis can all be present under certain conditions. The superposition of track signalling currents, with modulation and coding, on existing traction return currents, containing traction modulation harmonics and substation supply ripple frequencies, can produce intermodulation distortion. Frequencies consisting of products of these harmonics can then cause interference in safety signalling, broadcasting and telemetry circuits.

The approach described in this paper is to identify and measure the magnetic properties of rail that cause additional power loss (eddy current and hysteresis) and contibute to rail inductance. Experiments are described from which rail magnetic and electrical data can be obtained. Some simplified theoretical approaches are presented to quantify the results. Finally, some applications are described where traction and track circuit signals can combine to suffer distortion and create interference.

Rail Track Series Impedance

The magnetic and electrical phenomena that account for rail track impedance are well known, although theoretical procedures for identifying the various processes are less well established. In electromagnetic terms, the problem is to specify the series inductance and resistance of a pair of parallel ferrous conductors of irregular shape laid on a lossy ground plane in close proximity to each other. The rail material is neither a good conductor, nor a good insulator. Its permeability and conductivity are generally undefined, since the rail is manufactured for its mechanical and metallurgical, rather than electromagnetic properties.

The approach adopted by Trueblood and Wascheck [1] was to divide the series inductance into external and internal inductance. The former is that due to an equivalent circular rail, with the return circuit completed by a second, parallel, circular rail, while the latter depends on the material and geometry of the iron itself. It follows that only the internal inductance is dependent on material and enviromental properties. A more complete description of the rail inductance would divide the external reactance into two parts, with one dependent on the shape of the rail, and the other assuming circular rails as above. Thus

$$L_{rail} = L_{ext_1} + L_{ext_2} + L_{int} \qquad (1)$$

The rail resistance as identified by power losses is due to four factors:

- D.C. resistance loss, determined by the conductivity (σ), which is a function of temperature only.
- A.C. resistance loss, due to skin effect and manifesting itself as eddy current power loss.
- Hysteresis loss, caused by cyclic losses as the material orients itself round the B-H loop under A.C. conditions.
- Further magnetic loss mechanisms such as resonance and relaxation processes of non-macroscopic origin.

The presence of saturation in the iron modifies the magnitude of all the A.C. loss components, although it does not introduce further losses as such. It also affects

the rail internal inductance.

Unfortunately, it is not possible to represent all the above loss mechanisms in a single analytical model. This is because of the irregular rail shape and the nonlinear B-H relationship which includes both saturation and hysteresis.

It is possible to analytically model an equivalent rail of circular cross-section under linear B-H conditions, accounting for hysteresis loss, using a complex permeability function. Values for A.C. impedance will then include eddy current loss, hysteresis loss and internal inductance.

Experimental tests on rail material can generate the material B-H loop characteristics, enabling the combined effects of saturation on both the eddy current and hysteresis losses to be measured. Using Fourier analysis, harmonic coefficients of the magnetic flux density may be obtained, with frequency and peak magnetic field intensity as the independent variables.

Analytic Theory for Equivalent Circular Rail

The rail material is assumed to be both homogeneous and isentropic. Consider the circular equivalent rail shown in Figure 1. Ampere's law gives

$$H_\phi 2\pi r = I = \int_0^r J_z 2\pi r \, dr \qquad (2)$$

Differentiating with respect to r and rearranging

$$\frac{dH}{dr} + \frac{H}{r} = J \qquad (3)$$

The E.M.F. induced at radius r by the flux inside the conductor, i.e. the eddy current effect, is the difference between the volt drops at r and a (the surface). Hence

$$\frac{1}{\sigma}(J_z - J_{z0}) = -\frac{d}{dt}\int_r^a \mu H_\phi \, dr \qquad (4)$$

or

$$\frac{1}{\sigma}\frac{\partial J_z}{\partial r} = \frac{\partial}{\partial t}(\mu H_\phi) \qquad (5)$$

Representing the permeability by $\mu = \mu_1 - j\mu_2$,

$$\frac{dJ}{dr} = j\omega\sigma(\mu_1 - j\mu_2)H \qquad (6)$$

By differentiating Equation (3) with respect to r and using Equation (6),

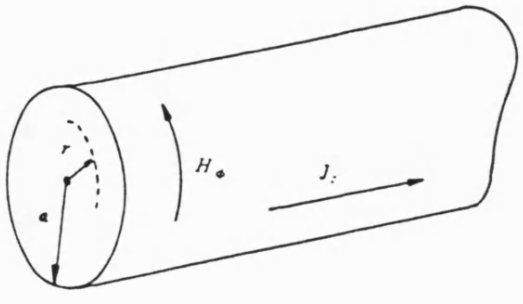

Figure 1. Equivalent Circular Rail Geometry

$$\frac{d^2H}{dr^2} + \frac{1}{r}\frac{dH}{dr} - \left|\alpha'^2 + \frac{1}{r^2}\right|H = 0 \qquad (7)$$

with

$$\alpha'^2 = j\omega\sigma(\mu_1 - j\mu_2)$$

After applying boundary conditions, the solution is

$$H = \frac{I}{2\pi a}\frac{I_1(\alpha' r)}{I_1(\alpha' a)} \qquad (8)$$

where $I_1(x)$ is the first order modified Bessel function of the first kind [6].

The current density is found by substituting in Equation (3) as

$$J = \frac{\alpha' I}{2\pi a}\frac{I_0(\alpha' r)}{I_1(\alpha' a)} \qquad (9)$$

The internal impedance per unit length of the conductor is then

$$R + jX = \frac{E|_{r=a}}{I} = \frac{\alpha'}{2\pi a\sigma}\frac{I_0(\alpha' a)}{I_1(\alpha' a)} \qquad (10)$$

Equation (10) gives numerical values of R and X for known geometrical and material properties. It is, however, instructive to consider certain limiting values of R and X.

- *High Frequency* i.e. conductor radius a >> skin depth δ. This is the case of a solid cylinder with the majority of the internal flux lying in a thin layer around the perimeter of the conductor. The solution is obtained by substituting for the skin depth $\delta\exp(j\theta/2)$, where θ is the hysteresis angle and simplifying [6] so that

$$Z_{hf} = \frac{1}{\pi a^2\sigma}\left|\frac{1}{4} + \left|\sqrt{2}\cos\left|\frac{\pi}{4} - \frac{\theta}{2}\right|\right|\left|\frac{a}{2\delta} + \frac{3}{32}\frac{\delta}{a}\right|\right| + j\left|\left|\sqrt{2}\sin\left|\frac{\pi}{4} - \frac{\theta}{2}\right|\right|\left|\frac{a}{2\delta} - \frac{3}{32}\frac{\delta}{a}\right|\right| \qquad (11)$$

  In this expression the term $\frac{1}{4\pi a^2\sigma}$ corresponds to the D.C. resistance. For real permeability ($\mu = \mu_1$), there are both resistance and reactance impedance components. For the case of imaginary permeability ($\mu = -j\mu_2$), there is no reactance, because the diffusion equation does not hold, there being no eddy currents. For complex permeability, Equation (11) is accurate for the fundamental component of hysteresis only, i.e. linear conditions. The eddy curerent loss and hysteresis loss cannot be separated.

- *Low frequency* i.e. conductor radius a << skin depth δ. The impedance is

$$Z_{lf} = \frac{1}{\pi a^2\sigma}\left|1 + \frac{a^2}{4\delta^2}\sin\theta + \frac{a^4}{48\delta^2}\cos 2\theta + j\left|\frac{a^2}{4\delta^2}\cos\theta - \frac{a^4}{48\delta^4}\sin 2\theta\right|\right| \qquad (12)$$

  For real permeability, there are again both resistance and reactance impedance components, and for imaginary permeability there is again only resistance.

The high frequency results show that the presence of hysteresis increases the losses by a factor

$$\frac{\cos\left|\frac{\pi}{4}-\frac{\theta}{2}\right|}{\cos\frac{\pi}{4}}$$

which is greater than unity. The reactance, however, is decreasd by the factor

$$\frac{\sin\left|\frac{\pi}{4}-\frac{\theta}{2}\right|}{\sin\frac{\pi}{4}}$$

The impedance angle reduces with hysteresis. With no hysteresis, it is $\frac{\pi}{4}$.

The effect of this simplified theory on rail impedance is as follows. In the absence of saturation, there are no harmonics and the rail reactance will reduce in the presence of hysteresis. The resistance, however will increase because the hysteresis loss is additional to the eddy current loss. However, the effects are not independent, since the hysteresis angle modifies the eddy current loss when hysteresis losses start to become important.

Finite Element Modelling (F.E.M.) for Internal Rail Reactance

A two-dimensional axisymmetric static and dynamic electomagnetic analysis package was used to obtain the resistance and internal inductance of both the rail and an equivalent cylindrical rod. The excitation was an imposed A.C. current characterised by its amplitude and frequency. The package carried out a nonlinear eddy current analysis. The case of a current-carrying steel conductor (rail) is unusual in electromagnetic terms since it is a magnetic conductor with the excitation current in the same medium as the eddy currents it produces.

From [7] it is found that the inductance per unit length is

$$l = \frac{1}{I^2}\sum_S \underline{A_s} \cdot \underline{J_s}\,\delta S \qquad (13)$$

where I is the total current, S is an elemental area. $\underline{A_s}$ is the vector potential associated with S, while $\underline{J_s}$ is the current density associated with S.

The A.C. resistance per unit length is given by

$$r = \frac{1}{I^2}\sum_S \frac{J_s^2}{\sigma}\delta S \qquad (14)$$

The package determines a solution by calculating the minimum energy state. The function to be minimised is obtained by considering the Helmholtz equation:

$$\nabla^2\underline{A} + \omega^2\mu\epsilon\underline{A} = -\mu\underline{J} \qquad (15)$$

By substituting $\nu = \frac{1}{\mu}$, this becomes

$$\nabla(\nu\nabla\underline{A}) + \omega^2\epsilon\underline{A} = -\underline{J} \qquad (16)$$

From [8], the function to be minimised is

$$F(A) = \frac{1}{2}\int_S (\nu(\nabla\underline{A})^2 - \omega^2\epsilon\underline{A}^2 - 2\underline{J}\underline{A})\,dS \qquad (17)$$

Hence Equations (13) and (14) can be evaluated. Typical results are given in Table 1.

	L ($\mu H\ m^{-1}$)	R ($m\,\Omega\ m^{-1}$)
Rail	14.4	0.75
Rod	1.46	0.49

Table1. Rail Impedance Evaluated by F.E.M. at 50 Hz and 30 A

The current distributions for both circular conductor and rail are shown in Figures 2 and 3.

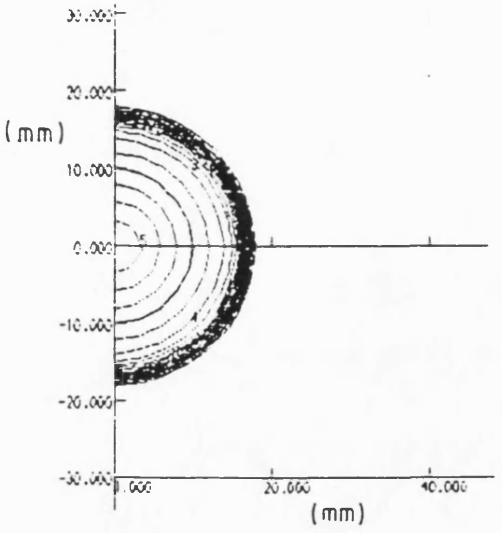

Figure 2. Current Distribution in Circular Conductor

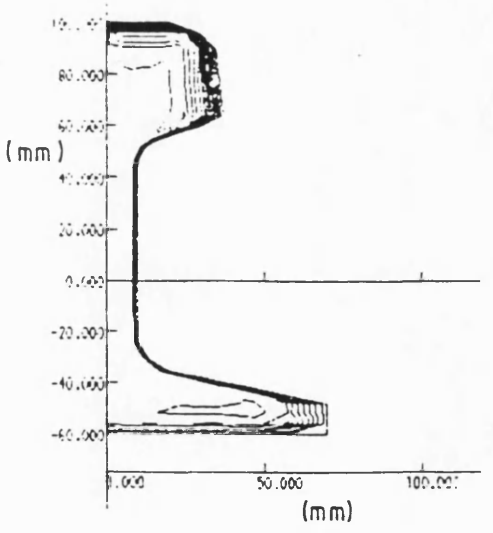

Figure 3. Current Distribution in Rail

Experimentally Derived Material Data

It is reasonable to assume that the resistivity of iron will not vary with frequency or current magnitude since the conduction process does not alter with either of these parameters. However, temperature variations do cause substantial changes in resistivity. Table 2 illustrates values, obtained experimentally, for a number of rail types (at a temperature of 298 K). A sample of mild steel is also included for comparison.

Sample Type	Resistivity (Ωm)
Bull-Head Rail	1.05×10^{-6}
Flat-Bottom Rail	1.7×10^{-6}
Mild Steel	9.1×10^{-7}

Table2. Experimental Conductivity Values

Toroidal samples were manufactured from known rail steel and a control sample of mild steel rod (i.e. of known composition). B-H loops were measured by applying low frequency signals of known amplitudes. Figure 4 shows the experimental equipment used and Figure 5 shows the results for a typical rail sample and circular steel conductor. From these measurements, values of permeability were obtained as defined by Von Hippel [9] and these are given in Table 3.

From the measured B-H loop, using real-time fast Fourier transform (F.F.T.) methods, harmonics of B were obtained for sinusoidal H excitation. An example of the spectral density and phase relationships, with frequency, are given in Figure 6. The results have the form

Sample Type	permeability (H m^{-1}) (initial)	(maximum)
Flat-Bottom Rail	150	530
Mild Steel	220	1250

Table3. Experimental Permeability Values

$$B = \sum_{n=1}^{\infty} B_n \cos(\omega_n y + \phi_n) \qquad (18)$$

Provided Equation (18) is evaluated for all values of H and of frequency, then for any applied waveform of H, the resulting B waveform can be predicted. Each harmonic of H then gives rise to a series of harmonics of B, as described by Equation (18).

Rail Impedance Measurements

Rail resistance and change in rail internal inductance were measured using the equipment devised by Trueblood and Wascheck [1] and further developed by Holmstrom [2]. The technique, as described by Holmstrom, is first to use a test conductor in the form of a hollow high-conductivity copper tube to obtain a reference setting. Subsequent measurements using the control (mild steel) rod and traction rail placed in the same physical location as the test sample, then produce measurements of absolute resistance, and changes in reactance, with excitation current and frequency. The changes in reactance are those outlined earlier i.e. L_{int_2} and L_{int}. The experimental equipment is illustrated in Figure 7.

The results are summarised in Figures 8 and 9, which show R and ΔL as functions of large signal A.C. current and frequency. Rail currents of up to 700 A (r.m.s.) at 50 Hz were used. This corresponds to a power of 17.5 MVA

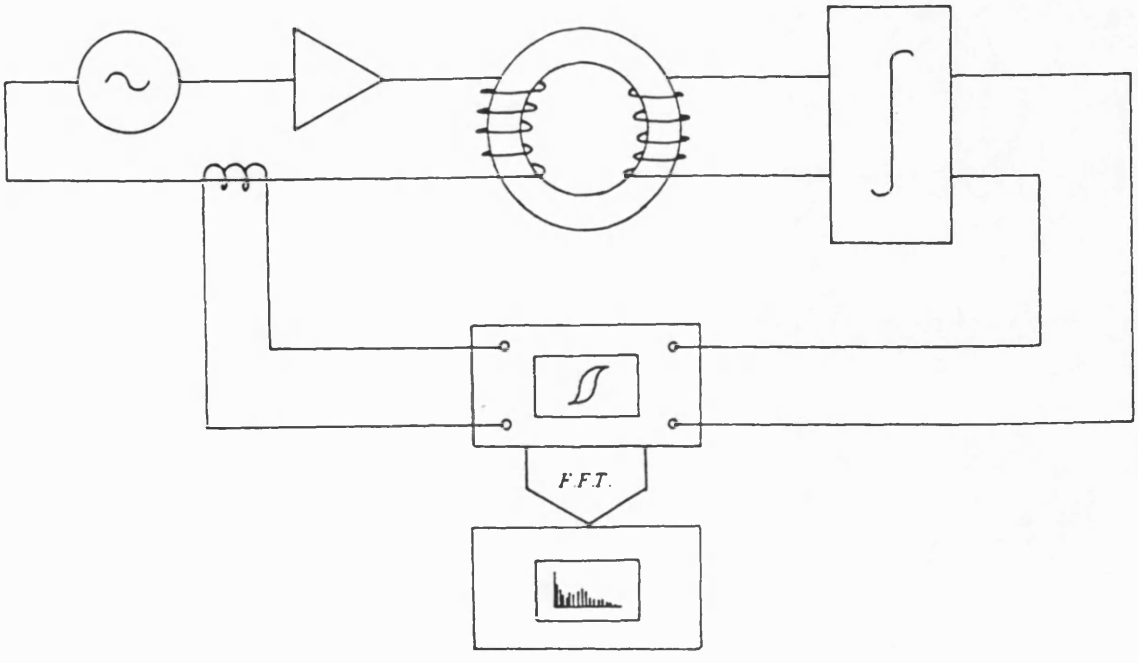

Figure 4. B-H Loop Test Equipment

for a 25 kV system. Since both rails are used, in parallel as return conductors, the tests simulated conditions in excess of 30 MVA (this being a typical substation rating for railway systems). The frequency response tests were carried out to simulate main line A.F. track circuit frequencies i.e. up to 3 kHz.

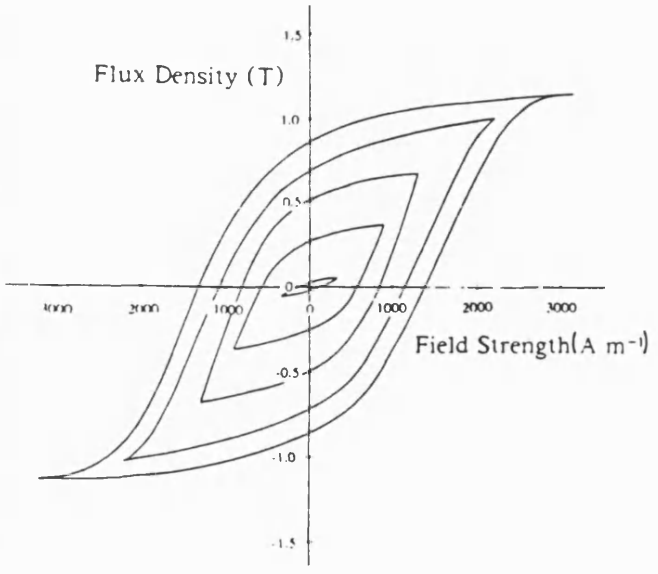

(a) Rail Sample

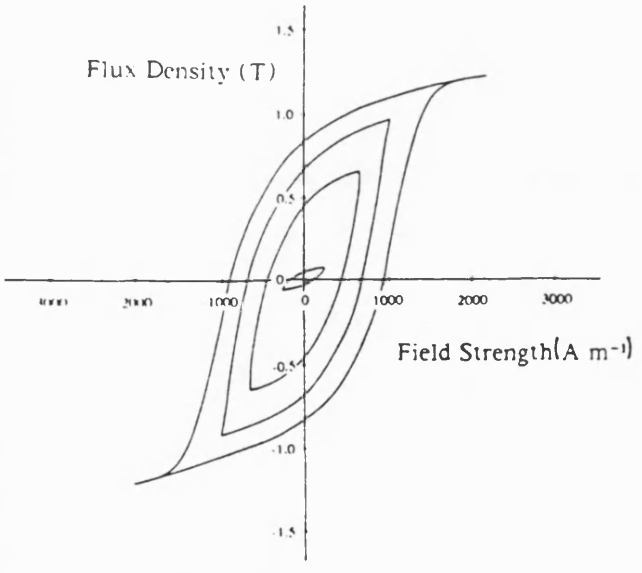

(b) Mild Steel Sample

Figure 5. Measured B-H Loops

Discussion of Experimental and Theoretical Results

The results show that the rail may be represented by an equivalent circular conductor only for far-field effects. At high frequencies, the perimeter of the rail correlates with the circumference of the circular conductor, due to small skin depth. At low frequencies, the areas of rail and

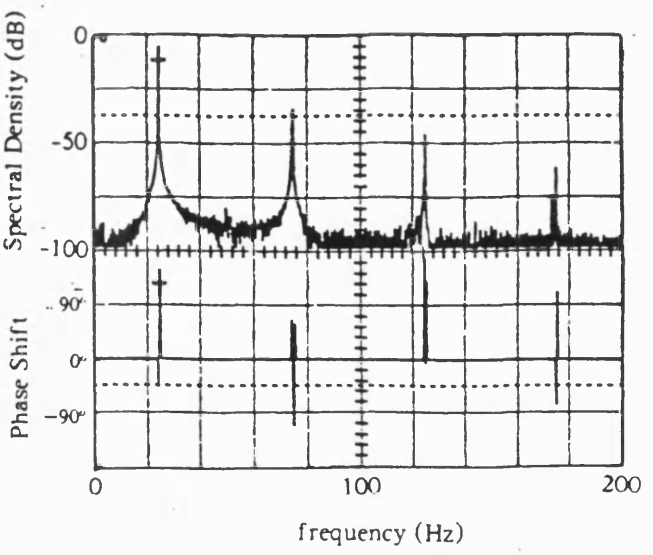

Figure 6. Spectral Density and Phase of Flux Density Waveform

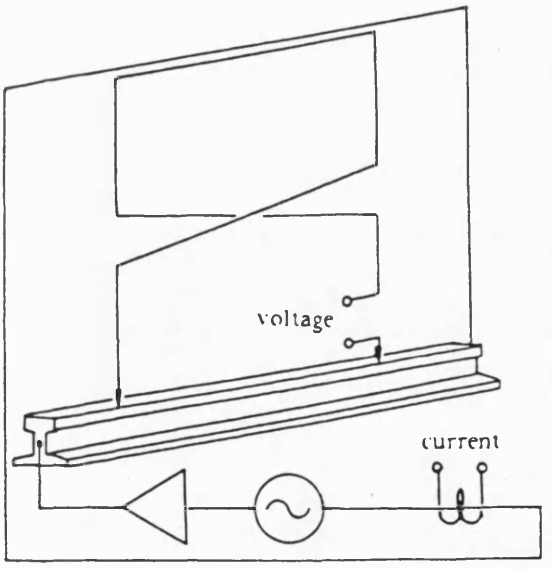

Figure 7. Impedance Measurement Equipment

circular conductor are equvalent as the skin depth is large. Although the A.C. resistance is predictable for linear conditions, the presence of magnetic saturation introduces harmonics which in turn cause additional losses. These additional losses may be modelled using a harmonic approach but the preliminary results reported in this paper suggest the additional losses due to saturation (both hysteresis and eddy current losses) are 13 dB lower than the regular losses. This applies for both circular conductor and rail.

The traction rail inductance (50 Hz) calculated using the F.E. model from stored energy considerations does not agree with the experimental measurements. Most of this inductance is due to near field effects ($L_{n.f.}$). For the circular steel conductor, however, the agreement is within 5%, explained by the limited disturbance of the near field

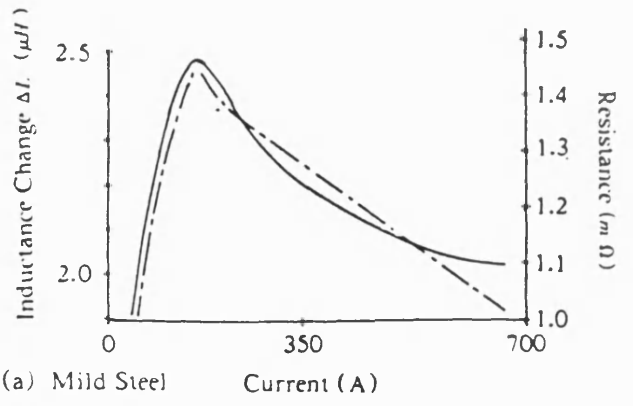

(a) Mild Steel

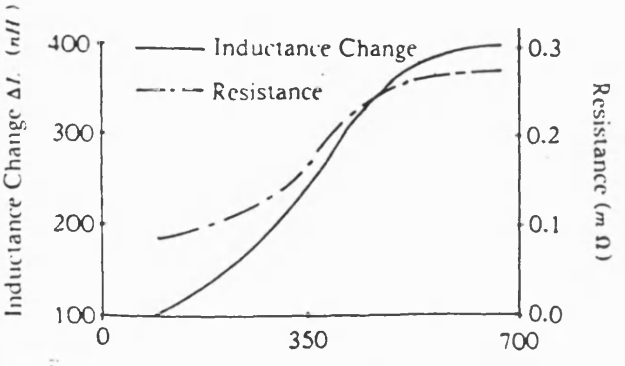

(b) Rail

Figure 8. Impedance Variation with Current

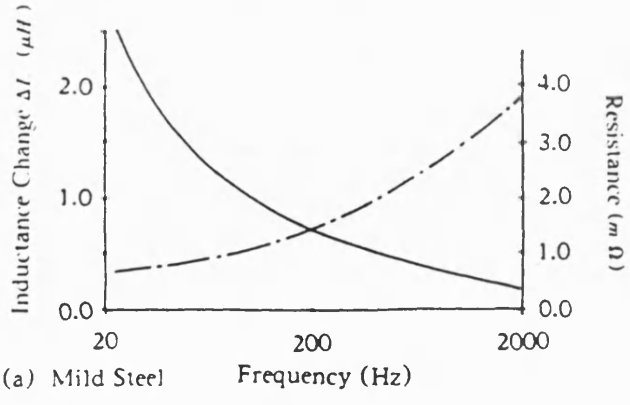

(a) Mild Steel

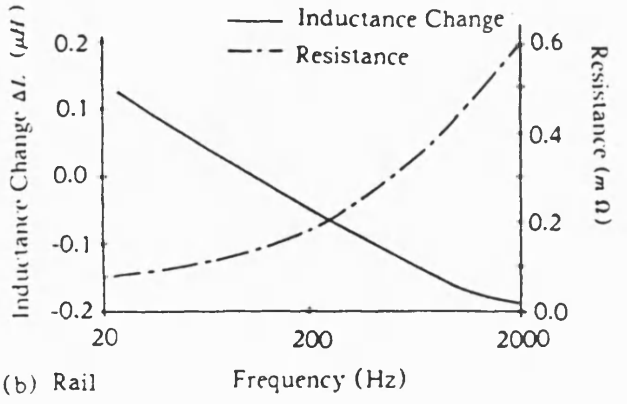

(b) Rail

Figure 9. Impedance Variation with Frequency

when the copper conductor is replaced by the steel conductor. These results do not include hysteresis loss.

The variation of both resistance and inductance with current magnitude for both samples depends upon the degree of saturation in the material. This is most noticable for the circular steel conductor which saturates at H = 1850 A m^{-1} (Figure 5b), corresponding to the peak in the inductance curve at 130 A in Figure 8. The rail, however, was unsaturated. Saturation, from the B-H waveform, occurs at 2900 A m^{-1}, which is equivalent to a current of 1740 A.Thus the rail inductance curve of Figure 8 retains a positive slope for the range of test currents applied.

Applications

Series rail impedance is a function of both current and frequency, because the magnetic material data indicates that permeability may be regarded as complex and hence represented as a function of both magnetic field intensity and frequency. Under these conditions, the material behaviour is completely specified and the rail internal reactance and resistance may be determined. However, it is not normally possible to completely separate out the effects of saturation, eddy currents and hysteresis due to their interdependency.

Once the series track impedance is known, it may be combined with the track admittance to obtain the track transfer function (Figure 10). The track impedance , Z , is a function of both frequency and current, although the track admittance, Y, is generally a function of frequency only. Knowledge of the track transfer function will enable quantification of the following situations:-

- With no propulsion current in the rails but with audio-frequency A.C. track circuit current, eddy currents and hysteresis will affect the phase and magnitude of signal transmission.
- With A.C. (sinusoidal) propulsion current of large magnitude and audio-freqency track circuit current, intermodulation distortion will generate interference signals consisting of products of the power frequency or traction modulation harmonics with the track circuit audio-frequency signals.
- With quasi-square wave propulsion current, corresponding to the practical case of a locomotive drawing "blocks" of current from an A.C. supply, intermodulation distortion again occurs with a wider range of interference frequencies produced.

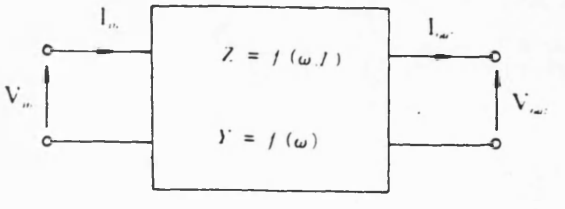

Figure 10. Rail Track Transfer Function Representation

Conclusions

It is not possible to devise a complete analytical model for series rail track impedance because nonlinear saturation effects produce harmonics which contribute to both the internal inductance and the A.C. resistance change. Separation of rail inductance into external and internal components, with external inductance depending on rail shape as well as position, is valid only for far-field effects. For near-field effects, such as required for cab signalling receiver studies, more accurate modelling is required and the most important determinator of induced voltage is the rail shape.

Acknowledgements

The work described in this paper has been financed by a research grant from the Science and Engineering Research Council, U.K.

References

1. H. M. Trublood and G. Wascheck, "Investigation of rail impedances," *AIEE Transactions* , vol. 53, pp. 1771-80, 1934.
2. F. R. Holmstrom, "The model of conductive interference in rapid transit signaling systems," *IEEE Transactions on Industry Applications* , vol. IA-22, pp. 756-62, July/Aug 1986.
3. S. K. Tso, F. K. Lam, F. H. Y. Chan and R. K. Edgley, "Attenuation effects of under track reinforcing on automatic train protection signalling systems," *Proceedings IEE* , vol. 128B, pp. 92-100, March 1981.
4. E. K. Stanek, T. Cataltepe and D. O. Wiitanen, "Phenomena that effect the calculation of the inductance and resistance of mine track/trolley systems," in *Conference Record 1984 IEEE IAS Meeting* , Chicago, 30 Sept-4 Oct 1984, pp. 100-101.
5. D. J. Tylavsky, "Impedance of track/trolley haulage systems," in *Conference Record 1985 IEEE IAS Meeting* , Toronto, 6-11 Oct 1985, pp. 206-212.
6. N. W. Mclachlan, *Bessel Functions for Engineers*. Oxford: Oxford University Press, 1955.
7. G. W. Carter, *The Electromagnetic Field in Engineering Aspects*. London: Longmans 1954.
8. P. P. Silvester and R. L. Ferrari, *Finite Elements for Electrical Engineers*. Cambridge: Cambridge University Press, 1983.
9. A. R. Von Hippel, *Dielectric Material and Applications*. New York: John Wiley 1954.

RAIL IMPEDANCE MODELLING FOR DC-FED RAILWAY TRACTION SIMULATION

David C. Carpenter and R. John Hill

School of Electrical Engineering, University of Bath
Claverton Down, Bath BA2 7AY, UK.

Abstract

A rail impedance model based on an equivalent circular conductor, with permeability and frequency as variables, gives good agreement with measurements of rail resistance and internal self-inductance for small-signal AC currents superimposed on a large DC current in the rail. The model requires experimentally-derived permeability data. The frequency range of validity for 54 kg/m flat-bottom rail is 40 Hz to 16 kHz.

KEY WORDS- Railway traction, rail impedance, saturation, skin effect.

1 INTRODUCTION

The running rails in DC-electrified railways carry DC propulsion return current in addition to AC track signalling current. The magnitude of the DC current may reach several thousand Amps, while the AC current is low in magnitude, but may have a spectrum containing utility frequency subharmonics as well as higher audio frequencies. Higher harmonic frequencies from rectifier substations and traction chopper or converter control systems are also usually present in the DC propulsion return current. The running rail impedance is dependent on its current and frequency, and for the accurate modelling of DC traction systems, its detailed knowledge is required. Applications of these models include calculation of the transfer impedance between track signalling transmitters and receivers; assessment of the possibility of intermodulation distortion in coded modulated information transmission systems; and measurement of energy losses due to eddy currents and hysteresis in the rail affecting the dynamic operation of track circuits.

In models of railway traction systems, the track is usually represented as a multiconductor coupled transmission line. The line voltages and currents are related to each other by the track impedance and admittance matrices [1]. The elements of the impedance matrix are the line self and mutual impedances, the self impedances being divided into internal and external components. The internal impedance includes the resistance and the inductance due to flux within the rail iron. Although in magnitude it is usually dominated by the external component, it can be important, for example, during traction fault conditions where large DC currents can saturate the iron [1] and where a modified current return path can reduce the external self-inductance. Complete knowledge of the internal impedance variation with both current and frequency is necessary to fully specify the track impedance matrix.

In most of the literature reporting traction simulation using multiconductor transmission line theory, the sensitivity of the analysis to internal impedance is claimed to be small and linear constant inductance models are used [2]. AC rail impedance is usually modelled assuming constant permeability [1, 3, 4]. This, however, is an acknowledged approximation and can be erroneous particularly for DC traction conditions, where AC and DC signals are both present, and where the large traction currents can saturate the rail.

In this paper the rail internal self-impedance is determined by modelling and measurement. The model is based on the AC impedance of an equivalent circular conductor, with appropriate experimentally-measured permeability data. The results demonstrate the dependence of the impedance on the rail permeability, which is a function of surface magnetic field or DC current, and on frequency. The rail impedance is also measured experimentally, and theory and experiment are in agreement in the frequency range 40 Hz - 16 kHz.

2 MATERIAL DATA

The permeability of a ferromagnetic material such as rail iron is a function of three vectors: magnetic flux density **B**, magnetic polarization **M**, and magnetic field strength **H**. The magnetic polarization can be expressed in terms of the field, giving a relationship between **B** and **H** as

$$\mathbf{B} = \mu(\mathbf{H}, \mathbf{B}, \omega)\mathbf{H} \qquad (1)$$

where μ is the material permeability and ω the angular frequency. When the material carries time-varying electric current, the impedance will depend on the permeability, and to obtain the general solution, the complete B-H relationship needs to be known.

Figure 1 shows the form of the static B-H loop for a ferromagnetic material, together with the relevant permeability definitions. If the material carries a net DC current, the normal magnetization curve defines an operating point according to the incremental and normal permeabilities μ_{inc} and μ_N. Small-amplitude AC signals then follow a subsidiary loop with slope given by the delta permeability μ_Δ. This permeability value defines the small-signal impedance through the skin effect. Application of AC fields to the material also cause extra energy losses in the material due to hysteresis. For small-signal AC conditions at low frequencies, the area of the hysteresis loop is small and the extra losses are minimal compared with eddy current and DC conductive losses. However at higher frequencies the hysteresis losses may become significant, and their magnitude may depend on the exact DC operating point on the B-H characteristics.

3 DELTA PERMEABILITY MEASUREMENTS

Samples of 54 kg/m flat-bottom (FB) rail iron were tested in order to evaluate the delta permeability as a function of magnetic field strength. The samples, filaments 1 mm square and at least 100 mm long, were subjected to an alternating magnetic field at 0.33 Hz in the direction of their longitudinal axis. The low excitation frequency removed the possibility of

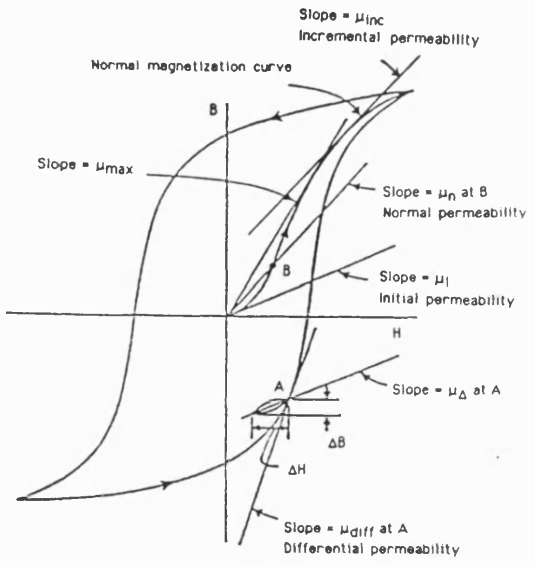

igure 1: Ferromagnetic material hysteresis loop and permeability definitions.

ddy current effects, because the skin depth was much greater han the filament width.

The material tests were primarily to determine the arge-signal AC hysteresis loops [5]. From these, the normal agnetization curve may be deduced, and hence also the delta ermeability. The result for FB rail iron is given in Figure 2 as function of magnetic field strength. The maximum value of elta permeability corresponds to the "knee" in the normal agnetization curve and hence defines the onset of saturation.

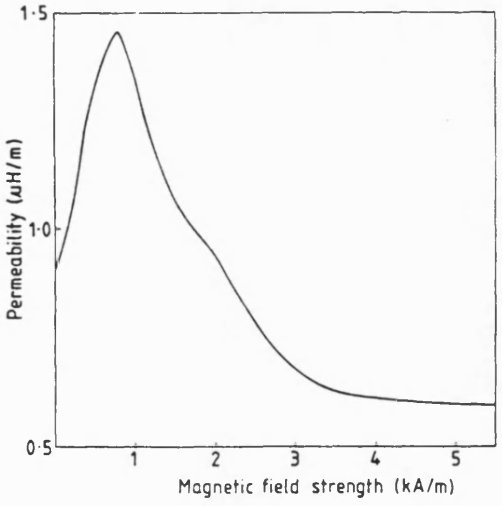

gure 2: Delta permeability as function of magnetic field strength for rail steel.

RAIL CONDUCTIVITY

The conductivity of rail iron was also accurately easured, using the same samples prepared for the B-H loop easurements. The conductivity can be expressed in the linearized form

$$\sigma = \sigma_{20}(1 + \alpha T)^{-1} \qquad (2)$$

where α is the temperature coefficient of resistivity (3.4×10^{-3} K^{-1} for FB rail), T is the temperature in K and σ_{20} is the conductivity at 20 K (4.44 MS/m for FB rail).

5 THEORETICAL MODELLING

The electrical impedance of a rail with time-varying current can be expressed as that of an equivalent circular magnetic conductor [6] as

$$R + jX = \frac{\alpha}{2\pi r_{eq}\sigma} \frac{I_0(\alpha a)}{I_1(\alpha a)} \qquad (3)$$

where $\alpha^2 = j\omega\sigma\mu$, r_{eq} is the rail equivalent radius, I_n are Bessel functions, and ω is the angular frequency. Expressing the skin depth as

$$\delta = \sqrt{(2/\omega\sigma\mu)} \qquad (4)$$

it may be shown [4] that for $r_{eq} \gg \delta$, a suitable approximation for the rail impedance is

$$R + jX = \frac{R_0}{4} \frac{1}{2\sqrt{(\pi r_{eq}\sigma)}} \sqrt{(\mu f)} + j\omega \frac{1}{4\pi r_{eq}\sqrt{(\pi\sigma)}} \frac{\sqrt{\mu}}{\sqrt{f}} \qquad (5)$$

where $R_0 = 1/\sigma\pi r_{eq}^2$ is the DC resistance. From Equation (5), it can be seen that the resistance is proportional to $\sqrt{(\mu f)}$ and the inductance is proportional to $\sqrt{(\mu/f)}$.

6 EXPERIMENTAL RESULTS

Measurements of small-signal AC rail internal self-impedance at variable frequency with a DC current offset were made using the apparatus of Figure 3. The technique, fully described in references [5] and [7], is a null-flux method using as a reference conductor a hollow copper shell the same shape as the rail. Results for resistance and inductance as functions of frequency, with DC current as parameter, and DC current, with frequency as parameter, are shown in Figures 4 and 5. The curves with frequency as the independent variable are plotted against the square root of frequency in the case of resistance and against the reciprocal of the square root of frequency for inductance.

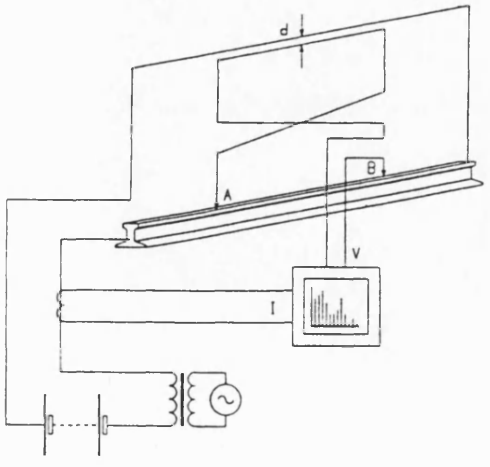

Figure 3: Experimental rail impedance measurement apparatus.

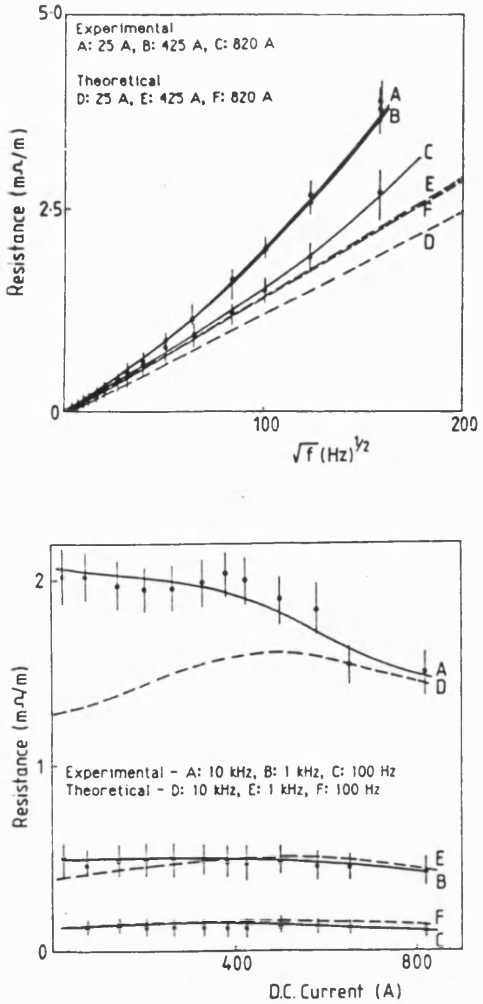

Figure 4: Experimental and theoretical rail resistance as function of frequency with DC current as parameter and DC current with frequency as parameter.

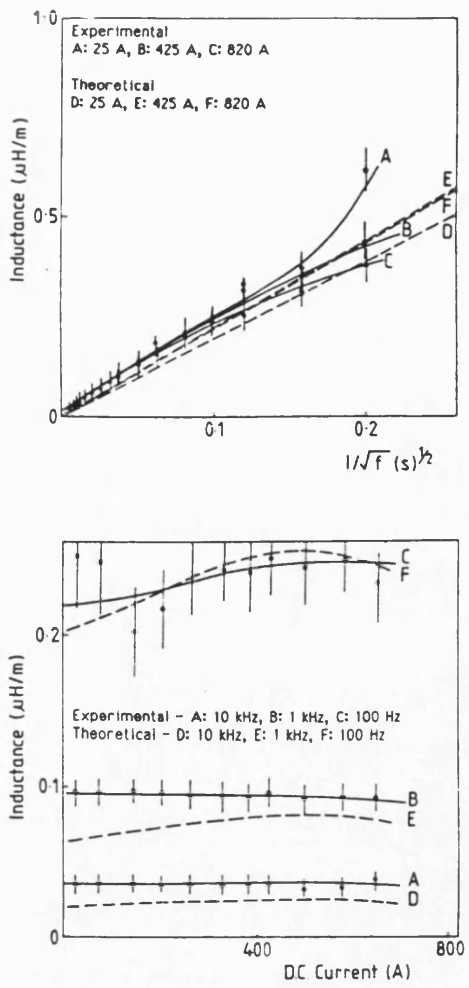

Figure 5: Experimental and theoretical rail internal self-inductance as function of frequency with DC current as parameter and DC current with frequency as parameter.

7 DISCUSSION

The theoretical resistances and internal self-inductances obtained from the model and given in Equation (5) are superimposed on the experimental results in Figures 4 and 5. In most cases, reasonable agreement is obtained, although relatively large experimental errors in some measurements make detailed comparison difficult.

In the results with frequency as the independent variable, the theoretical curves reflect the different values of permeability as determined by the magnitude of the DC offset. The delta permeabilities for DC currents of 425A and 820A are located either side of the maximum in the curve and are almost equal, so the theoretical curves for those currents coincide.

In the results with DC current as the independent variable, the permeability variation is reflected in the gradual peak of the theoretical curves. The maximum DC current applied to the rail during the experimental impedance measurements was sufficient to drive the rail past the maximum delta permeability point, but complete rail saturation was not obtained. The deviation of the experimental and theoretical resistances at 10 kHz at lower DC currents is possibly due to hysteresis.

The model allows normalization of the impedances, and Figure 6 shows all the experimental and theoretical curves plotted together. These results demonstrate the range of validity of the theory, and the effect of the various assumptions made.

The approximation of the rail shape being represented as circular holds at high frequencies when the skin depth is small. For example, for the FB rail tested, r_{eq} = 0.1 m, and the skin depth increases to one tenth of the radius at a frequency of 5 Hz, assuming a delta permeability value of 0.145 mH/m, corresponding to about 600A DC (and 7 Hz at 0.1 mH/m or 400A and 800A DC). In this case the equivalent rail radius may be found from equating the the rail perimeter to an equivalent circular perimeter. Below the critical value of frequency, an alternative impedance model is necessary, based on the inequality $\delta \gg r_{eq}$. In this case, the equivalent rail radius should be calculated from the rail cross section area.

From the results in Figure 6 the deviation of the experimental and theoretical inductance at about

$$\sqrt{(\mu/f)} > 1.5 \text{ m (Hs/m)}^{1/2} \qquad (6)$$

gives the lower limit of frequency as a function of permeability. For a peak μ_Δ of 0.145 mH/m, this frequency is 65 Hz, and for an average μ_Δ of 0.1 mH/m, it is 45 Hz. These values should

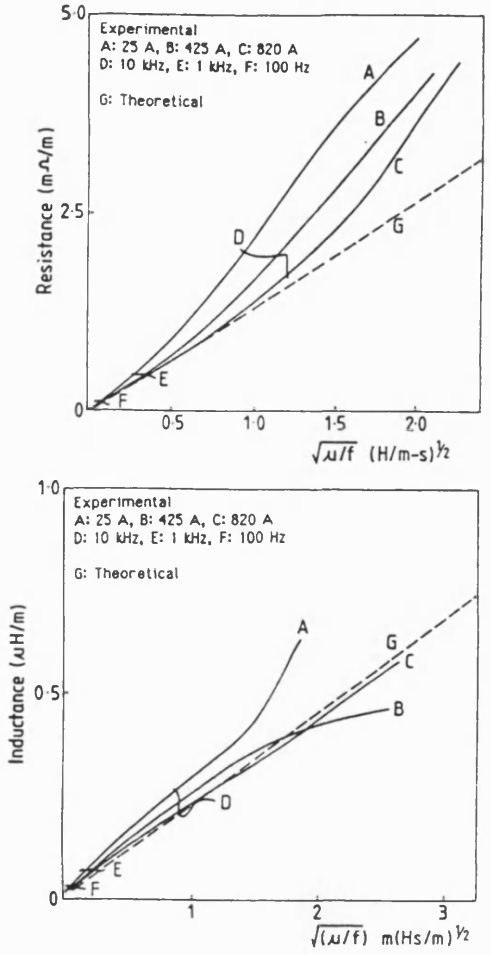

Figure 6: Rail impedance: resistance as function of $\sqrt{(\mu f)}$ and internal self-inductance as function of $\sqrt{(\mu/f)}$.

define the lower limit of model applicability, rather than the skin depth considerations above.

Also in Figure 6 can be seen that at high frequencies, the experimental values of resistance exceed the theoretical values. This is probably due to extra losses from hysteresis. The deviation becomes apparent at a value $\sqrt{(\mu f)} = 1.3$ $(H/m.s)^{1/2}$, corresponding to a frequency of 12 kHz at the peak $\mu_\Delta = 0.145$ mH/m (or 16 kHz at $\mu_\Delta = 0.1$ mH/m). This phenomenon has also been reported by Holmstrom [4].

8 CONCLUSIONS

- A model for AC small-signal rail impedance in the presence of DC current has been proposed. The rail resistance and the internal self-inductance are analytic functions of the frequency and the delta permeability.

- Rail sample measurements of delta permeability as a function of magnetic field strength, and electrical conductivity as a function of temperature, yield accurate data for the theoretical model.

- Experimental measurements of rail resistance and internal self-inductance have been made with variable DC current and frequency, and confirm the theoretical model at audio frequencies (45 Hz - 16 kHz). Below about 45 Hz the inaccuracy shows that the rail shape must be taken into account. Above about 16 kHz, hysteresis effects are probably significant.

- The model can be used to calculate the internal impedance terms of the diagonal components in the track impedance matrix, for use as data in traction network circuit simulation studies, and to accurately predict the AC rail impedance for track signalling system design.

9 ACKNOWLEDGEMENTS

This research was financed by the Science and Engineering Research Council, UK.

10 REFERENCES

[1] D. J. Tylavsky and A.Y Kulkarmi, "Inductance Calculations for Earth-Return Trolley Systems," Proc. 1988 IEEE Industry Applications Society Annual Meeting, Pittsburgh PA, 2-7 Oct. 1988 (New York: IEEE 1988), vol. 2, pp. 1216-1223.

[2] B. Mellitt, J. Allan, Z. Y. Shao, W.B. Johnston and C.J. Goodman, "Computer-Based Methods for Induced-Voltage Calculations in AC Railways," IEE Proc., vol. 137B, no. 1, Jan. 1990, pp. 59-72.

[3] E.K. Stanek, T. Cataltepe and D.O. Wiitanen, "Phenomena that Affect the Calculation of the Inductance and Resistance of Mine Track/Trolley Systems," Proc. 1984 IEEE Industry Applications Society Annual Meeting, Chicago IL, 30 Sept. - 4 Oct. 1984 (New York: IEEE 1984), pp. 100-106.

[4] F.R. Holmstrom, "Conductive Interference in Rapid Transit Signaling Systems. Volume 1: Theory and Data," Report No. UMTA-MA-06-0153-85-5, U.S. Dept. of Transportation, Washington DC, Nov. 1985, 94 pp.

[5] R.J. Hill and D.C. Carpenter, "Modelling of Nonlinear Rail Impedance in AC Traction Power Systems," Proc. Int. Conf. on Harmonics in Power Systems, ICHPS IV, Budapest, 4-6 Oct. 1990, 7 pp.

[6] -, "Mutual Design: Overhead Transmission Lines and Railroad Facilities. Susceptibility Program," Report EPRI EL-6462, Electric Power Research Institute, Palo Alto CA, 31 July 1989, 160 pp.

[7] D.C. Carpenter and R.J. Hill, "The Effect of Magnetic Saturation, Hysteresis and Eddy Currents on Rail Track Impedance," Proc. IEEE/ASME Joint Railroad Conference, Philadelphia PA, 25-27 April 1989 (New York: IEEE 1989), pp. 73-79.

MODELLING OF NONLINEAR RAIL IMPEDANCE IN AC TRACTION POWER SYSTEMS

Dr R. John Hill

Mr David C. Carpenter

University of Bath, School of Electrical Engineering
Claverton Down, Bath BA2 7AY, UK

Abstract - Nonlinearity in the internal self-impedance of railroad rail can give rise to power frequency harmonics in traction systems. Limiting case analytical models of rail impedance, based on linear complex permeability and complete saturation, are compared with measurements for currents to 800A and frequencies to 10 kHz. The results show that for accurate representation an effective permeability of the material must be defined by prior modelling of the eddy current flux distribution within the rail iron. The usual assumption of rail internal self-impedance invariance with current is shown to be unrealistic.

INTRODUCTION

In AC-electrified railways, electric power is delivered from transformer substations via overhead catenary and returned through the running rails to electrical connections with return feeder cables or autotransformers. The traction power transmission system comprises the catenary, auxiliary feeder, return conductor and rail track. Electrically, this forms a coupled multiconductor transmission line, the behaviour of which is described by a matrix equation relating the phase voltages V_i to the line currents I_i, as follows:

$$\frac{d}{dx}[V_i] = [z_{ij}][I_j]. \qquad (1)$$

In this equation, the coefficients of the system impedance matrix are diagonal terms z_{ii}, the self-impedance of each conductor i with earth return, and off-diagonal terms z_{ij}, the mutual impedance between conductors i and j with earth return. The self-impedance terms are the sum of external and internal impedances. The former are functions mainly of circuit geometry, but the latter are determined by the flux within the rail iron. They depend on the excitation current and frequency, and are sources of nonlinearity in the power transmission path.

The elements of the track impedance matrix are required as data for system simulation studies, the objectives of which are to model energy flow, power supply/signal interference and harmonic effects. Harmonic currents generated by rail nonlinearities can propagate back into the power system and couple with communications and track signalling circuits. They can cause power supply problems such as network distortion, line resonance, and power factor deterioration, and are also important for fault condition and transient studies.

In most simulation studies reported in the literature, rail internal self-impedance is treated as an analytic function with value equal to the impedance of an equivalent circular conductor. Rail iron permeability is treated as a constant [1,2], so both resistance and inductance are assumed constant with AC current. The internal inductance reduces and the resistance rises with frequency due to flux reduction and redistribution within the iron from the skin effect. In the steady state, the external self-inductance is usually considered to dominate the internal self-inductance [2], the former being approximated with sufficient accuracy using the Carson-Pollaczek equations assuming the earth to have a finite, constant conductivity. Stanek et al [3], however, show that for transient studies, the rail internal self-impedance may be significant compared with the external component, and that the nature of fault transients indicates that knowledge of its impedance variation with current and frequency is essential for successful modelling of traction fault currents. Significant impedance change occurs from the effects of saturation and hysteresis in the rail iron, both phenomena modifying rail energy losses and reactive power flow. Holmstrom [4] has stated that rail hysteresis may give rise to intermodulation distortion in power and audio frequency track signalling systems.

The problem of the determination of rail self-impedance is concerned with the analysis of power frequency magnetic systems. The literature on this subject has concentrated on modelling saturation and hysteresis effects in electrical machines and transformers by accurate field computational techniques. These applications do not in general deal with magnetic conductors but the analytic methods can still be used with advantage. Burais [5], for example, demonstrates a technique to separate hysteresis from eddy current losses for a non-oriented material steel plate taking into account saturation. The method combines the finite element technique for space, and finite difference for time discretization. A similar problem is approached in a different way by Labridis [6] who assumes an equivalent fictitious material with relative permeability constant in time but variable in space, and related to the saturation B-H curve by a stored magnetic co-energy density. The effect of harmonic fluxes has also been evaluated numerically for transformer cores, and Hsu [7] shows that iron loss can be reduced for saturated conditions where hysteresis loss is large.

The modelling of internal impedance in an irregular-shaped ferromagnetic conductor such as railroad rail suffers practical difficulties due to its shape and variable material permeability. In this paper, the objectives of the modelling of rail internal impedance are to determine the regimes where hysteresis and saturation effects are significant. Linear analytic models with actual material data based on measurements of rail material permeability and resistivity are presented. The rail internal self-impedance term in the track impedance matrix is evaluated as a function of both frequency and AC current. The result can then be used to give a quantitative assessment of the extent of power frequency harmonic propagation in the power delivery process.

RAIL MATERIAL DATA

The Ferromagnetic B-H Loop

The permeability (μ) of ferromagnetic material is a function of the field vectors **B** (magnetic induction), **M** (magnetic polarization), and **H** (magnetic field), according to

$$\mathbf{B} = \mu_0(\mathbf{H} + \mathbf{M}) = \mu\mathbf{H} \qquad (2)$$

For isotropic and homogenous materials, the permeability is invariant with direction and position. For ferromagnetic materials, the magnetization process is time-dependent and B is a nonlinear, multivalued function of **H** as well as a function of frequency, with

$$\mathbf{B} = \mu(\mathbf{H}, \mathbf{B}, \omega)\,\mathbf{H} \qquad (3)$$

To determine the flux distribution within these materials, and hence electrical impedance, the complete B-H relationship needs to be specified. Figure 1 shows a typical ferromagnetic material static B-H characteristic together with the associated permeability definitions. Of principal interest for large-signal AC conditions are the initial, normal, incremental and differential permeabilities.

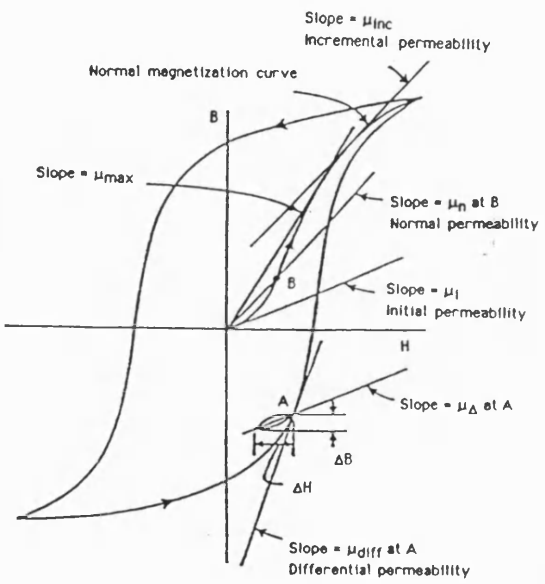

Fig. 1. Ferromagnetic material B-H loop and permeability definitions.

Time dependency in the magnetization process may be accounted for by introducing a complex permeability to describe the phase lag between the **H** and **B** vectors. Thus

$$\mathbf{B}\,e^{j\omega t} = |\mu^*|\,\mathbf{H}\,e^{j(\omega t-\phi)} = (\mu' - j\mu'')\,\mathbf{H}e^{j\omega t} \qquad (4)$$

where μ^* is the complex permeability. Physically, the phase angle accounts for energy losses associated with magnetic resonance and relaxation phenomena arising from the reorientation of magnetic moments of microscopic origin [8]. However a similar representation can also give accurate estimates of material behaviour in the macroscopic region if there is no material saturation, so that the vectors **B** and **H** are linearly related. The B-H characteristic then becomes elliptical. Even for practical materials with nonlinear permeability, approximating the B-H loop by an ellipse allows complex permeability data to be extracted by considering the fundamental frequency relationship.

Experimental Material Tests

Various material samples were machined from railroad rail in order to evaluate the actual permeabilities as specified in Figure 1. The static B-H loop was determined using filaments of material 2 mm square and with length at least 100 mm. Each filament was subjected to an alternating magnetic field with frequency 0.33 Hz in the direction of its longitudinal axis. This low excitation frequency ensured that the skin depth was much greater than the filament width (d):

$$\delta = \sqrt{(2/\omega\sigma\mu)} \gg d \qquad (5)$$

Three filaments from orthogonal directions were tested to confirm the material isotrophy. Graphical results for low, medium and high values of surface field strength H_S are shown in Figure 2. Table 1 shows the evaluated energy per cycle in each of the three hysteresis loops. The variations of normal and incremental permeability as a function of surface magnetic field strength, extracted from the measured data of Figure 2, are reproduced in Figure 3.

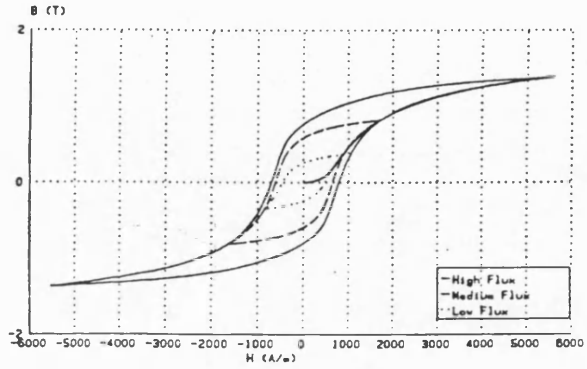

Fig. 2. Measured B-H loops for 54 kg/m flat-bottom rail material.

From the B-H loops, complex permeability data has been evaluated in two ways:

- Assuming sinusoidal magnetic field excitation, the B-H loop has been analysed by the Fast Fourier Transform technique to obtain the fundamental and harmonic magnitudes and phases of the flux density. Only the odd harmonics are significant, and the results for the first three are shown in Table 1. In this method, the sum of the fundamental and harmonic losses will equal the total loss as given by the loop area.
- For linear modelling it may be more accurate to equate the total loop area with the area of an equivalent fundamental ellipse. Thus all harmonic losses would be included within the fundamental. The orientation of the ellipse, defined by coercive force and remanent flux density, is that defined by the original hysteresis loop.

Figure 4 shows the resulting complex permeability functions derived from each model.

Rail Resistivity

The resistivity of the rail iron is also a fundamental material property and appears as a constant in the skin depth function. It can be expressed in the form

$$\rho = \rho_{20}(1 + \alpha T) \qquad (6)$$

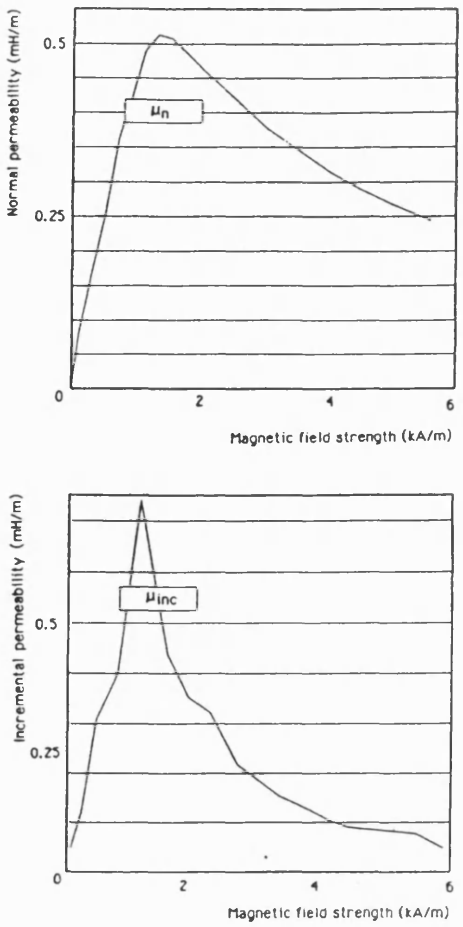

g. 3. Derived normal and incremental permeabilities for 54 kg/m rail material.

here α is the temperature coefficient of resistivity, nearized over the temperature range of interest, T is the mperature (K), and ρ_{20} is the restivity at 20 K.

The resistivity of the rail samples used in the material sts was measured by applying constant currents and easuring voltage over a suitable temperature range. ypical results at 20 K are

$\alpha = 3.4\ 10^{-3}\ K^{-1}$
$\rho_{20} = 0.225\ 10^{-6}\ \Omega\ m$

lth conductivity

$\sigma_{20} = 4.44\ 10^{6}\ S\ m^{-1}$.

ANALYTICAL MODELLING

The objective of analytical modelling is to predict the pendency of rail internal self-impedance on AC current id frequency. Simple modelling can reveal order of agnitude estimates for the fundamental and harmonic wer loss for the base cases of:

Linear complex permeability, no saturation.

No hysteresis loss, high saturation.

rther analysis is necessary to establish the optimum ffective permeability to use in each model, as a function of rface magnetic field H_s.

Peak surface magnetic field H_s (A m^{-1})	Fundamental B_1 (T)	Φ_1 (°)	3rd harmonic B_3 (T)	Φ_3 (°)	5th harmonic B_5 (T)	Φ_3 (°)	7th harmonic B_7 (T)	Φ_7 (°)
5600	1.65	-9	0.39	-29	0.19	-46	0.105	-65
1700	0.95	-25	0.19	-74	0.075	+65	0.04	+20.5
900	0.394	-26	0.065	+64	0.017	-20	0.006	-73

Table 1. Flat-bottom Rail Hysteresis Loop Harmonic Analysis.

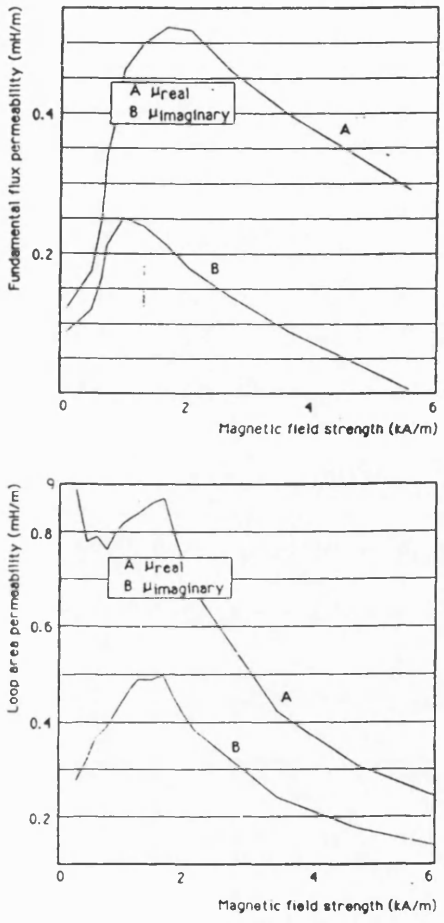

Fig. 4. Complex permeability with fundamental flux and B-H loop area approximations.

Linear Hysteresis Model

The rail is treated as a magnetic conductor made from homogenous, isotropic material with constant permeability μ^*. Assuming an equivalent circular solid conductor, the solution for magnetic field and hence current density within the material is found from solving the diffusion equation [9]. The conductor impedance is then found as a function of conductor radius and skin depth:

$$R + jX = \frac{\alpha}{2\pi a \sigma} \frac{I_0(\alpha a)}{I_1(\alpha a)} \qquad (7)$$

where

$$\alpha^2 = j\omega\sigma\mu^* \qquad (8)$$

is the complex skin depth function, a is the conductor

radius, σ is the conductivity and I_n are n^{th} order modified Bessel functions of the first kind.

After manipulation, it may be shown that the internal impedance of the conductor takes limiting values at low and high frequencies as follows [10]:

Low frequency: $a \ll \delta$

$$z_{lf} = \frac{1}{\pi a^2 \sigma}\left\{\left[1 + \frac{a^2}{4\delta^2}\sin\theta + \frac{a^4}{48\delta^2}\cos 2\theta\right] + j\left[\frac{a^2}{4\delta^2}\cos\theta - \frac{a^4}{48\delta^4}\sin 2\theta\right]\right\} \quad (9)$$

High frequency: $a \gg \delta$

$$z_{hf} = \frac{1}{\pi a^2 \sigma}\left\{\left[\frac{1}{4} + \sqrt{2}\cos\left(\frac{\pi}{4} - \frac{\theta}{2}\right)\right]\left(\frac{a}{2\delta} + \frac{3}{32}\frac{\delta}{a}\right) + j\left[\sqrt{2}\sin\left(\frac{\pi}{4} - \frac{\theta}{2}\right)\right]\left(\frac{a}{2\delta} - \frac{3}{32}\frac{\delta}{a}\right)\right\} \quad (10)$$

where θ is the hysteresis angle. For complex permeability, equations (9) and (10) describe the behaviour at the fundamental frequency, and the eddy and hysteresis losses cannot be separately identified.

The impedance angle reduces with hysteresis from the asymptotic value of π/4. The model shows that losses are increased in the presence of hysteresis by a factor

$$\frac{[\cos(\pi/4 - \theta/2)]}{\cos\pi/4}$$

and the rail reactance is decreased by the factor

$$\frac{[\sin(\pi/4 - \theta/2)]}{\sin\pi/4}.$$

Saturation Effects

The linear model gives the equivalent rail impedance as that of an inductance, associated with energy storage, and a resistance, associated with energy dissipation. In electrical circuits, a nonlinear resistance behaves like a reactive power generator, although it has no energy-storage capacity. This is also the case for a saturated magnetic system, where the nonlinearity modifies the reactive, as well as the active power. An approximate model to take account of saturation in rail can represent the iron B-H characteristic by a step function according to

$$B = \begin{cases} +B_A & H > 0 \\ -B_A & H < 0 \end{cases} \quad (11)$$

It can be shown [9] that for this material property, magnetic flux waves with a constant magnitude of $|B_A|$ will penetrate the boundary under the influence of sinusoidal surface magnetic field excitation ($H_S \sin \omega t$). The maximum penetration depth is:

$$\delta_A = \sqrt{[2H_S/\omega\sigma B_A]} \quad (12)$$

which is in the same form as the skin depth equation (5), with the effective permeability, μ, replaced by B_A/H_S. The average power in the material is

$$P_{av} = \frac{8}{3\pi}\frac{H_S^2}{\sigma\delta_A} \quad (13)$$

which is a factor 70% greater than that in the linear case with δ set equal to δ_A).

Eddy Current Loss Model

The approximate models described so far represent limiting conditions of linear permeability and complete saturation. In most cases, the rail material saturates gradually, accompanied by distortion in the hysteresis loop. The balance between hysteresis and eddy current losses then changes.

The effect of nonlinear permeability in the presence of hysteresis is to produce harmonics with associated extra losses. To predict the rail impedance variation under these conditions a suitable effective permeability value must be selected. The modified eddy current distribution within the material can be calculated numerically taking account of the known dependency of permeability on magnetic field strength. The approach adopted is to use a finite difference technique, the Du Fort-Frankel scheme [11], to calculate the spatial and temporal decay in the magnetic field intensity within the material and hence estimate the effective complex skin depth.

The finite difference technique gives an explicit equation with attractive stability properties. Applied to a semi-infinite slab of material, the magnetic field strength is given by

$$\frac{\partial^2 H}{\partial y^2} = \sigma\mu(H)\frac{\partial H}{\partial t} \quad (14)$$

The associated difference equation is:

$$H_{i,k+1} = r H_{i+1,k} + (1-2r) H_{i,k} + r H_{i-1,k} \quad (15)$$

where $r = p/\sigma\mu h^2$, p being the time step length and h the spatial step length. By substituting for the present nodal value the average of the previous and next values,

$$H_{i,k} = (H_{i,k+1} + H_{i,k-1})/2 \quad (16)$$

the explicit difference equation is formed:

$$H_{i,k+1} = H_{i,k-1} + \frac{2r}{2r+1}(H_{i+1,k} - 2H_{i,k-1} + H_{i-1,k}). \quad (17)$$

The distribution of H in the material can then be determined by varying the surface magnetic field strength $H_{0,k}$ as a sine wave. Figure 5 shows the computed result of $|H_S|$ vs depth, for various initial surface field strengths. At high field strengths, the material becomes saturated near the surface and the magnitude of H falls away steeply in the interior, but for low initial field strengths, there is little deviation from the linear model.

EXPERIMENTAL RAIL IMPEDANCE MEASUREMENTS

Order of Magnitude Estimate for Hysteresis and Eddy Losses

In order to determine the relative importance of hysteresis and eddy current losses, iron losses were measured as a function of frequency in a toroid manufactured from rail iron. The dimensions of the toroid were: radius 30 mm, thickness 3 mm and length 10 mm, and the winding comprised 250 turns of 1 mm copper wire. The results, shown in Figure 6 with the static B-H loop loss per cycle superimposed, show that at power frequencies the hysteresis loss and eddy loss per cycle are comparable. This indicates that for the range of rail excitation expected in practice, neither the linear nor the heavily saturated model alone is realistic.

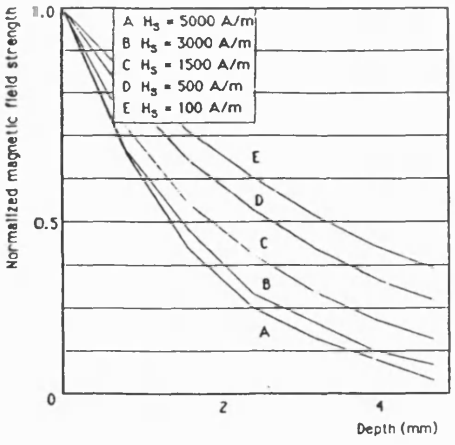

g. 5. Magnetic field strength as a function of depth in a semi-infinite slab of ferromagnetic material.

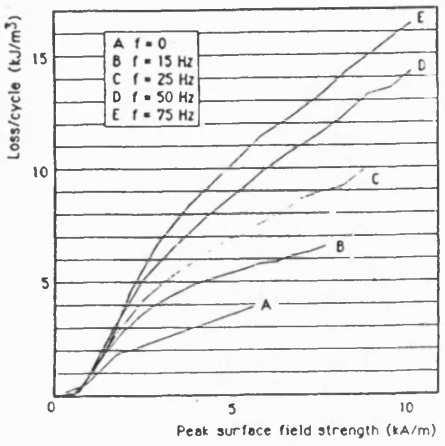

6. Measured iron loss in toroid sample of rail material.

Impedance Measurement Apparatus

To accurately measure the rail internal -impedance, the circuit inductance due to the test ent return path and the flux disturbance from sample e effects must both be eliminated. The experimental nique used was developed from equipment described by nstrom [4] for null-flux measurement of the -inductance change in an isolated rail, using as a rence conductor a copper tube. The method was ified so that absolute measurements of internal edance could be made. The apparatus (Figure 7) relies the prior use of a reference conductor, which is a cially-constructed hollow copper shell of identical shape he test rail and having negligible internal inductance [10] high frequency. This enables the impedance surement loop to be adjusted in position (distance d in re 7) such that zero inductance is obtained in ration.

When the rail sample is placed in the same physical tion as the copper shell, measurements of the change in ctance will thus represent the true internal -inductance. The resistive part of the impedance ains an absolute measurement of internal resistance. effects are negligible since the measurement points (A, Figure 7) are maintained a suitable distance from the luctor ends. An on-line FFT analyser provides noise unity and accurate phase and frequency measurement.

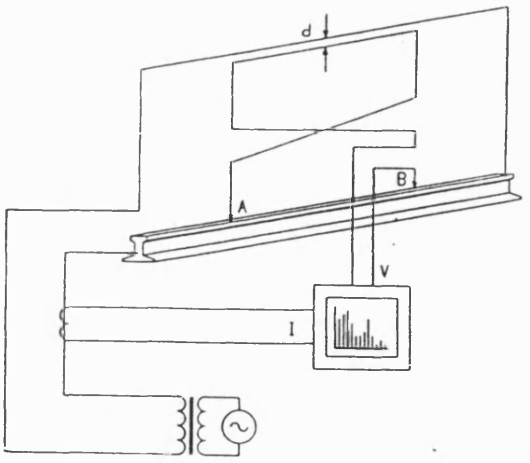

Fig. 7. Experimental apparatus for measurement of rail impedance.

Rail Impedance as Function of Current and Frequency

Measurement results of impedance as a function of current at 50 Hz are shown in Figure 8. Both resistance and inductance increase with current magnitude for the range of currents generated. To assess rail impedance at harmonic frequencies, measurements at a constant amplitude of 6 A were made for frequencies up to 10 kHz. The results are shown in Figure 9. As expected, the resistance increases and the inductance decreases with increasing frequency due to the skin effect.

DISCUSSION

Superimposed on the experimental curves of Figures 8 and 9 are theoretical calculations derived from the various assumptions on the modelling of hysteresis loss and the variation in material permeability. The increase of rail impedance with AC current indicates that the material is far from saturation even with the highest current applied. This is because of the large rail cross sectional area ($7.5\ 10^{-3}$ m^2). The most accurate resistance model is with an effective permeability function at low excitation, and with complex permeability obtained by the B-H loop area approximation (i.e. incorporating total harmonic losses within the fundamental) at high excitation. The use of normal and incremental permeability from Figure 3 is inappropriate in the model due to the importance of hysteresis loss. The effective permeability used is constant throughout the AC cycle, but with magnitude dependent on the level of current excitation as determined from Figure 5 (it has been termed *linearized* permeability). The inductance variation shows good agreement with the model using complex permeability obtained from the fundamental of the B-H loop, with better agreement at very low excitations from the linearized model of permeability as described above.

The variation in rail resistance with frequency, for low excitation currents, shows good agreement with the complex permeability model based on total loop area for high frequencies, and that based on the fundamental component for low frequencies. For rail inductance, the fundamental complex permeability model is more accurate at high frequencies, with the experimental curve lying between this model and the linearized model of permeability at lower frequencies.

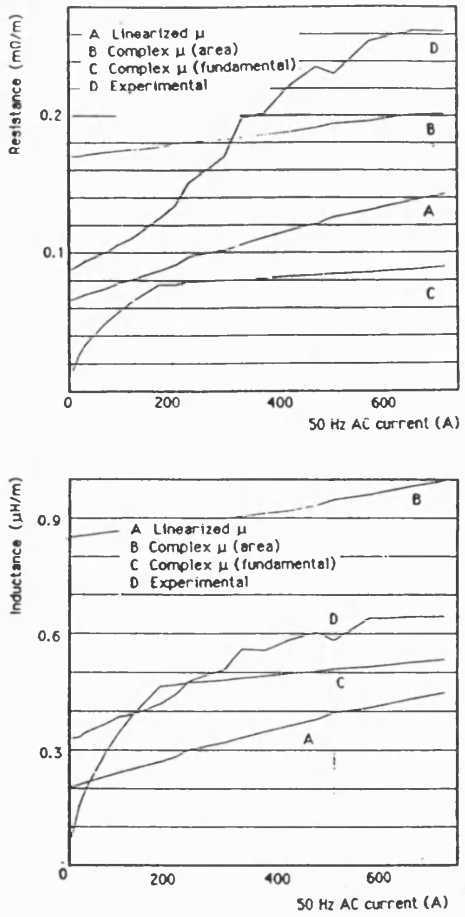

Fig. 8. Experimental and theoretical rail internal self-impedance as a function of AC current at 50 Hz.

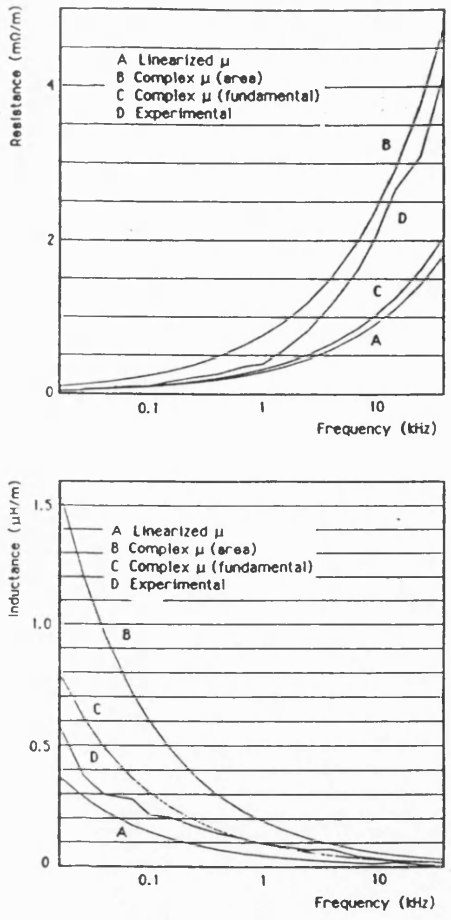

Fig. 9. Experimental and theoretical rail internal self-impedance as a function of frequency at 6A.

The complex permeability model based on loop area is more accurate for rail resistance modelling at high currents and frequencies. This model necessarily includes higher harmonic losses which increase with greater excitation. For the rail induction variation with current, ignoring the harmonics produces closer agreement with the experimental measurements. However the inductance is defined only at the fundamental frequency and the total VARs would necessarily need to include higher harmonics.

More accurate models are required to represent the rail impedance over the complete range of current and frequency. For example, accurate computations using combined finite element and finite difference techniques could incorporate exact differential permeability data, and hence enable identification of the separate fundamental and harmonic losses.

CONCLUSIONS

An analytical model with linear complex permeability, based on experimental determination of the material B-H loop, gives good agreement with measurements of rail impedance for moderate rail currents. The conditions correspond to hysteresis but not saturation, and will be of use in the modelling of power harmonic propagation in track signalling systems. At low excitations, better agreement is found by neglecting hysteresis and using an effective permeability obtained by modelling the flux distribution within the rail, using as data experimentally derived normal permeability as a function of surface magnetic field strength.

A saturation model ignoring hysteresis is suggested as suitable for transient studies and fault condition analyses which would be obtained with high excitation currents. The large magnitude of current at 50 Hz necessary to achieve rail saturation was not achieved in the reported experiments.

Results presented for rail internal self-impedance will enable the rail resistance and inductance at specific power frequency harmonics to be determined. The impedance is a function of current and frequency and cannot be obtained as a closed-form expression. It could, however, be expressed as a polynomial.

ACKNOWLEDGEMENTS

This research was supported by the Science and Engineering Research Council, UK.

REFERENCES

[1] D. J. Tylavsky and A. Y. Kulkarmi, "Inductance calculations for earth-return trolley systems," Proceedings of *1988 IEEE Industry Applications Society Annual Meeting*, Pittsburgh PA, 2-7 October 1988 (New York: IEEE 1988), vol. 2, pp. 1216-1223.

[2] B. Mellitt, J. Allan, Z. Y. Shao, W. B. Johnston and C. J.

Goodman, "Computer-based methods for induced-voltage calculations in AC railways," *IEE Proceedings,* vol. 137B, no. 1, pp. 59-72, January 1990.
E. K. Stanek, T. Cataltepe and D. O. Wiitanen, "Phenomena that affect the calculation of the inductance and resistance of mine track/trolley systems," Proceedings of *1984 IEEE Industry Applications Society Annual Meeting,* Chicago IL, 30 September - 4 October 1984 (New York: IEEE 1984), pp. 100-106.
F. R. Holmstrom, "The model of conductive interference in rapid transit signaling systems," *IEEE Transactions on Industry Applications,* vol. IA-22, no. 4, pp. 756-762, July/August 1986.
N. Burais and G. Grellet, "Numerical modelling of iron losses in ferromagnetic steel plate," *IEEE Transactions on Magnetics,* vol. MAG-18, no. 2, pp. 558-61, March 1982.
D. Labridis and P. Dokopoulos, "Calculation of eddy current losses in nonlinear ferromagnetic materials," *IEEE Transactions on Magnetics,* vol. MAG-25, no. 3, pp. 2665-2669, May 1989.
J. S. Hsu, H. H. Woodson and S.-S. P. Liou, "Experimental study of harmonic-flux effects in ferromagnetic materials," *IEEE Transactions on Magnetics,* vol. MAG-25, no. 3, pp. 2678-2685, May 1989.
D. J. Epstein, "Permeability". In: *Dielectric Materials and Applications* [Editor: A. R. Von Hippel]. New York: Technology Press M.I.T./Wiley 1954.
P. Hammond. *Applied Electromagnetism.* Oxford UK: Pergamon Press 1981.
D. C. Carpenter and R. J. Hill, "The effect of magnetic saturation, hysteresis and eddy currents on rail track impedance," Proceedings of *IEEE/ASME Joint Railroad Conference,* Philadelphia PA, 25-27 April 1989 (New York: IEEE 1989), pp. 73-79.
[11] E. C. Du Fort and S. P. Frankel, "Stability conditions in numerical treatment of parabolic differential equations," *Mathematical Tables and Aids Computation,* vol. 7, pp. 135-152, 1953.

R. John Hill was born in Somerset, England, on July 3, 1948. He received the degrees of B.Eng. in Electronics and Ph.D. in Power Electrical Engineering from the University of Liverpool, England, in 1969 and 1973, and M.A. from the University of Cambridge, England, in 1983.

From 1973-1980 he was a Design and Development Engineer for London Underground Railways working on automatic train control systems. In 1980 he became a Lecturer at Cambridge University Engineering Department and in 1983 a Fellow of King's College, Cambridge. Since 1986 he has been a Lecturer at the Universaity of Bath, England.

Dr Hill is a Member of the IEE (UK) and the Institute of Physics (UK). In 1988 he was awarded the IEEE Vehicular Technology Society prize for the best paper presented at the Joint ASME/IEEE Railroad Conference.

David C. Carpenter was born in England on September 8, 1956. He received the degrees of B.Sc. from the University of Southampton, England, in 1978 and M.Phil. from Coventry Polytechnic, England, in 1989.

In 1979 he became a Computer-Aided Design Engineer at GEC Machines Ltd, Rugby, England, and in 1980 a Lecturer (Senior Lecturer from 1984) in Electrical Engineering at Coventry Polytechnic, England. From 1986-1987 he was a Visiting Professor at Lakehead University, Canada. Since 1988 he has been a Research Officer at the University of Bath, UK, working on the modelling of electric traction systems.

Mr Carpenter is a Member of the IEE (UK).

UITP91

INTERNATIONAL EXHIBITION OF PUBLIC TRANSPORT UITP 91

in conjunction with the 49th Congress of the International Union of Public Transport

STOCKHOLM, SWEDEN
3 - 6 June 1991

This is the only Exhibition, supported by UITP and its members, with worldwide coverage for the suppliers to urban public transport systems. Exhibits will show the whole range of products used in urban public transport systems, from rolling stock & revenue/passenger controlling equipment to the most sophisticated new electronic devices and software.

Further information - and entry forms - can be obtained from the

BRUSSELS INTERNATIONAL TRADE FAIR
Parc des Expositions, place de Belgique, B-1020 Brussels (Belgium)
Tel. 322+ 477 04 77 - Telex 046+ 23643 - Fax 322+ 478 80 23

Rail track modelling for signalling and electrification system simulation studies

Detailed knowledge of the electrical behaviour of rail track is necessary for the simulation of signalling and electrification systems. Research is described here to determine the equivalent values of the rail track transmission line distributed impedance and admittance. The numerical values may be found by a combination of modelling and practical measurement.

Dr. R.J. Hill, Senior Lecturer, & Mr. D.C. Carpenter, Research Officer, School of Electronic and Electrical Engineering, University of Bath, U.K.

For the simulation of railway signalling and electric power systems, accurate models are required both for the electrical equipment connected to the track, and for the track itself. The track consists of a number of parallel lines — rails, and power, signal and communication cables — which have electrically distributed properties. The values of their equivalent impedances and admittances define the track transfer function and govern longitudinal and lateral signal and power flows.

Considerable difficulties exist in accurately specifying the equivalent electrical component values for rails. Making in-situ measurements is extremely difficult because the rail track is fixed in place, and access to an absolute remote earth is not available. Models must account for non-linearities with frequency and/or current due to the material properties of the rail iron, soil and substructure. Non-linearities are especially significant when determining the mixing behaviour of power and signal currents, and for electromagnetic compatibility studies. Furthermore, the equivalent element values also vary with environmental conditions such as temperature and humidity.

In the literature, the determination of the track equivalent impedances and admittances has been reported only as a supporting activity for simulation studies. In particular, track data is usually oversimplified with regard to its variability. Mellitt [1], for example, used estimates of self and mutual track impedance and, apart from the AC skin effect behaviour, assumed linearity. Other approximations usually made in simulation include linear rail permeability with variable current and frequency, and constant soil conductivity and permittivity with variable depth and frequency. Although over simplification of the track model precludes parametric studies involving the track/ground interaction, linear approximations are sufficient for many applications since many simulation models are system specific, e.g. the prediction of harmonic propagation in railway overhead power lines [2], and the calculation of induced voltages in adjacent cables [3].

In this article, modelling and experimental techniques are described to obtain values of the track impedances and admittances as functions of excitation frequency and current. The models treat rail track as a coupled multiconductor line.

and specific numerical results for the equivalent component values are given for a single track with no parallel signal or electric cables. Finally, a brief outline of some simulation applications is given.

Multiconductor line model of rail track

The model of rail track as a multiconductor coupled transmission line must include the running rails, parallel electric power rails and cables, and signalling/telecommunications cables. Fig. 1 shows the line representation in terms of self and mutual impedances and admittances, with only two lines shown for clarity. The usefulness of the line model is that standard electrical transmission line equations may be used to obtain the line voltages and currents for any given line excitation. This procedure can most conveniently be carried out in software using an electric circuit simulation package.

The general line equations for an n-phase line (i.e. for n rails and cables) relate the distance-dependent voltages and currents to the line impedance and admittance matrices according to the wave equations

$$\frac{d^2[V]}{dx^2} = [Z][Y][V] \quad (1)$$

and

$$\frac{d^2[I]}{dx^2} = [Y][Z][I] \quad (2)$$

where [Z], [Y] are square matrices of order n with elements z_{ij}, y_{ij}. The elements z_{ii} and y_{ii} are the unit length self impedances and self admittances, and z_{ij} and y_{ij} are the unit length mutual impedances and admittances.

The modal transformation solution technique is commonly used for electric power line analysis [4], since it removes the mutual dependencies. Modal voltage and current vectors are introduced such that after the transformations, the new differential equations are essentially those of independent, single-phase lines with unique voltage and current distributions, propagation constants and characteristic impedances. Generally, however, these latter parameters are frequency dependent, so it is important to have detailed line data to determine the line behaviour at variable frequency.

For the single track (two-rail) line, the modal analysis may be simplified since spatial symmetry can be assumed in the conductor (rail) positions. The modes then correspond to line excitation with differential (or balanced) and common (or unbalanced) voltages. In railway traction, this is the case with line operation with track circuit and traction power return current as shown in Fig. 2.

The differential and common modes have their individual characteristic impedances (z_0) and propagation constants (γ) determined from the line element data, as follows:

$$z_{0,d} = \sqrt{[(z_{11} - z_{12})/(y_{11} - y_{12})]} \quad (3)$$

and

$$\gamma_d = \sqrt{[(z_{11} - z_{12})(y_{11} - y_{12})]} \quad (4)$$

for the differential mode, and

$$z_{0,c} = \sqrt{[(z_{11} + z_{12})/(y_{11} + y_{12})]} \quad (5)$$

and

$$\gamma_c = \sqrt{[(z_{11} + z_{12})(y_{11} + y_{12})]} \quad (6)$$

for the common mode. The above argument considers the two-line case, but the general principles apply equally well to any general n-phase line. However, for n modes, the physical significance of each of mode tends to become lost in simulation without detailed consideration of the modal characteristic impedances and propagation constants.

Modelling and measuring the rail equivalent components

Exact determination of the values of the rail impedance and admittance equivalent components is difficult due to their variation from:

- *rail iron material properties,* giving frequency and current dependency;
- *environmental changes,* giving dependencies on temperature and ground water content;
- *ground geological structure,* affecting the soil conductivity and permittivity profiles with depth;
- *rail and track substructure,* including rail shape and weight, ballast and sleeper type, and affecting the leakage admittance.

Modelling of the equivalent components should commence with determination of the material properties of the rails and ground. The relevant rail properties are iron permeability and conductivity, and the main relevant ground properties are soil/substrata conductivity and permittivity variations with depth and frequency.

The second stage in modelling is to use the material data to create impedance and admittance component models, and to verify the models with practical tests. At the University of Bath, this has been facilitated by the installation of a 36 m long test rail track (Fig. 3). The track is laid on limestone ballast with a depth of 300 mm, with both wood and concrete sleeper sections, and bull-head and flat-bottom rail, with provision for third and fourth rail electrification.

In-situ measurement of rail track elements

In practice, considerable difficulties exist in measuring the equivalent impedance and admittance matrix elements in situ, because:

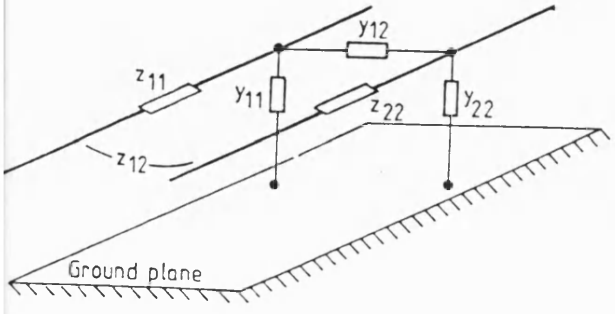

Fig. 1. Multiconductor line model for a single rail track

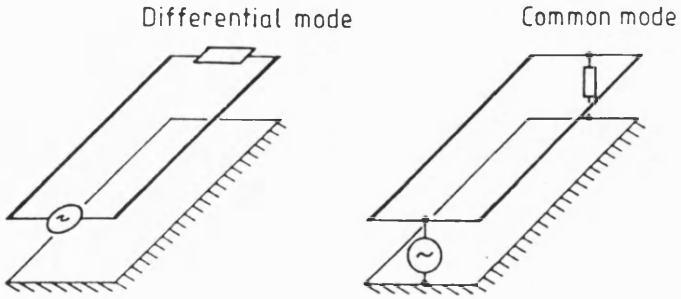

Fig. 2: Line excitation modes for two-rail line with earth return

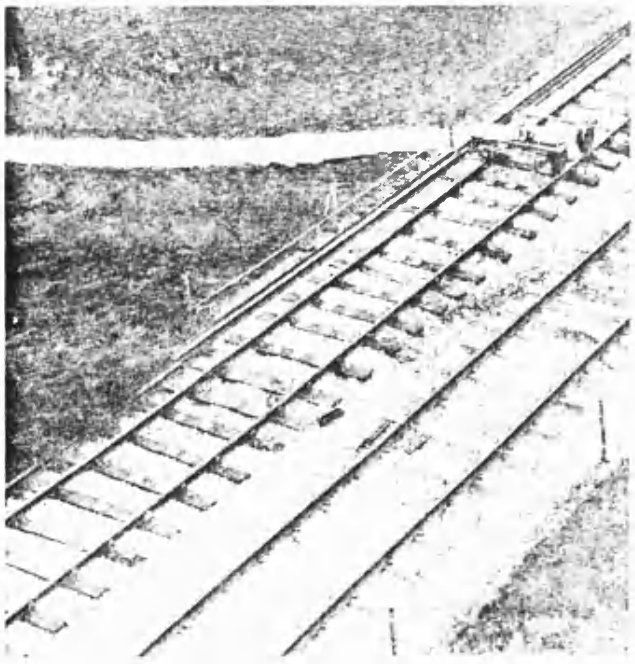

Fig. 3. Test rail track

— rail joint connections and stray capacitance and inductance may be dominant;
— the components are distributed along the track length, so the inadvertent creation of measurement loops should be avoided;
— access to an absolute earth reference is not possible.

Null measurement methods such as bridge techniques are attractive in principle, but difficult to perform because of electrical interference which has a serious effect due to the distributed nature of the system. Power measurements are more convenient, but a major consideration is that the value of certain elements vary with current and frequency. In devising track tests, a significant consideration is that the number of accessible measurement terminals is low, compared with the number of unknowns to be determined.

In making experimental measurements on rail track, it is important to note that rails are designed neither for efficient energy transfer (as in overhead power transmission lines) nor for distortionless signal propagation (as in communications lines), so the usual assumptions such as loss-free operation do not apply. However, for in-situ tests, advantage may be taken of the short measurement length on the University test track, and its isolation from adjoining track sections. Thus

$$z_{ij}l \ll 1/(y_{ij}l) \quad \text{for all } i, j \tag{7}$$

where l is the length, so the impedance and admittance measurements may be performed independently. The consequence of this inequality is that it is fairly straightforward to devise approximate experiments giving confirmation of some of the models.

Effect of conducting earth

Determination of the rail track equivalent matrix element values must take into account the proximity of the earth which is a semi-infinite weakly conducting medium. The single track rail line comprises twin ferromagnetic conductors connected electrically to the ground surface by metallic fastenings to sleepers at periodic intervals. The ground itself has conductivity, permittivity and in some cases permeability, which are all generally both depth and frequency dependent. Currents flowing along the rails will cause additional currents to flow in the earth from both conductive and inductive coupling.

For the simplified case of the symmetrical two-rail line, the general line excitation can be represented as a linear combination of the common and differential modes shown in Fig. 2. A large common-mode current flows in the earth, from conductive and inductive coupling, together with a smaller current from inductive coupling of the differential-mode current.

The effect of the conducting earth on the rail self impedance arises from spreading of the earth return current in the soil due to the low soil conductivity. The physical model proposes the generation of eddy currents within the soil by induction, to oppose the field generated by the rail current. Current actually flows in the ground near the rail in the form of an image conductor, so the loop impedance is modified. For perfectly conducting earth, the image conductor will be located beneath the ground at a depth equal to the rail height, but for lossy ground the depth increases and the current spreads out further, thus increasing the loop inductance. Eddy current power losses also arise in the ground, so the equivalent self resistance also increases.

Similar considerations apply for the mutual impedance between the lines. This is defined as the mutual coupling between circuits comprising each line with its earth return. The conducting earth acts as a screen, reducing the mutual impedance value as the earth conductivity is raised. Separate image conductors exist for each rail, so the mutual impedance will have several distinct terms as described later.

The finite ground conductivity is also responsible for shunt losses in the track transmission line system, and physically the model is represented by self and mutual conductances. The resistance of the rail fastenings, sleepers and ballast also contribute to these leakage currents. The depth profile of ground conductivity determines the values of these track conductances. A similar ground permittivity variation with depth accounts for self and shunt capacitance in the admittance model.

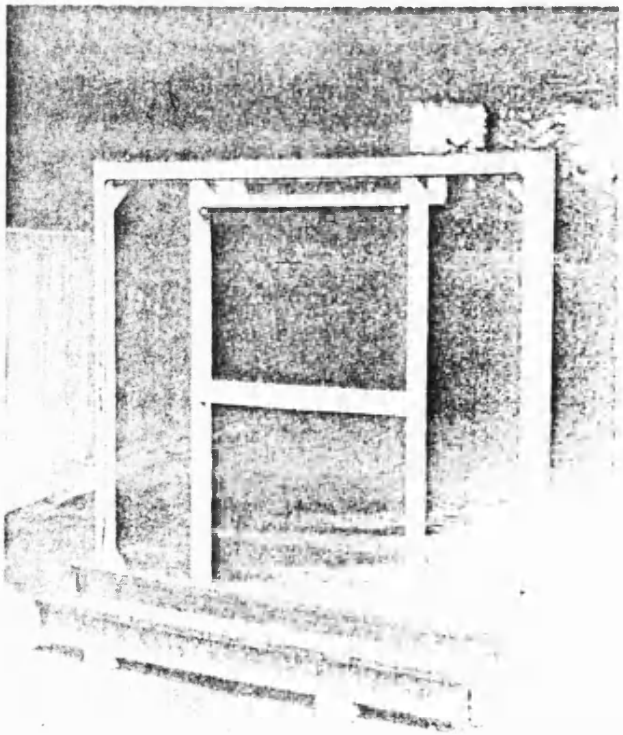

Fig. 4. Measurement apparatus for rail internal impedance

Series self and mutual impedance

The self impedance of each rail in the track multiconductor system is the sum of internal and external components. The internal inductance is due to stored magnetic field energy, and the internal resistance is due to dissipated energy, both within the rail. The former may represent an appreciable proportion of the total rail self impedance. It is nonlinear with both current and frequency because of the variation in iron permeability. A complete model of the internal impedance is difficult due to the presence of rail saturation and hysteresis [5, 6], but its laboratory measurement is fairly straightforward using a null flux technique and apparatus of the form shown in Fig. 4. Sample results for the internal impedance for flat-bottom rail with small signal AC excitation are given in Fig. 5.

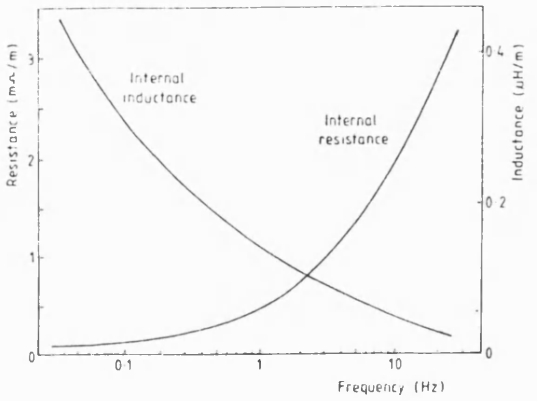

Fig. 5: Rail internal self impedance as function of frequency

The external impedance, due to the stored and dissipated energy outside the conductor, is the circuit inductance and resistance of the loop comprising the rail current with earth return. The electromagnetic theory necessary to model the self impedance was originally evaluated by Carson, Polaczek and Haberman, and the resulting equations have since been applied to a variety of transmission line configurations. For the model of rail track impedance, the theory developed by Bickford [7] may be conveniently used assuming a two-layer earth conductivity function. Bickford's equation for the external self impedance is

$$z_s = j\omega\left(\frac{\mu_1\mu_0}{2\pi}\right)\ln\left(\frac{2h}{\alpha}\right) + j\omega\left(\frac{\mu_1\mu_0}{\pi}\right)J_s \quad \Omega/m \qquad (8)$$

where

$$J_s = \int_0^\infty \frac{\mu_2 \exp -2h\lambda}{[\mu_2\lambda+\mu_1 A(\lambda)]}\, d\lambda \qquad (9)$$

$$A(\lambda) = \gamma_2\left(\frac{\mu_3\gamma_2\sinh(d\gamma_2) + \mu_2\gamma_3\cosh(d\gamma_2)}{\mu_3\gamma_2\cosh(d\gamma_2) + \mu_2\gamma_3\sinh(d\gamma_2)}\right) \qquad (10)$$

and

$$\gamma n^2 = \lambda^2 + j\omega\mu_n\mu_0\sigma_n. \qquad (11)$$

The subscripts 1, 2 and 3 refer to air, the upper ground layer and the lower ground layer respectively, d is the depth of layer 2 beneath the ground surface, ω the angular frequency, μ the permeability, h the rail height, α the rail radius, λ a varaible of integration and σ the conductivity. Equations (8) – (11) express the impedance as the value assuming a perfectly conducting earth, together with a correction term.

The mutual impedance per unit line length with earth return is derived from similar considerations. Bickford's equations again give the mutual impedance as the value assuming a perfectly conducting earth with a correction factor:

$$z_m = j\omega\left(\frac{\mu_1\mu_0}{2\pi}\right)\ln\sqrt{\frac{(h_k+h_m)^2+d^2}{(h_k-h_m)^2+d^2}} + j\omega\left(\frac{\mu_1\mu_0}{\pi}\right)J_m \quad \Omega/m \qquad (12)$$

where

$$J_m = \int_0^\infty \frac{\mu_2\cos[\lambda(h_k-h_m)]\exp -h\lambda\, d\lambda}{[\mu_2\lambda+\mu_1 A(\lambda)]} \qquad (13)$$

$A(\lambda)$ again being defined by Equations (10) and (11), and the subscripts k and m referring to the two rails.

The physical interpretation of the mutual impedance relies on visualising the field round the rails. The general form of mutual impedance is

$$z_m = r + j\omega(L_A + L_B). \qquad (14)$$

The positive real component (r) is the mutual resistance and represents the ground eddy current loss. The two rails have different ground return paths, and L_A is the contribution to the mutual inductance from the wire geometry, with L_B the contribution from the ground return paths. Actually, for pairs of running rails, the ground return paths will almost coincide in space, and the DC term will be small. Fig. 6 shows theoretical values of self and mutual impedance evaluated from Equations (8) - (13) using the two-layer soil conductivity model.

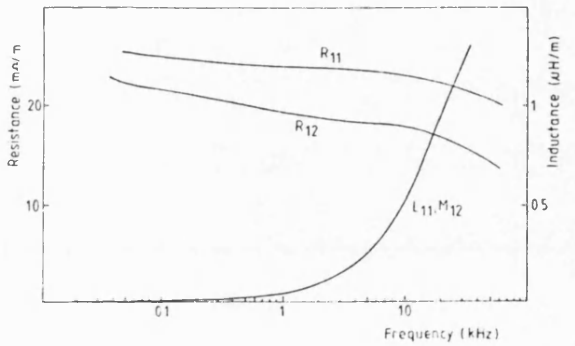

Fig. 6: Series self and mutual impedance as function of frequency

Shunt and mutual admittance

The model of track admittance may be derived by considering continuous or discrete function conductivity and permittivity models of the earth. Approximate estimates may be made assuming a single or two-layer earth model [8]. Experimental verification is difficult due to the inaccessibility of the remote earth, to which the self admittance is referenced. However, an estimate of track admittance can be made using the *broken rail* technique illustrated in Fig. 7, and assuming lumped rail admittances. This method involves making a break in one of the rails, applying an excitation signal at one end, with a suitable load admittance, comparable in magnitude to the track admittance, applied at the other. The source voltage (V_s) and current (I_s), and load admittance (y_L), voltage (V_L) and current (I_L) are measured. Circuit analysis by solution of the equivalent loop equations then yields the self and mutual admittances. Fig. 8 gives some typical results for flat-bottom rail with concrete sleepers.

Model applications

A complete track transmission line equivalent circuit with current and frequency dependency can be used to represent the signal transmission path in simulation studies concerned with both signal and power transmission.

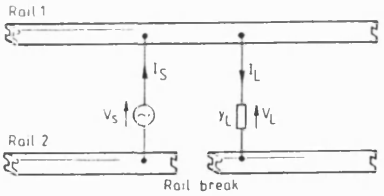

Fig. 7: Broken rail test for measurement of rail admittance

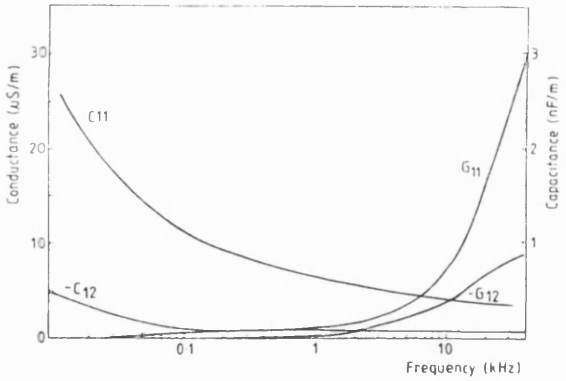

Fig. 8: Shunt self and mutual admittance as function of frequency

Signalling system simulation

The design of audio frequency (AF) track circuits with signal modulation and coding can be facilitated by simulation. AF track circuit carrier frequencies are in the range 1.6 kHz to 20 kHz, and typical operating lengths are 300 m to 800 m. The first task of simulation is the optimisation of the basic track circuit characteristics in the train shunt and broken rail modes of operation. Then, to determine the capacity for information transmission, the signal mixing behaviour in the termination areas may be modelled.

To adequately model the above conditions, the full track section model must be used. Although in normal operation, the track circuit is excited by the differential mode, in general the track will exhibit asymmetric properties because of ballast asymmetry, drainage conditions and track curvature. Thus there will also be common mode excitation and ground current will flow. In the broken rail mode of operation, severe unbalanced currents flow in addition to a small differential mode current. Further information on the simulation of track circuits can be obtained in reference [9].

Electrification system simulation

The propagation of harmonic currents in AC or DC fed electric railway traction systems can also be modelled with advantage if a complete track section model is available. Although return currents normally flow along the running rails in parallel, by common mode excitation, in practice differential mode currents will also flow, for example through unbalanced traction currents arising from asymmetries such as rail curvature. In general, this will cause harmonics of the traction current to penetrate the ground at different depths and to be present in the various modes with different magnitudes. Modelling and simulation of the electric traction power system can also give information about energy transmission efficiency, line regulation and load power factor.

Conclusions

Rail track electrical equivalent circuit component data necessary for accurate simulation models can be obtained by a combination of modelling and experimental measurement. The variation of the data with current and frequency, and with environmental conditions, is particularly useful. In order to complete the track data knowledge base, research is proceeding on the following enhancements:

— the in-situ measurement of track parameters without the need to make approximations, and which applies to both short and long lines.
— a ground capacitance model with ground permittivity variation with depth.
— a method to assess the relative importance of the self and mutual impedances.
— the variation of the shunt admittance components with environmental and geological conditions.

Acknowledgement

This research was performed with financial aid from the UK Science and Engineering Research Council (Grant GR/E/58816).

References:

[1] Mellitt B, Allan J., Shao Z.Y., Johnston W.B. and Goodman C.J.: Computer-based methods for induced-voltage calculations in AC railways. IEE Proceedings, January 1990, v. 137 B, n. 1, pp. 59-72.

[2] Holtz J. and Klein H.-J.: The propagation of harmonic currents generated by inverter-fed locomotives in the distributed overhead supply system. IEEE Transactions on Power Electronics, April 1989, v. PE-4, n. 2, pp. 168-74.

[3] Machczynski, W.: Currents and potentials in earth-return circuits exposed to alternating current electric railways. IEE Proceedings, September 1982, v. 129 B, n. 5, pp. 279-88.

[4] Wedepohl, L.M.: Application of matrix methods to the solution of travelling-wave phenomena in polyphase systems. Proceedings IEE, December 1963, v. 110, n. 12, pp. 2200-12.

[5] Hill R.J. and Carpenter D.C.: Modelling of nonlinear rail impedance in AC traction power systems. 4th International Conference on Harmonics in Power Systems: ICHPS IV, Budapest, 4-6 October 1990, pp. 268-74.

[6] Carpenter D.C. and Hill R.J.: Rail impedance modelling for DC-fed railway traction simulation. IASTED International Symposium on Applied Modelling and Simulation, Lugano, 18-21 June 1990 (Anaheim CA: Acta Press 1990), 5 pp.

[7] Bickford J.P., Mullineux N. and Reed J.R.: Computation of Power System Transients. London: Peter Peregrinus 1976.

[8] Hill R.J., Carpenter D.C. and Tasar T.: Railway track admittance, earth-leakage effects and track circuit operation. 1989 ASME/IEEE Joint Railroad Conference, Philadelphia, 25-27 April 1989 (New York: IEEE 1989), pp. 55-62.

[9] Hill R.J., Yu S.L. and Dunn N.J.: Rail transit chopper traction interference modelling using the SPICE circuit simulation package. IEEE Transactions on Vehicular Technology, November 1989, v. VT-38, n. 4, pp. 237-46.

FEM APPLIED TO RAILROAD TRACK ELECTRICAL IMPEDANCE AND ADJACENT TRACK CROSSTALK MODELLING

David C. Carpenter, R. John Hill

School of Electrical Engineering, University of Bath
Claverton Down, Bath BA2 7AY, UK

Abstract - In a multiple-track railroad, the conductors form mutually-coupled ground return circuits. Accurate electrical circuit analysis, required for signalling, traction and electromagnetic compatibility analysis, is difficult to achieve because of the variability in the equivalent electrical components from their material properties and environmental conditions. This paper describes an application of the finite element method to the electromagnetic analysis of rail track. After validation by benchmark tests using single rail, single & three-rail track, the technique is used to predict crosstalk between adjacent tracks of a two-track electric railroad.

INTRODUCTION

Evaluating crosstalk effects between adjacent tracks in an electrified railway is of considerable significance for the safe and reliable operation of automatic train control systems. Because of crosstalk, harmonics of the traction currents, generated from power supply substation ripple and power electronic traction drive modulation components, can appear in signalling circuits on adjacent tracks. If the received signal harmonic spectrum is within the bandwidth of the track or train receiver, the interference currents may defeat the safety signalling system. Even if sufficient safety checks are made, the presence of crosstalk can still give rise to safe failures with associated equipment reliability problems. In this paper, a method is presented to predict crosstalk voltages and currents by computer simulation, using the finite element method (FEM) of electromagnetic system analysis.

It is difficult to model crosstalk analytically by conventional circuit analysis because the track transfer functions are imprecise. These depend on detailed knowledge of the track impedance matrix [Z] and admittance matrix [Y]. The former consists of the line self and mutual impedances, and the latter the line self and mutual admittances. The [Z] and [Y] matrices are not known to a high accuracy since the elements may be frequency, current and/or environmentally dependent. Previous attempts at analytical modelling of crosstalk have therefore met with only limited success [1]. Generally, for existing railroads, site measurements are required to verify the impedance and admittance models, and Mellitt et al [2] have displayed some ingenuity in using a computer program with data which could be varied with longitudinal position along the track section.

The finite element method was first applied to plain stress and strain problems in structural mechanics for the analysis of continua in 1953. In the 1960s, it was used to solve field problems in fluid dynamics, heat flow and electromagnetics, with problems of wave propagation in waveguides, and eddy currents in ferromagnetic materials receiving considerable attention. Recently, transient solutions for moving conductor systems such as electrical machines and electromagnetic launchers have been published. Several software packages for FEM are now available. References [3] and [4] summarize the existing state of the art.

Application of FEM to rail track signal analysis is not complicated. The technique is used to calculate the stored and dissipated system electromagnetic energy components, from which the electrical circuit impedance (resistance and inductance) may be determined. For long lengths, rail track can be regarded as a two-dimensional structure, so creation of the initial FEM net is straightforward, and computer run time and storage requirements are reasonable. The main problems lie in selecting accurate data for the rail ferromagnetic material and the ballast/ground structure, and in dealing with frequency and current dependency in those data. In particular, rail iron is nonlinear and exhibits hysteresis, and ground conductivity and permittivity vary with depth below the ground surface. The rails, however, can be modelled satisfactorily using a quasi-analytic approach [5], and the ground by using layered approximations [6].

In this paper, the model of rail track impedance is explained in terms of internal and external self-inductance, mutual inductance and resistance. The relationship of those variables to circuit impedance for various track configurations is given. FEM is described in terms of a physical understanding, and its practical application to rail track analysis is illustrated. To verify the accuracy of the technique, benchmark tests using single rail, single track and power-rail-electrified single track are described, the FEM model being compared with both analytic calculations and experimental results. Sample crosstalk voltages and currents, obtained by FEM and practical experimentation, are then presented.

THE MODEL OF RAIL TRACK IMPEDANCE

Rail track consists of two or more parallel ferromagnetic conductors laid on the surface of the ground. Together, the conductors form a coupled transmission line, whose electrical behaviour may be mathematically modelled using matrix algebra after setting up the track impedance and admittance matrices. The elements of these matrices are determined by the rail ferromagnetic material, line shape, physical geometry

and ground properties, and are represented schematically as shown in Figure 1. The impedance matrix contains the rail self impedances as the diagonal terms and the inter-rail mutual impedances as the off-diagonal terms. The self impedance of each rail consists of internal inductance, arising from the flux within the rail iron, external inductance, from the flux outside the rail surface, and resistance. The mutual impedance between lines also has both real and imaginary components. It can be interpreted physically by considering the nature of the earth-return circuit. Because of the weakly conducting earth, there is an additional loss mechanism from ground eddy currents, and an extended distribution of magnetic flux within the ground.

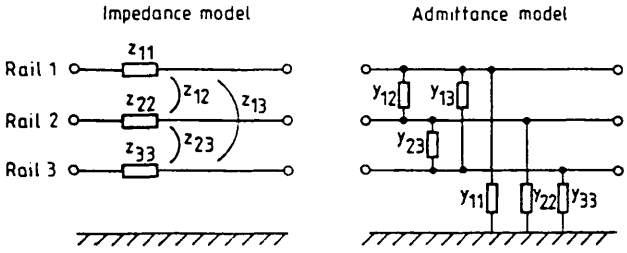

Figure 1: Rail track impedance and admittance model

The magnetic coupling between the rails is affected by their proximity to the ground. The track exhibits distinct propagation modes, the number of modes being equal to the number of lines. For a two-rail track, the modes relate to differential and common mode excitation (Figure 2). An approximate circuit analysis, ignoring the effect of line admittance, gives the impedances seen by the signal source to be

$$z_d = z_{11} + z_{22} - 2z_{12} \quad (1)$$

for differential mode excitation, and

$$z_c = z_{11} + z_{22} + 2z_{12} \quad (2)$$

for common mode excitation. The accurate transmission line analysis results in wave equations for the line voltage and current, characterized by propagation constants and characteristic impedances. The latter are

$$Z_{od} = \sqrt{[(z_{11} + z_{22} - 2z_{12})/(y_{11} + y_{22} - 2y_{12})]} \quad (3)$$

for differential mode excitation, and

$$Z_{oc} = \sqrt{[(z_{11} + z_{22} + 2z_{12})/(y_{11} + y_{22} + 2y_{12})]} \quad (4)$$

for common mode excitation.

The impedances in equations (1) and (2) form the basis for verification of the FEM results using the benchmark tests, since they may also be obtained approximately by analytic theory and/or experiments. However, direct experimental measurements of the track impedances for some configurations are extremely difficult due to the inaccessibility of the remote earth. A combination of experiment and analytical models must therefore normally be used.

The model of the internal self impedance must account for ferromagnetic material properties such as saturation and hysteresis and has been evaluated for both DC and AC

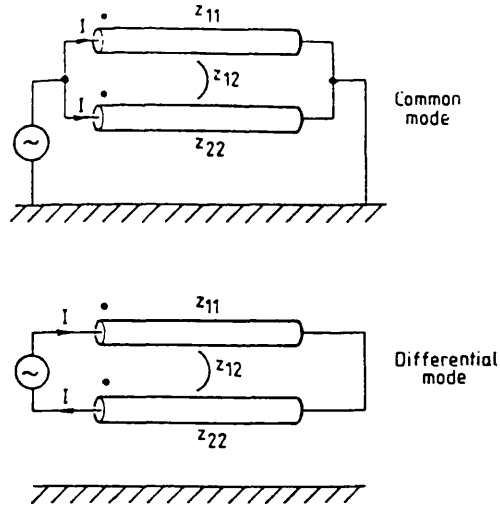

Figure 2: Common and differential mode track excitation

excitation [5, 7]. The model for the external self and mutual impedances must include the effects of the rail ground return circuits. The impedance of ground-return conductors laid on the ground surface has been considered in detail by various researchers, and Carson, Pollaczek, and Haberland have all produced analytic equations suitable for use at power and audio frequencies. Suitable approximations are normally necessary to model the variation of ground conductivity with depth. Bickford [8], for example, has adopted a two-layer earth conductivity stratification, modifying Carson's equations to obtain the self impedance as

$$z_{ii} = j\omega \frac{\mu_1\mu_0}{2\pi} \ln \frac{2h}{a} + j\omega \frac{\mu_1\mu_0}{\pi} J_s \quad \Omega/m \quad (5)$$

and the mutual impedance as

$$z_{ij} = j\omega \frac{\mu_1\mu_0}{2\pi} \ln \sqrt{\frac{(h_k+h_m)^2+d^2}{(h_k-h_m)^2+d^2}} + j\omega \frac{\mu_1\mu_0}{\pi} J_m \quad \Omega/m \quad (6)$$

In equations (5) and (6),

$$J_s = \int_0^\infty \frac{\mu_2 \exp(-2h\lambda)}{[\mu_2\lambda+\mu_1 A(\lambda)]} \, d\lambda \quad (7)$$

$$J_m = \int_0^\infty \frac{\mu_2 \cos[\lambda(h_k-h_m)] \exp(-2h\lambda)}{[\mu_2\lambda+\mu_1 A(\lambda)]} \, d\lambda \quad (8)$$

$$A(\lambda) = \gamma_2 \frac{\mu_3\gamma_2 \sinh(d\gamma_2)+\mu_2\gamma_3 \cosh(d\gamma_2)}{\mu_3\gamma_2 \cosh(d\gamma_2)+\mu_2\gamma_3 \sinh(d\gamma_2)} \quad (9)$$

and

$$\gamma_n^2 = \lambda^2 + j\omega\mu_n\mu_0\sigma_n \quad (10)$$

where the subscripts 1, 2 and 3 refer to air, ground layer and the lower ground layer respectively, d is the depth of layer 2 beneath the ground surface, ω the angular frequency, μ the permeability, h the rail height, *a* the rail radius, λ a variable of integration, σ the conductivity, and the subscripts k and m

refer to the two rails. Equations (5) and (6) express the impedance as the value assuming a perfectly conducting earth, together with a correction term.

THE FINITE ELEMENT METHOD

FEM applied to magnetic systems analysis

Generally, the finite element method can be implemented using either the electric field and magnetic vector potential, or the magnetic field and electric vector potential, to model the field in eddy current regions. In addition, nodal or edge variables may be used, and the field equations may be solved either by their differential or integral formulation [3]. The package used here implements the electric field method, with the differential form of the equations using nodal variables.

The problem space is categorized according to its material properties. In non eddy current regions, the magnetic scalar potential is sufficient to describe the field. In eddy current regions with no iron, the magnetic vector potential must be used, and in regions containing source current both the magnetic vector potential and electric scalar potential are required.

The finite element method models the appropriate field equations for each region, and then solves the equations numerically using, for example, the Galerkin weighted residual method [3]. An approximate expression is then created for the stored energy associated with the potential at each spatial point in the problem region, usually by assuming that the potential can be expressed as simple functions with undetermined coefficients. Computation then determines the coefficients for the minimum non-trivial energy condition. Silvester and Ferrari [9] show that this non-trivial solution is unique, and, furthermore, that the form of the solution implies that the calculation of system properties such as stored energies, power losses and impedances will be accurate, even for substantial local approximations in the potential distribution.

In non-conducting regions, the magnetic scalar potential (u) in regions of zero conductivity can be expressed by Laplace's equation

$$\nabla^2 u = 0. \qquad (11)$$

The boundary conditions are that the magnetic scalar potential is constant along ferromagnetic surfaces, and that it has zero normal derivative at planes of symmetry. The minimum potential energy condition implies a minimisation of the stored field energy per unit length, so the function

$$\min \{ W(u) = 0.5 \int |\nabla u|^2 \, dS \} \qquad (12)$$

is determined, with the integration carried over the complete two-dimensional problem region. Mathematically, a potential distribution satisfying Equation (11) will also minimise the energy as in Equation (12).

In regions containing currents, the magnetic vector potential A, satisfying a vector Poisson equation, must be used. For a two-dimensional system geometry, this degenerates to the scalar equation

$$\nabla^2 A = - \mu_0 J. \qquad (13)$$

The constant value of A corresponds to a magnetic flux line, thus defining the boundary conditions. The variational problem is then to find the function

$$\min \{ F(u) = 0.5 \int |\nabla u|^2 \, dS - \mu_0 \int \mu J \, dS \}. \qquad (14)$$

Silvester and Ferrari [9] show that F(u) reaches its minimum for u = A, given by the solution of Equation (13). The field energy is then calculated from the equivalent expression

$$W = 0.5 \int |\nabla A|^2 \, dS = 0.5 \, \mu_0 \int A \, J \, dS. \qquad (15)$$

To obtain a FEM solution, the problem space is divided into elements, exploiting symmetry to reduce their number. In principle, the elements may be any shape, since the method requires continuity across adjacent element boundaries. Once the potential at each element corner is known, the potential everywhere within the element may be found by interpolation. Common element shapes are triangular and quadrilateral. The former has the advantage of a linear interpolation procedure, and the latter of the need for fewer elements. The elemental assembly procedure is a non-trivial task that must take account of the structure shape and field charge density.

The stages of representing and solving a problem by FEM are: create the mesh, define the sources and boundary values, construct in software the matrix representation of each element, assemble the elemental equations, solve them, and display the results.

FEM for rail track impedance determination

The task of creating a finite element mesh for rail track is fairly straightforward since the track is longitudinally symmetric. Additional planes of symmetry can be exploited in the cases of a single rail, and a two-rail track. The irregular shape of the rails themselves requires care in apportioning the elements, and the elemental size must reduce in regions of high flux density magnitude or direction change. The aspect ratio of the meshes should, however, be maintained

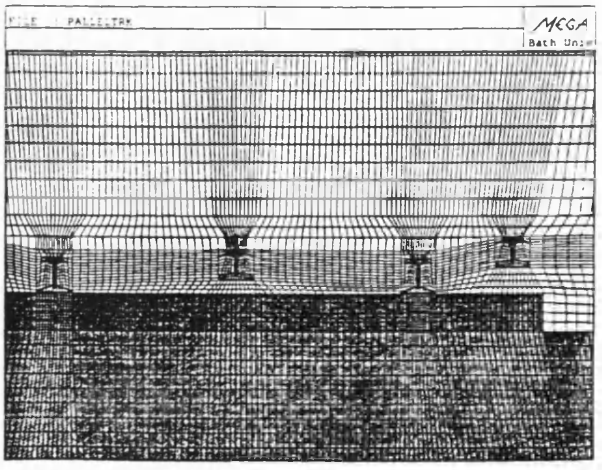

Figure 3: Elemental net for FEM of rail/track structure

approximately unity. The electrically conducting earth must also be divided into elements, and its conductivity variation may be represented as horizontal stratification of the elements.

The FEM package used employed quadrilateral elements, ensuring efficiency in the number required, but at the expense of computational complexity. Figure 3 shows the elemental net for the complete rail track structure, which includes the facility for twin-track third and third/fourth rail electrification. The smallest elements are located around the rail in regions of high flux density. The sleeper and ground are modelled as separate regions, since they have different electrical conductivities. The model specifies various regions, such as rails, sleepers, ground and air. The computation process evaluates the stored and dissipated energy in each of these regions after the excitation conditions have been defined. The stored and dissipated energies are then interpreted in terms of circuit resistance and inductance.

FEM TRACK MODELLING

To validate the FEM model, and to gain confidence in the accuracy of the material data used, preliminary benchmark tests were performed with simple geometries, with supporting experiments and analytical models. All the experiments, models and FEM results were obtained with a constant excitation frequency of 50 Hz.

Single rail with earth return

The self impedance of a single rail with earth return is represented by z_{ii} (Figure 1). Its impedance may be determined using FEM by constraining the rail current to return via the ground and evaluating the stored and dissipated energy components in the magnetic fields. The vector potential contours of such an analysis are shown in Figure 4. The inductance and resistance are then determined from

$$L = 2E_S/I^2 \qquad (16)$$

and

$$R = P_d/I^2 \qquad (17)$$

where E_S and P_d are the total system stored energy and power loss, and I is the rail current. The rail impedance is the sum of the internal and external components. The internal component has been modelled analytically by assuming an equivalent circular magnetic conductor. This is described in references [5] and [10], which also give the results of corresponding laboratory experiments. The external component has been evaluated using the Carson-Bickford equation (5). Table 1 gives the rail reactance and resistance, and the earth-return resistance, for all the above models and measurements.

The two-rail track

The mutual impedance between two rails with earth return combines with the rail self impedances according to the rail excitation mode, as given in Equations (1) and (2). Both excitation modes were modelled by FEM, and the impedance results compared with those using the Carson-Bickford equations (5) and (6). The FEM-generated magnetic vector

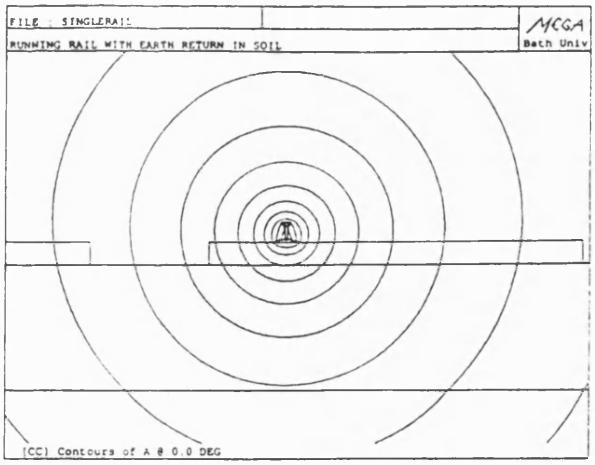

Figure 4: Single rail vector potential contour calculation by FEM

Table 1: Single-rail impedance at 50 Hz

Rail type		FEM	Bickford theory (z_{ii} ext)	Lab expt (z_{ii} int)
Flat-bottom rail	Reactance (mΩ/m)	j0.395	j0.387	j0.104
	Inductance (μH/m)	1.258	1.232	0.33
	Resistance (mΩ/m)	0.403	0.05	0.09
	Earth-return resistance (mΩ/m)	112.2	-	-
Power rail	Reactance (mΩ/m)	j0.356	j0.400	-
	Inductance (μH/m)	1.133	1.273	-
	Resistance (mΩ/m)	0.341	0.05	-
	Earth-return resistance (mΩ/m)	112.2	-	-

potential contours for the two excitation modes are shown in Figure 5. Only the differential mode excitation can be directly checked by track experiments, since the remote ground is not accessible for common mode excitation measurements.

The differential and common mode reactances and resistances have been evaluated by FEM from the stored and dissipated system energies according to Equations (16) and (17). Table 2 gives all the FEM, experimental and analytic theoretical results for both differential-mode and common-mode excitation.

The three-rail track

Analysis of a three-rail track is necessary to evaluate harmonic propagation effects in a DC-electrified railway.

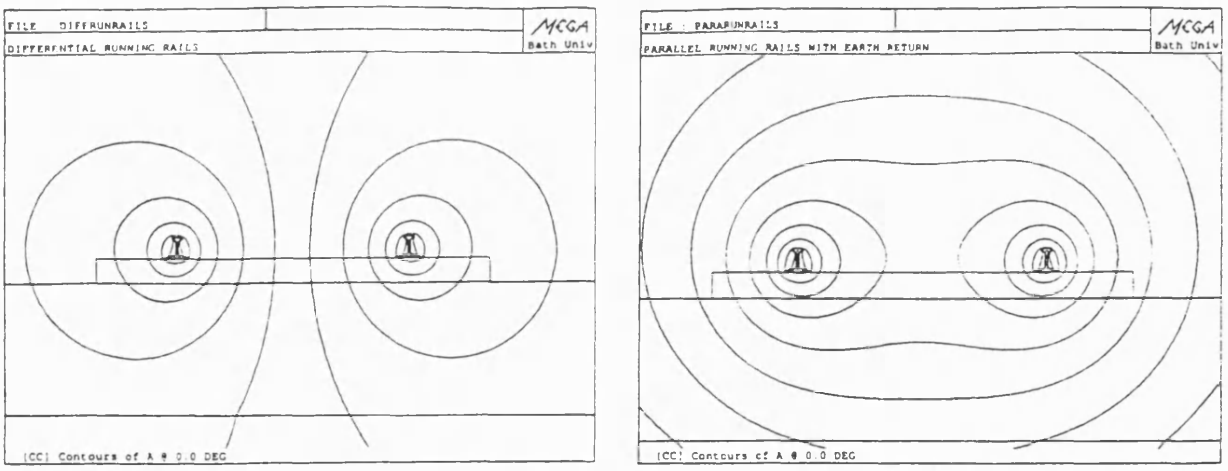

Figure 5: Single track vector potential contour calculation by FEM

Table 2: Single-track impedance at 50 Hz

Configur-ation		DIFFERENTIAL MODE			COMMON MODE	
		FEM	Bickford theory	Track expt.	FEM	Bickford theory
Both	Reactance (mΩ/m)	j0.615	j0.074	j0.889	j0.246	j1.47
running	Inductance (μH/m)	1.96	0.236	2.83	0.784	4.67
rails	Resistance (mΩ/m)	0.184	0	0.80	0.253	0.196
	Earth-return resistance (mΩ/m)	-	-	-	128.0	-
Power	Reactance (mΩ/m)	j0.414	j0.037	j0.611	-	j1.539
rail & near	Inductance (μH/m)	1.32	0.118	1.95	-	4.90
running	Resistance (mΩ/m)	0.160	0	1.589	-	0.196
rail	Earth-return resistance (mΩ/m)	-	-	-	-	-
Power	Reactance (mΩ/m)	j0.617	j0.089	j1.05	-	j1.49
rail & far	Inductance (μH/m)	1.96	0.283	3.342	-	4.74
running	Resistance (mΩ/m)	0.159	0	1.89	-	0.196
rail	Earth-return resistance (mΩ/m)	-	-	-	-	-

Usually the power rail is located close to one of the running rails, with power current returning via the combination of the running rais in parallel. The vector potential contours for such a case is shown in Figure 6. The FEM model result, obtained from Equations (16) and (17) using the single-conductor excitation current, and the experimentally measured circuit resistance and inductance are both given in Table 3.

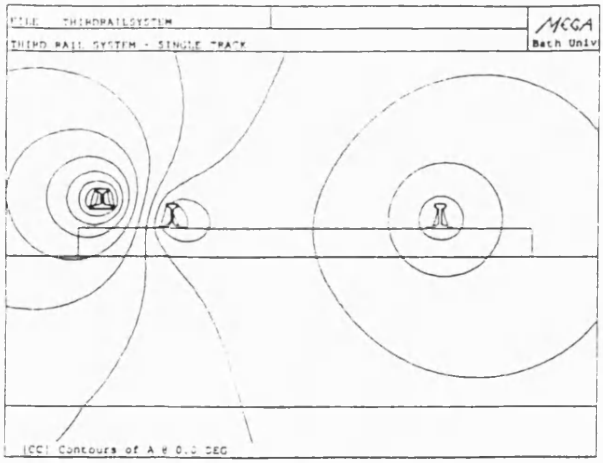

Figure 6: Three-rail track vector potential contour calculation by FEM

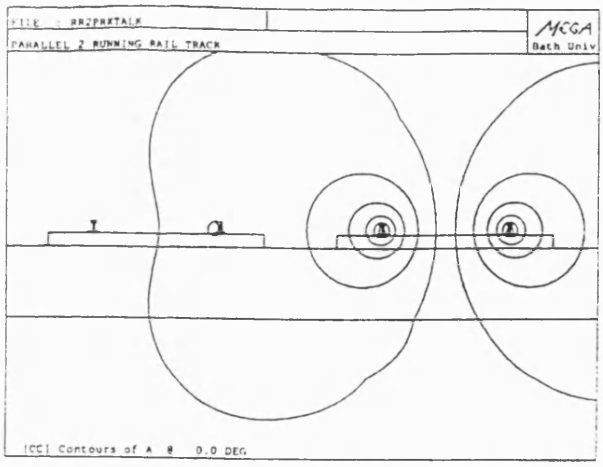

Figure 7: Crosstalk to adjacent track from signalling rail currents

Table 3: Three-rail track impedance at 50 Hz (power rail with running rails in parallel)

	FEM	Track experiment
Reactance (mΩ/m)	j0.340	j0.546
Inductance (μH/m)	1.08	1.74
Resistance (mΩ/m)	0.118	1.71

CROSSTALK BETWEEN PARALLEL TRACKS

Due to the variability of rail and ground material data, it is difficult to create accurate analytical models of complex track configurations. Using FEM, once the mesh has been set up, and the material data specified, the geometry may be altered easily to simulate different track configurations. Two crosstalk effects were investigated, to simulate the magnetic interference on a track circuit from parallel track signalling currents, and from traction currents.

Crosstalk from signalling current

The model of signalling current crosstalk treats one running rail loop as the excitation, with the other as the receiver. Figure 7 shows the contours of vector potential generated by the FEM package in such a model. The FEM results have been obtained for three excitation conditions:

- no restriction on receiver track currents
- receiver track rail currents forced to be equal and opposite
- receiver track rail currents forced to be zero.

These conditions correspond to infinite length track, and short circuit & open circuit operation respectively. The FEM and experimental results are given in Table 4, together with a theoretical value calculated from Faraday's law and ignoring the effect of the finite ground conductivity.

Table 4: Crosstalk between parallel tracks at 50 Hz from signalling currents

FEM: Floating rails	Inter-rail voltage (μV per A excitation current)	5.06 + j2.71
	Near rail current transfer (mA per A excitation current)	68 + j17
	Far rail current transfer (mA per A excitation current)	27 + j1.7
FEM: Equal rail currents	Receiver track current (mA per A excitation current)	20.1 - j7.5
FEM: Zero rail currents	Receiver track voltage (μV per A excitation current)	12.6 + j0.36
Experiment	Short-circuit current (mA per A excitation current)	3.6 - j6.1
	Open-circuit voltage (mV per A excitation current)	7.68 - j8.15
Theory	Receiver track induced voltage (μV per A excitation current)	13.8

Crosstalk from traction current

When the excitation is from traction current flowing in a circuit comprising a third rail with return through the parallel combination of the running rails, the inter-rail voltages and rail currents appearing in the receiver track differ from the previous case. The contours of vector potential for the three-rail excitation case are displayed in Figure 8, with all the results in Table 5.

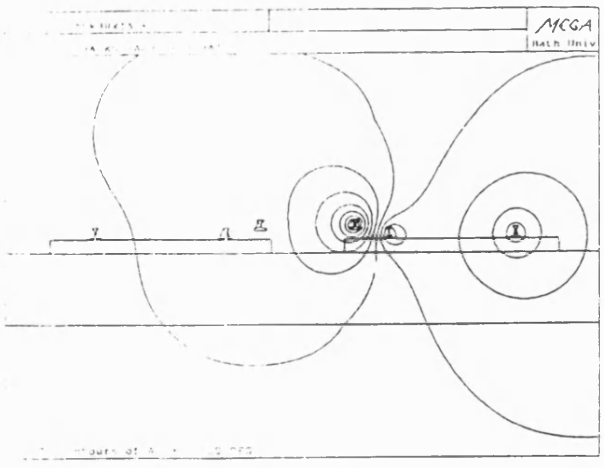

Figure 8: Crosstalk to adjacent track from traction currents

Table 5. Crosstalk between parallel tracks at 50 Hz from traction currents

FEM: Floating rails	Inter-rail voltage (μV per A excitation current)	1.76 - j2.07
	Near rail current transfer (mA per A excitation current)	23.0 - j7.0
	Far rail current transfer (mA per A excitation current)	7.0 - j4.0
	Power rail current transfer (mA per A excitation current)	66.0 + j17.0
FEM: Equal rail currents	Receiver track current: with power rail floating (mA per A excitation current)	7.3 - j1.6
	Receiver track current: with zero power rail current (mA per A excitation current)	17.7 - j5.4
FEM: Zero rail currents	Receiver track voltage (μV per A excitation current)	10.9 - j0.19
Experiment	Short-circuit current (mA per A excitation current)	5.2 - j8.4
	Open-circuit voltage (mV per A excitation current)	9.1 - j 8.8
Theory	Receiver track induced voltage (μV per A excitation current)	15.5

DISCUSSION

General considerations

Most of the results in Tables 1-5 demonstrate agreement between the FEM results, analytical models based on the Carson-Bickford equations, and laboratory and track experiments to within an order of magnitude. The deviations are due to a number of factors listed below.

Magnitude of impedances - The self and mutual rail impedance values are extremely small in magnitude and are strongly affected by changes in ground material properties. The ground conductivity is particularly significant, and varies with depth in a manner dependent on local geology as well as the environment. Thus errors will accrue unless the conductivity is measured at the same time as the track impedance experiments are performed.

Rail joints - The experimental test track used for the practical measurements consisted of four, 9 m rail lengths connected together with copper cable, so poor cable joint impedances could represent a significant fraction of the measured impedance. The presence of joint resistance errors is consistent with the larger experimental values compared with both theoretical model and FEM results.

Rail permeability - The FEM results which depend on internal self impedance are sensitive to the magnitude of rail permeability, which is in general a function of frequency as well as current magnitude [5]. For example, at 50 Hz, a rail permeability change from 350 mH/m to 100 mH/m results in a 50% reduction in rail resistance. However, for low power frequency currents, the variation in the permeability magnitude is small. In general, the measured inductance is not seriously affected by permeability variation since, apart from the case of rail self inductance with earth return, it is mainly determined by the circuit geometry.

Rail shape - The irregular rail shape may also explain the disagreement between FEM, experiment and theory in some individual results, for example those of Table 1. The magnetic flux distortion around the rail surface causes the vector potential contours to cut the rail boundary at the top and bottom of the rail web, as seen in Figure 4, and this produces inaccuracies in the computed result. The elemental net within the rail cross section is coarse because of computational restrictions, and this also produces inaccuracies. A further source of error is that the theoretical model assumes a circular equivalent conductor, rather than the special rail shape.

It is believed that further refinement of the modelling process, and the use of more accurate material data, would enhance the achievable accuracy.

Benchmark tests

Considering the above comments, some detailed observations may be drawn about specific results. In Table 1, the Carson-Bickford equations model the external impedance only, with the assumptions of infinite rail permeability and conductivity. If the Carson-Bickford result is added to the laboratory measured value of internal rail reactance, then agreement, to within 20%, is obtained with the FEM result. A similar correction could also be made for the internal

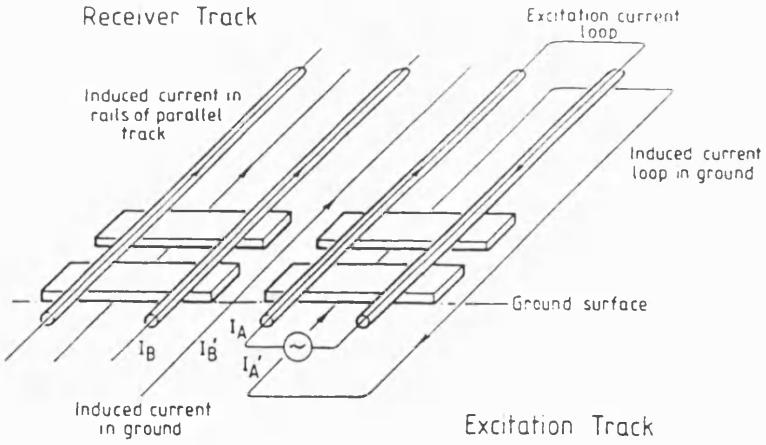

Figure 9: Physical model of rail track crosstalk current loops

reactances in the other benchmark tests, recorded in Tables 2 and 3. However, in those results, the significance of the internal inductance is less due to the relatively large circuit inductance owing to the wide rail spacing.

In Table 2, the FEM results for the common and differential mode inductances indicate that the size of the current loop for the common mode case will be less than that for the differential mode case. Hence the rail current images must lie close to the ground surface, at a depth less than the inter-rail spacing.

Crosstalk

With the receiver track rails unrestricted in length, the physical model predicts induced currents in each rail, with associated eddy currents in the ground, as shown in the simplified representation of Figure 9. There is an image conductor for each of the four rails, located beneath the ground at a distance determined by the ground conductivity, permeability and the signal frequency. The primary eddy current loop is induced from the transmitter track current. Further coupling will exist between all the ground current components.

For the case of crosstalk from signalling currents, experimental validation of the FEM results was obtained for the short-circuit current condition to within an order of magnitude (Table 4), the difference in the in-phase parts, as before, probably being due to significant rail joint resistance. Confirmation of the open-circuit voltage result by experiment was more difficult to achieve, due to the extremely low voltages involved. However, an approximate validation, to within 10%, was obtained by calculating the voltage between two infinite coils spaced at the track gauge using Faraday's law, and assuming an insulating earth. The experimental measurement of open-circuit voltage given in Table 4 corresponds to the case when both ends of the receiver track were left open circuit, it being confirmed that when one track end was closed, the detected open-circuit voltage reduced towards the value predicted by the FEM model.

The condition of crosstalk from traction currents also shows close correspondence between FEM and experiment for the short-circuit current condition (Table 5). However, the screening effect from the receiver track power rail must be considered in interpreting the results. The FEM model shows that when the power rail current is allowed to acquire its floating value (i.e. when the rail is of infinite length), the short-circuit current magnitude in the running rails is reduced. The experimental measurement agrees most closely with the FEM result where the receiver track power rail current is forced to be zero. The open-circuit voltages obtained by FEM, experiment and theory are also shown in Table 5, and similar considerations apply to those given for the signalling current crosstalk condition.

CONCLUSIONS

The use of FEM to determine rail track impedance has been demonstrated. Various physical layouts and excitation modes have been modelled, and a validation procedure based on the Carson-Bickford equations and practical measurement of rail impedance demonstrated. Preliminary results for crosstalk at 50 Hz between adjacent tracks of a two-track railway have been presented, for both signalling current and power current excitation.

ACKNOWLEDGEMENTS

This research was financed by the UK Science and Engineering Research Council under research grant #GR/E/58816. The authors are grateful to Professor David Rodger at the University of Bath for use of the FEM software (MEGA), and to him and Dr Paul Leonard for practical advice concerning its use.

REFERENCES

[1] P. R. G. Hopkins, "Crosstalk between track circuits on adjacent roads of a railway system," M.Phil Thesis, Brunel University, London UK, 1981.

[2] B. Mellitt, J. Allan and J. A. Taufiq, "Electromagnetic compatibility in DC railways," 6th International Conference on Electromagnetic Compatibility, York UK, 12-15 September 1988 (London UK: IERE 1988), pp. 347-354.

[3] J. F. Eastham and D. Rodger, "Differential methods, finite elements and applications," in: Industrial Applications of Electromagnetic Computer Codes (Editors - Y. R. Crutzen, G. Molinari and G. Rubinacci). Dordrecht: Kluwer 1990.

[4] A. B. J. Reece, "Electrical machines and electro-mechanics - computer aids to design," Power Engineering Journal, November 1988, v. 2, n. 6, pp. 315-321.

[5] R. J. Hill and D. C. Carpenter, "Modelling of nonlinear rail impedance in AC traction power systems," 4th International Conference on Harmonics in Power Systems: ICHPS IV, Budapest, 4-6 October 1990, pp. 268-274.

[6] R. J. Hill, D. C. Carpenter and T. Tasar, "Railway track admittance, earth-leakage effects and track circuit operation," 1989 IEEE/ASME Railroad Conference, Philadelphia, 25-27 April 1989 (New York: IEEE 1989), pp. 55-62.

[7] D. C. Carpenter and R. J. Hill, "Rail impedance modelling for DC-fed railway traction simulation," IASTED International Symposium on Applied Modelling and Simulation, Lugano, Switzerland, 18-21 June 1990 (Anaheim CA: IASTED 1990), pp. 105-108.

[8] J. P. Bickford, N. Mullineux and J. R. Reed. Computation of Power System Transients. London UK: Peter Peregrinus 1976.

[9] R. P. Silvester and R. L. Ferrari. Finite Elements for Electrical Engineers. Cambridge UK: Cambridge University Press 1983.

[10] D. C. Carpenter and R. J. Hill, "The effect of magnetic saturation, hysteresis and eddy currents on rail track impedance," 1989 IEEE/ASME Railroad Conference, Philadelphia, 25-27 April 1989 (New York: IEEE 1989), pp. 73-79.

USING THE CIRCUIT SIMULATION PACKAGE EMTDC FOR AUDIO FREQUENCY TRACK CIRCUIT DESIGN

R J Hill [1], M L Berova [1],
D C Carpenter [1] and G J W Meecham [2].

1 School of Electrical Engineering, University of Bath, Claverton Down. Bath, BA2 7AY, UK.

2 Westinghouse Brake and Signal Ltd., Signal Division, PO Box 79, Pew Hill, Chippenham, SN15 1JD.

ABSTRACT

A method is proposed for the optimal design of audio frequency track circuits. After the approximate area of existence of track circuits is defined by formal mathematical models, simulation, using a commercial circuit simulation package, is used for the final design. Simulation results are presented for the train shunt and broken rail modes of operation. The detailed behaviour in the tuned termination area is also shown.

1 INTRODUCTION

Many automatic train control (ATC) systems use audio frequency (AF) track circuits for the automatic train protection (ATP) functions of train location detection and track-to-train data transmission of safety speed codes. The advantages of AF track circuits include the elimination of insulating rail blockjoints, enhanced data transmission capability and with the addition of suitable signal processing, immunity from electromagnetic interference (EMI). The problem addressed in this paper is the achievement of optimal AF track circuit design by computer methods using a commercially available electric circuit simulation package.

The design of AF track circuits has in the past largely been achieved by continuous development of existing equipment using ad-hoc methods based on previous engineering experience. A considerable pool of practical knowledge exists on joined DC and AC power frequency track circuits, derived from their use over many years and summarised in a number of publications [1, 2]. However, compared with their jointed counterparts, AF track circuits are complex systems. The attenuation along the track circuit is sensitive to ground conditions and they are terminated using tuned areas. Detailed knowledge of the properties of the rail track-to-ground system and of the rails themselves is thus necessary for design. A number of solutions to the AF track circuit design problem have been proposed, reviewed in references [3, 4], but all are sub-optimal in that they represent acceptable solutions for particular combinations of operational conditions, such as length, frequency and environmental variations. Attempts to formalise the design procedures and produce a universal AF track circuit have been made, based on gaining a thorough understanding through analysis [5]. Although a large quantity of data has been collected, the problem of optimal design, however, is still unsolved.

In this paper, the basic problem of AF track circuit design is stated and the use of a circuit simulation package (EMTDC) to assist in the design process is described. the design procedure starts with the method of linear programming to define the area of existence, with circuit simulation used for final optimisation. The simulation technique eliminates much of the practical site testing otherwise required in prototype designs.

An important aspect of the model is the correct characterisation of the track-to-ground behaviour. Example simulations are presented for train position detection along the track circuit, broken rail detection and for detailed operation in the tuned termination area.

2 TRACK CIRCUIT DESIGN

The primary function if a track circuit is that of fail-safe, train position sensing. Information is generated about the presence of a vehicle or vehicular string (train) on a particular track section within the complete range of track circuit operating conditions. Other functions of track circuits are train-to-train data transmission for cab signalling and automatic train control (ATC) and broken rail detection.

The track circuit functions within a particular environment. This includes the complete set of input effects which can affect the track circuit performance. These cover variations in the external environment (for example, temperature, humidity and geological conditions) and the effects of EMI.

The track circuit design procedure may be divided into two parts. The first task is to establish the area of existence of the track circuit to achieve fail-safe train detection and broken rail detection. The parameters to be considered in the area of existence include length, power and cost. A necessary concomitant is that a quantative requirement of fail-safe operation must be established. The second task is to define a particular location within the area of existence where the track circuit has the optimal design according to the previously chosen criteria of maximum operating length, minimum power consumption or minimum cost. This can be achieved by creating and maximising a coefficient of performance for the track circuit incorporating all the chosen criteria.

3 TRACK CIRCUIT DESIGN AND OPTIMISATION METHODS

The AF jointless track circuit has been developed from the jointed DC and AC power frequency track circuits which have been in use for many years. In addition to raising the carrier frequency to audio levels, signal modulation and coding have been introduced to provide immunity from EMI and for track-to-train data transmission using train-mounted cab signal receivers. The uses of mathematical analysis and electric circuit simulation for AF track circuit design may be regarded as complementary rather than alternative, as shown by the following optimal design procedure.

3.1. Analytical mathematical method

Any rigorous design of electrical equipment should follow a design procedure that yields unique optimal results for a given specification. A formal description of the equipment operation is required so that the design problem may be expressed and solved as a series of mathematical equations. In formal mathematical language, this may be presented as a nonlinear programming problem of the form.

Minimise:

$$F(X),\ x = (x_1, x_2, \ldots x_n)$$

subject to:

$$H_j(x) = (i = 1,2,..m)$$
$$G_j(x) < 0 (j=1,2,.....p)$$

F(x) is a function of optimal design according to the chosen criteria, H(x) = 0 and G(x) < 0 are functional constraints which define the alogorithm of operation and x includes additional conditions. The method has been widely applied to engineering system design, for example for power transformers [6], and requires both the function and the criteria of optimisation to be expressed in terms of the general design parameters.

pplied to track circuit design, (x) and G(x) define the area of xistence of track circuits and x rovides additional information, or example that the length and ermination impedance are ositive. The basic relations from he function of optimisation in the ase of track circuits are the athematical expressions of track ircuit algorithm, which is the rack circuit transfer function etween transmitter and receiver or the various operational modes such as train detection and broken ail detection).

This analytical method of track circuit design and synthesis has been applied and fully developed for both AC power frequency and DC track circuits [2]. The principal ideas can be extended to the design of AF track circuits provided the analytical expressions of the track circuit transfer function are known. The applicability of the method has been demonstrated for AF track circuits with a current receiver [7].

The analytical method is a fundamental technique that can be very effective. Its main disadvantage is that the complexity of the analytical expressions increases for sophisticated systems. However, the use of more powerful computational methods can obviate this difficulty.

3.2. Electrical circuit simulation

In simulation, a physical model of the system is devised, expressed as an equivalent electrical circuit and some initial approximate values are assigned to the circuit components. A computer programme then solves the circuit using one of the classical solution techniques. Both steady state and transient solutions may be obtained, with post-processing activities giving additional circuit properties such as harmonic performance. Usually, many simulations must be performed to obtain the particular set of parameters which ensure the best system performance.

Applied to AF track circuit design, the problem is to create an accurate physical model, taking account of both discrete components in the terminations and distributed components in the track and ground. A significant difficulty is in obtaining accurate data for the distributed parts of the model.

3.3. Comparison and necessary models

The effectiveness of each of the above methods of track circuit design depends on the track circuit model on which it operates. The analytical model, if developed on the basis of versatility, is a powerful tool for the analysis and solution of general problems of AF track circuit design. For complex problems, such as the prediction of parallel track crosstalk and traction generated EMI, it is likely to be too complicated in its use. For such cases, a simulation model of an equivalent physical representation of the track to ground system with data based on experiment and solution by computer may be appropriate. The simulation method is flexible and straightforward to implement. It is most convenient to use when the areas of existence and a crude optimisation have already been achieved by the analytical method. This implies that simulation should mainly be used to improve an existing design.

4 MODELLING AF TRACK CIRCUITS WITH A CIRCUIT SIMULATION PACKAGE

Physical systems must be represented as equivalent electrical components for their solution in circuit simulation packages. The exact representation depends on the particular package used, but some general principles will apply irrespective of the particular solution technique employed. The following description is given in general terms, with additional details as necessary applied to the Westinghouse FS2000 AF jointless track circuit and the circuit simulation package EMTDC.

4.1. Main features of the package EMTDC

EMTDC is a discrete vent simulation package, originally intended for power system modelling. It functions in the time domain by modelling the dynamic operation of electric circuits with a fixed number of nodes. It is possible to make dynamic changes in the circuit topology through the insertion of switches in the model. The solution proceeds by creating nodal voltage equations to build up circuit admittance matrix. Special subroutines are available for semiconductors and nonlinear functions and user-written dynamic and output subroutines may be provided. Access to the source code is available.

.2 Rail track modelling

he package allows both discrete mponent and disturbed circuits to solved. This means that the il track section of the track rcuit may be modelled by stributed parameter transmission nes or discrete component lumped ementary circuits in cascade. e latter requires choice of the mped section length. The optimum del choice depends on the plication and requirements of the ysical mode. For instance, where balanced two-wire line is fficient, for example short rail gths within the tuned mination areas, a lumped mponent model will suffice. ever, on long open line sections h parallel signal and traction er cables, the transmission line roach must be used for putational efficiency. These ernative rail line models are ustration in Figure 1, with the ual trial data used shown in le 1.

value of using a transmission model of the track becomes rent when the physical nature the transmission system is ined. Even for a single track no electrification or parallel al or communications cables, concept of a two-conductor transmission line over a conductive earth surface must be invoked. This is because asymmetries in the line, such as those caused by broken rails, will create imbalance, so necessitating the consideration of the individual transmission modes [8]. It is straightforward to extend the model to a general rail traction and signalling network using the concept of a multiconductor transmission line over a conductive earth. The definition and determination of the model equivalent components, however, is a non-trivial task, for which some experimentation is usually necessary.

4.3 Practical details of using EMTDC

The data required by the EMTDC package, for rail systems modelling, is structured to suit modal, time domain operation. Key information includes power frequency, signalling frequency, ground mode shaping time constant and metallic mode steep front shaping factor. For each transmission line mode, the package also requires travelling time, characteristic impedance, resistance per unit track length at both power and signalling frequencies and the row of the current modal transformation matrix. In the case of an existing track, most of the data can be determined from measurement. Where the simulation is to be used ahead of the construction of the railway, for example in tendering or feasibility studies, EMTDC provides a utility programme for modal evaluation of the transmission line (EMTTL). The example transmission line data given in Table 1 was evaluated using EMTTL according to the basic transmission line model of Figure 1. The data in the table is based on a track gauge of 1.435 m and flat-bottom rail running rail. The evaluation of the material properties of the rail as well as the information needed for correct ballast and soil representation may be found in references [9 - 11].

The number of line sections is limited by the array dimensioning. Although the number of line sections may be increased from the default value of ten, computer memory often provides a practical limitation. Relating to this is the consideration of line section length, especially where short and long lengths are to be used in the same circuit. A conflict arises when very short line lengths occur in the same model as relatively long lengths, for example when a tuned area is modelled in conjunction with a 1 km long track circuit, when the travelling time for the two line sections will be very different. The restriction then exists that the time step value of the simulation must be small enough to correctly model the short section. This implies that the long section will have many time steps associated with it. Although the maximum (default) of 500 steps per line section can be increased, again computer hardware limitations may impose a practical limit. An alternative solution is to use discrete components to model the line section. However, when multiple lines are to be simulated, this can become a circuit analysis problem.

A practical advantage of using transmission lines is that they provide an extremely simple interface between subsystems of the model. As a subsystem defines the nodes associated with a particular admittance matrix, if the number of nodes in a subsystem is small and the nodes are highly interconnected, the computation time is reduced since small and dense, rather than large and sparse, matrices are formed. In addition, when switching occurs, as in the case of the simulation of train axle movement, the matrix which contains the nodes of the switch has to be inverted (once for each switch operation). Efficient computation requires that such a matrix is small and this is achieved by dividing such modal areas into subsystems.

4.4 Track circuit equipment modelling

Generally, the track circuit transmitter and receiver may be modelled for incorporation in the package using a discrete component representation. Normally, only the signal power output stage needs to be taken into consideration. Some components, for example the track feed transformer, may have to be laboratory tested to reveal the linearised equivalent components necessary for the model. Where cabling parallels the track, coupling and screening coefficients have to be evaluated and incorporated in the model. Figure 2 shows the discrete component models of the track transmitter/receiver, together with the sections of the track circuit to which they are connected.

4.5 Modelling the track circuit operational modes

Once the simulation is set up, various modes of operation may be modelled, including the train shunt mode and the broken rail mode. The modelling technique is to incorporate switches at various locations in the complete circuit model. In addition to the considerations of section 4.3, the choice between transmission line and lumped circuit model for each application must also reflect the ease with which train movement and broken rail simulation can be carried out. Figure 3 shows the facilities necessary for the simulation of the train shunt operation mode, the broken rail mode and for train shunting over the tuned termination area of the track circuit.

5 TRACK CIRCUIT DESIGN BY EMTDC SIMULATION

5.1 Running the simulation programme

The process of designing track circuits by the method of direct simulation requires repeated simulation of the circuit performance for a number of static or dynamically changing operating

conditions, and for varying values of the design parameters. Many simulations are therefore normally required to check the correct functioning of a track circuit under design with all possible operating conditions and to find the optimal design according to the given criteria.

To carry out the design, a procedure must be established for determining the order of simulations. The objective is to ensure that the solution obtained will be optimal in a mathematical sense and also obtained using a minimum of computer resources (computation time and memory). As the area in which the solution can be found is initially large and the number of simulations required to solve the problem is very high, the procedure must be incorporated within a control programme. This programme (the Track Circuit Design Programme, TCDP) performs two main tasks:

It controls the search for the solution through the specified area by specifying the input conditions for every single simulation

It stores and processes the output data from all simulations in order to determine which set of design parameters is a solution of the problem and which is the optimum solution.

In general, TCDP solves the nonlinear programming problem described in section 3.1. The programme itself is not described here and the simulation results presented below are for only one simple set of simulations carried out within TCDP.

5.2 Simulation results

Simulations have been performed to model the operation of a Westinghouse FS2000 AF jointless track circuit with a carrier frequency of 4.01 kHz. The initial simulations used a single track model with no parallel electrification of signalling/communications cables. Only the carrier frequency was considered in the signal transmitter. The simulation results are presented in Figures 4-6. These are non optimal in the sense that they were obtained with nominal track and track circuit data.

The train shunt operation mode result of Figure 4 shows the receiver voltage gain as the train proceeds along the section. The broken rail mode of operation is shown in Figure 5, with the broken rail position along the track circuit as the second variable. The track circuit receiver voltage gain is an order of magnitude lower than that in the train shunt mode because of the low conduction path provided by the track admittance.

Operational conditions in the tuned termination area are critical for the design of the overlap region between adjacent track circuits. Simulation results for the train shunt mode in this case are shown in Figure 6. The results indicate that the exact track circuit resolution length is determined by the equivalent component values in the double circuit bond area.

6 CONCLUSIONS

- A formal design procedure for AF track circuits has been proposed consisting of initial determination of the area of existence using linear programming, followed by optimal design with a circuit simulation package.

- In a practical design procedure, an additional user-defined shell would be required which calls the circuit simulation programme as a subroutine. This routine should take into account the circuit topology which changes with train and/or broken rail position. Additional data manipulation is also necessary to recognise optimality in the solution.

- The rail track should be represented in the circuit simulation by a multiconductor line over a weakly conducting earth place, in order to achieve a realistic model of asymmetric conditions in the running rails. A discrete component representation is adequate for the tuned areas.

- The representation of moving train shunts and variable broken rail positions can be achieved by closing switches in the model at discrete time intervals during run time.

- The example simulations presented include the shunt and broken rail modes, with further details of the shunt mode operation when the train shunt is within the tuned termination area.

7 ACKNOWLEDGEMENT

This work was performed with financial aid from the UK Science and Engineering Research Council under research grant GR/E/58816. Full acknowledgement is given to Westinghouse Signals, Chippenham, UK for the use of AF track circuit design and to the Manitoba HVDC Research Centre (University of Manitoba), Winnipeg, Canada for the use of the EMTDC package.

8 REFERENCES

[1] Gall, D. C., 1933, Railway Track Circuits. London: Pitman

[2] Brileev, A. A., Kravtzov, J. A. and Shishliakov, A. V., 1978, Theory Design and Operation of Track Circuits. Moscow: Transport Publishing Co.

[3] Hill, R. J., 1985, Train position detection and track-train data transmission using audio frequency track circuits, Journal of Electrical and Electronics Engineering, Australia, v. 5, n. 4, pp. 267-77.

[4] Brown, C., 1984-5, A review of jointless track circuits, Proceedings of Institution of Railway Signal Engineers, pp. 111-28.

[5] Kalra, P., 1973. Track circuits for modern rapid transit systems, ASME Intersociety Conference of Transportation, Denver CO, 23-27 September 1973 (New York: ASME 1973), paper 73-ICT-62, 8pp.

[6] Poloujadoff, M. and Findlay, R. D., 1986, Procedure for illustrating the effect of variation of parameters on optimal transformer design, IEEE Transactions on Power Systems, v. PWRS-1, n. 4, pp. 202-206.

[7] Iancu, O. D. and Giuhat, R., 1976, Non-insulated track circuits with direct-coupled receiver: analysis relations, method of calculation, Rail International, v. 7, n. 11, pp. 638-45.

[8] Hill, R. J., Yu S. L. and Dunn, N. J., 1989, Rail transit chopper traction interference modelling using the SPICE circuit simulation package, IEEE Transactions on Vehicular Technology, v. VT-38, n. 4, pp. 237-46.

[9] Hill, R. J. and Carpenter, D. C., 1990, Rail track modelling for signalling and electrification system simulation studies, Rail Engineering International, v. 19, n. 4.

10] Carpenter, D. C. and Hill, R. J., 1989, The effect of magnetic saturation, hysteresis and eddy currents on rail track impedance, IEEE/ASME Joint Railroad Conference, Philadelphia, 25-27 April 1989 (New York: IEEE 1989), pp 73-9.

11] Hill, R> J>, Carpenter, D. C. and Tasar, T., 1989, Railway track admittance, earth-leakage effects and track circuit operation, IEEE/ASME Joint Railroad Conference, Philadelphia, 25-27 April 1989 (New York: IEEE 1989), pp. 55-62.

Table 1: Model transmission line data for single track section with no electrification

Phases . .	2	Power frequency	50 Hz
Sending-end subsystem	3	Signal frequency	4.08 kHz
Receiving-end subsystem	4	Line section length	50 m

Mode type	Common	Differential
Sending-end node	1	2
Receiving-end node	2	4
Travelling Time us	4.85	2.16
Character impedance (z_0)	297.8	135.3
Modal resistance (R_{50}) m /m	0.131	0.033
Modal resistance ($R_{4.08k}$)m /m	2.075	1.079

IST OF FIGURES

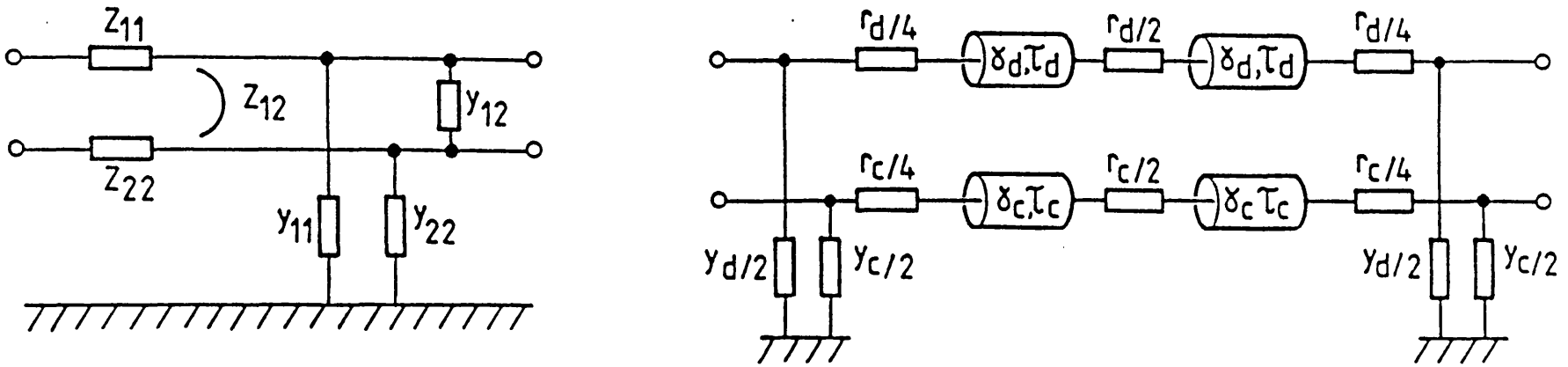

Fig.1. Track model as discrete component & transmission line representation

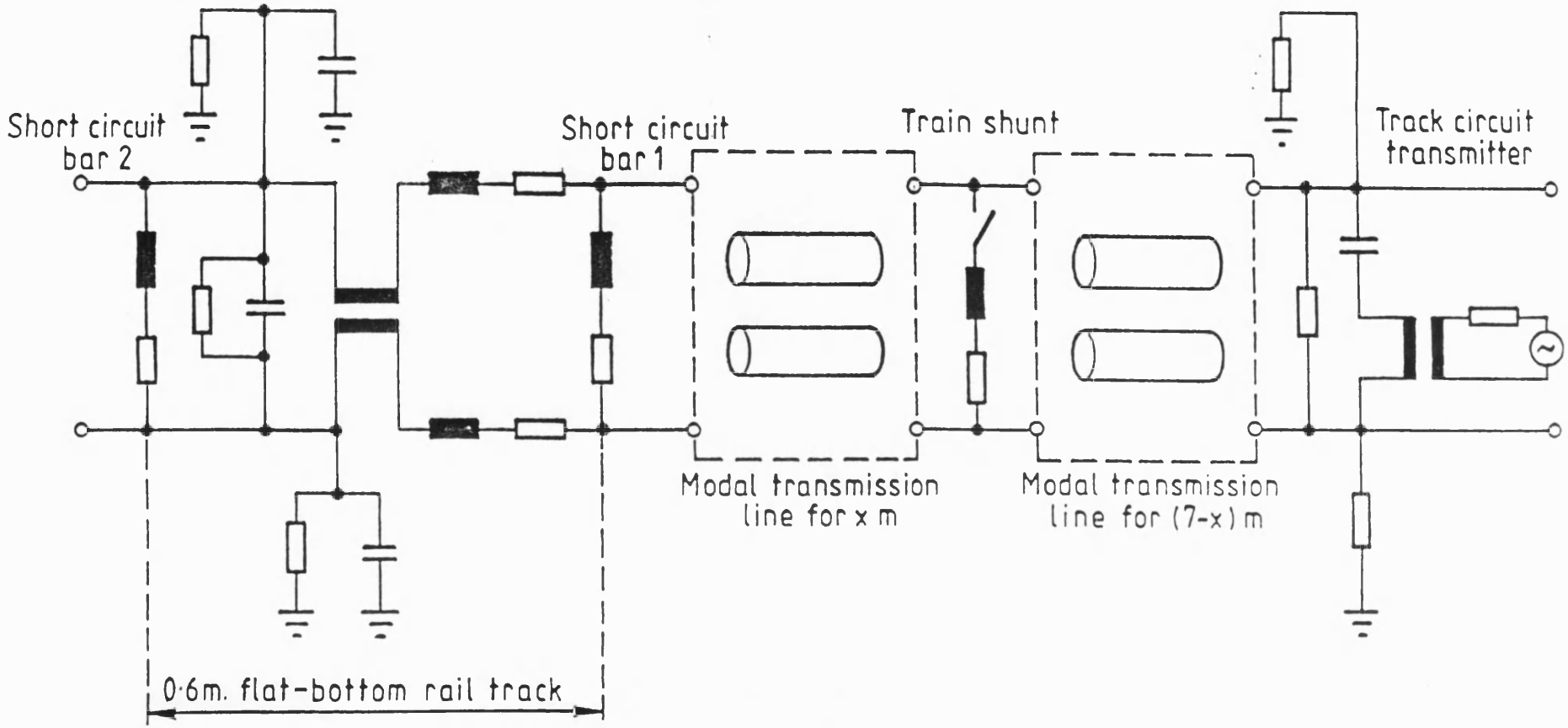

Fig. 2. Track circuit transmitter model

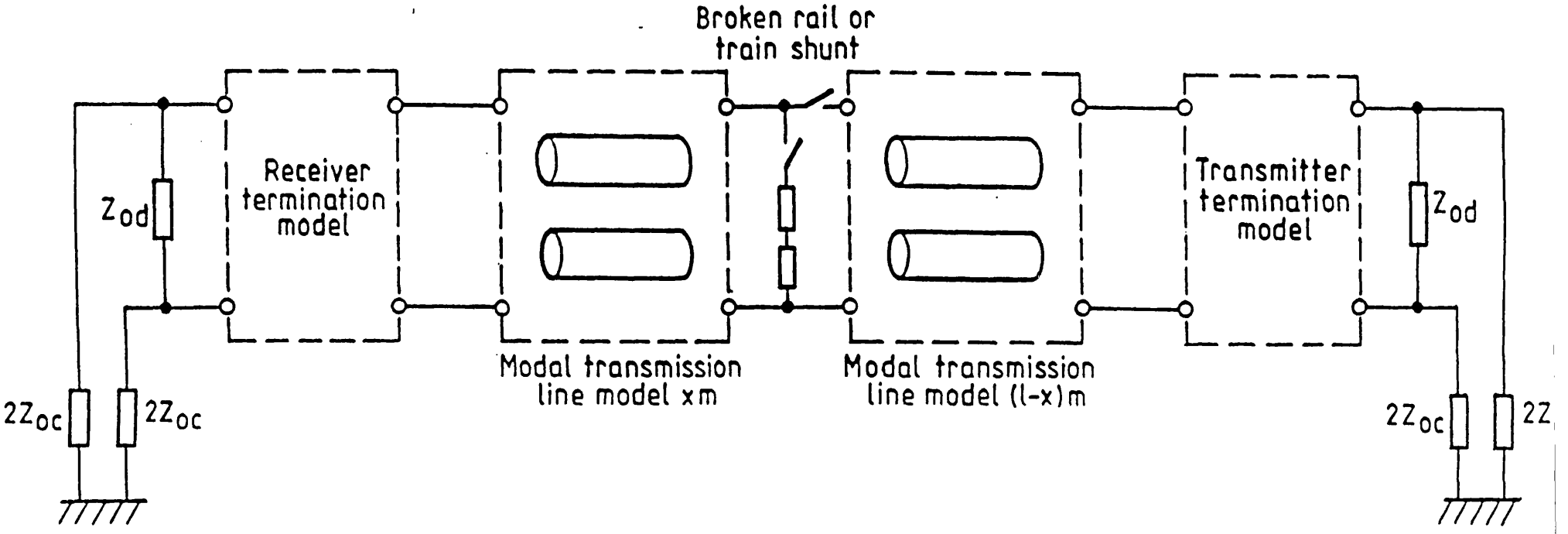

Fig. 3. Simulation circuit model

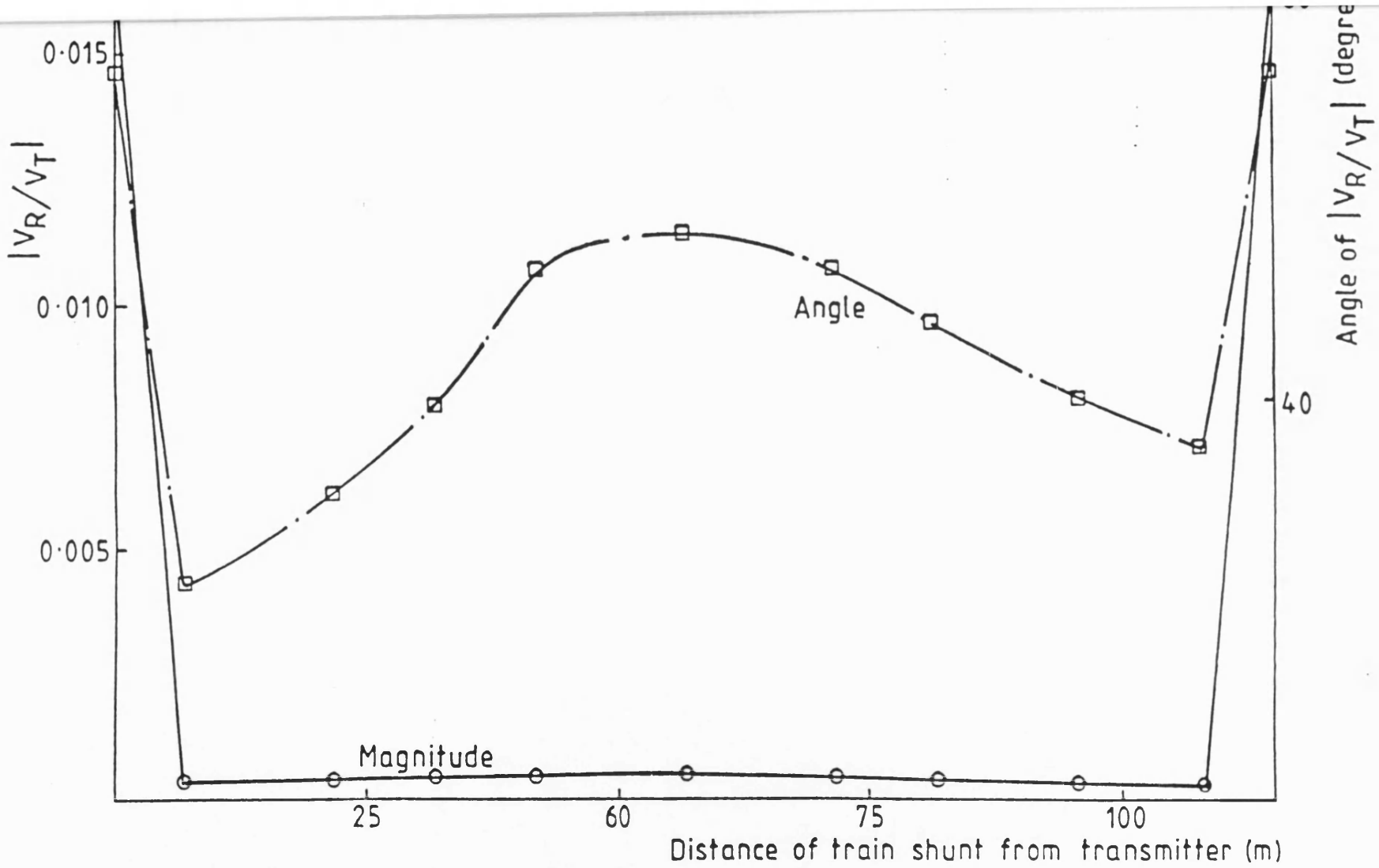

Fig. 4. Simulation of voltage transfer function for train shunt mode

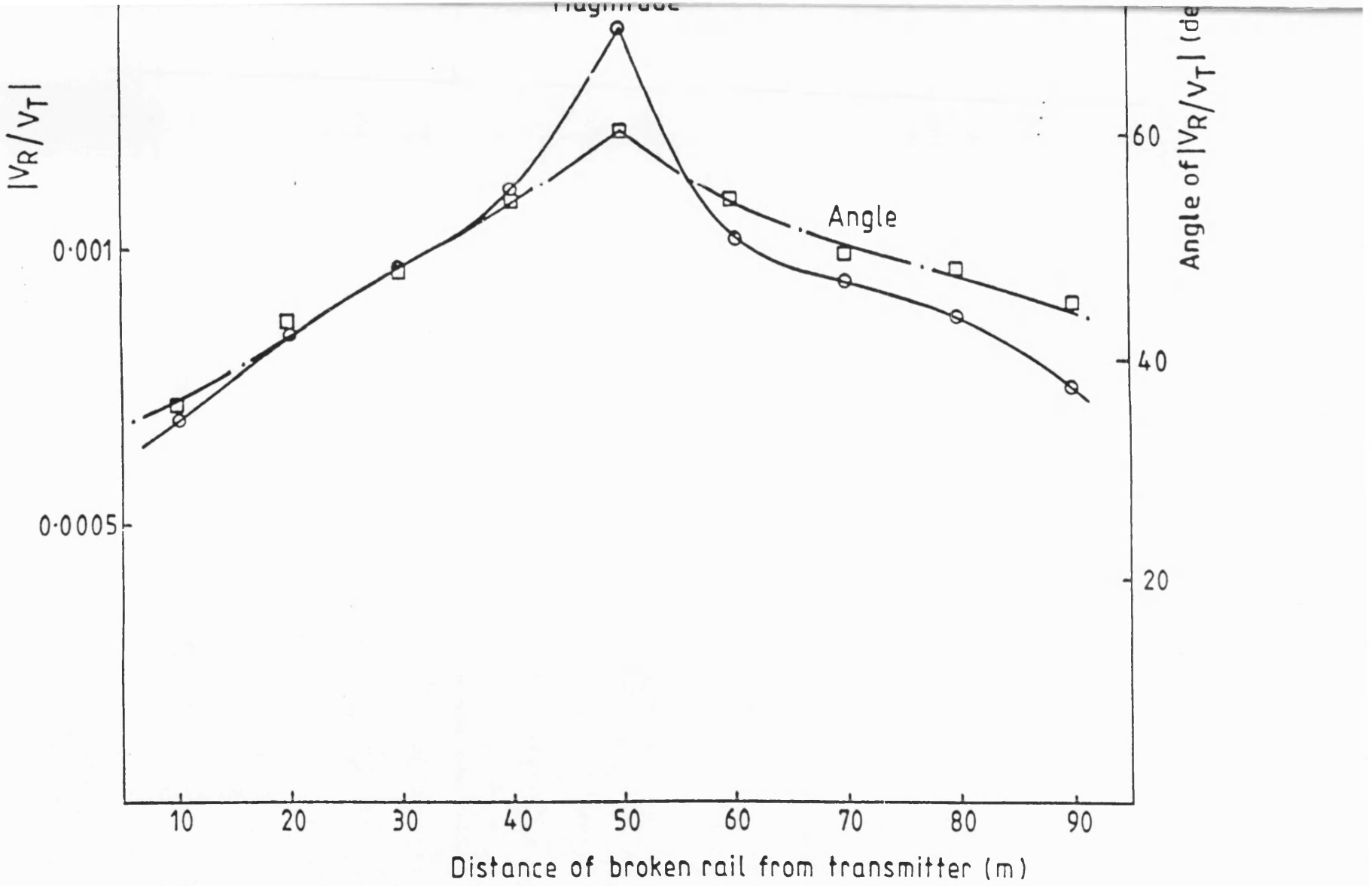

Fig.5. Simulation of voltage transfer function for broken rail mode

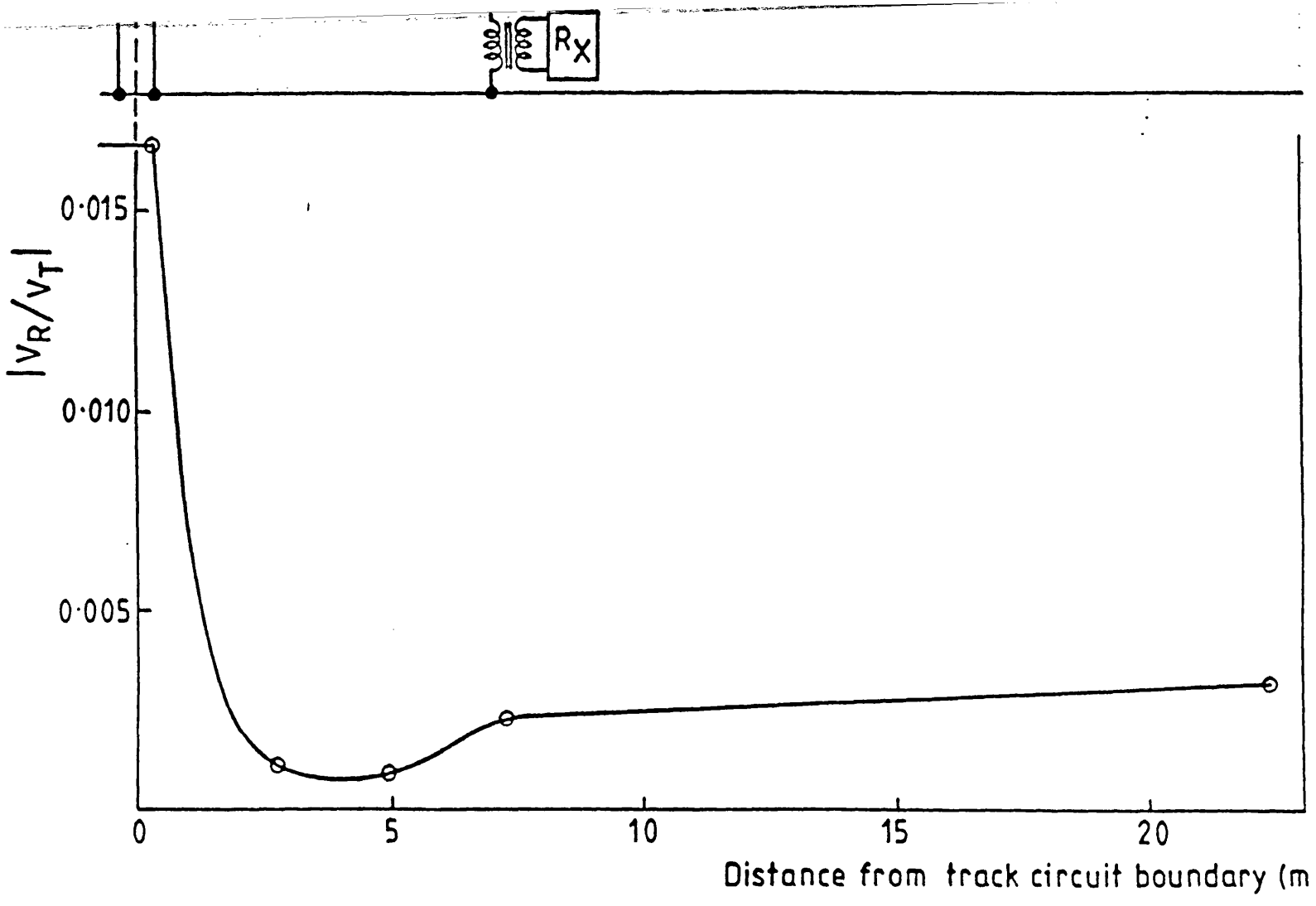

Fig. 6. Simulation of voltage transfer function for train shunt within tuned termination area

E Transactions on Power Delivery, Vol. 6, No. 4, October 1991

MODELLING OF NONLINEAR RAIL IMPEDANCE IN AC TRACTION POWER SYSTEMS

Dr R. John Hill

Mr David C. Carpenter

University of Bath, School of Electrical Engineering
Claverton Down, Bath BA2 7AY, UK

Abstract - Nonlinearity in the internal self-impedance ailroad rail can give rise to power frequency harmonics raction systems. Limiting case analytical models of rail edance, based on linear complex permeability and plete saturation, are compared with measurements for ents to 800A and frequencies to 10 kHz. The results y that for accurate representation an effective neability of the material must be defined by prior elling of the eddy current flux distribution within the iron. The usual assumption of rail internal impedance invariance with current is shown to be alistic.

INTRODUCTION

In AC-electrified railways, electric power is delivered n transformer substations via overhead catenary and rned through the running rails to electrical connections return feeder cables or autotransformers. The tion power transmission system comprises the nary, auxiliary feeder, return conductor and rail track. trically, this forms a coupled multiconductor smission line, the behaviour of which is described by a rix equation relating the phase voltages V_i to the line ents I_i, as follows:

$$\frac{d}{dx}[V_i] = [z_{ij}][I_i]. \qquad (1)$$

his equation, the coefficients of the system impedance rix are diagonal terms z_{ii}, the self-impedance of each ductor i with earth return, and off-diagonal terms z_{ij}, mutual impedance between conductors i and j with earth rn. The self-impedance terms are the sum of external internal impedances. The former are functions mainly circuit geometry, but the latter are determined by the within the rail iron. They depend on the excitation rent and frequency, and are sources of nonlinearity in power transmission path.

The elements of the track impedance matrix are uired as data for system simulation studies, the ectives of which are to model energy flow, power supply/ al interference and harmonic effects. Harmonic rents generated by rail nonlinearities can propagate k into the power system and couple with communications track signalling circuits. They can cause power supply blems such as network distortion, line resonance, and power factor deterioration, and are also important for fault condition and transient studies.

In most simulation studies reported in the literature, rail internal self-impedance is treated as an analytic function with value equal to the impedance of an equivalent circular conductor. Rail iron permeability is treated as a constant [1,2], so both resistance and inductance are assumed constant with AC current. The internal inductance reduces and the resistance rises with frequency due to flux reduction and redistribution within the iron from the skin effect. In the steady state, the external self-inductance is usually considered to dominate the internal self-inductance [2], the former being approximated with sufficient accuracy using the Carson-Pollaczek equations assuming the earth to have a finite, constant conductivity. Stanek et al [3], however, show that for transient studies, the rail internal self-impedance may be significant compared with the external component, and that the nature of fault transients indicates that knowledge of its impedance variation with current and frequency is essential for successful modelling of traction fault currents. Significant impedance change occurs from the effects of saturation and hysteresis in the rail iron, both phenomena modifying rail energy losses and reactive power flow. Holmstrom [4] has stated that rail hysteresis may give rise to intermodulation distortion in power and audio frequency track signalling systems.

The problem of the determination of rail self-impedance is concerned with the analysis of power frequency magnetic systems. The literature on this subject has concentrated on modelling saturation and hysteresis effects in electrical machines and transformers by accurate field computational techniques. These applications do not in general deal with magnetic conductors but the analytic methods can still be used with advantage. Burais [5], for example, demonstrates a technique to separate hysteresis from eddy current losses for a non-oriented material steel plate taking into account saturation. The method combines the finite element technique for space, and finite difference for time discretization. A similar problem is approached in a different way by Labridis [6] who assumes an equivalent fictitious material with relative permeability constant in time but variable in space, and related to the saturation B-H curve by a stored magnetic co-energy density. The effect of harmonic fluxes has also been evaluated numerically for transformer cores, and Hsu [7] shows that iron loss can be reduced for saturated conditions where hysteresis loss is large.

The modelling of internal impedance in an irregular-shaped ferromagnetic conductor such as railroad rail suffers practical difficulties due to its shape and variable material permeability. In this paper, the objectives of the modelling of rail internal impedance are to determine the regimes where hysteresis and saturation effects are significant. Linear analytic models with actual material data based on measurements of rail material permeability and resistivity are presented. The rail internal self-impedance term in the track impedance matrix is evaluated as a function of both frequency and AC current. The result can then be used to give a quantitative assessment of the extent of power frequency harmoni

RAIL MATERIAL DATA

The Ferromagnetic B-H Loop

The permeability (μ) of ferromagnetic material is a function of the field vectors **B** (magnetic induction), **M** (magnetic polarization), and **H** (magnetic field), according to

$$\mathbf{B} = \mu_0 (\mathbf{H} + \mathbf{M}) = \mu \mathbf{H} \qquad (2)$$

For isotropic and homogenous materials, the permeability is invariant with direction and position. For ferromagnetic materials, the magnetization process is time-dependent and **B** is a nonlinear, multivalued function of **H** as well as a function of frequency, with

$$\mathbf{B} = \mu (\mathbf{H}, \mathbf{B}, \omega) \mathbf{H} \qquad (3)$$

To determine the flux distribution within these materials, and hence electrical impedance, the complete B-H relationship needs to be specified. Figure 1 shows a typical ferromagnetic material static B-H characteristic together with the associated permeability definitions. Of principal interest for large-signal AC conditions are the initial, normal, incremental and differential permeabilities.

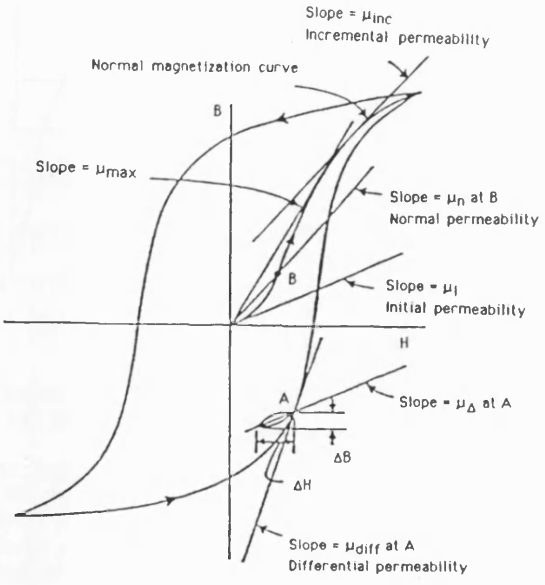

Fig. 1. Ferromagnetic material B-H loop and permeability definitions.

Time dependency in the magnetization process may be accounted for by introducing a complex permeability to describe the phase lag between the **H** and **B** vectors. Thus

$$\mathbf{B}\, e^{j\omega t} = |\mu^*|\, \mathbf{H}\, e^{j(\omega t - \phi)} = (\mu' - j\mu'')\, \mathbf{H} e^{j\omega t} \qquad (4)$$

where μ^* is the complex permeability. Physically, the phase angle accounts for energy losses associated with magnetic resonance and relaxation phenomena arising from the reorientation of magnetic moments of microscopic origin [8]. However a similar representation can also give accurate estimates of material behaviour in the macroscopic region if there is no material saturation, so that the vectors **B** and **H** are linearly related. The B-H characteristic then becomes elliptical. Even for practical materials with nonlinear permeability, approximating the B-H loop by an ellipse allows complex permeability data to be extracted by considering the fundamental frequency relationship.

Experimental Material Tests

Various material samples were machined from railroad rail in order to evaluate the actual permeabilities as specified in Figure 1. The static B-H loop was determined using filaments of material 2 mm square and with length at least 100 mm. Each filament was subjected to an alternating magnetic field with frequency 0.33 Hz in the direction of its longitudinal axis. This low excitation frequency ensured that the skin depth was much greater than the filament width (d):

$$\delta = \sqrt{(2/\omega\sigma\mu)} \gg d \qquad (5)$$

Three filaments from orthogonal directions were tested to confirm the material isotrophy. Graphical results for low, medium and high values of surface field strength H_S are shown in Figure 2. Table 1 shows the evaluated energy per cycle in each of the three hysteresis loops. The variations of normal and incremental permeability as a function of surface magnetic field strength, extracted from the measured data of Figure 2, are reproduced in Figure 3.

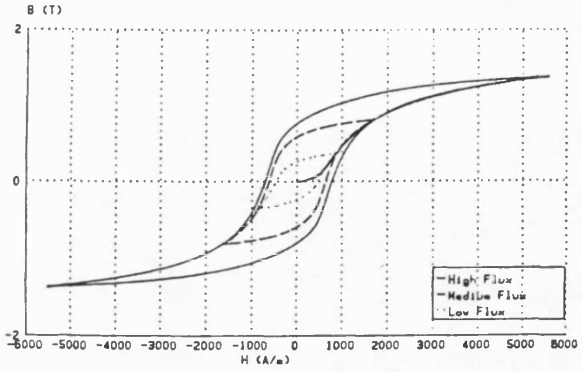

Fig. 2. Measured B-H loops for 54 kg/m flat-bottom rail material.

From the B-H loops, complex permeability data has been evaluated in two ways:

- Assuming sinusoidal magnetic field excitation, the B-H loop has been analysed by the Fast Fourier Transform technique to obtain the fundamental and harmonic magnitudes and phases of the flux density. Only the odd harmonics are significant, and the results for the first three are shown in Table 1. In this method, the sum of the fundamental and harmonic losses will equal the total loss as given by the loop area.
- For linear modelling it may be more accurate to equate the total loop area with the area of an equivalent fundamental ellipse. Thus all harmonic losses would be included within the fundamental. The orientation of the ellipse, defined by coercive force and remanent flux density, is that defined by the original hysteresis loop.

Figure 4 shows the resulting complex permeability functions derived from each model.

Rail Resistivity

The resistivity of the rail iron is also a fundamental material property and appears as a constant in the skin depth function. It can be expressed in the form

$$\rho = \rho_{20}(1 + \alpha T) \qquad (6)$$

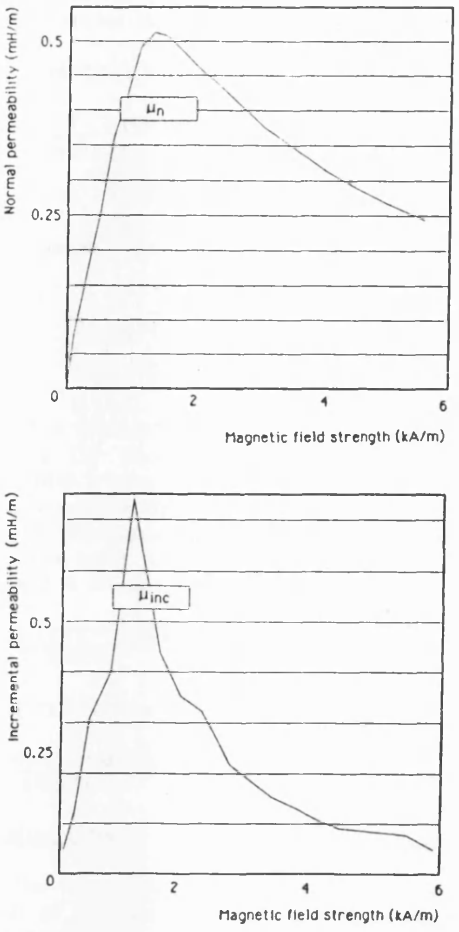

3. Derived normal and incremental permeabilities for 54 kg/m rail material.

e α is the temperature coefficient of resistivity, ·ized over the temperature range of interest, T is the erature (K), and ρ_{20} is the restivity at 20 K.

The resistivity of the rail samples used in the material was measured by applying constant currents and uring voltage over a suitable temperature range. al results at 20 K are

= $3.4\ 10^{-3}\ K^{-1}$
$_0$ = $0.225\ 10^{-6}\ \Omega$ m

conductivity

$_0$ = $4.44\ 10^6\ S\ m^{-1}$.

ANALYTICAL MODELLING

The objective of analytical modelling is to predict the dency of rail internal self-impedance on AC current requency. Simple modelling can reveal order of tude estimates for the fundamental and harmonic loss for the base cases of:
ear complex permeability, no saturation.
hysteresis loss, high saturation.
r analysis is necessary to establish the optimum ive permeability to use in each model, as a function of e magnetic field H_s.

Peak surface magnetic field H_s (A m^{-1})	Fundamental B_1 (T)	Φ_1 (°)	3rd harmonic B_3 (T)	Φ_3 (°)	5th harmonic B_5 (T)	Φ_3 (°)	7th harmonic B_7 (T)	Φ_7 (°)
5600	1.65	-9	0.39	-29	0.19	-46	0.105	-65
1700	0.95	-25	0.19	-74	0.075	+65	0.04	+20.5
900	0.394	-26	0.065	+64	0.017	-20	0.006	-73

Table 1. Flat-bottom Rail Hysteresis Loop Harmonic Analysis.

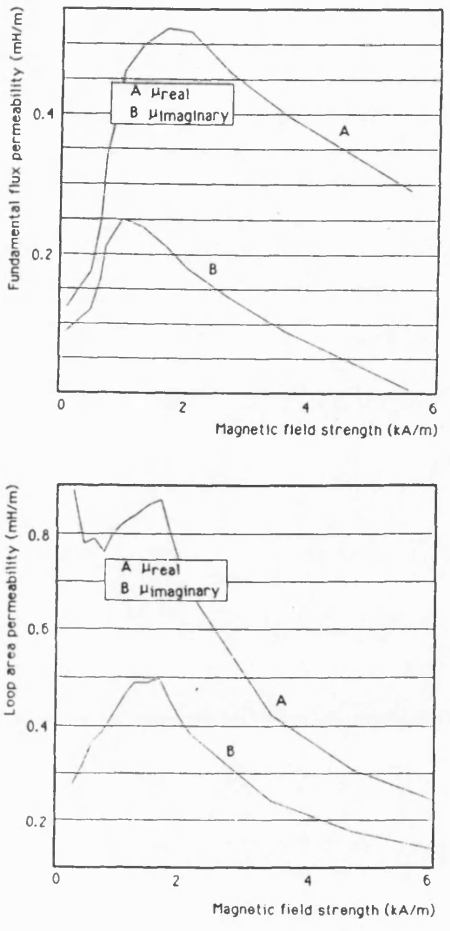

Fig. 4. Complex permeability with fundamental flux and B-H loop area approximations.

Linear Hysteresis Model

The rail is treated as a magnetic conductor made from homogenous, isotropic material with constant permeability μ^*. Assuming an equivalent circular solid conductor, the solution for magnetic field and hence current density within the material is found from solving the diffusion equation [9]. The conductor impedance is then found as a function of conductor radius and skin depth:

$$R + jX = \frac{\alpha}{2\pi a\sigma} \frac{I_0(\alpha a)}{I_1(\alpha a)} \qquad (7)$$

where

$$\alpha^2 = j\omega\sigma\mu^* \qquad (8)$$

is the complex skin depth function, a is the conductor

radius, σ is the conductivity and I_n are n^{th} order modified Bessel functions of the first kind.

After manipulation, it may be shown that the internal impedance of the conductor takes limiting values at low and high frequencies as follows [10]:

Low frequency: $a \ll \delta$

$$z_{lf} = \frac{1}{\pi a^2 \sigma}\left\{\left[1 + \frac{a^2}{4\delta^2}\sin\theta + \frac{a^4}{48\delta^2}\cos 2\theta\right] + j\left[\frac{a^2}{4\delta^2}\cos\theta - \frac{a^4}{48\delta^4}\sin 2\theta\right]\right\} \quad (9)$$

High frequency: $a \gg \delta$

$$z_{hf} = \frac{1}{\pi a^2 \sigma}\left\{\left[\frac{1}{4} + \sqrt{2}\cos\left(\frac{\pi}{4} - \frac{\theta}{2}\right)\right]\left(\frac{a}{2\delta} + \frac{3}{32}\frac{\delta}{a}\right) + j\left[\sqrt{2}\sin\left(\frac{\pi}{4} - \frac{\theta}{2}\right)\right]\left(\frac{a}{2\delta} - \frac{3}{32}\frac{\delta}{a}\right)\right\} \quad (10)$$

where θ is the hysteresis angle. For complex permeability, Equations (9) and (10) describe the behaviour at the fundamental frequency, and the eddy and hysteresis losses cannot be separately identified.

The impedance angle reduces with hysteresis from the asymptotic value of π/4. The model shows that losses are increased in the presence of hysteresis by a factor

$$\frac{[\cos(\pi/4 - \theta/2)]}{\cos\pi/4}$$

and the rail reactance is decreased by the factor

$$\frac{[\sin(\pi/4 - \theta/2)]}{\sin\pi/4}.$$

Saturation Effects

The linear model gives the equivalent rail impedance as that of an inductance, associated with energy storage, and a resistance, associated with energy dissipation. In electrical circuits, a nonlinear resistance behaves like a reactive power generator, although it has no energy-storage capacity. This is also the case for a saturated magnetic system, where the nonlinearity modifies the reactive, as well as the active power. An approximate model to take account of saturation in rail can represent the iron B-H characteristic by a step function according to

$$B = \begin{cases} +B_A & H > 0 \\ -B_A & H < 0 \end{cases} \quad (11)$$

It can be shown [9] that for this material property, magnetic flux waves with a constant magnitude of $|B_A|$ will penetrate the boundary under the influence of sinusoidal surface magnetic field excitation ($H_S \sin \omega t$). The maximum penetration depth is:

$$\delta_A = \sqrt{[2H_S/\omega\sigma B_A]} \quad (12)$$

which is in the same form as the skin depth equation (5), with the effective permeability, μ, replaced by B_A/H_S. The average power in the material is

$$P_{av} = \frac{8}{3\pi}\frac{H_S^2}{\sigma\delta_A} \quad (13)$$

which is a factor 70% greater than that in the linear case (with δ set equal to δ_A).

Eddy Current Loss Model

The approximate models described so far represent limiting conditions of linear permeability and complete saturation. In most cases, the rail material saturates gradually, accompanied by distortion in the hysteresis loop. The balance between hysteresis and eddy current losses then changes.

The effect of nonlinear permeability in the presence of hysteresis is to produce harmonics with associated extra losses. To predict the rail impedance variation under these conditions a suitable effective permeability value must be selected. The modified eddy current distribution within the material can be calculated numerically taking account of the known dependency of permeability on magnetic field strength. The approach adopted is to use a finite difference technique, the Du Fort-Frankel scheme [11], to calculate the spatial and temporal decay in the magnetic field intensity within the material and hence estimate the effective complex skin depth.

The finite difference technique gives an explicit equation with attractive stability properties. Applied to a semi-infinite slab of material, the magnetic field strength is given by

$$\frac{\partial^2 H}{\partial y^2} = \sigma\mu(H)\frac{\partial H}{\partial t} \quad (14)$$

The associated difference equation is:

$$H_{i,k+1} = r H_{i+1,k} + (1-2r) H_{i,k} + r H_{i-1,k} \quad (15)$$

where $r = p/\sigma\mu h^2$, p being the time step length and h the spatial step length. By substituting for the present nodal value the average of the previous and next values,

$$H_{i,k} = (H_{i,k+1} + H_{i,k-1})/2 \quad (16)$$

the explicit difference equation is formed:

$$H_{i,k+1} = H_{i,k-1} + \frac{2r}{2r+1}(H_{i+1,k} - 2H_{i,k-1} + H_{i-1,k}). \quad (17)$$

The distribution of H in the material can then be determined by varying the surface magnetic field strength $H_{0,k}$ as a sine wave. Figure 5 shows the computed result of $|H_S|$ vs depth, for various initial surface field strengths. At high field strengths, the material becomes saturated near the surface and the magnitude of H falls away steeply in the interior, but for low initial field strengths, there is little deviation from the linear model.

EXPERIMENTAL RAIL IMPEDANCE MEASUREMENTS

Order of Magnitude Estimate for Hysteresis and Eddy Losses

In order to determine the relative importance of hysteresis and eddy current losses, iron losses were measured as a function of frequency in a toroid manufactured from rail iron. The dimensions of the toroid were: radius 30 mm, thickness 3 mm and length 10 mm, and the winding comprised 250 turns of 1 mm copper wire. The results, shown in Figure 6 with the static B-H loop loss per cycle superimposed, show that at power frequencies the hysteresis loss and eddy loss per cycle are comparable. This indicates that for the range of rail excitation expected in practice, neither the linear nor the heavily saturated model alone is realistic.

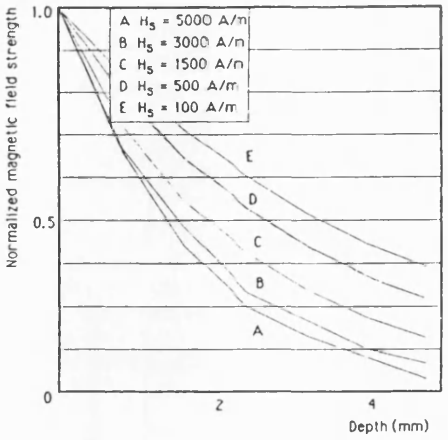

ig. 5. Magnetic field strength as a function of depth in a semi-infinite slab of ferromagnetic material.

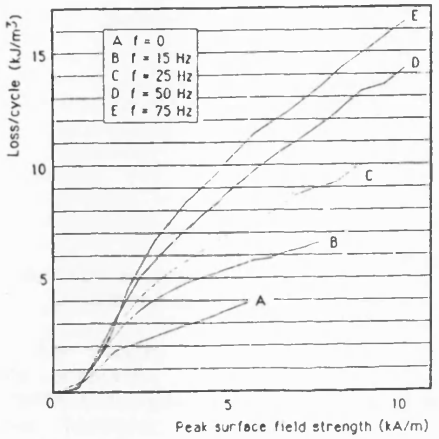

g. 6. Measured iron loss in toroid sample of rail material.

ail Impedance Measurement Apparatus

To accurately measure the rail internal elf-impedance, the circuit inductance due to the test urrent return path and the flux disturbance from sample hape effects must both be eliminated. The experimental echnique used was developed from equipment described by olmstrom [4] for null-flux measurement of the elf-inductance change in an isolated rail, using as a eference conductor a copper tube. The method was odified so that absolute measurements of internal npedance could be made. The apparatus (Figure 7) relies n the prior use of a reference conductor, which is a pecially-constructed hollow copper shell of identical shape o the test rail and having negligible internal inductance [10] t high frequency. This enables the impedance easurement loop to be adjusted in position (distance d in igure 7) such that zero inductance is obtained in alibration.

When the rail sample is placed in the same physical osition as the copper shell, measurements of the change in nductance will thus represent the true internal elf-inductance. The resistive part of the impedance emains an absolute measurement of internal resistance. nd effects are negligible since the measurement points (A, in Figure 7) are maintained a suitable distance from the onductor ends. An on-line FFT analyser provides noise nmunity and accurate phase and frequency measurement.

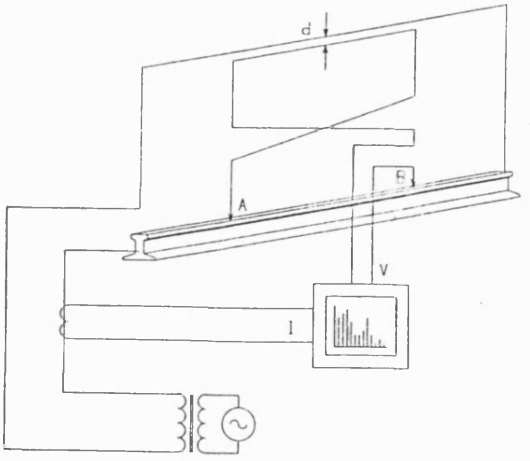

Fig. 7. Experimental apparatus for measurement of rail impedance.

Rail Impedance as Function of Current and Frequency

Measurement results of impedance as a function of current at 50 Hz are shown in Figure 8. Both resistance and inductance increase with current magnitude for the range of currents generated. To assess rail impedance at harmonic frequencies, measurements at a constant amplitude of 6 A were made for frequencies up to 10 kHz. The results are shown in Figure 9. As expected, the resistance increases and the inductance decreases with increasing frequency due to the skin effect.

DISCUSSION

Superimposed on the experimental curves of Figures 8 and 9 are theoretical calculations derived from the various assumptions on the modelling of hysteresis loss and the variation in material permeability. The increase of rail impedance with AC current indicates that the material is far from saturation even with the highest current applied. This is because of the large rail cross sectional area ($7.5\ 10^{-3}$ m^2). The most accurate resistance model is with an effective permeability function at low excitation, and with complex permeability obtained by the B-H loop area approximation (i.e. incorporating total harmonic losses within the fundamental) at high excitation. The use of normal and incremental permeability from Figure 3 is inappropriate in the model due to the importance of hysteresis loss. The effective permeability used is constant throughout the AC cycle, but with magnitude dependent on the level of current excitation as determined from Figure 5 (it has been termed *linearized* permeability). The inductance variation shows good agreement with the model using complex permeability obtained from the fundamental of the B-H loop, with better agreement at very low excitations from the linearized model of permeability as described above.

The variation in rail resistance with frequency, for low excitation currents, shows good agreement with the complex permeability model based on total loop area for high frequencies, and that based on the fundamental component for low frequencies. For rail inductance, the fundamental complex permeability model is more accurate at high frequencies, with the experimental curve lying between this model and the linearized model of permeability at lower frequencies.

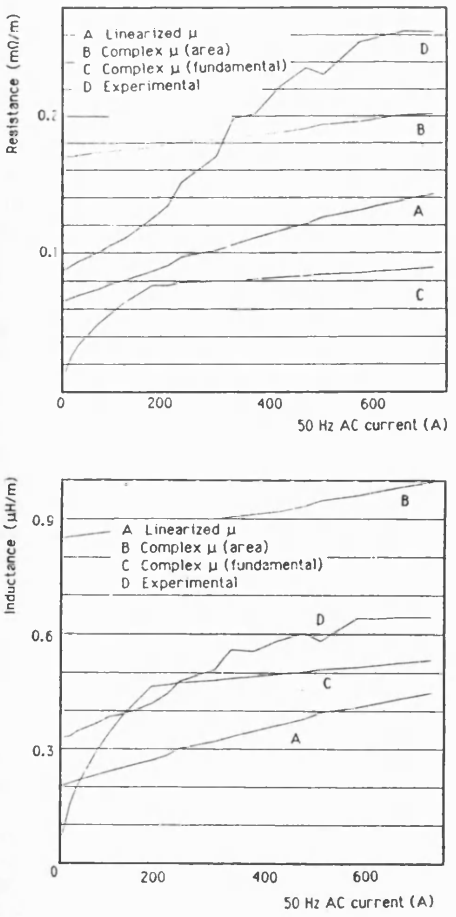

Fig. 8. Experimental and theoretical rail internal self-impedance as a function of AC current at 50 Hz.

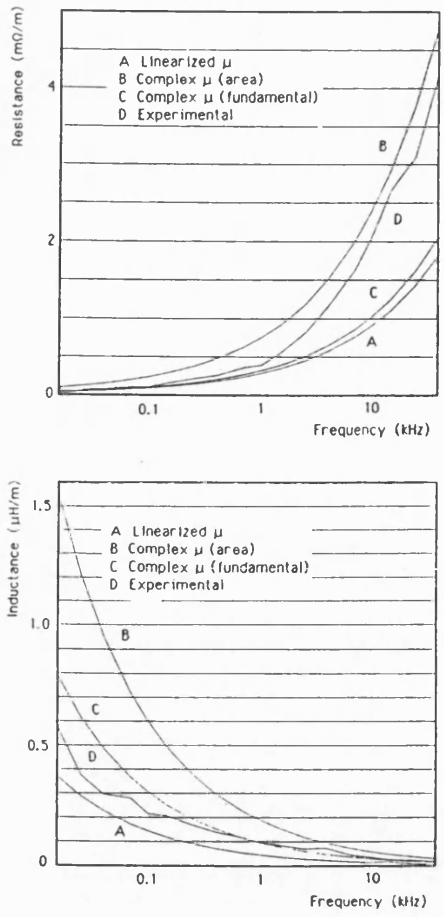

Fig. 9. Experimental and theoretical rail internal self-impedance as a function of frequency at 6A.

The complex permeability model based on loop area is more accurate for rail resistance modelling at high currents and frequencies. This model necessarily includes higher harmonic losses which increase with greater excitation. For the rail induction variation with current, ignoring the harmonics produces closer agreement with the experimental measurements. However the inductance is defined only at the fundamental frequency and the total VARs would necessarily need to include higher harmonics.

More accurate models are required to represent the rail impedance over the complete range of current and frequency. For example, accurate computations using combined finite element and finite difference techniques could incorporate exact differential permeability data, and hence enable identification of the separate fundamental and harmonic losses.

CONCLUSIONS

An analytical model with linear complex permeability, based on experimental determination of the material B-H loop, gives good agreement with measurements of rail impedance for moderate rail currents. The conditions correspond to hysteresis but not saturation, and will be of use in the modelling of power harmonic propagation in track signalling systems. At low excitations, better agreement is found by neglecting hysteresis and using an effective permeability obtained by modelling the flux distribution within the rail, using as data experimentally derived normal permeability as a function of surface magnetic field strength.

A saturation model ignoring hysteresis is suggested as suitable for transient studies and fault condition analyses which would be obtained with high excitation currents. The large magnitude of current at 50 Hz necessary to achieve rail saturation was not achieved in the reported experiments.

Results presented for rail internal self-impedance will enable the rail resistance and inductance at specific power frequency harmonics to be determined. The impedance is a function of current and frequency and cannot be obtained as a closed-form expression. It could, however, be expressed as a polynomial.

ACKNOWLEDGEMENTS

This research was supported by the Science and Engineering Research Council, UK.

REFERENCES

[1] D. J. Tylavsky and A. Y. Kulkarmi, "Inductance calculations for earth-return trolley systems," Proceedings of *1988 IEEE Industry Applications Society Annual Meeting*, Pittsburgh PA, 2-7 October 1988 (New York: IEEE 1988), vol. 2, pp. 1216-1223.

[2] B. Mellitt, J. Allan, Z. Y. Shao, W. B. Johnston and C. J.

Goodman, "Computer-based methods for induced-voltage calculations in AC railways," *IEE Proceedings,* vol. 137B, no. 1, pp. 59-72, January 1990.

[3] E. K. Stanek, T. Cataltepe and D. O. Wiitanen, "Phenomena that affect the calculation of the inductance and resistance of mine track/trolley systems," Proceedings of *1984 IEEE Industry Applications Society Annual Meeting,* Chicago IL, 30 September - 4 October 1984 (New York: IEEE 1984), pp. 100-106.

[4] F. R. Holmstrom, "The model of conductive interference in rapid transit signaling systems," *IEEE Transactions on Industry Applications,* vol. IA-22, no. 4, pp. 756-762, July/August 1986.

[5] N. Burais and G. Grellet, "Numerical modelling of iron losses in ferromagnetic steel plate," *IEEE Transactions on Magnetics,* vol. MAG-18, no. 2, pp. 558-61, March 1982.

[6] D. Labridis and P. Dokopoulos, "Calculation of eddy current losses in nonlinear ferromagnetic materials," *IEEE Transactions on Magnetics,* vol. MAG-25, no. 3, pp. 2665-2669, May 1989.

[7] J. S. Hsu, H. H. Woodson and S.-S. P. Liou, "Experimental study of harmonic-flux effects in ferromagnetic materials," *IEEE Transactions on Magnetics,* vol. MAG-25, no. 3, pp. 2678-2685, May 1989.

[8] D. J. Epstein, "Permeability". In: *Dielectric Materials and Applications* [Editor: A. R. Von Hippel]. New York: Technology Press M.I.T./Wiley 1954.

[9] P. Hammond. *Applied Electromagnetism.* Oxford UK: Pergamon Press 1981.

[10] D. C. Carpenter and R. J. Hill, "The effect of magnetic saturation, hysteresis and eddy currents on rail track impedance," Proceedings of *IEEE/ASME Joint Railroad Conference,* Philadelphia PA, 25-27 April 1989 (New York: IEEE 1989), pp. 73-79.

[11] E. C. Du Fort and S. P. Frankel, "Stability conditions in numerical treatment of parabolic differential equations," *Mathematical Tables and Aids Computation,* vol. 7, pp. 135-152, 1953.

R. John Hill was born in Somerset, England, on July 3, 1948. He received the degrees of B.Eng. in Electronics and Ph.D. in Power Electrical Engineering from the University of Liverpool, England, in 1969 and 1973, and M.A. from the University of Cambridge, England, in 1983.

From 1973-1980 he was a Design and Development Engineer for London Underground Railways working on automatic train control systems. In 1980 he became a Lecturer at Cambridge University Engineering Department and in 1983 a Fellow of King's College, Cambridge. Since 1986 he has been a Lecturer at the Universaity of Bath, England.

Dr Hill is a Member of the IEE (UK) and the Institute of Physics (UK). In 1988 he was awarded the IEEE Vehicular Technology Society prize for the best paper presented at the Joint ASME/IEEE Railroad Conference.

David C. Carpenter was born in England on September 8, 1956. He received the degrees of B.Sc. from the University of Southampton, England, in 1978 and M.Phil. from Coventry Polytechnic, England, in 1989.

In 1979 he became a Computer-Aided Design Engineer at GEC Machines Ltd, Rugby, England, and in 1980 a Lecturer (Senior Lecturer from 1984) in Electrical Engineering at Coventry Polytechnic, England. From 1986-1987 he was a Visiting Professor at Lakehead University, Canada. Since 1988 he has been a Research Officer at the University of Bath, UK, working on the modelling of electric traction systems.

Mr Carpenter is a Member of the IEE (UK).

Determination of rail internal impedance for electric railway traction system simulation

R.J. Hill
D.C. Carpenter

Indexing term: Railway electrification

Abstract: Theoretical models for rail internal self-inductance and resistance are proposed which include material saturation and hysteresis. Model data are obtained using experimentally derived ferromagnetic material *B-H* loops. Analytical methods for deriving the impedance variations with current and frequency for large-signal AC and incremental AC superimposed on DC excitation are in agreement with experimental measurements.

List of symbols

a	= equivalent radius of circular conductor, m
A, A_s	= vector potential, vector potential associated with element S, Tm
B	= magnetic flux density, T
d	= depth within material from surface, m
h, p	= spatial step, m, time step length, s
H, H_s, H_{sp}	= magnetic field, surface field, peak surface field strength, A/m
i, k	= spatial, time counters
I	= current, A
$[I]$	= column vector of rail currents, A
I_n, K_n	= nth order modified Bessel function of first kind, second kind
J, J_s	= current density, current density associated with element S, A/m^2
ℓ	= inductance per unit length, H/m
M	= magnetic polarisation, A/m
P, P_A	= active (dissipated) power, W, apparent power, VA
P_H, P_R, P_W	= harmonic (distortion), fundamental reactive, total reactive power, VAr
r	= resistance per unit track length, Ω
s	= conductor cross-section area, m^2
S	= elemental area, m^2
$[V]$	= column vector of rail voltages with respect to earth, V
y	= depth co-ordinate, m
y_{ii}	= self admittance of rail i per unit track length, S
y_{ij}	= mutual admittance between rails i and j per unit track length, S
$[Y]$	= track admittance matrix, S/m
z	= internal impedance per unit length, Ω/m
z_{ii}	= self impedance of rail i per unit track length, Ω/m
z_{ij}	= earth-return mutual impedance of rail i with respect to rail j, Ω/m
$[Z]$	= track impedance matrix, Ω/m
α	= complex skin depth function, m^{-1}
β	= conductivity coefficient, K^{-1}
δ, δ_{eff}	= skin depth, effective skin depth, m
ε	= permittivity, F/m
$\mu, \mu^* (=\mu' - j\mu'')$	= permeability, complex permeability, H/m
μ_0	= permeability of free space, H/m
$\mu_{\Delta AC}, \mu_{\Delta DC}, \mu_{diff}$	= AC delta, DC delta, differential permeability, H/m
μ_{eff}, μ_{inc}	= effective, incremental permeability, H/m
μ_i, μ_n	= initial, normal permeability, H/m
σ, σ_1	= electrical conductivity, reference electrical conductivity, S/m
θ	= hysteresis angle, rad
ϕ	= phase lag of B behind H, rad
ω	= angular frequency, rad/s

Paper 8156B (P2), first received 20th November 1990 and in revised form 18th April 1991

The authors are with the School of Electrical Engineering, University of Bath, Claverton Down, Bath BA2 7AY, United Kingdom

1 Introduction

In electric railways with track-circuit based data transmission, both power and information signals propagate along the track. Unwanted coupling between the traction power and signal/communication subsystems is determined by the track transfer function, which is governed by the transmission parameters and specified by the track impedance and admittance matrices. These matrices are defined from the variation of voltages and currents along the track according to

$$\frac{d}{dx}[V] = -[Z][I] \tag{1}$$

and

$$\frac{d}{dx}[I] = -[Y][V] \tag{2}$$

The matrices $[Z]$ and $[Y]$ are composed of diagonal coefficients z_{ii}, y_{ii} and off-diagonal coefficients z_{ij}, y_{ij}. The rail self impedance z_{ii} consists of an internal and an external component. The internal component is determined by the distribution of magnetic flux within the rail iron and the external component arises from flux outside the conductor. Whereas the former is material-dependent, the latter is largely determined by circuit geometry.

This paper is concerned with accurate determination of the internal component of the rail self impedance. This parameter is nonlinear with respect to current and frequency, and is of considerable significance in the simulation of electrified rail networks, for modelling signal propagation in studies concerning:

(i) Signalling system design, e.g. to obtain the transfer impedance between track signalling transmitters and receivers

(ii) Traction system design, e.g. to calculate energy flow, harmonic overvoltages, network distortion effects and supply power factor

(iii) Traction fault assessment, where large direct or alternating currents can saturate the rail iron causing a redistribution of rail current to alternative paths such as the earth

(iv) Electromagnetic compatibility assurance, where traction current harmonics couple with communications and signal currents to generate interference, e.g. producing intermodulation distortion in coded information track transmission systems.

In most reported rail traction simulation studies, the internal rail self impedance is regarded as a constant. This is reasonable because for many applications, the internal self impedance is only a small part of the total circuit impedance. The sensitivity of simulation results to variations in rail impedance will then be small. For studies including the internal rail impedance, constant iron permeability, no hysteresis and an equivalent circular conductor may be assumed. This implies that the resistance will increase and the inductance reduce with increasing frequency due to flux redistribution from the skin effect. Further, for the modelling of overhead catenary supply systems, it is usually considered unnecessary to model the rail internal impedance accurately, running rail impedance data based on a single equivalent rail being sufficient [1]. Detailed consideration of internal rail impedance can only be attempted by physically removing the rail from the track, as reported by Trueblood & Waschek [2] and, more recently, by Holmstrom [3], who also considered the effect of rail saturation, but not hysteresis, on rail impedance for DC railways. Tylavsky [4] and Stanek [5], modelling faults in mining railway traction systems, also report studies of rail impedance taking into account iron saturation.

Analytical techniques for field computation in power frequency magnetic systems have some relevance to the modelling of rail track impedance. However, the special condition of the rail is that it is an electrical conductor exhibiting ferromagnetic saturation and hysteresis effects. The problem is essentially one of time and two-dimensional-space magnetic field computation. Burais [6], for example, demonstrates a technique in which hysteresis and eddy current losses can be separated in non-oriented saturated steel plate, combining finite element modelling (FEM) for space discretisation, and finite difference modelling (FDM) for time discretisation. Labridis [7], however, assumes an equivalent fictitious material with constant permeability (for time) and variable permeability (for space) and involving evaluation of the stored magnetic co-energy density. Further, Hsu [8] has shown that harmonic fluxes lead to a reduction in iron loss at saturation where hysteresis loss is large.

The objective of this paper is to specify completely the current and frequency dependency of the rail internal self inductance and resistance for frequencies in the power and audio range (12 Hz–30 kHz). Current excitation can be from AC or DC traction systems, the latter implying that the rail carries an incremental alternating current superimposed on the DC excitation. The technique proposed considers the iron magnetic characteristics, constructs an analytical model for impedance, and then defines the areas of validity. The theory has been verfied by experimental measurements and, where appropriate, validated by FEM. It is shown that for large-signal AC conditions, the hysteresis loss can represent a substantial proportion of the total energy loss, and that in DC railways the impedance reduction for AC signals at large traction currents can be significant.

2 Rail iron material data

2.1 Rail physical dimensions

The results reported are specifically for British BS 113A flat-bottom rail, with nominal weight 56.4 kg/m. The data for this, and for other rail types considered, is given in Table 1. In practice, partially worn rail samples were available, with the data in the Table representing practical, rather than new, values, providing realistic results with respect to work hardening and magnetic orientation.

Table 1: Rail data

Rail type	Nominal weight (kg/m)	Actual weight (kg/m)	Perimeter (m)	Area (m^2)	Equivalent radius	
					area (m)	perimeter (m)
Flat bottom BS 113A	56.4	51.5	0.63	0.0075	0.034	0.100
Bull head	—	37.1	0.48	0.0054	0.029	0.092
Conductor	—	52.2	0.58	0.0076	0.035	0.076

2.2 Permeability

2.2.1 Ferromagnetic material: The electromagnetic behaviour of ferromagnetic material is expressed in terms of field vectors according to the relationship

$$\boldsymbol{B} = \mu_0(\boldsymbol{H} + \boldsymbol{M}) = \mu \boldsymbol{H} \tag{3}$$

For isotropic, homogenous material, the permeability is a scalar. In ferromagnetic materials, time-dependency in the magnetisation process implies that the magnetic flux density lags the magnetic field excitation, so that the flux density will be a multivalued function of the magnetic field strength. In addition, material saturation introduces nonlinearity. Finally, frequency dependency occurs through loop widening as a second-order effect [9]. Hence eqn. 3 can be more rigorously expressed as

$$\boldsymbol{B} = \mu(\boldsymbol{H}, \boldsymbol{B}, \omega)\boldsymbol{H} \tag{4}$$

where the time dependency is included in the frequency variable due to cyclic excitation. The internal electrical impedance of a current-carrying conductor is affected by its field distribution. To determine this, the complete material *B-H* relationship is required, as shown in Fig. 1. The permeability definitions necessary to model electrical impedance are also shown in the Figure, and are the initial, normal, incremental, delta and differential permeabilities [10]. All of the time and frequency effects above can be accounted for by introducing a complex permeability to describe the phase lag between the mag-

netic flux density and magnetic field vectors, according to

$$Be^{j\omega t} = |\mu^*| He^{j(\omega t - \phi)}$$
$$= (\mu' - j\mu'')He^{j\omega t} \quad (5)$$

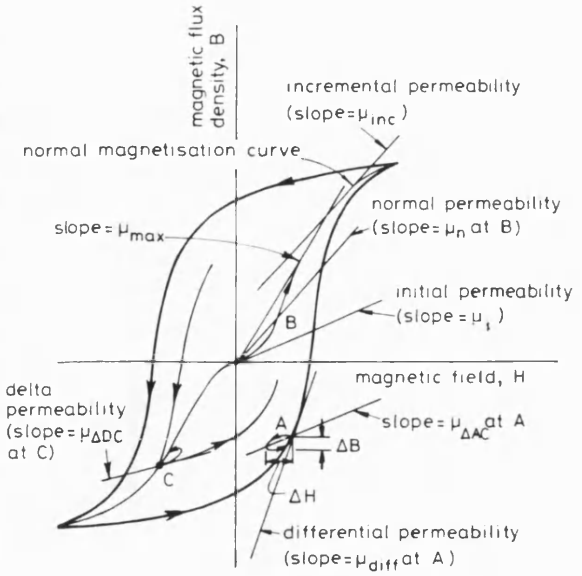

Fig. 1 *Ferromagnetic material B-H loop and permeability terminology*

Although this representation is usually applied to account for energy losses associated with magnetic resonance and relaxation phenomena from reorientation of microscopic magnetic moments [10], it can also be applied to linear macroscopic conditions, where the *B-H* curve is elliptical.

For excitation with a net DC, there is an operating point on the normal magnetisation curve with specific incremental and normal permeabilities. Superimposed alternating currents then follow a small hysteresis loop (at point C in Fig. 1) with a specific value of delta permeability ($\mu_{\Delta DC}$) for each direct current. The AC incremental impedance may be evaluated using this value of delta permeability. Hysteresis loss is not considered important in this case as the loop area is small, and even at high frequency the additional loss involved is much less than the losses due to AC eddy currents and DC ohmic heating.

For excitation with a large amplitude AC signal, an effective permeability must be calculated which accounts for loop distortion due to saturation. This is considered in detail later.

2.2.2 Permeability measurements: Material samples of dimensions 1 × 1 × 100 mm were machined from the rail. The material *B-H* loops were obtained by subjecting these samples to an axial magnetic field at 0.33 Hz in the longitudinal direction. The low excitation frequency ensured that eddy currents were negligible, i.e.

$$\delta = \sqrt{\left(\frac{2}{\omega\sigma\mu}\right)} \gg d \quad (6)$$

Material isotropy was confirmed by testing samples from three orthogonal directions. Fig. 2 shows a typical test result. The nested loops are for low, medium and high surface magnetic field strengths. From these curves, values of normal, incremental and delta permeability as functions of magnetic field strength were extracted, as shown in Fig. 3. All curves demonstrate the onset of saturation which is given by the point of maximum slope in the normal magnetisation curve of Fig. 1.

2.2.3 Effective permeability: The effect of saturation is to produce additional harmonic (distortion) power in the

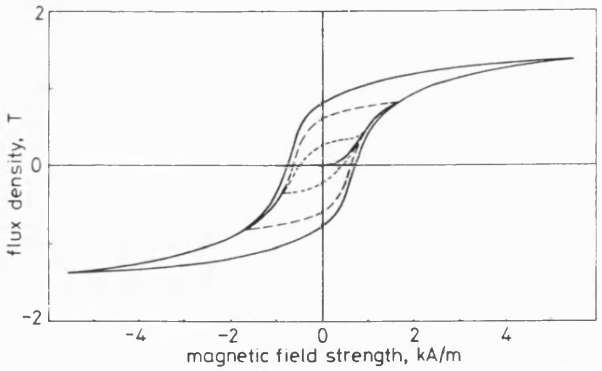

Fig. 2 *B-H loop measured characteristics*

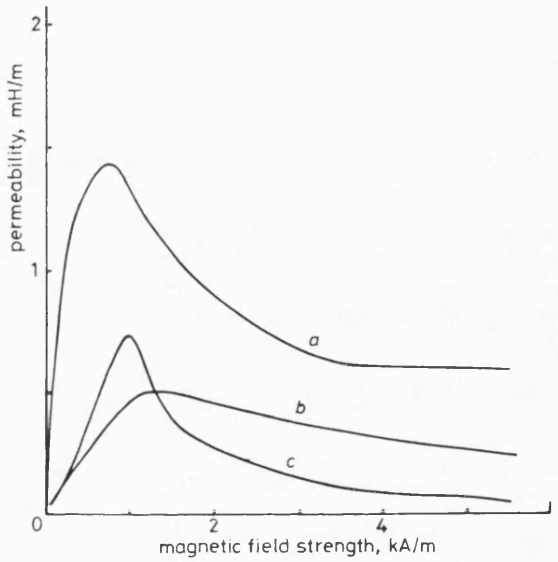

Fig. 3 *Normal, incremental and delta permeability as function of surface peak magnetic field*

a Delta permeability
b Normal permeability
c Incremental permeability

material. To demonstrate this effect, Hammond [11] has carried out an extreme-case analysis with a step function for magnetic flux density of $\boldsymbol{B} = +\boldsymbol{B}_A$ for positive excitation field and $\boldsymbol{B} = -\boldsymbol{B}_A$ for negative field. The average power loss in the material is found to be 70% greater than in the corresponding linear case, due to the modified magnetic flux distribution near the material surface.

To quantify the effect of saturation in the analytic model, the field within a semi-infinite slab of nonlinear ferromagnetic material was determined using a FDM technique. The objective was to obtain an effective permeability as a function of surface magnetic field strength. For linear conditions, electromagnetic theory predicts a fall in magnitude of magnetic field strength with depth, together with a phase shift. On saturation, the magnitude and phase variations will deviate from the linear case.

The FDM technique models the space and time decay of magnetic field strength within the material by solving

the diffusion equation

$$\frac{\partial^2 \boldsymbol{H}}{\partial y^2} = \sigma \mu_{\text{inc}}(\boldsymbol{H}) \frac{\partial \boldsymbol{H}}{\partial t} \tag{7}$$

The associated difference equation for a general element $\boldsymbol{H}_{i,k+1}$ is:

$$\boldsymbol{H}_{i,k+1} = u\boldsymbol{H}_{i+1,k} + (1 - 2u)\boldsymbol{H}_{i,k} + u\boldsymbol{H}_{i-1,k} \tag{8}$$

where

$$u = \frac{p}{\sigma \mu_{\text{inc}} h^2} \tag{9}$$

The variation of magnetic field strength within the material is determined by applying a sinusoidal surface magnetic field strength $\boldsymbol{H}_{0,k}$. The results are shown in Fig. 4 for a peak surface field strength of 3500 A/m. The

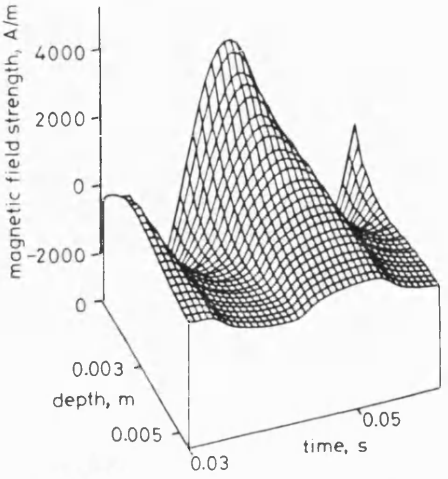

Fig. 4 *FDM-generated magnetic field within semi-infinite slab of nonlinear magnetic material*
Frequency = 50 Hz

amplitude clearly decreases with depth. The phase shift change with depth can be seen by following the grid line corresponding to the maximum surface field strength (depth = 0, $\boldsymbol{H}$ = 3.5 kA/m) into the material. The distortion of the sinusoidal field within the material can most clearly be seen at a depth of 5 mm. For a given surface field strength, the effective permeability (μ_{eff}) can be defined from the effective skin depth (δ_{eff}) according to

$$\mu_{\text{eff}}(\boldsymbol{H}_{sp}) = \frac{2}{\delta_{\text{eff}}^2 \sigma \omega} \tag{10}$$

where δ_{eff} is the depth at which the maximum field strength has fallen to $1/e$ of its surface value. Fig. 5 shows the resulting values of effective skin depth and effective permeability as a function of the peak surface magnetic field.

2.2.4 Saturation with hysteresis: The *B-H* loops in Fig. 2 suggest that hysteresis loss may become significant at higher frequencies. To evaluate the effect of hysteresis on the field waveform within the material, time waveforms of magnetic field have been calculated by FDM at the effective skin depth for saturated conditions with hysteresis. The effect of adding hysteresis to the model is illustrated in Fig. 6 which shows the distortion in magnetic field strength in a slice 1.4 mm within the material. It can be seen that the main effects are a small additional phase shift and extra distortion in the flux density waveform. For high accuracy, further adjustment of the effective permeability value would be appropriate.

The shape of the *B-H* loop is an ellipse for linear conditions, distorting with saturation. Its shape may be specified by assuming a sinusoidal magnetic field excita-

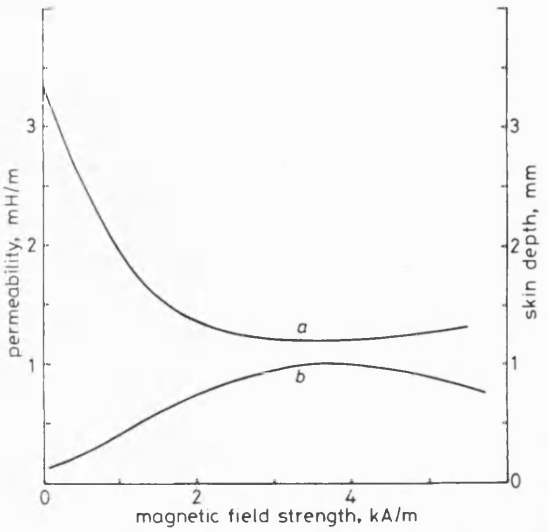

Fig. 5 *Effective skin depth and effective permeability as function of surface peak magnetic field for a semi-infinite nonlinear magnetic material slab*

a Effective skin depth
b Effective permeability

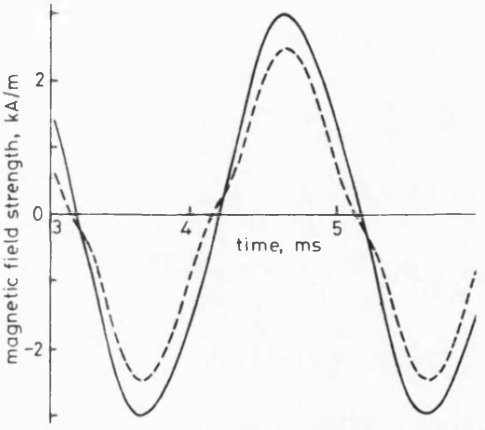

Fig. 6 *FDM-generated magnetic field within semi-infinite slab of nonlinear magnetic material at a depth of 1.4 mm with and without hysteresis*

---- With hysteresis
——— Without hysteresis

tion waveform and evaluating the fundamental and harmonics of the resulting flux density waveform by fast Fourier transforms (FFT). Table 2 gives the results of such an analysis.

Table 2: Harmonic analysis of *B-H* loops for flat-bottom rail

Rail type	$\hat{H}$ (A/m)	Harmonic magnitude B_n (T) Harmonic angle θ_n (°)					
		$n=1$	$n=3$	$n=5$	$n=7$	$n=9$	$n=11$
Flat Bottom	5600	1.65 8	0.38 28	0.17 45	0.11 65	0.07 83	0.05 100
	1750	0.94 21	0.19 74	0.07 117	0.04 160	0.03 225	0.01 245
	900	0.39 31	0.06 115	0.02 200	0.01 253	— —	— —

A quantitative assessment of loop shape distortion has been made by evaluating the apparent, dissipated, fundamental stored and harmonic stored energy densities from

Table 3: Evaluated energy densities for flat-bottom rail

$\hat{H}$ (A/m)	Flat-bottom rail energy densities (J/m³)					Loop area (J/m³)
	Apparent	Dissipated	Fundamental stored	Harmonic stored	Total stored	
5600	43225	4039	28746	32028	43036	3908
1750	6732	1852	4843	4295	6473	1805
900	1262	571	945	613	1126	506

the harmonics of flux density as given in Table 3. From these the corresponding real and reactive powers have been evaluated (Appendix 9.1). The significance of these quantities is derived from nonlinear electric circuit analysis, where it is known that a nonlinear resistance will behave like a reactive power generator while having no energy-storage elements, by the generation of harmonic, rather than reactive, power [12]. Distortion of the *B-H* loop through saturation will similarly introduce harmonic power as additional reactive power (P_H), whereas the active power (P) and fundamental reactive power (P_W) will depend only on the fundamental flux density and magnetic field values as determined in the Fourier analysis.

The effective permeability defined above is thus considered to be the magnitude of a complex effective permeability. The angle of the complex permeability is determined from the loop harmonic analysis according to

$$\theta(H_{sp}) = \arctan\left(\frac{P}{P_w}\right) \tag{11}$$

where

$$P_w = \sqrt{(P_R^2 + P_H^2)} \tag{12}$$

with the apparent power given by

$$P_A = \sqrt{(P^2 + P_w^2)} \tag{13}$$

The resulting complex effective permeability, as a function of peak surface magnetic field strength, is given in Fig. 7, together with the value derived from the fundamental of the flux density.

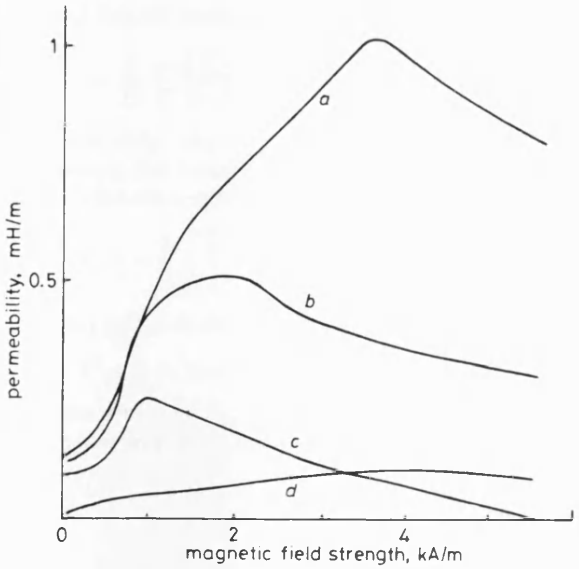

Fig. 7 *Fundamental and effective complex permeability as functions of surface peak magnetic field*

a Complex effective permeability (real)
b Complex permeability from fundamental flux component (real)
c Complex permeability from fundamental flux component (imaginary)
d Complex effective permeability (imaginary)

2.3 Electrical conductivity

The conductivity of rail iron is a fundamental material property and is temperature dependent. For small temperature excursions, the coefficient of resistivity may be linearised with the conductivity expressed by the relationship

$$\sigma = \sigma_1(1 + \beta T)^{-1} \tag{14}$$

The conductivity of the rail samples tested was determined using constant currents over a measured temperature range. The results are in Table 4.

Table 4: Rail resistivity at 293 K

Sample	Resistivity ($\mu\Omega m$)	Temp. coeff. (K^{-1})
Flat-bottom rail	0.225	0.0034
Bull-head rail	0.202	0.0031
Conductor rail	0.113	0.008

3 Rail internal impedance

3.1 Large-signal AC rail impedance

3.1.1 Large-signal equivalent circular model: A linear impedance model for a current-carrying ferromagnetic conductor can be used to account for the frequency dependency if the rail is treated as an equivalent circular solid conductor with constant permeability. The value of permeability is a function of the peak surface magnetic field strength and hence the current. The magnetic field and hence current density within the material, found from the solution of the diffusion equation, both decay exponentially from the surface. The conductor impedance is a function of the equivalent radius and skin depth, and can be calculated by considering Ampere's law (Appendix 9.2). The result is

$$z = r + j\omega l = \frac{\alpha}{2\pi a\sigma}\frac{I_0(\alpha a)}{I_1(\alpha a)} \tag{15}$$

where

$$\alpha^2 = j\omega\sigma\mu^* \tag{16}$$

The impedance takes limiting values at low frequency ($a \ll \delta$) and high frequency ($a \gg \delta$) as follows:

$$z_{lf} = \frac{1}{\pi a^2\sigma}\left\{\left(1 + \frac{a^2}{4\delta^2}\sin\theta + \frac{a^4}{48\delta^2}\cos 2\theta\right) + j\left(\frac{a^2}{4\delta^2}\cos\theta - \frac{a^4}{48\delta^2}\sin 2\theta\right)\right\} \tag{17}$$

$$z_{hf} = \frac{1}{\pi a^2\sigma}\left\{\left[\frac{1}{4} + \sqrt{(2)}\cos\left(\frac{\pi}{4} - \frac{\theta}{2}\right)\right]\left(\frac{a}{2\delta} + \frac{3\delta}{32a}\right) + j\left[\sqrt{(2)}\sin\left(\frac{\pi}{4} - \frac{\theta}{2}\right)\right]\left(\frac{a}{2\delta} - \frac{3\delta}{32a}\right)\right\} \tag{18}$$

Although the eddy current and hysteresis losses cannot be separated in this model, the effect of hysteresis is to:

(*a*) reduce the impedance angle from $\pi/4$ at high frequency.

(*b*) increase the AC resistance by $[\cos(\pi/4 - \theta/2)]/\cos\pi/4$: physically, the area of the hysteresis loop represents hysteresis loss per cycle.

(*c*) decrease the reactance by $[\sin(\pi/4 - \theta/2)]/\sin\pi/4$, by reducing the stored energy in the material.

The linear model represents the rail impedance as a pure resistance in series with a pure inductance, associated respectively with the active and reactive power.

3.1.2 Effect of rail shape: It is known that the geometric mean distance (GMD) of an irregularly shaped conductor from itself, interpreted as a circular conductor, is needed for inductance calculations at frequencies where the skin depth is significant compared with the conductor dimensions [13]. For rail, the phenomenon is apparent in the power and audio frequency range. Evaluation of the internal rail inductance for quasilinear conditions for the equivalent circular conductor model thus requires the evaluation of an effective radius by numerical evaluation of the GMD. This is justified by the agreement between the theoretical and experimental evaluation of inductance reported later. The evaluation of the GMD is described in Appendix 9.3 and for 56.4 kg/m flat-bottom rail the GMD is 0.11 m.

For resistance evaluation at very low frequencies, the rail area determines the equivalent radius. At frequencies above about 12 Hz, where the skin depth is small for rail ferromagnetic material, an equivalent radius based on the rail perimeter must be used. The boundary frequency can be taken as that at which the skin depth is very much smaller than the radius ($\delta = 0.1r$). At intermediate frequencies interpolation can be used.

3.1.3 Finite-element modelling: For nonlinear materials, local saturation at sharp corners of the rail boundary may occur, introducing errors in the quasilinear model. The above analytic theory has therefore been verified at high currents using FEM. The FEM model requires definition of an elemental net, which can be reduced in size in regions of high flux density. It then performs a two-dimensional axisymmetric static and dynamic electromagnetic analysis, assuming sinusoidal current excitation. The internal inductance is obtained from evaluation of the stored energy in the material:

$$\ell = \frac{2}{I^2} \int \boldsymbol{H} \cdot d\boldsymbol{B} \tag{19}$$

and the AC resistance per unit length from

$$r = \frac{1}{I^2} \sum_s \left(\frac{\boldsymbol{J}_s}{\sigma}\right) \cdot \delta \boldsymbol{S} \tag{20}$$

Essentially, the method is to find the solution by determining the minimum energy state through minimisation of a function such as

$$F(A) = \frac{1}{2} \int_s \left[\left(\frac{\nabla \boldsymbol{A}}{\mu}\right)^2 - \omega^2 \varepsilon \boldsymbol{A}^2 - 2\boldsymbol{J} \cdot \boldsymbol{A} \right] d\boldsymbol{S} \tag{21}$$

[14] which is derived from the Helmholtz equation:

$$\nabla^2 \boldsymbol{A} + \omega^2 \mu \varepsilon \boldsymbol{A} = -\mu \boldsymbol{J} \tag{22}$$

The contours of vector potential for a typical analysis are shown in Fig. 8. Table 5 gives some typical results for rail inductance and resistance, and confirms the applicability of the equivalent rail radii. For the rail section used in the tests, the values of current achieved represent the approach of saturation. The FEM results for inductance and resistance are in reasonable agreement with the measured and model values. The FEM model does not include the effect of hysteresis, so at 50 Hz the hysteresis loss must be small.

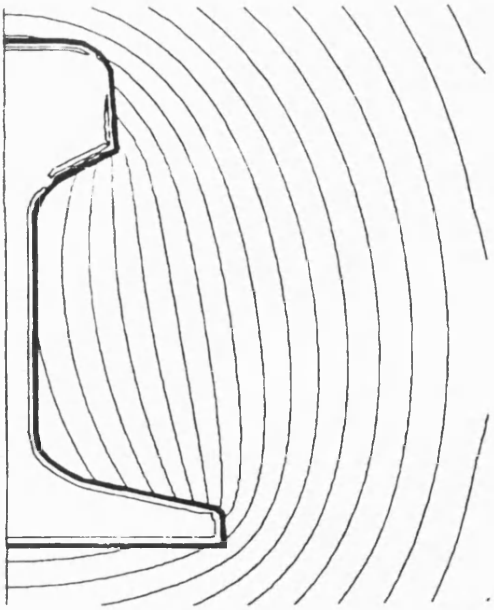

Fig. 8 *FEM vector potential contours for nonlinear rail material*

3.1.4 Accurate impedance model: The following steps summarise the modelling procedure for internal rail impedance for large-signal AC excitation:

(i) Determine *B-H* loops of rail material (Fig. 2).

(ii) Obtain effective permeability magnitude from normal curve and FDM (Fig. 5).

(iii) Evaluate P, P_R, P_H, P_W by harmonic analysis of *B-H* loops (Tables 2 and 3).

(iv) Determine angle of complex permeability (eqns. 11, 12).

(v) Calculate rail GMD and perimeter-equivalent radius (Table 1 and Appendix 9.3).

(vi) Use linear relationship to obtain inductance and resistance per unit length (eqn. 15).

3.2 Incremental AC impedance

In DC rail networks, the traction current flowing along the running rails defines the magnetic operating point as being on the normal magnetisation curve. The DC traction current usually contains ripple at harmonics of the power supply utility frequency and traction convertor modulation frequency, and the rails may also contain signalling current at audio frequencies. As indicated in

Table 5: FEM results at 50 Hz for rail and circular equivalent conductor for saturated conditions

Excitation current ($\hat{A}$)	FEM		Analytical model		Experimental result	
	L (μH/m)	R (mΩ/m)	L (μH/m)	R (mΩ/m)	L (μH/m)	R (mΩ/m)
800	0.672	0.231	0.670	0.220	0.635	0.252
900	0.647	0.233	0.705	0.228	0.641	0.259
1000	0.615	0.235	0.719	0.233	0.644	0.263

Section 2.2.1, in the modelling of incremental AC impedance, hysteresis loss is assumed negligible due to the small amplitude of the excursions involved. The delta permeability, as a function of H_{sp}, is evaluated experimentally by finding the operating point and using Ampere's law

$$\int H_{sp} \cdot dl = I_{DC} \tag{23}$$

The equivalent rail radii given in Section 3.1.2 and Table 1 are then used to calculate the resistance and inductance, using eqn. 15.

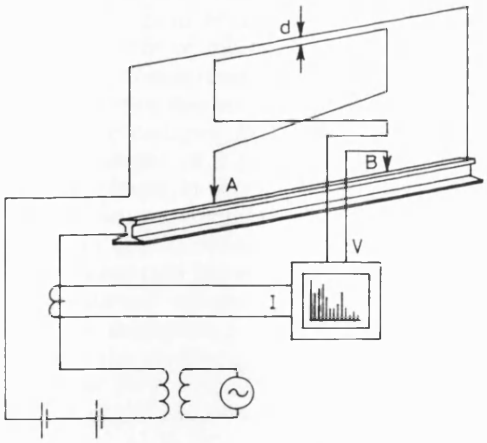

Fig. 9 *Experimental apparatus for rail internal impedance measurements*

4 Experimental measurements

4.1 Apparatus and technique

Measurements of rail internal self impedance were made in the laboratory on an isolated rail, using the apparatus shown in Fig. 9. The experimental equipment was adapted from that described by Holmstrom [3] for measurement of inductance change in an isolated rail, using, as a reference conductor, a circular copper tube. However, the method was developed further to enable absolute internal impedance measurements to be determined, by prior use of a reference conductor, which was a

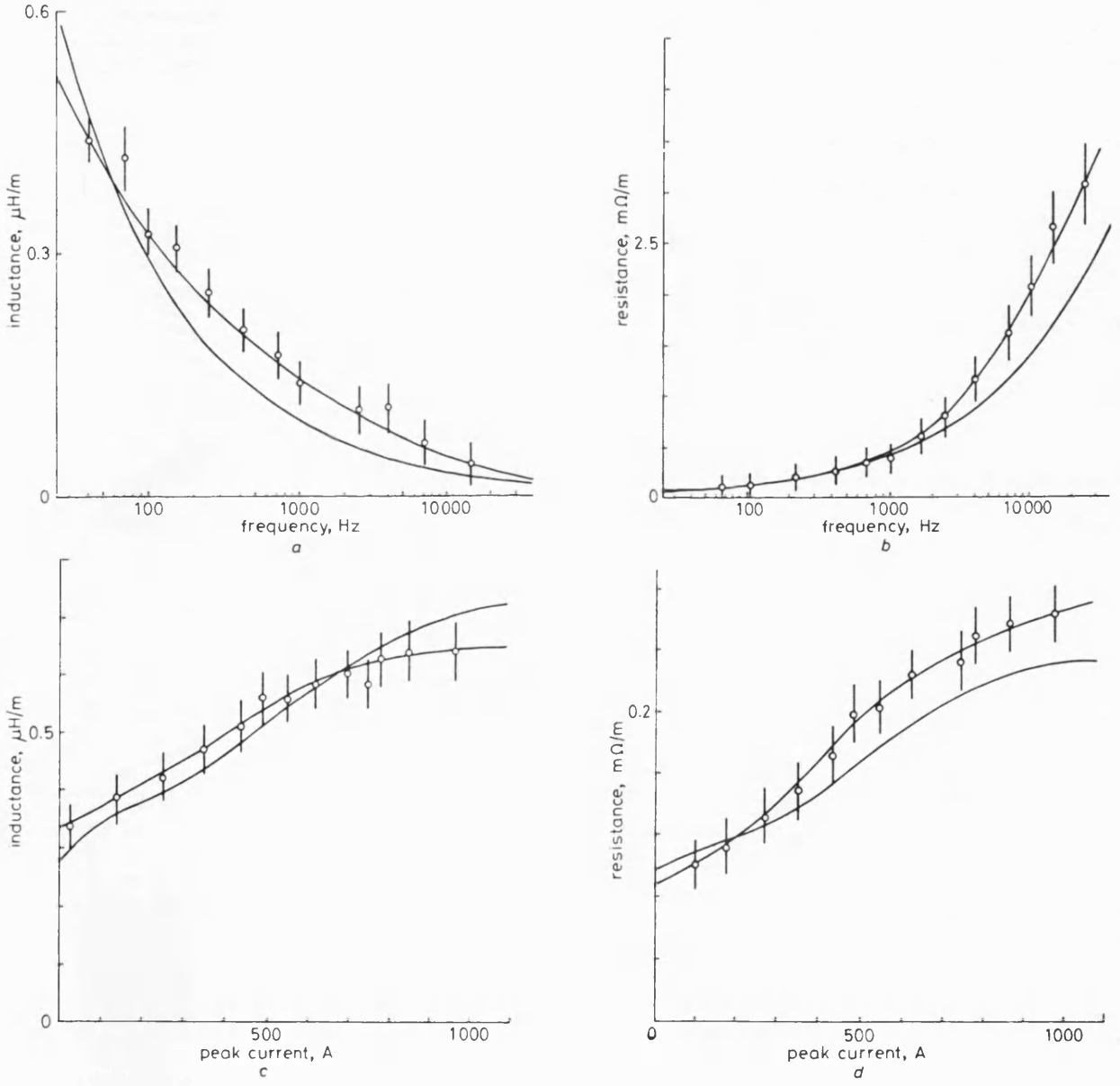

Fig. 10 *Rail self-inductance and resistance for large-signal AC excitation*

—○— experiment ——— theory

hollow copper rail the same shape and size as the test rail. This copper rail had negligible internal inductance at high frequency and so enabled the impedance measurement loop to be calibrated by adjusting its position to obtain zero circuit inductance.

The measurement procedure was to null the circuit inductance due to the test current return loop by adjusting the distance d (typically 25 mm for a measurement loop height of 2 m). The rail sample (2 m in length) is then placed in the same physical position as the copper shell, so measurements of the inductance change will represent true internal self inductance. The resistive part of the measured impedance is also an absolute measurement of internal resistance. In the apparatus, end effects are made negligible by fixing the measurement points 0.5 m from the conductor ends. The results are processed using online FFT analysis to provide noise immunity and accurate phase and frequency measurement.

4.2 Experimental results

4.2.1 Large-signal AC impedance: Measurement results of rail impedance as a function of current at 50 Hz, and as a function of frequency at 6 A, are shown in Fig. 10. At constant frequency, both resistance and inductance continually increase with current magnitude for the measurements made, indicating that a completely saturated condition was not reached. At constant current, the resistance increases and the inductance decreases with increasing frequency. Frequency variation is more significant than permeability variations because from the skin depth relationship (eqn. 6), frequency and permeability both appear with equal weighting, and the variation in frequency is much greater than that in permeability.

4.2.2 Incremental AC impedance: Results for small-signal AC rail internal impedance and variable frequency with a DC offset are shown in Fig. 11, for resistance and inductance as functions of frequency with DC as the parameter, and of DC with frequency as the parameter. When frequency is the independent variable, the square root of frequency or its reciprocal is used for the abscissa, to demonstrate the effect of variable permeability in causing deviations from linearity. As indicated in Fig. 11*c* and *d*, the variations of inductance and resistance with frequency confirm the validity of the model frequency dependency. However the current variations are small, suggesting that the change in permeability and the effect of hysteresis within the measurement range are less significant.

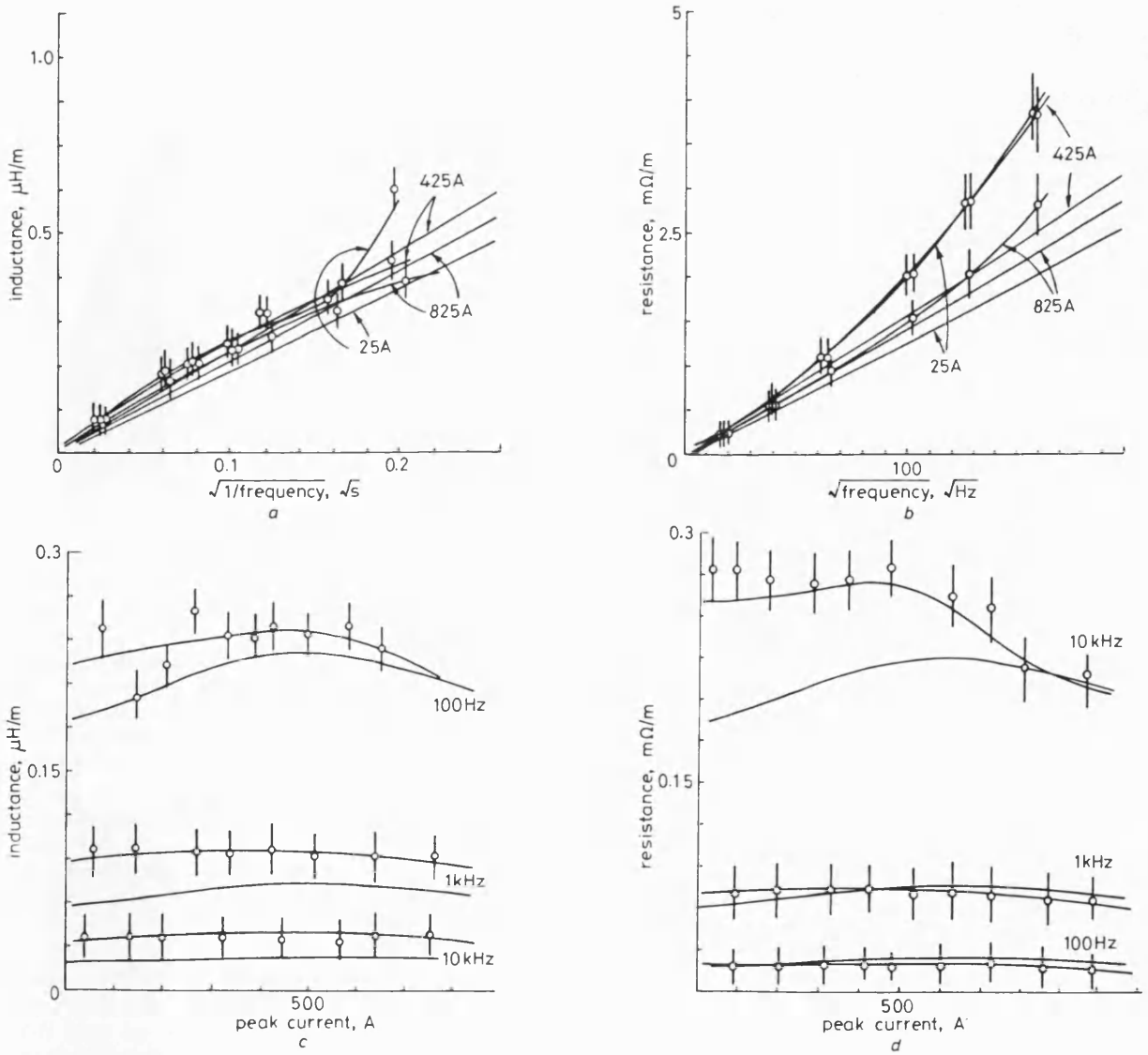

Fig. 11 *Rail self-inductance and resistance for incremental AC with steady DC excitation*

—○— experiment ——— theory

5 Discussion and model applicability

Superimposed on Figs. 10 and 11 are theoretical curves derived from the models described in Sections 3 and 4. The validated models have been used to generate rail internal self inductance and resistance as functions of AC, DC and frequency. These are shown in Figs. 12 and 13. Although most of the inductance variation occurs at low frequency, this is not the case for resistance. The variations of inductance and resistance with large signal AC are consistent with the permeability changes.

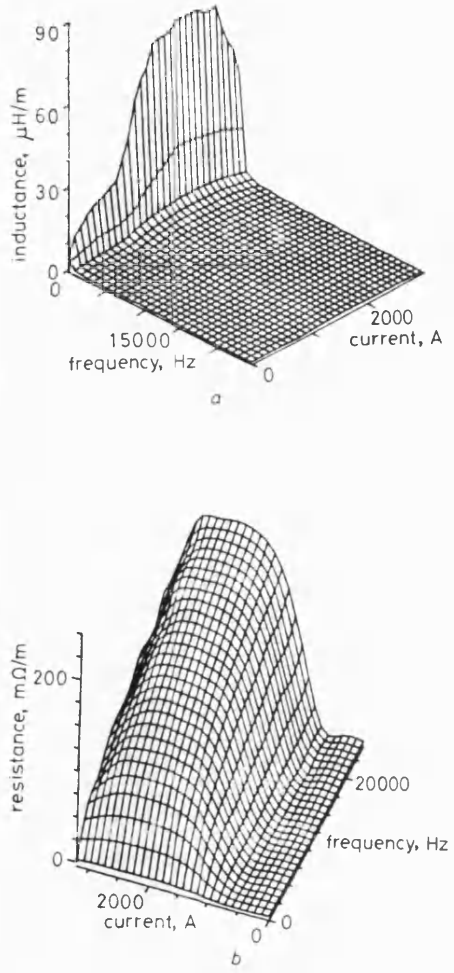

Fig. 12 *Model self-inductance and resistance for large-signal AC excitation*

The following considerations apply when using the rail internal self impedance model:

(*a*) *Saturation* — The increased loss with rail saturation can be explained in terms of the increase in magnitude of the fundamental flux density for sinusoidal field excitation.

(*b*) *Hysteresis* — The effect of hysteresis is to increase the loss and decrease the inductance from nominal values, seen through the change in impedance angle. This is explained by an increase in loop area and a reduction of stored energy. With saturation, a first approximation can be made by assuming the magnitude of the effective skin depth remains unchanged. This is a reasonable assumption because the effect of hysteresis is to enlarge the *B-H* loop by introducing harmonics, rather than to change the magnitude of the fundamental flux. However, a skin depth variation does accompany the magnetic field phase change within the material. Fig. 6 shows that the addition of hysteresis increases the phase change at the effective skin depth. Quantification of the increase could be used as a further correction factor to the calculated angle of complex effective permeability. However, the effect is small and has thus been neglected in the model.

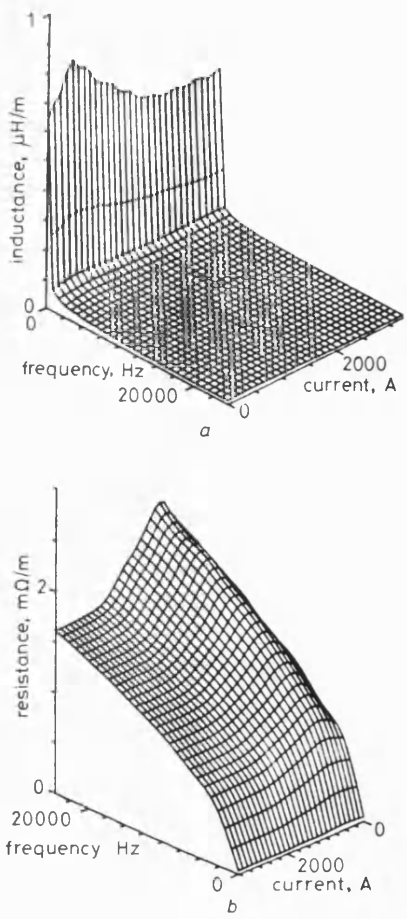

Fig. 13 *Model self-inductance and resistance for incremental AC with steady DC excitation*

(*c*) *Rail shape and frequency* — The resistance model, with perimeter equivalent radius, does not hold when the skin depth is large compared with the radius. In that case, an area equivalent radius should be used. In a similar way, for the inductance model the GMD must be recalculated based on the conductor area. This, however, is not apparent in Fig. 10 due to the low frequency at which the theoretical and experimental curves should deviate (below about 12 Hz). The difference in theory and experiment at high frequencies is thought to be due to the phenomenon of loop widening which gives rise to extra losses, with the hysteresis loss exceeding the frequency proportionality criterion [9].

(*d*) *Rail type* — For high-conductivity rail such as conductor rail in DC railways, the hysteresis loop has been found to be narrower (Table 2). Hence the FEM technique would be expected to show closer agreement with experimental measurements.

Extension of the work to the case of audio frequency superimposed on a power frequency signal would be relatively straightforward using the same techniques as for the superimposed DC case. Because the delta permeability would be constantly changing throughout the power frequency cycle (point A in Fig. 1), a single effective value would have to be evaluated, using iterative computation.

6 Conclusion

A technique has been proposed which enables rail internal self inductance and resistance to be calculated analytically from a knowledge of the ferromagnetic material properties. It takes account of saturation and hysteresis and hence considers both current and frequency dependency. The model has been rigorously tested by experiment.

7 Acknowledgments

This work was performed with financial support from the UK Science & Engineering Research Council (research grant GR/E/58816). The authors acknowledge Prof. Eastham at the University of Bath, UK, for advice on magnetic material measurements, and Dr. D. Rodger and Dr. P. Leonard for help concerning FEM calculations.

8 References

1 KRITTIAN, F.: 'Contribution to calculations of interference by thyristorized units to cables alongside a railway line', *Rail Int.*, 1981, **12**, (6), pp. 245–256
2 TRUEBLOOD, H.M., and WASCHEK, G.: 'Investigation of rail impedances', *AIEE Trans.*, 1934, **53**, pp. 1771–1780
3 HOLMSTROM, F.R.: 'The model of conductive interference in rapid transit signaling systems', *IEEE Trans.*, 1986, **IA-22**, (4), pp. 756–762
4 TYLAVSKY, D.J., and KULKARMI, A.Y.: 'Inductance calculations for earth-return trolley systems'. Proc. 1988 IEEE IAS Annual Meeting, Pittsburgh PA, 2–7 October 1988 (New York: IEEE 1988), **2**, pp. 1216–1223
5 STANEK, E.K., CATALTEPE, T., and WIITANEN, D.O.: 'Phenomena that affect the calculation of the inductance and resistance of mine track/trolley systems'. Proc. 1984 IEEE Industry Applications Society Annual Meeting, Chicago IL, 30 September–4 October 1984 (New York, IEEE, 1984), pp. 100–106
6 BURAIS, N., and GRELLET, G.: 'Numerical modelling of iron losses in ferromagnetic steel plate', *IEEE Trans.*, 1982, **MAG-18**, (2), pp. 558–561
7 LABRIDIS, D., and DOKOPOULOS, P.: 'Calculation of eddy current losses in nonlinear ferromagnetic materials', *IEEE Trans.*, 1989, **MAG-25**, (3), pp. 2665–2669
8 HSU, J.S., WOODSON, H.H., and LIOU, S.-S.P.: 'Experimental study of harmonic flux effects in ferromagnetic materials', *IEEE Trans.*, 1989, **MAG-25**, (3), pp. 2678–2685
9 MARTINEZ, M.C., MUNOZ, V., and SUCH, V.: 'L'influence du type de caracteristique magnetique utilise sur le calcul du champ electromagnetique dans les plaques d'acier massif', *EDF Bulletin de la Direction des Etudes et Recherches — Serie B Reseaux Electriques Materiels Electriques*, 1987, **1**, pp. 5–24
10 EPSTEIN, D.J.: 'Permeability', *in* VON HIPPEL, A.R. (Ed.): 'Dielectric materials and applications' (Technology Press M.I.T./Wiley, 1954)
11 HAMMOND, P.: 'Applied electromagnetism' (Pergamon Press, 1981)
12 RISSIK, H.: 'The influence of mercury-arc rectifiers upon the power factor of the supply system', *J. IEE*, 1933, **72**, pp. 435–455
13 GROVER, F.W.: 'Inductance calculations' (Dover, 1973)
14 SILVESTER, P.P., and FERRARI, R.L.: 'Finite elements for electrical engineers' (Cambridge University Press, 1983)

9 Appendix

9.1 B-H loop distortion analysis

Applying a sinusoidal magnetic field excitation to a sample of ferromagnetic material will produce a periodic, nonsinusoidal, flux density, which can be expressed as the sum of harmonics according to

$$H = H_1 \sin \omega_1 t \tag{24}$$

and

$$B = \sum_n^{\infty} B_n \sin (\omega_n t + \phi_n) \tag{25}$$

The energy loss density per cycle is calculated from the loop area. The power loss is associated with the fundamental flux density and is

$$\int_0^{2\pi} H\, dB = \frac{1}{n}\int_0^{2\pi} H_1 B_n \times \sin \omega_1 t \sum_n^{\infty} \cos (\omega_n t + \phi_n) d(\omega_1 t) \tag{26}$$

$$= \frac{1}{n}\sum_n^{\infty}\int_0^{2\pi} H_1 B_n \times \sin \omega_1 t \cos (n\omega_n t + \phi_n) d(\omega_1 t) \tag{27}$$

and when $n \neq 1$, the integral vanishes. For the fundamental ($n = 1$), the energy loss density per cycle is

$$= \int_0^{2\pi} H_1 B_1 \sin \omega_1 t \cos (\omega_1 t + \phi_1) d(\omega_1 t)$$

$$= H_1 B_1 \pi \sin \phi_1 \tag{28}$$

The power loss density (per unit volume) is given by the rate of loss of energy and at frequency f is

$$P = \pi f H_1 B_1 \sin \phi_1 \tag{29}$$

The maximum power loss density occurs when the phase difference is $\phi_1 = \pi/2$. By similar argument, the fundamental reactive power density is

$$P_R = \pi f H_1 B_1 \cos \phi_1 \tag{30}$$

with the maximum occurring at $\phi_1 = 0$. The treatment of distortion and harmonics in circuits with nonsinusoidal waveforms is achieved by defining distortion and harmonic power densities, which are not dissipative in nature, due to cross-products of the harmonics. The total apparent power density can be defined in a similar way as

$$P_A = \pi f H_1 \sum_n^{\infty} (nB_n) \tag{31}$$

As power and reactive power densities are vector components of the apparent power density,

$$P_H^2 = P_A^2 - P^2 - P_R^2$$

$$= (\pi f)^2 \left[H_1^2 \sum_n^{\infty} (n^2 B_n^2) - H_1^2 B_1^2 \sin^2 \phi_1 - H_1^2 B_1^2 \cos^2 \phi_1 \right]$$

$$= (\pi f)^2 H_1^2 \sum_n^{\infty} (n+1)^2 B_{n+1}^2 \tag{32}$$

The harmonic power density is

$$P_H = \pi f H_1 \sqrt{\left[\sum_{n=2}^{\infty} (nB_n)^2 \right]} \tag{33}$$

Rissik [12] shows that this adds to the reactive power density as a vector sum to give the Wattless power which does not contribute to the power losses. However, it does modify the magnitude of the flux density and so will influence the effective inductance. It is included in the calculation of effective inductance by calculating the inphase (Wattless) power density as

$$P_w^2 = \sqrt{(P_R^2 + P_H^2)}$$

$$= \pi f H_1 \sqrt{\left[B_1^2 \cos^2 \phi_1 + \sum_{n=2}^{\infty} (nB_n)^2 \right]} \tag{34}$$

An effective permeability angle may then be defined as

$$\theta_{\mu eff} = \arctan \frac{P}{\sqrt{(P_R^2 + P_H^2)}} \tag{35}$$

The various power loss density components can be determined from the energy loss densities found from the harmonic analysis of the *B-H* loop by multiplying by the frequency. Although this does assume that the *B-H* loop shape does not vary with frequency, Martinez *et al.* [9], considering the dynamic and static *B-H* loop analysis, show that there is only a small frequency variation (termed loop widening), which could cause modelling errors at high frequencies.

9.2 Impedance of circular conductor

The impedance of a circular conductor may be found by considering the eddy currents in an isolated conductor of circular cross-section. Consider such a conductor with radius a, with a current I flowing along the axis of the conductor in the z direction. The current density is therefore J_z, and the magnetic field is H_φ in the circumferential direction. At radius r within the conductor, Ampere's law gives

$$2\pi r H_\varphi = \int_0^r 2\pi r J_z \, dr \tag{36}$$

which when differentiated with respect to r gives

$$r \frac{\partial H_\varphi}{\partial r} + H_\varphi = r J_z \tag{37}$$

or in phasor notation

$$\frac{dH}{dr} + \frac{H}{r} = J \tag{38}$$

The EMF induced in the conductor at radius r by the flux inside the conductor is given by the difference between the resistance drops at r and a. Hence

$$\frac{1}{\sigma}(J_z - J_{z0}) = -\frac{d}{dt}\int_r^a \mu_0 H_\varphi \, dr \tag{39}$$

where J_{z0} is the surface current density. Differentiating with respect to r

$$\frac{1}{\sigma}\frac{\partial J_z}{\partial r} = \mu_0 \frac{\partial H_\varphi}{\partial t} \tag{40}$$

or in phasor notation

$$\frac{dJ}{dr} = j\omega\sigma\mu_0 H \tag{41}$$

Differentiating eqn. 36 with respect to r and substituting from eqn. 41

$$\frac{d^2H}{dr^2} + \frac{1}{r}\frac{dH}{dr} - \left(\alpha^2 + \frac{1}{r^2}\right)H = 0 \tag{42}$$

where $\alpha^2 = j\omega\sigma\mu_0$. The solution of eqn. 42 is

$$H = AI_1(\alpha r) + BK_1(\alpha r) \tag{43}$$

where A and B are arbitrary constants found from the boundary conditions. By considering the values of H at $r = 0$ and $r = a$, the constants are

$$A = \frac{I}{2\pi a I_1(\alpha a)} \tag{44}$$

and

$$B = 0 \tag{45}$$

Hence eqn. 43 becomes

$$H = \frac{I}{2\pi a}\frac{I_1(\alpha r)}{I_1(\alpha a)} \tag{46}$$

From eqn. 38

$$J = \frac{I}{2\pi a}\frac{1}{I_1(\alpha r)}\left[\frac{d}{dr}[I_1(\alpha r)] + \frac{1}{r}I_1(\alpha r)\right] \tag{47}$$

$$= \frac{\alpha I}{2\pi a}\frac{I_0(\alpha r)}{I_1(\alpha a)} \tag{48}$$

The internal impedance per unit length of the conductor is

$$z = r + j\omega\ell = (E)_{r=a} = \frac{\alpha}{2\pi a\sigma}\frac{I_0(\alpha r)}{I_1(\alpha a)} \tag{49}$$

since $J = \sigma E$.

9.3 Rail geometric mean distance

The geometric mean distance (GMD) between two conductor cross-sections is found by taking $1/n$ of the sum of n values of the logarithms of the distances between n pairs of points of the two cross-sections [13]. The resulting GMD can be considered as the effective distance between two filament conductors which gives the same mutual inductance as the original conductors.

If a single conductor is now considered, it may be thought of as being made up of a number of filament conductors. The internal self inductance of the conductor is the sum of the mutual inductances between filaments.

This introduces the concept of the GMD of an area from itself, since the mutual inductances of all the actual filaments are equivalent to the mutual inductances of two filaments separated by a distance equal to the GMD of the actual filaments from each other.

If the actual filaments have cross-sectional areas of δA_m and distances between any two filaments of ℓ_m, then the GMD of the conductor from itself is

$$\ln R = \sum_m \frac{\delta A_m \ln(\ell_m)}{\ell_m} \tag{50}$$

This may be evaluated numerically for rails. Assuming that all the current flows within the skin depth, the equivalent conductor with a cross-section of an annulus must be determined. Thus, to use the analytical model, the annular GMD must be converted to that of a solid circular cross-section by the relationship [14]

$$\frac{\text{GMD of annulus}}{\text{GMD of circle}} = 0.7788 \tag{51}$$

FOR YOUR DIARY

EuroModal '92
Copenhagen, Denmark, 12-13 March 1992
International conference organised by the International Union of Railways (UIC) and Danish State Railways (DSB) on intermodal freight transport.
Further information: UIC, Communications Department, 14 rue Jean Rey, F-75015 Paris, France. Fax: +33 1 42730140.

IEEE/ASME
JOINT RAILROAD CONFERENCE
Atlanta, Georgia, USA, 31 March-2 April 1992
Further information: Mr. Aaron C. James, Meetings Chairman, Land Transportation Division, IEEE-VTS, Booz, Allen & Hamilton Inc., 707 North First Street, 2nd Floor, St. Louis, Missouri 63102, USA. Fax: +1 314 982-1464/1470.

UIC/CER
EURAILSPEED '92
Brussels, Belgium, 27-29 April 1992
International Conference organised by the International Union of Railways (UIC) and the Community of European Railways (CER) which looks at the technological, political, economic, environmental, financing and investment aspects of high-speed rail transport.
Further information: UIC, Communications Department, 14 rue Jean Rey, F-75015 Paris, France. Fax: +33 1 42730140.

IMechE Conference
Maintenance — The Business Challenge
Birmingham, UK, 16-17 June 1992
Further information: Conference Department, C445, Institution of Mechanical Engineers, 1 Birdcage Walk, London SW1H 9JJ, UK. Fax: +44 71 222 9881.

Cost Effective
Maintenance of Railway Track
London, UK, 25-26 June 1992
Further information: Mr. Belgin Mustafa, Conference Office, Institution of Civil Engineers, 1-7 Great George Street, London SW1P 3AA, UK. Fax: +44 71 233 1743.

Fourth RIA Track Sector Course
Railway Track Engineering
Nottingham, UK, 12 July-21 August 1992
Further information: Mr. S.A. Kercher, Training Manager, Railway Industry Association, 6 Buckingham Gate, London SW1E 6JP, UK. Fax: +44 71 821 1640.

Electromagnetic field modelling of rail track using the finite-element method

Computer simulation of the electromagnetic field around an electrified rail track can give information about track impedance and admittance useful for the design of traction and signalling systems. This article describes a comprehensive field model with solution based on the finite-element method. Field plots and impedance results are presented for several track excitation conditions.

By: Dr. R.J. Hill, Senior Lecturer, School of Electronic and Electrical Engineering, University of Bath, U.K. & Mr. D.C. Carpenter, Applications Engineer, Vector Fields Ltd, Kidlington, Oxford, U.K.

Circuit simulation models of railway traction and signalling networks are useful for the design of power and signalling circuits and the assessment of electromagnetic interference and earth leakage currents. A distributed parameter multiconductor transmission line representation of rail track, shown in Fig. 1, is suitable for inclusion in such simulation models provided the values of the equivalent distributed components are known [1].

In a transmission line, energy transfer takes place through the surrounding electric and magnetic fields which are perpendicular to the longitudinal direction. The primary line distributed components are the self and mutual impedance and admittance. A remote earth reference is necessary to define these equivalent impedances and admittances. In rail track, current is carried by both the electrical conductors and the ground itself. Because of the ground currents, the associated energy flow is diffuse. To verify the applicability of the transmission line model for a rail track system, it must therefore be confirmed that energy flows far from the track are insignificant, and that the presence of the remote earth does not destroy the line propagation characteristics.

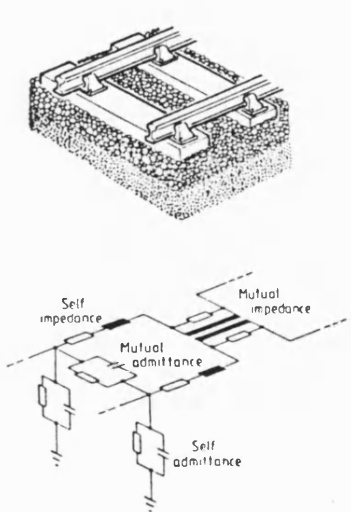

Fig. 1: Rail track substructure and equivalent transmission line network

The research described in this article is being carried out to verify the above conditions, with the additional objective of determining the values of the track equivalent circuit parameters. The importance of the work is demonstrated by the difficulty of accurate experimental determination of the track parameters. This is because of variability in environmental and ground conditions, imprecise knowledge of rail material and substructure properties and practical difficulties in making extensive measurements on a real rail track, with the associated problems of electrical interference and earth inaccessibility.

Previously published accounts of the flow of power signals along rail track rely on the theory of leaky ground-return conductors to obtain the propagation characteristics. Fundamental analysis of current propagation in and over a weakly conducting earth by Carson [2], using the method of image conductors, predicts a significant earth surface skin effect at traction frequencies. More recently, Machczynski [3] has considered both conductive and inductive transfer of current into the ground in connection with the study of earth currents in traction systems. In both cases, to obtain analytic solutions, oversimplified conditions or linear material properties were assumed. With modern computing power, much greater accuracy can be obtained using numerical field modelling to account for space and time varying parameters and material non-linearity.

In this article, the theory necessary to construct a two-dimensional numerical electromagnetic field model of the track and track-ground structure is presented. The problem space is divided into uniform elements, each with specified conductivity, permittivity and permeability. After setting the boundary and excitation conditions, the finite element method (FEM) is used to calculate the field distribution necessary to achieve a minimum energy condition. The stored and dissipated energies in the subregions of interest are then summed to obtain the circuit impedances and admittances.

The finite-element technique

The electromagnetic field around any system is known from Maxwell's equations. For rail track, only an unrealistically simple model (uniform, cylindrical rails and cables over the surface of a uniform, weakly conducting earth) may be solved analytically. The irregular rail shape, proximity of power and signalling cables and non-uniform ground substructure require the use of sophisticated models with numerical solution. The numerical methods available include finite differences, ladders and cells, and finite elements. All construct a mathematical representation of the system energy state in terms of the electromagnetic field variables, but the finite element method is the most advanced, providing an efficient technique for modelling complex shapes, taking account of material non-linearities and boundary conditions. In constructing the system model, a mesh is created with each material modelled as a distinct region or several regions, which are then subdivided into finite elements.

The numerical technique utilised for the FEM solution analyses the system under static, transient and steady state excitation conditions, and deals with non-linear material properties, so the computation and storage requirements for the code are usually severe. The FEM package used in this study obtains a quasi non-linear solution for the steady state analysis. A complete AC solution is thus possible by applying a sinusoidal waveform to a transient analysis.

Generally, there are a number of solution approaches available, including the calculus of variation and the residual techniques. The calculus of variation technique attempts to solve the equations by determining and minimising an energy functional. The second method, however, takes a more straightforward approach by equating the system energy equations to a residual, which is then reduced to a small value.

To create a FEM model, the system is first described using the Maxwell equation

$$\text{curl}\,\mathbf{H} + \sigma\mathbf{E} = \mathbf{J_s}$$

where **H** and **E** are the magnetic and electric fields, σ is the electrical conductivity and $\mathbf{J_s}$ represents the source current density. Expansion gives

$$\text{curl}\left(\frac{1}{\mu}\text{curl}\,\mathbf{A}\right) + \sigma\left(\frac{\delta \mathbf{A}}{\delta t} + \text{grad}\,V\right) = \mathbf{J_s} \qquad (2)$$

where μ is the permeability, **A** is the vector potential defined by curl **A** = **B**, with **B** the magnetic flux density, and V is the potential. Simplifying to two dimensions, the equation becomes

$$-\text{div}\left(\frac{1}{\mu}\text{grad}\,A_z\right) + \sigma\frac{\delta A_z}{\delta t} = J_{sz} \qquad (3)$$

since A and J_s now have only z-components, and V has arbitrarily been set to zero.

The objective is to reduce the residual

$$R = \text{div}\left(\frac{1}{\mu}\text{grad}\,A_z\right) - \sigma\frac{\delta A_z}{\delta t} = J_{sz} \qquad (4)$$

to zero, so numerically the problem is to determine an acceptably small value for R. This is achieved by weighting it by a factor W and minimising the integral

$$\int_\Omega WR\,d\Omega = \int_\Omega\left[\text{div}\left(\frac{1}{\mu}\text{grad}\,A_z\right) - \sigma\frac{\delta A_z}{\delta t} + J_{sz}\right]d\Omega \qquad (5)$$

where Ω is the complete problem space. This is carried out by dividing the problem space into a large number of small areas, known as meshing. W is then directly related to the finite element mesh by the local Galerkin procedure [4]. The size of the mesh is dependent on the local flux density and its rate of change.

The mesh necessary for modelling a single rail track with electrical catenary is shown in Fig. 2. Large elements are sufficient a long way from the track where the fields are low, but smaller meshes are necessary near and within the rails where the field gradients change rapidly. In computational trials, it has been found that the far field boundaries should be at a distance of about 20 times the largest dimension of the track cross-section. Because the rails act as magnetic conductors with significant permeability and conductivity, the skin effect ensures that the meshes within the rails themselves are very small near the surface, and larger in the interior (Fig. 3). Triangular elements are used near the rail surface to provide more flexibility when modelling complex shapes.

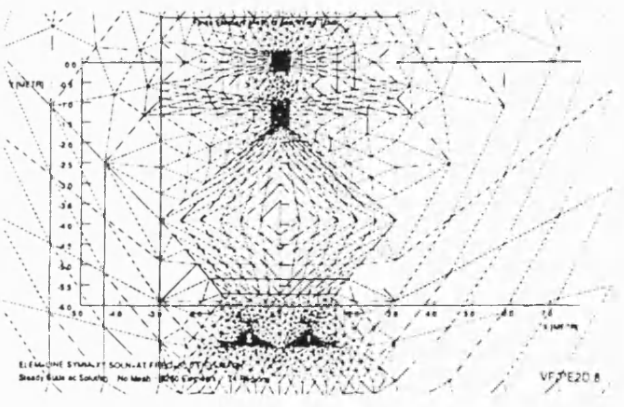

Fig. 2: FEM elemental mesh for overhead line electrified single track

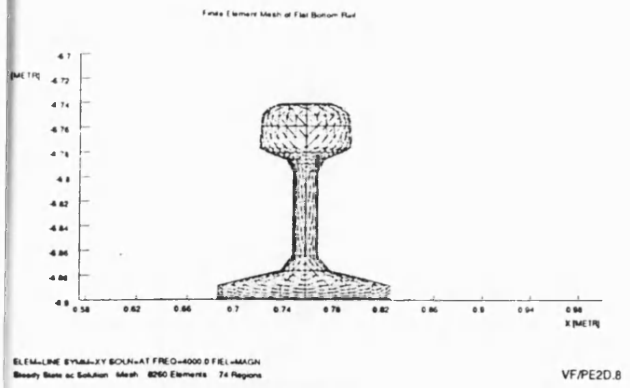

Fig. 3: FEM elemental mesh for flat-bottom rail

Inductance and resistance modelling

Equation (5) is used directly to model the electromagnetic field distribution. Since the source current density J_{sz} is known as an excitation condition, a suitable value of vector potential A_z as a function of position may be found to minimise the weighted residual. This value of vector potential then describes the minimum system energy state, so that the other electromagnetic variables, such as magnetic flux density and magnetic field, may be determined.

The circuit inductance L is found from integrating the stored system energy over the appropriate area S using

$$E_{stored} = \tfrac{1}{2}\, LI^2 = \int_s \mathbf{H}.\mathbf{B}\, dS \qquad (6)$$

where I is the known excitation current.

The system resistance R is determined from the dissipated power

$$P_{diss} = I^2R = \int_s \frac{J^2}{\sigma} dS \qquad (7)$$

where J is the conductor current density.

Fig. 4 shows the vector potential around an overhead electrified single track railway obtained using the above model. The current flows along the catenary and, equally divided, back along the rails. With a frequency of 50 Hz and a catenary current of 100 A, the vector potential line intervals are spaced at 5 μWb m^{-1}. The magnetic flux density and magnetic field lines follow the same profile as the vector potential in both air and ground since both regions are non-magnetic. From the model, the catenary track inductance is 1.95 μH m^{-1}.

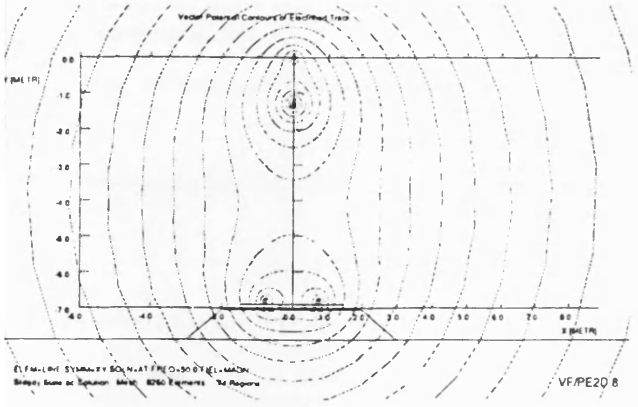

Fig. 4: Vector potential contours for overhead line electrified track

Part of the series impedance is internal to the catenary wire and rails. Fig. 5 shows a model of the rail cross-section with flux density contours generated by a sinusoidal current at 50 Hz. The result shows that the flux is concentrated near the rail surface, since the skin depth at that frequency is very small. Because of the known rail shape and material properties, it is possible to devise very accurate models of the rail internal impedance, taking into account both current and frequency [5]. The internal resistance and inductance are found as before by integrating across the rail cross-section, typical impedances at 50 Hz being 0.65 μH m^{-1} and 0.23 mΩ m^{-1}.

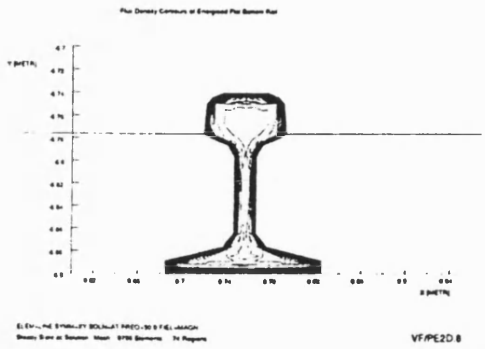

Fig. 5: Magnetic flux density contours for current-carrying flat-bottom rail

Conductance and capacitance modelling

FEM modelling of the admittance between the catenary and rails, and between the rails themselves, may be carried out in a similar way to that for impedance, by exploiting electromagnetic-electrostatic duality. For the determination of conductance, the duals are obtained by replacing A_z by H_z, J by B, E by H, μ by σ and σ by μ. The system equation is now

$$-\text{div}\left(\frac{1}{\sigma}\text{grad}\, H_z\right) = -\mu\frac{\delta H_z}{\delta t} \qquad (8)$$

and by analogy the dissipated power is

$$P_{diss} = GV^2 = \int_s \mathbf{E}.\mathbf{J}\, dS \qquad (9)$$

where G is the conductance. To determine the conductance, the boundary conditions of H_z are set by using Ampère's law ($\int H\, dl = I$).

The use of the model is illustrated in Fig. 6, which shows rail-rail current flow through the weakly conducting ground. Due to the symmetric system geometry, only half the model is shown. Fig. 6a shows lines of current flow from one rail to the centre plane, Fig. 6b gives an indication of the current magnitude from the arrow size, and Fig. 6c depicts the equipotentials. The ground is assumed to have a uniform conductivity of 3.33 mS m^{-1}. To obtain the rail-rail conductance, the package calculates the magnitude of current and potential within each region, matching boundary conditions across boundaries. Typical currents are several μA for rail-rail potential differences of a few volts, the conductance being 0.5 μS m^{-1} at a frequency of 50 Hz.

The capacitance between conductors may be determined from an electrostatic analysis. From equation (3), a static analysis with no source currents gives

$$-\text{div}\left(\frac{1}{\mu}\text{grad}\, A_z\right) = 0 \qquad (10)$$

By analogy, replacing H with D (the electric induction), A_z with V and μ with ε^{-1} (the reciprocal of permittivity), equation (10) becomes

$$-\text{div}\,\varepsilon\,\text{grad}\, V = 0 \qquad (11)$$

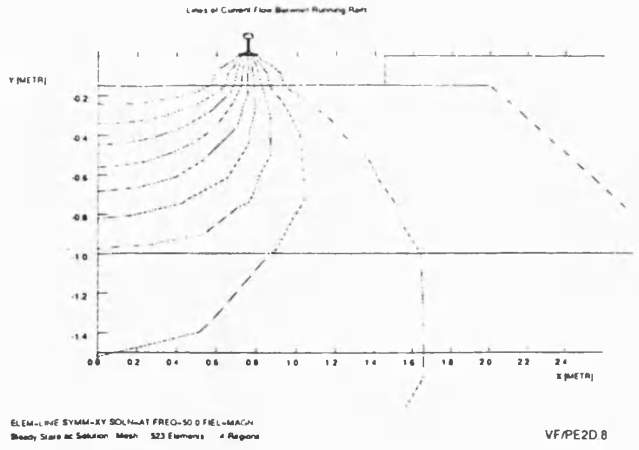

a. Current flow lines

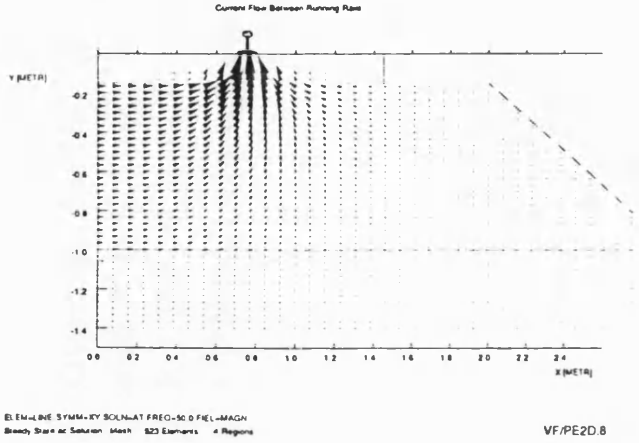

b. Current magnitude

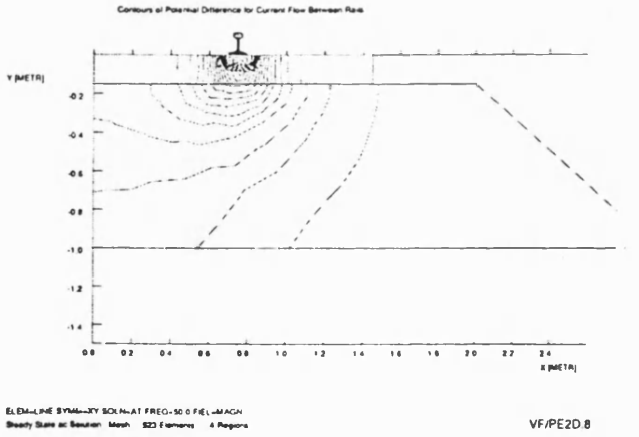

c. Equipotential lines

Fig. 6: Rail-rail ground currents for differential track excitation

The capacitance C is then obtained from the stored system energy

$$E_{stored} = \tfrac{1}{2}\ CV^2 = \int_s \mathbf{E.D}\ dS \qquad (12)$$

by setting the potential V as a boundary condition.

The model can be used to obtain the capacitance between any combination of conductors. Fig. 7 shows the model applied to an overhead electrified single track railway at 25 kV and 50 Hz. The figure shows the electric potential lines between the catenary and one rail. The contour interval is 625 V and with an effective ground permittivity of 600, the system capacitance is 11.96 pF m^{-1}.

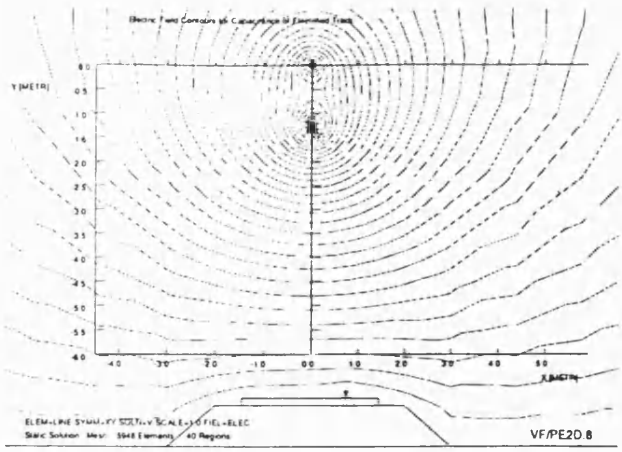

Fig. 7: Electric field equipotentials for overhead line electrified track

Conclusions

The general applicability of FEM for the analysis of railway traction systems has been demonstrated. The main difficulties in modelling a traction network for finite element solution have been that:

— the electromagnetic fields extend far from the track, which conflicts with the need to use a bounded FEM mesh;
— the permittivity, permeability and conductivity of the rails, catenary, track substructure and ground must be accurately known, including any non-linearities with current, frequency and temperature; and
— the optimum number and size of mesh elements is unknown and must be found by experience.

Before the model can be put to productive use with confidence, verification should be carried out using experiments and benchmark testing.

Further applications of FEM in rail traction systems include:

— modelling interference noise from traction drive components such as line and motor smoothing reactors;
— predicting induced voltages on buried metal pipes and cables near rail track, and crosstalk on parallel tracks [6]; and
— designing track-train transmission based signalling systems, including determining the effects of traction and signalling bonding, and other track-connected equipment.

Acknowledgement

The authors would like to acknowledge Vector Fields Ltd, UK for the use of the FEM package PE2D.

References

[1] Hill R.J. and Carpenter D.C.: Rail track modelling for signalling and electrification system simulation studies. Rail Engineering International, 1990, vol. 19, no. 4, pp. 16-20.

[2] Carson J.R.: Wave propagation in overhead wires with ground return. Bell System Technical Journal, October 1926, vol. 5, pp. 539-556.

[3] Machczynski W.: Currents and potentials in earth-return circuits exposed to alternating current electric railways. IEE Proceedings-B, September 1982, vol. 129, no. 5, pp. 279-288.

[4] Eastham J.F. and Rodger D.: Differential methods, finite elements and applications. In: Industrial Applications of Electromagnetic Computer Codes (Editors — Y.R. Crutzen, G. Molinari and G. Rubinacci). Dordrecht: Kluwer 1990, pp. 51-79.

[5] Hill R.J. and Carpenter D.C.: Determination of rail internal impedance for electric railway traction system simulation. IEE Proceedings-B, November 1991, vol. 136, no. 6, pp. 311-321.

[6] Hill R.J. and Carpenter D.C.: FEM applied to railroad track electrical impedance and adjacent track crosstalk modelling. 1991 Joint IEEE/ASME Railroad Conference, St. Louis, 21-23 May 1991 (New York: IEEE 1991), pp. 87-95.

Finite Element Method Modelling of Overhead Catenary Rail Track Impedance and Admittance

R.J. Hill (*), D.C. Carpenter (**)

(*) School of Electronic and Electrical Engineering, University of Bath, Claverton Down, Bath BA2 7AY, U.K.

(**) Vector Fields Inc., 1700 N. Farnsworth Avenue, Aurora IL 60505, U.S.A.

ABSTRACT

An electromagnetic field model is described for the determination of the electrical equivalent distributed impedances and admittances of catenary electrified rail track. The model solution, obtained using the finite-element method, takes account of the complete track-ground substructure. Sample results are presented of the calculated field lines for various track excitation conditions. Post-processing field integration gives the stored and dissipated system energy and hence the track self and mutual impedance and admittance as functions of frequency.

INTRODUCTION

A rigorous model suitable for the accurate simulation of a traction network must include the fixed electric power and signalling plant, the moving traction vehicles and the rail track. Electromagnetically, the rails and parallel conductors comprising the track act as a coupled multiconductor transmission line. The rails are laid on the surface of, and in contact with, the ground, which has finite conductivity and permittivity. An accurate and complete electric circuit model of the track is difficult to achieve due to the distributed nature of the substructure and because the rails contain ferrous material which is nonlinear with current and frequency.

In overhead catenary electrified railways, traction current flow is usually distributed between several parallel conductors, the rails and the ground. It is important to quantify the ground current effect since

the induction loop consisting of catenary and ground acts as an electromagnetic noise source, giving rise to power and harmonic frequency interference in parallel communications lines.

Considerable effort has been expended in the past in the creation of analytical models for the self and mutual impedances of conductors laid over a weakly conducting earth. The Carson/Pollaczek equations, for example, apply the theory of leaky ground-return conductors using the concept of image conductors to quantify the earth currents which flow due to induction and conduction [1]. The model predicts a significant earth surface skin effect at traction frequencies. This analytical solution, however, relies on simplified conditions, including a uniform or horizontally stratified earth conductivity. In addition to removing these restrictions, the advantage of the numerical method presented here is that a complete electromagnetic field model is created which can give the admittance as well as the impedance of a conductor set.

In this paper, a two-dimensional electromagnetic field model is described which gives the magnetic and electric fields around a section of track with an overhead catenary. After material and geometrical properties are specified, the track excitation conditions are defined and a solution obtained by the finite element method (FEM). The field vectors are integrated over appropriate regions of the model to obtain the dissipated and stored energies. The track impedance is then obtained directly. The track admittance is determined using electromagnetic-electrostatic duality transformations. Results for track impedance and admittance as functions of frequency are presented, and confirmed from published data reported in the literature.

TRANSMISSION LINE RAIL TRACK MODEL

The track model shown in Figure 1 represents a distributed coupled transmission line and consists of series self and mutual impedance and shunt self and mutual admittance. The individual lines represent rails, power conductors or signalling cables. The element values are generally nonlinear with respect to both frequency and current. To fully define the model, experimental determination of the parameters by conventional short circuit and open circuit tests is not possible because the equivalent components in the model are referenced to a remote, inaccessible earth.

In reality, the track is surrounded by current and field distributions which are influenced by the ground and rail material properties and the track geometry. Energy transfer takes place through the electric and magnetic fields which for long track sections are perpendicular to

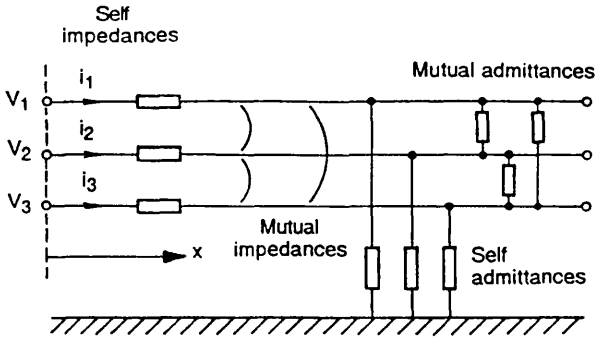

Figure 1. Rail track substructure and equivalent transmission line network

the longitudinal direction. To fully understand the physical nature of the equivalent circuit components in the model, the surrounding fields must be calculated for typical track excitation conditions. Although this implies that conditions away from the track vicinity must be considered, the reduced magnitude of the fields far from the track limits energy flow at those locations. Implementing and solving a field model in terms of the electrical equivalent parameters then overcomes the restriction of the lack of knowledge of the remote ground point.

FINITE ELEMENT MODELLING

Theoretical basis of FEM

FEM is a versatile numerical analytic technique in widespread use for the solution of static and time-varying electomagnetic field problems. Its application to problems involving magnetic stored and dissipated energy is well established, and computation times for systems with two-dimensional geometrical symmetry are reasonable with modern computer workstations. The FEM technique applies given boundary and excitation conditions to a defined physical system and results in generation of the field lines at discrete points corresponding to a minimum system energy condition. It is attractive for the rail track problem because the rails and trackbed do not have a regular geometric shape and the rails are in close proximity to each other. The difficulties in applying FEM to rail track modelling are concerned with selecting the optimum mesh size to achieve reasonable computation times, and setting appropriate model boundaries to achieve acceptable computational accuracy.

The theoretical model starts with a description of the field problem using Maxwell's equations. A detailed exposition is available in

specialist articles [2] and the following is a summary together with interpretive information resulting in the integral formulation as required by the FEM package used.

In general, the problem space is characterised by separate regions with various conductivity, permeability and permittivity values. In the present case, ferrous hysteresis is ignored, although saturation is permitted. In regions of nonzero conductivity and constant permeability, small source current loops are allowed, but otherwise no current flows. Hence

$$\nabla \times H_s = J_s \tag{1}$$

where J_s is the current density of all sources. Let

$$H_d = H_1 - H_s \tag{2}$$

where H_1 is the total field in the region. Then

$$\nabla \times H_1 = \nabla \times H_s \tag{3}$$

so $$\nabla \times H_d = 0. \tag{4}$$

Let $$H_d = \nabla\Phi \tag{5}$$

where Φ is a scalar potential function. Since

$$\nabla \times \nabla\Phi = 0 \tag{6}$$

and from Maxwell's Equation

$$B = 0 \tag{7}$$

then using the material relationship

$$B = \mu H \tag{8}$$

$$\nabla.(\mu H_1) = 0 \tag{9}$$

so $$-\nabla.\nabla\Phi + \nabla.(\mu H_s) = 0. \tag{10}$$

Hence $$-\nabla.(\mu\nabla\Phi) = 0. \tag{11}$$

Equation (11) must be solved over the complete problem region, i.e.

$$\int_\Omega N_i[\nabla.(\mu\nabla\Phi)]d\Omega = 0 \tag{12}$$

where N_i are the set of weighting (shape) functions and Ω is the whole region. From Green's theorem.

$$\int_\Omega \mu\nabla N_i.\nabla\Phi\, d\Omega - \int_\Gamma \mu N_i \frac{\partial\Phi}{\partial n}\, d\Gamma = 0 \tag{13}$$

where Γ is the region boundary line. For each element, the scalar potential is made up of

$$\Phi = \sum_1^k N_i\Phi_i \tag{14}$$

with k the number of nodes in the element. For the element e,

$$\int_{\Omega e} \mu_e \sum_1^k \left[\frac{\partial N_i}{\partial x}\frac{\partial N_j}{\partial x} + \frac{\partial N_i}{\partial y}\frac{\partial N_j}{\partial y}\right]\Phi_j\, d\Omega - \int_\Gamma \mu_e N_i \frac{\partial\Phi}{\partial n}\, d\Gamma = 0. \tag{15}$$

In regions where $\sigma \neq 0$ and is discontinuous, then $V \neq 0$ because of the boundary conditions. From the definition of vector potential

$$\nabla \times A = B \tag{16}$$

and Maxwell's Equation,

$$\nabla \times E = -\frac{\partial B}{\partial t} = -\frac{\partial}{\partial t}(\nabla \times A). \tag{17}$$

Integrating, the electric field becomes

$$E = -\left[\frac{\partial A}{\partial t} + \nabla V\right] \tag{18}$$

where V is the electric scalar potential. Using the material relationship

$$J = \sigma E \tag{19}$$

and $$\nabla \times H = J \tag{20}$$

then $$\nabla \times H = \sigma E = -\sigma\left[\frac{\partial A}{\partial t} + \nabla V\right] \tag{21}$$

The electromagnetic problem solved by FEM is then

$$\nabla \times \frac{(\nabla \times A)}{\mu} = -\sigma\left[\frac{\partial A}{\partial t} + \nabla V\right]. \tag{22}$$

with $$\nabla\sigma.\left[\frac{\partial \mathbf{A}}{\partial t} + \nabla V\right] = 0 \qquad (23)$$

and the Colomb Gauge

$$\nabla.\mathbf{A} = 0. \qquad (24)$$

The equation to solve in integral form is

$$\int_{\Omega e} N_i.\left[\nabla \times \frac{(\nabla \times \mathbf{A})}{\mu} + \sigma \frac{\partial \mathbf{A}}{\partial t}\right] d\Omega = 0. \qquad (25)$$

Again, using Green's theorem, for each element

$$\int_{\Omega e}\left\{\frac{(\nabla \times N_i).(\nabla \times \mathbf{A})}{\mu_e} + \sigma N_i.\left[\frac{\partial \mathbf{A}}{\partial t} + \nabla V\right]\right\} d\Omega - \int_{\Gamma} N_i.\left[\frac{(\nabla \times \mathbf{A}) \times \mathbf{n}}{\mu_e}\right] d\Gamma = 0 \qquad (26)$$

and $$\int_{\Omega e} \sigma \nabla\left\{N_i\left[\frac{\partial \mathbf{A}}{\partial t} + \nabla V\right]\right\} d\Omega - \int_{\Gamma} \sigma N_i\left\{\left[\frac{\partial \mathbf{A}}{\partial t} + \nabla V\right].\mathbf{n}\right\} d\Gamma = 0 \qquad (27)$$

To include the Coulomb gauge, a penalty technique is added to the above equation of the form

$$\alpha(\nabla.\mathbf{A})^2 = 0 \qquad (28)$$

which is valid over the complete problem region. In a static problem, $\partial A/\partial t = 0$ and if $V = 0$ is arbitrarily chosen, Equation (22) is simplified to

$$\nabla \times \frac{(\nabla \times \mathbf{A})}{\mu} = 0. \qquad (29)$$

To set up the FEM model, the problem region is divided into an elemental net, the extremities of which coincide with the boundary conditions. The net size is determined by the rate of change of field within it. Examples of nets for individual rails and for the complete system are shown in Figure 2. Large elements may be used a long distance from the track where the fields are low but smaller meshes are necessary near the rail surface where the field changes greatly from the skin effect. In practice, the far boundary is set at about 20 times the track lateral dimension.

FEM determination of track impedance

Solution of Equation (29) results in the calculation of values for the vector potential within each element for the minimum energy state.

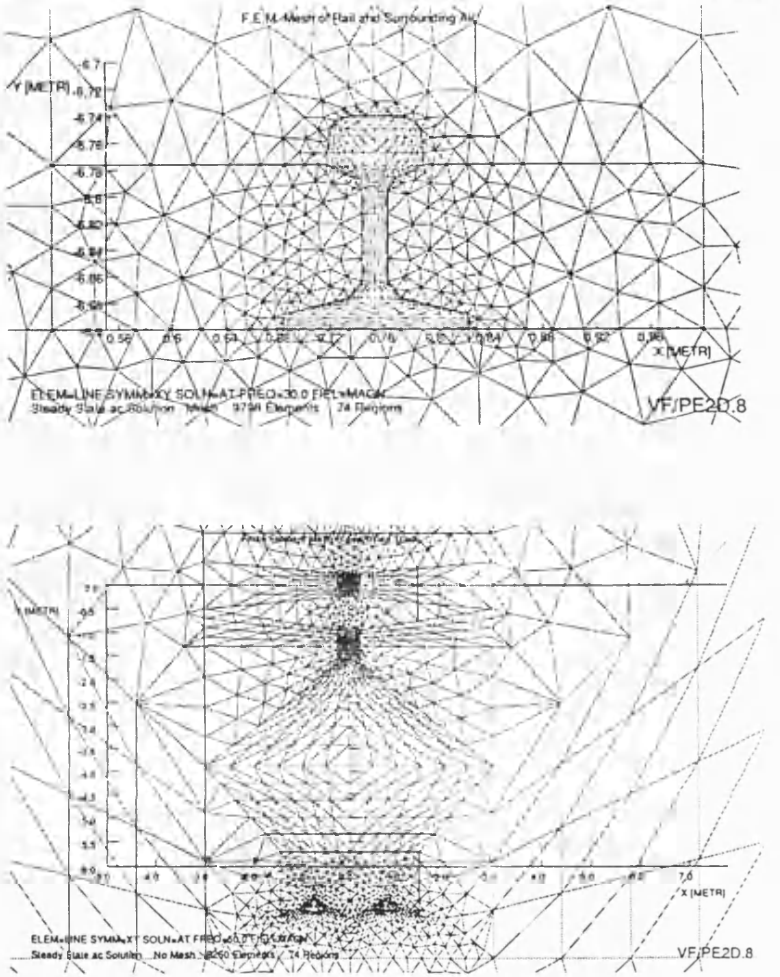

Figure 2. FEM meshes for field calculations near rail and around track

From this the values of other fixed variables such as magnetic flux density and magnetic field can be obtained and the system magnetic stored and dissipated energies evaluated.

The circuit inductance L is determined by integrating the stored system energy using the equation

$$E_{stored} = 0.5\, L\, I^2 = \int_s H.B\, dS \qquad (30)$$

where I is the known excitation current and S is the circuit area.

The system resistance R is determined from the dissipated power

$$P_{diss} = I^2R = \int_s J^2/\sigma \, dS \qquad (31)$$

where J is the conductor current density and S is the conducting area.

Figure 3 shows typical results for the vector potential distribution necessary to calculate the self impedance Z_{11} and mutual impedance

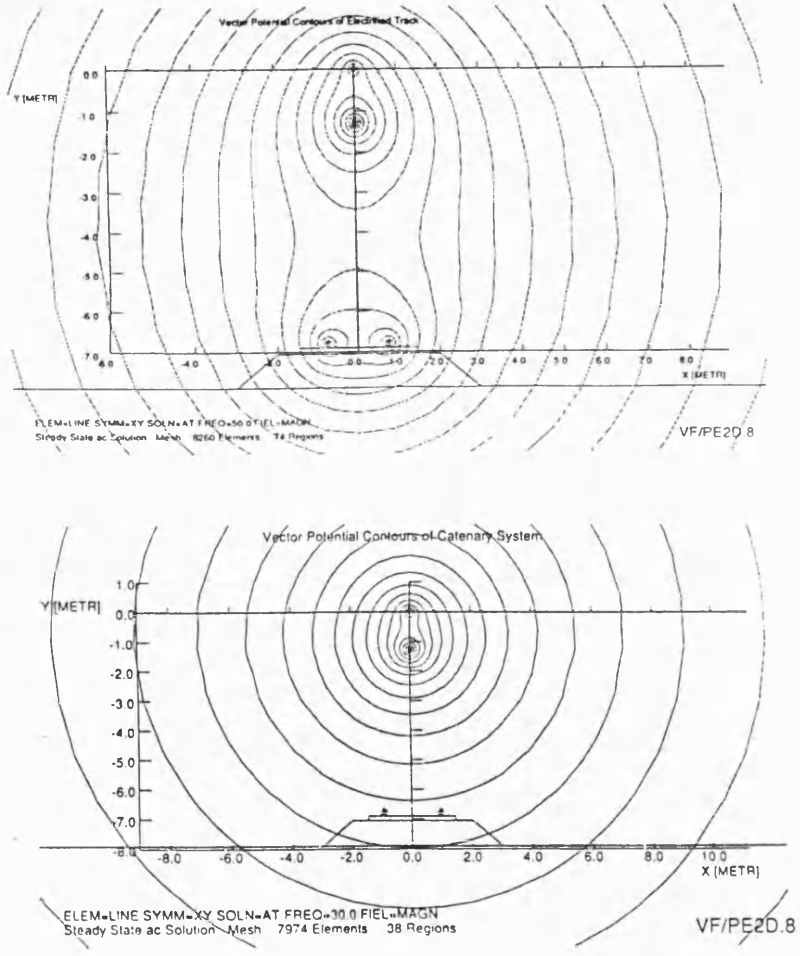

Figure 3. Vector potential contours for overhead catenary electrified single track railway: catenary with earth return,

Z_{1r}. In the former case current excitation is applied along the catenary (conductor 1) with earth return, and in the latter case, it is applied along the catenary with return through the parallel combination of the running rails. With a frequency of 50 Hz and a catenary current of 100A, the vector potential line intervals are spaced at 5 μTm. The magnetic flux density and magnetic field lines follow the same profile as the vector potential in both air and ground since both regions are non-magnetic.

Part of the series impedance is internal to the catenary wire and rails. Figure 4 shows a model of the rail cross section with current contours generated at a frequency of 50 Hz. The current is concentrated near the rail surface, since the skin depth at that frequency is very small. Because of the known rail shape and material properties, it is possible to devise very accurate models of the rail internal impedance, taking into account both current magnitude and frequency [3]. The internal resistance and inductance are found by integrating across the rail cross section.

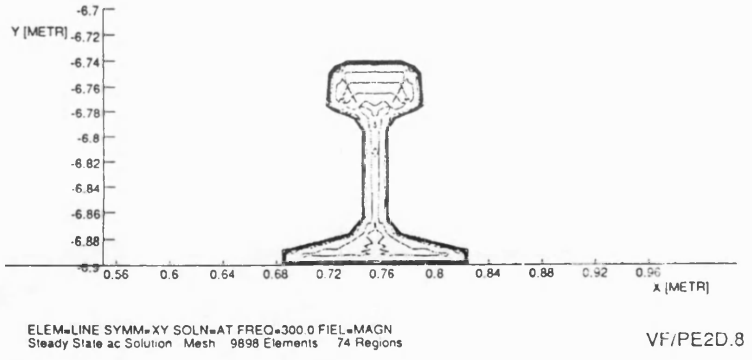

Figure 4. Current density contours in flat-bottom rail

Track admittance modelling

FEM modelling of the self and mutual admittance may be carried out in a similar way to that for impedance, by exploiting electromagnetic-electrostatic duality. For the determination of conductance, the duals are obtained by replacing A_z by H_z, J by B, E by H, μ by σ and σ by μ. The system equation becomes

$$\nabla.\left(\frac{\nabla H_z}{\sigma}\right) = -\mu \frac{\partial H_z}{\partial t} \qquad (32)$$

and by analogy the dissipated power is

$$P_{diss} = GV^2 = \int_s E.J\, dS \qquad (33)$$

where G is the conductance.

To determine the conductance, the boundary conditions of H_z are set using Ampère's law ($\int H.dl = I$). Results from the model are given in Figure 5, which shows current flow through the weakly conducting ground from a single rail to remote earth. The lines of current flow and the equipotentials are orthogonal. The model gives the self conductance g_{1e} directly by summing the magnitude of current and potential within each region and matching boundary conditions across boundaries. For g_{12}, excitation is applied between the running rails.

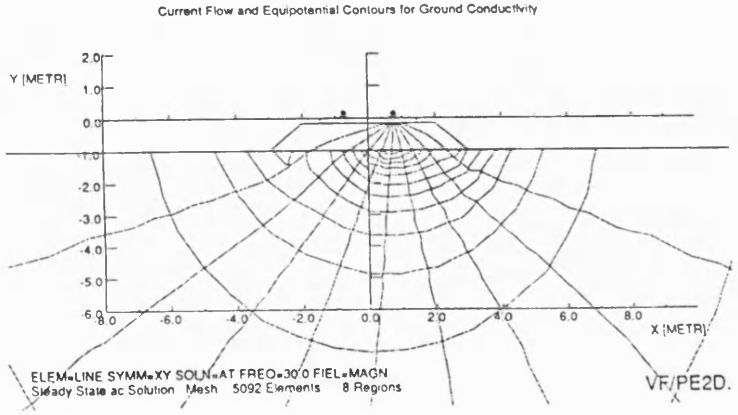

Figure 5. Current flow and equipotential lines for track conductance model (ground conductivity = 3.33 mS/m)

The capacitance between conductors may be determined from an electrostatic analysis. A static analysis with no source currents gives

$$-\frac{\nabla.(\nabla A_z)}{\mu} = 0. \qquad (34)$$

By analogy, replacing H with D (the electric induction), A_z with V and μ with $1/\varepsilon$, equation (34) becomes

$$-\nabla.(\varepsilon \nabla V) = 0. \qquad (35)$$

$$E_{stored} = 0.5\, C\, V^2 = \int_s E.D\, dS \qquad (36)$$

by setting the potential V as a boundary condition.

The model has been used to obtain the capacitance between combinations of conductors. Figure 6 shows results from an overhead electrified single track railway at 25 kV and 50 Hz. The electric potential lines between the catenary and the rail are at 625 V intervals.

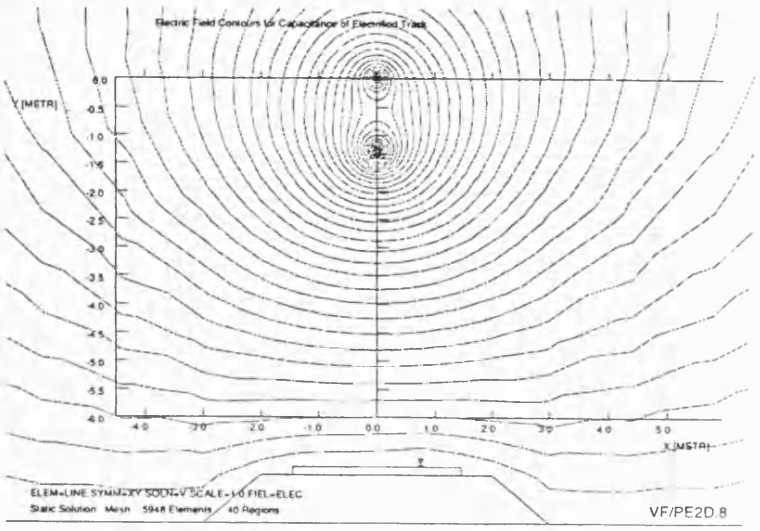

Figure 6. Electric field equipotentials between catenary and rail

TRACK IMPEDANCE AND ADMITTANCE

The models described have been solved with a commercial FEM package and the field plots generated were integrated to find the stored and dissipated energy and hence the self and mutual impedances and admittances. The results as a function of frequency are given in Figure 7, where line 1 refers to the overhead catenary and lines 2 and 3 are the running rails.

The results for phase impedance include inductance and resistance. The former, obtained by integrating across the complete field internal and external to the rail, indicates that the catenary-rail circuit inductance value is 1.95 mH/km at 50 Hz, which is in agreement

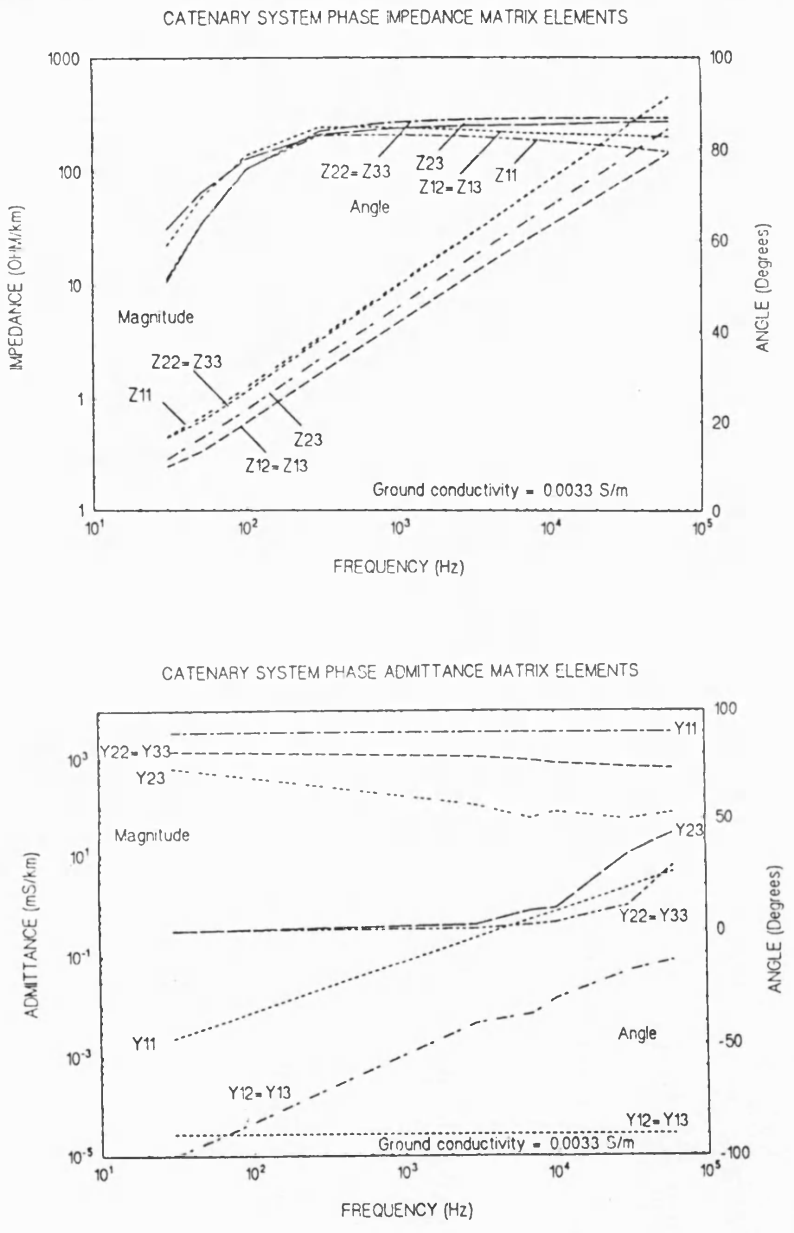

Figure 7. Phase impedance and admittance for single rail catenary electrified track

with published traction power system studies [4]. The series resistance has been calculated by integrating across the rail cross section only, a typical value at 50 Hz being 0.23 Ω/km.

The phase admittance results have been obtained from the scaling factors used in the duality transformation. To determine the conductance, the excitation currents are typically several μA for rail-rail potential differences of a few volts. The results depends critically on the value of ground conductivity selected, the rail-rail conductance being about 0.5 mS km^{-1} at a frequency of 50 Hz for a ground conductivity value of 3.3 mS/m. The catenary-rail capacitance is in agreement with published data, and is typically about 12 nF km^{-1} for an relative ground effective permittivity of 600.

CONCLUDING REMARKS

FEM analysis is a viable modelling technique to determine the impedance and admittance of railway traction networks. The main difficulties are that since the electromagnetic fields extend far from the track, careful choice of the model boundary is necessary; that the permittivity, permeability and conductivity of the rails, catenary, track substructure and ground must be accurately known; and that the optimum number and size of mesh elements has a large effect on computation time and storage and must be found from experience.

The technique is now being further developed for application in rail traction systems to model interference noise from traction drive components such as line and motor smoothing reactors, to predict induced voltages on buried metal pipes and cables near rail track, and crosstalk on parallel tracks [5] and to design track-train transmission based signalling systems based on track conductors.

ACKNOWLEDGEMENTS

The authors would like to acknowledge Vector Fields Ltd, UK for the use of the FEM package PE2D.

REFERENCES

[1] Carson, J.R. "Wave Propagation in Overhead Wires with Ground Return" *Bell System Technical Journal,* Vol. 5, pp. 539-556, 1926.

[2] Eastham, J.F. and Rodger, D. "Differential Methods, Finite Elements and Applications" *Industrial Applications of Electromagnetic Computer Codes* ed. Crutzen, Y.R., Molinari, G. and Rubinacci, G.

pp. 51-79, Kluwer, Dordrecht, 1990.

[3] Hill, R.J. and Carpenter, D.C. "Determination of Rail Internal Impedance for Electric Railway Traction System Simulation" *IEE Proceedings-B,* Vol. 136, pp. 311-321, 1991.

[4] Krittian, F. "Contribution to Calculations of Interference by Thyristorized Units to Cables alongside a Railway Line" *Rail International,* Vol. 12, pp. 245-256, 1981.

[5] Hill, R.J. and Carpenter, D.C. "FEM Applied to Railroad Track Electrical Impedance and Adjacent Track Crosstalk Modelling" pp. 87-95, *Proceedings of 1991 Joint IEEE/ASME Railroad Conference,* St Louis MO, 1991. IEEE, New York, 1991.

In Situ Determination of Rail Track Electrical Impedance and Admittance Matrix Elements

R. John Hill, *Senior Member, IEEE*, and David C. Carpenter

Abstract—**A novel differential excitation technique is described for the experimental determination of the elements of rail track impedance and admittance matrices from measurements of rail voltages and currents on a short, isolated track section. The establishment of a common earth point along the track is unnecessary, although rail breaks and driven earth rods at the feed and remote ends of the test section are required. Rail self and mutual impedance and admittance measurements are reported for a single railway track, for a frequency of 50 Hz.**

I. Introduction

An electric railway traction system consists of power and signal sources and receivers connected through the track bed structure and electrically conducting earth. The rails are coupled to parallel power lines and signal and communications cables, and the whole track system behaves as a spatial, linear, distributed network. The track voltages and currents are determined by the transmission line equations

$$\frac{d[\mathbf{V}]}{dx} = -[\mathbf{Z}][\mathbf{I}] \tag{1}$$

and

$$\frac{d[\mathbf{I}]}{dx} = -[\mathbf{Y}][\mathbf{V}] \tag{2}$$

where [V], [I] are column vectors of the track conductor phase voltages and currents, and [Z], [Y] are the track impedance and admittance matrices. The problem considered in this paper is the experimental determination of the elements of the track [Z] and [Y] matrices by site measurements.

Accurate knowledge of the values of the track impedance and admittance matrix elements is important for the electrical circuit simulation of traction systems. The elements define the track transfer function which governs power flows between substations and electric vehicles. They also determine the mixing behavior of power and signal currents in track signaling systems, and affect the sensitivity of track signaling receivers in data transmission systems using modulated carrier signals. Element nonlinearities with respect to current and frequency are also important, for example, in electromagnetic compatibility studies to predict intermodulation distortion.

Determination of the track elements has been reported in the literature only as a peripheral problem in traction simulation. In defining the element values, simplifying assumptions are usually made about material properties (rail iron conductivity and permeability, and earth conductivity and permittivity), and the nature of the track substructure. Early studies by Riordan [1] and Sunde [2] used estimated values of the single-track propagation constant. Other reported track experimental measurements consider only the differential mode propagation constant and characteristic impedance as applied to unbalanced excitation, for track signaling applications [3]. Many simulations do not consider the differential excitation of the running rails with electrical signals, and so treat the rails as a single conductor located near the ground. Examples are the modeling of harmonic propagation along the overhead catenary [4], earth currents [5], and telecommunications interference [6]. In these cases, the line inductance and capacitance are calculated from the track and cable geometric positions [7]. For more exact studies, the rail internal self-impedance may be assumed to be frequency dependent due to skin effect in the iron [8], and the external rail self-impedance and interrail mutual impedance may be estimated using the Carson–Pollaczek equations assuming a uniform earth conductivity [9].

The main difficulties in making experimental measurements of the track matrix elements are that access to an absolute earth reference is not possible, and that differential voltage and phase measurements between points at each end of the track cannot be made, because the distances are long, and the measurement instrumentation creates additional earth loops. The technique described in this paper determines all the track parameters in a single set of tests. It requires the establishment of reference probes at the sending and receiving ends of a track section. These probes have a finite earth impedance, which is also determined experimentally. After the track excitation voltages and currents have been measured, phasor diagrams are constructed, and the measured phasors are

Manuscript received August 30, 1991. This work was financed by the U.K. Science and Engineering Research Council under Grant # GR/E/58816.

R. J. Hill is with School of Electronic and Electrical Engineering, University of Bath, Claverton Down, Bath BA2 7AY, UK.

D. C. Carpenter was with School of Electronic and Electrical Engineering, University of Bath, Claverton Down, Bath BA2 7AY, UK. He is now with Vector Fields Limited, 24 Bankside, Kidlington, Oxford OX5 1JE, UK.

IEEE Log Number 9202730.

examined for consistency to provide error information. The corrected phasors are then treated as the variables in a track transmission line model enabling calculations to be made of all the track matrix element values.

II. Propagation of Signals Along Rail Track

A. Wave Propagation

The theory of wave propagation along multiconductor transmission lines is well known [10], [11]. Considering the distributed-parameter line of Fig. 1, the distance-dependent voltages and currents are related by the impedance and admittance matrices. In these matrices, the elements are z_{ij} and y_{ij} ($i, j = 1$ to n for an n-phase line), where z_{ii} and y_{ii} are the line self-impedances and admittances per unit length, and z_{ij} and y_{ij} are the mutual impedance per unit length of line i with respect to line j with earth return, and the mutual admittance per unit length between lines i and j, consistent with the equivalent circuit of Fig. 2. Combining (1) and (2) gives the wave equations:

$$\frac{d^2[\mathbf{V}]}{dx^2} = [\mathbf{Z}][\mathbf{Y}][\mathbf{V}] = [\mathbf{P}][\mathbf{V}] \tag{3}$$

and

$$\frac{d^2[\mathbf{I}]}{dx^2} = [\mathbf{Y}][\mathbf{Z}][\mathbf{I}] = [\mathbf{P}_I][\mathbf{I}] \tag{4}$$

since $z_{ij} = z_{ji}$ and $y_{ij} = y_{ji} (i \neq j)$. Equations (3) and (4) are solved by means of a modal transformation by determining the eigenvalues of $[\mathbf{P}]$. Introducing a diagonal matrix $[\mathbf{Q}]$ and column vectors of modal voltages $[\mathbf{V}_m]$ and currents $[\mathbf{I}_m]$, it may be shown that [10]

$$\frac{d^2[\mathbf{V}_m]}{dx^2} = [\mathbf{Q}][\mathbf{V}_m] \tag{5}$$

and

$$\frac{d^2[\mathbf{I}_m]}{dx^2} = [\mathbf{Q}][\mathbf{I}_m] \tag{6}$$

where $[\mathbf{Q}]$ contains as elements the modal propagation constants

$$[\mathbf{Q}] = \begin{bmatrix} \gamma_1^2 & 0 & \cdots \\ 0 & \gamma_2^2 & \cdots \\ \cdots & \cdots & \gamma_n^2 \end{bmatrix}. \tag{7}$$

The modal voltages and currents each satisfy the equations of a single-phase line with a unique voltage and current distribution, propagation constant and characteristic (surge) impedance at any frequency. Equations (5) and (6) can be solved independently since mutual components are eliminated. After solution, the combination of the n modes satisfies the line boundary conditions.

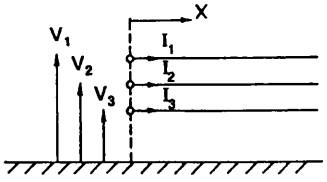

Fig. 1. Line excitation voltages and currents.

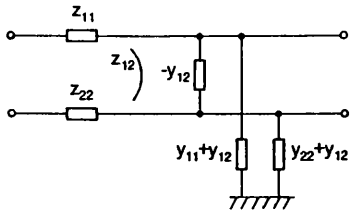

Fig. 2. Impedance and admittance model for a two-wire line with earth return.

B. Single-Rail Excitation

For a single conductor in the presence of an infinite earth plane, the impedance and admittance per unit length are z_{11} and y_{11}, and the propagation constant is

$$\gamma = \sqrt{P} = \sqrt{(z_{11}y_{11})}. \tag{8}$$

The phase voltage has components corresponding to forward and backward traveling waves. Each component produces an associated current, with the currents and voltages related by the characteristic impedance

$$z_0 = \sqrt{(z_{11}/y_{11})}. \tag{9}$$

C. The Two-Rail Line: Single-Track Railway

The two-rail line corresponds to a single rail track with no parallel electric power or signal/communications cables. The problem is considerably simplified if spatial symmetry is assumed in the conductor positions such that $z_{11} = z_{22}$ and $y_{11} = y_{22}$. Equations (3) and (4) then become

$$\frac{d^2}{dx^2}\begin{bmatrix} V_1 \\ V_2 \end{bmatrix} = \begin{bmatrix} P_1 & P_2 \\ P_2 & P_1 \end{bmatrix}\begin{bmatrix} V_1 \\ V_2 \end{bmatrix} \tag{10}$$

and

$$\frac{d^2}{dx^2}\begin{bmatrix} I_1 \\ I_2 \end{bmatrix} = \begin{bmatrix} P_1 & P_2 \\ P_2 & P_1 \end{bmatrix}\begin{bmatrix} I_1 \\ I_2 \end{bmatrix} \tag{11}$$

where

$$P_1 = y_{11}z_{11} + y_{12}z_{12} \tag{12}$$

and

$$P_2 = y_{11}z_{12} + y_{12}z_{11} \tag{13}$$

according to the element notation given in the unit length model of Fig. 2. The two propagation modes are each associated with a pair of forward and backward traveling waves. The modes may be related to differential (bal-

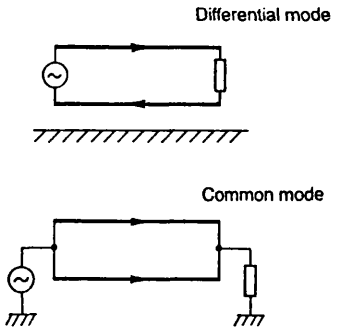

Fig. 3. Differential and common mode excitation.

anced) and common (unbalanced) excitation, as illustrated in Fig. 3. In rail track, these correspond to arrangements for track circuit excitation, where a signal source and load are connected across a length of track, and a propulsion current return path, where power is injected to the rails by a moving train and extracted at a substation or transformer connection point.

For differential mode excitation, $I_1 = -I_2$, and

$$\frac{d^2 I_1}{dx^2} = (P_1 - P_2) I_1 \tag{14}$$

with

$$\gamma_d = \sqrt{(P_1 - P_2)} = \sqrt{[(z_{11} - z_{12})(y_{11} - y_{12})]} \tag{15}$$

and

$$z_{0,d} = \sqrt{[(z_{11} - z_{12})/(y_{11} - y_{12})]}. \tag{16}$$

For common mode excitation, $V_1 = V_2$ and $I_1 = I_2$. Hence

$$\gamma_c = \sqrt{(P_1 + P_2)} = \sqrt{[(z_{11} + z_{12})(y_{11} + y_{12})]} \tag{17}$$

with

$$z_{0,c} = \sqrt{[(z_{11} + z_{12})/(y_{11} + y_{12})]}. \tag{18}$$

D. Parallel Lines and Tracks

The above considerations can be extended to the general n-phase transmission line system corresponding to rail tracks with parallel power and signal cables. The line voltages and currents are determined in terms of propagation modes, the dominant mode being determined by the power feeding arrangements. In the solution of modal systems, multiple-track railways can exploit planes of symmetry, rather like the case of symmetrical components for three-phase power lines [10].

III. Theory of In Situ Track Parameter Measurement

A. Excitation of a Line Pair with Earth Return

Consider two conductors 1 and 2 with different excitation voltages $V_1(x)$ and $V_2(x)$ and carrying different currents $I_1(x)$ and $I_2(x)$ as shown in Fig. 4. The source impedances are z_1 and z_2, and the two lines are loaded with equal impedances z_L. The excitation voltage source and load are each earthed with an impedance of z_E.

For homogenous lines, the solution of (10) for this line geometry may be expressed in terms of exponential functions as:

$$\begin{bmatrix} V_1(x) \\ V_2(x) \end{bmatrix} = \begin{bmatrix} T_{11} & T_{12} \\ T_{21} & T_{22} \end{bmatrix} \begin{bmatrix} A_1 \exp - \gamma_1 x + B_1 \exp \gamma_1 x \\ C_1 \exp - \gamma_2 x + D_1 \exp \gamma_2 x \end{bmatrix} \tag{19}$$

where T_{ij} and A_1, B_1, C_1, and D_1 are constants determined by the line boundary conditions. The matrix [T] may be evaluated using (10) and (19) since

$$\begin{bmatrix} T_{11} & T_{12} \\ T_{21} & T_{22} \end{bmatrix} \begin{bmatrix} \gamma_1^2 & 0 \\ 0 & \gamma_2^2 \end{bmatrix} = \begin{bmatrix} P_1 & P_2 \\ P_2 & P_1 \end{bmatrix} \begin{bmatrix} T_{11} & T_{12} \\ T_{21} & T_{22} \end{bmatrix} \tag{20}$$

from which, associating γ_c with γ_1 and γ_d with γ_2, (15) and (17),

$$T_{11} = T_{21} \tag{21}$$

and

$$T_{12} = -T_{22}. \tag{22}$$

The line voltages are thus, from (19),

$$\begin{bmatrix} V_1(x) \\ V_2(x) \end{bmatrix} = \begin{bmatrix} T_{11} & -T_{22} \\ T_{11} & T_{22} \end{bmatrix} \cdot \begin{bmatrix} A_1 \exp - \gamma_1 x + B_1 \exp \gamma_1 x \\ C_1 \exp - \gamma_2 x + D_1 \exp \gamma_2 x \end{bmatrix} = \begin{bmatrix} 1 & -1 \\ 1 & 1 \end{bmatrix} \begin{bmatrix} A \exp - \gamma_1 x + B \exp \gamma_1 x \\ C \exp - \gamma_2 x + D \exp \gamma_2 x \end{bmatrix} \tag{23}$$

and the line currents are

$$\begin{bmatrix} I_1(x) \\ I_2(x) \end{bmatrix} = \begin{bmatrix} z_{11} & z_{12} \\ z_{21} & z_{22} \end{bmatrix}^{-1} \begin{bmatrix} dV_1(x)/dx \\ dV_2(x)/dx \end{bmatrix}. \tag{24}$$

If the lines are symmetric, $z_{11} = z_{22}$, and since $z_{21} = z_{12}$,

$$\begin{bmatrix} I_1(x) \\ I_2(x) \end{bmatrix} = k_1 \begin{bmatrix} -1 & 1 \\ -1 & 1 \end{bmatrix} \begin{bmatrix} A \exp - \gamma_1 x \\ B \exp \gamma_1 x \end{bmatrix} + k_2 \begin{bmatrix} 1 & -1 \\ -1 & 1 \end{bmatrix} \begin{bmatrix} C \exp - \gamma_2 x \\ D \exp \gamma_2 x \end{bmatrix} \tag{25}$$

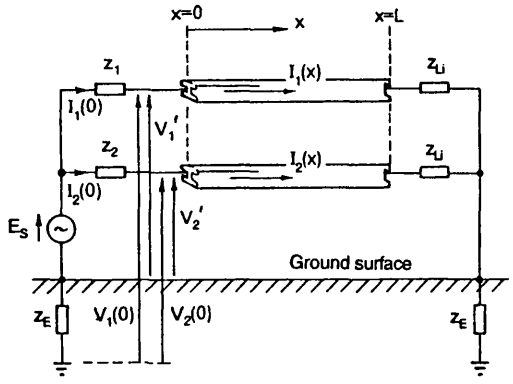

Fig. 4. Experimental arrangement.

where k_1 and k_2 are constants determined by the line geometry. Equations (23) and (25) may be solved to give the impedance matrix elements in terms of the constants γ_1, γ_2, k_1 and k_2. The result, shown in Appendix I, is

$$z_{11} = 0.5\left\{\frac{\gamma_1}{k_1} + \frac{\gamma_2}{k_2}\right\} \tag{26}$$

$$z_{12} = 0.5\left\{\frac{\gamma_1}{k_1} - \frac{\gamma_2}{k_2}\right\}. \tag{27}$$

The admittance matrix elements are obtained from (15), (17), (26), and (27) as

$$y_{11} = \frac{(z_{11} - z_{12})\gamma_1^2 + (z_{11} + z_{12})\gamma_2^2}{\det [\mathbf{Z}]} \tag{28}$$

and

$$y_{12} = \frac{(z_{11} - z_{12})\gamma_1^2 - (z_{11} + z_{12})\gamma_2^2}{\det [\mathbf{Z}]}. \tag{29}$$

B. Sending-End and Receiving-End Boundary Conditions

Knowledge of the receiving-end currents and voltages for known values of z_L enables the constants A, B, C, and D to be found in terms of k_1, k_2, γ_1, γ_2 and z_E. The line voltages at the load end are

$$\begin{bmatrix} V_1(L) \\ V_2(L) \end{bmatrix} = \begin{bmatrix} (z_L + z_E) & z_E \\ z_E & (z_L + z_E) \end{bmatrix} \begin{bmatrix} I_1(L) \\ I_2(L) \end{bmatrix}. \tag{30}$$

From (23) and (25), the line voltages and currents at $x = L$ may also be determined in terms of k_1, k_2, γ_1, γ_2, A, B, C, and D. Further, at the sending-end with $x = 0$, using (25),

$$\begin{bmatrix} I_1(0) \\ I_2(0) \end{bmatrix} = k_1 \begin{bmatrix} -1 & 1 \\ -1 & 1 \end{bmatrix} \begin{bmatrix} A \\ B \end{bmatrix} + k_2 \begin{bmatrix} 1 & -1 \\ -1 & 1 \end{bmatrix} \begin{bmatrix} C \\ D \end{bmatrix}. \tag{31}$$

Equations (23) and (25) with $x = L$, and (30) and (31), may thus be solved for the coefficients A, B, C, and D as functions of z_L, z_E, k_1, k_2, γ_1, and γ_2 and the variables $I_1(0)$ and $I_2(0)$. The result is given in Appendix II.

Since the absolute values of $V_1(0)$ and $V_2(0)$ cannot be measured, further consideration of the sending-end conditions is necessary to obtain an expression to eliminate the additional voltage drop across the unknown sending-end earth impedance z_E. Only the potentials $V_1'(0)$ and $V_2'(0)$, relative to the excitation voltage terminals, and the currents $I_1(0)$ and $I_2(0)$ may be determined experimentally. Because there are five unknowns (the four track elements and the earth impedance), sufficient independent experiments must be performed to derive five independent equations. To achieve this, three different load impedances are used to make three independent sets of measurements.

If the lines are equally loaded at $x = L$ with impedance z_{Li} (i = 1 to 3), the sending-end ($x = 0$) voltages are related to the measured line voltages and currents by

$$\begin{bmatrix} V_{1i}'(0) \\ V_{2i}'(0) \end{bmatrix} = \begin{bmatrix} V_{1i}(0) \\ V_{2i}(0) \end{bmatrix} + z_E \begin{bmatrix} 1 & 1 \\ 1 & 1 \end{bmatrix} \begin{bmatrix} I_{1i}(0) \\ I_{2i}(0) \end{bmatrix}. \tag{32}$$

The solution technique, summarized in Appendix III, is to find analytical expressions for the measured line voltages in terms of the basic unknowns z_E, k_1, k_2, γ_1 and γ_2, using the constants A, B, C, and D from (B1)–(B4). The track matrix elements are then found from (26)–(29).

IV. Expermental Measurements

A. Line Excitation

The choice of excitation voltage, source impedance, and load impedance depends on the relative magnitudes of those impedances relative to the track matrix elements and earth impedance. The series impedance of rail track is normally much less than the reciprocal of the shunt admittance. Moreover, it is generally not possible to reduce the value of the earth impedance below a certain value by installing more earth rods, due to the finite ground conductivity. Therefore, in the rail track circuit, most of the series voltage drop appears across the earth impedances, rather than the line.

The line excitation must produce a high voltage differential between the two rails to create an appreciable transverse current flow through the interrail admittance, and high currents through the rails to create an appreciable longitudinal voltage drop along the rails. These conditions are satisfied by choosing the source impedances so that the rail circuit is in parallel resonance. Further, the source and load impedances must be of comparable magnitude to the line impedance. Fig. 5 shows a phasor diagram for a typical measurement where these conditions are satisfied.

B. Results

Measurements on a 36 m length of rail track were made at 50 Hz, with the excitation voltage, source impedances and load impedances shown in Table I. Also shown in that table are the measured sending-end voltages and currents. The primary results, in the form of the line self and mu-

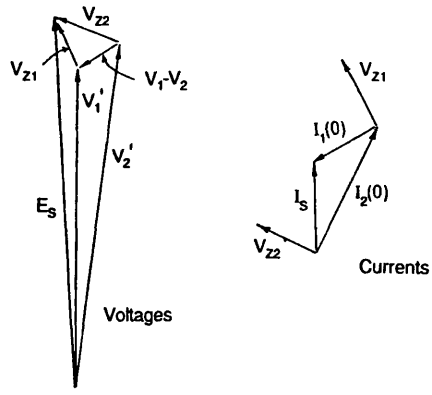

Fig. 5. Phasor diagrams for line voltages and currents.

TABLE I
EXPERIMENTAL CONDITIONS AND RESULTS

Test Number	$i = 1$	$i = 2$	$i = 3$
Load impedance Z_{Li} (Ω)	$0.099 + j0$	$0.198 + j0$	$0.298 + j0$
Supply voltage E_s (V)	$243.9 + j0$	$243.5 + j0$	$240.9 + j0$
Rail voltage V_{1i} (V)	$243.4 - j8.5$	$243.0 - j8.5$	$241.3 - j6.7$
Rail voltage V_{2i} (V)	$242.7 - j8.5$	$241.5 - j8.4$	$239.2 - j6.7$
Supply current I_{si} (A)	$3.84 - j0.317$	$3.83 - j0.32$	$3.80 - j0.27$
Line 1 current $I_{1i}(0)$ (A)	$2.01 - j0.16$	$2.23 - j0.17$	$2.54 - j0.15$
Line 2 current $I_{2i}(0)$ (A)	$1.83 - j0.16$	$1.60 - j0.15$	$1.26 - j1.34$
Sending end series impedance Z_1 (Ω)		$0.12 - j4.21$	
Sending end series impedance Z_2 (Ω)		$0.27 + j4.65$	

TABLE II
IMPEDANCE, ADMITTANCE AND GROUND RETURN IMPEDANCE RESULTS

Parameter	Value
Sef impedance z_{11} (mΩ/m)	$0.55 + j0.49$
Mitual impedance z_{12} (mΩ/m)	$0.51 + j0.31$
Sef admittance y_{11} (μS/m)	$0.38 + j0.93$
Mitual admittance y_{12} (μS/m)	$0.048 + j0.061$
Gound impedance (Ω)	$63.0 + j3.7$

TABLE III
DERIVED PROPAGATION CONSTANTS AND CHARACTERISTIC IMPEDANCES

	Propagation constant γ (Napier/m)	Characteristic impedance z_0 (Ω)
Sngle rail	$(2.34 + j2.98)10^{-5}$	$33.91 - j8.96$
Dfferential mode	$(3.77 + j1.25)10^{-5}$	$14.04 + j1.03$
Ommon mode	$(1.57 + j2.22)10^{-5}$	$26.38 - j6.11$

tial impedances and admittances, and the ground-return inpedance, are given in Table II, and the calculated characteristic impedances and propagation constants are given in Table III.

V. DISCUSSION

Measurement errors in voltage, current and phase readings are inherently large due to instrumentation inaccuracies, and in the difficulty in reading small differential voltages and phase angles. An error assessment was made using the phasor diagram representation of Fig. 5. The shift in phasor magnitude and direction arising from erroneous readings was used to estimate possible variations in the parameters, by substituting extreme, as well as nominal, phasor voltage and current values in the model. For the short track section used for the reported measurements, errors were estimated at greater than 50%. This was due to the difficulty in ensuring low rail-to-cable joint impedances, compared with the self and mutual impedance values under determination. Indeed, the short track length dictated extreme measurement accuracy, with the use of a stable power supply and linear external series components. To reduce the error, a longer measurement track section would be required.

The differential mode propagation constants and characteristic impedances evaluated from the self and mutual impedances and admittances are comparable to those obtained using conventional short-circuit and open-circuit tests, where connection to the ground is not required [3]. The various rail types and track geometries in service explain small differences between the results and other reported impedance measurements [12], [13], differences in admittance being explained by ground and environmental conditions.

The technique can readily be used for multiple-track lines, by making measurements between successive pairs of rails or conductors. However, the assumptions about track symmetry ($z_{11} = z_{22}$ and $y_{11} = y_{22}$) may not be valid for asymmetric track positioning. The presence of unex-

cited conductors will not affect the results for any rail pair. The assumption about equal earth impedances at the excitation source and load earth points is also unimportant since the reference potential is automatically adjusted to be midway between those points.

Although the short measurement track length in the reported test represented much less than a quarter wavelength at 50 Hz, the technique is unrestrictive as to the length required. Indeed, the necessity to create a pseudoresonance condition for the measurements would no longer apply since the phasors in Fig. 5 would be more widely spread due to the inherent transmission line effects.

The technique could also be used to determine any length dependency in the values of the line impedances and admittances. The models for these parameters rely on the presence of the weakly conducting earth to remove such length dependency, so for insulating earth it would be expected that the line parameters would themselves depend on the length of line involved.

VI. Concluding Remarks

- The differential rail excitation technique described enables rail track impedance and admittance matrix elements to be determined, and hence the transmission line parameters to be evaluated, for any length of track. It is applicable to any pair of parallel similar conductors laid on the surface, and in contact with, the earth.
- The method does not rely on the prior establishment of a perfect earth plane, nor on the removal of the track from the ground. It requires rail breaks to be established and earth rods to be installed at the beginning and end of the measurement section.
- The results show that at 50 Hz, no assumptions may be made regarding the relative magnitudes of the in-phase and quadrature components of the track impedances and admittances. This is significant since the propagation wavelength for the differential excitation mode of a single-rail track would be long compared with typical block section lengths employed in railway signaling systems.

Appendix I
Impedance and Admittance Matrix Coefficients

Differentiating (23) and substituting into (24),

$$\begin{bmatrix} I_1(x) \\ I_2(x) \end{bmatrix} = \begin{bmatrix} z_{11} & z_{12} \\ z_{12} & z_{11} \end{bmatrix}^{-1} \gamma_1 \cdot \begin{bmatrix} -A \exp -\gamma_1 x + B \exp \gamma_1 x \\ -A \exp -\gamma_1 x + B \exp \gamma_1 x \end{bmatrix} + \gamma_2 \begin{bmatrix} C \exp -\gamma_2 x - D \exp \gamma_2 x \\ -C \exp -\gamma_2 x + D \exp \gamma_2 x \end{bmatrix}. \quad \text{(A1)}$$

Equating (A1) and (25),

$$\begin{bmatrix} k_1 & k_2 \\ k_1 & -k_2 \end{bmatrix} \begin{bmatrix} -A \exp -\gamma_1 x + B \exp \gamma_1 x \\ C \exp -\gamma_2 x - D \exp \gamma_2 x \end{bmatrix} = \frac{1}{\det [Z]} \begin{bmatrix} z_{11} & -z_{12} \\ -z_{12} & z_{11} \end{bmatrix} \begin{bmatrix} \gamma_1 & \gamma_2 \\ \gamma_1 & -\gamma_2 \end{bmatrix} \cdot \begin{bmatrix} -A \exp -\gamma_1 x + B \exp \gamma_1 x \\ C \exp -\gamma_2 x - D \exp \gamma_2 x \end{bmatrix}. \quad \text{(A2)}$$

Adding (A2),

$$k_1(-A \exp -\gamma_1 x + B \exp \gamma_1 x) = \frac{\gamma_1}{\det [Z]} [(z_{11} - z_{12})(-A \exp -\gamma_1 x + B \exp \gamma_1 x)]$$

or

$$k_1 = \frac{\gamma_1}{z_{11} + z_{12}}. \quad \text{(A3)}$$

Subtracting (A2), it may be shown that

$$k_2 = \frac{\gamma_2}{z_{11} - z_{12}}. \quad \text{(A4)}$$

The values of z_{11} and z_{12} are determined from (A3) and (A4), and are given in (26) and (27).

The admittance matrix elements are derived from (15), (17), (26), and (27), since

$$y_{11} - y_{12} = \frac{\gamma_2^2}{z_{11} - z_{12}} \quad \text{(A5)}$$

and

$$y_{11} + y_{12} = \frac{\gamma_1^2}{z_{11} + z_{12}}. \quad \text{(A6)}$$

The resulting values for y_{11} and y_{12} are given in (28) and (29).

Appendix II
Evaluation of Constants from Line Boundary Conditions

From the solution of (23) and (25) with $x = L$, (25) with $x = 0$, and (30), the constants A, B, C, and D may

be evaluated as:

$$A = -\frac{I_1(0) + I_2(0)}{2k_1} \frac{[1 - k_1(z_L + 2z_E)]}{\{[1 - k_1(z_L + 2z_E)] + [1 + k_1(z_L + 2z_E)] \exp - 2\gamma_1 L\}} \quad \text{(B1)}$$

$$B = \frac{I_1(0) + I_2(0)}{2k_1} \frac{[1 + k_1(z_L + 2z_E)]}{\{[1 + k_1(z_L + 2z_E)] + [1 - k_1(z_L + 2z_E)] \exp 2\gamma_1 L\}} \quad \text{(B2)}$$

$$C = \frac{I_1(0) - I_2(0)}{2k_2} \frac{(1 - z_L k_2)}{[(1 - z_L k_2) + (1 + z_L k_2) \exp - 2\gamma_2 L]} \quad \text{(B3)}$$

$$D = -\frac{I_1(0) - I_2(0)}{2k_2} \frac{(1 + z_L k_2)}{[(1 + z_L k_2) + (1 - z_L k_2) \exp 2\gamma_2 L]}. \quad \text{(B4)}$$

Appendix III
Solution in Terms of Measured Line Voltages and Currents

Equations (23) and (32) can be combined as

$$\begin{bmatrix} V'_{1i}(0) \\ V'_{2i}(0) \end{bmatrix} = \begin{bmatrix} 1 & -1 \\ 1 & 1 \end{bmatrix} \begin{bmatrix} A \exp - \gamma_1 x + B \exp \gamma_1 x \\ C \exp - \gamma_2 x + D \exp \gamma_2 x \end{bmatrix} + z_E \begin{bmatrix} 1 & 1 \\ 1 & 1 \end{bmatrix} \begin{bmatrix} I_{1i}(0) \\ I_{2i}(0) \end{bmatrix}. \quad \text{(C1)}$$

Using (B1)–(B4), and rearranging.

$$\exp 2\gamma_1 L = \frac{[1 + k_1(z_{Li} + 2z_E)](1 - 2k_1 z_{ABi})}{[1 - k_1(z_{Li} + 2z_E)](1 + 2k_1 z_{ABi})} \quad \text{(C2)}$$

and

$$\exp 2\gamma_2 L = \frac{(1 + z_{Li}k_2)(1 - 2k_2 z_{CDi})}{(1 - z_{Li}k_2)(1 + 2k_2 z_{CDi})} \quad \text{(C3)}$$

where

$$z_{ABi} = \frac{V'_{1i}(0) + V'_{2i}(0)}{2[I_1(0) + I_2(0)]} - z_E \quad \text{(C4)}$$

and

$$z_{CDi} = \frac{V'_{1i}(0) - V'_{2i}(0)}{2[I_1(0) - I_2(0)]}. \quad \text{(C5)}$$

Equation (C3) may be solved for k_2 by equating the value of $\exp 2\gamma_2 L$ for two values of load ($i = 1, 2$). The result is

$$k_2 = \pm \frac{(z_{L2} - z_{L1}) + 2(z_{CD1} - z_{CD2})}{2[z_{L1} z_{L2}(z_{CD1} - z_{CD2}) + 2z_{CD1} z_{CD2}(z_{L2} - z_{L1})]}. \quad \text{(C6)}$$

Substituting k_2 into (C3) then gives γ_2. By similar substitution of $i = 1, j$ into (C2), the value of k_1 becomes

$$k_1 = \pm \frac{(z_{Lj} - z_{L1}) + 2(z_{AB1} - z_{ABj})}{2[(z_{L1} + 2z_E)(z_{Lj} + 2z_E)(z_{AB1} - z_{ABj}) + 2z_{AB1} z_{ABj}(z_{Lj} - z_{L1})]}. \quad \text{(C7)}$$

By setting $j = 2, 3$, the two resulting solutions for k_1 may be equated, yielding

$$z_E = \frac{-G \pm \sqrt{(G^2 - 4FH)}}{2F} \quad \text{(C8)}$$

where

$$F = 2(2z_{P2}\,\delta z_3 - 2z_{P3}\,\delta z_2 + z_{P2}\,\delta z_{L3} - z_{P3}\,\delta z_{L2}) \quad \text{(C9)}$$

$$G = 2[z_{P2}(z_{L3} + z_{L1})\,\delta z_3 - z_{P2}\,\delta z_{L3}(z_{Q1} + z_{Q3}) - z_{P3}(z_{L2} + z_{L1})\,\delta z_2 + z_{P3}\,\delta z_{L2}(z_{Q1} + z_{Q2})] \quad \text{(C10)}$$

and

$$H = z_{L1}(z_{P2} z_{L3}\,\delta z_3 - z_{P3} z_{L2}\,\delta z_2) + 2\,z_{Q1}(z_{Q3} z_{P2}\,\delta z_{L3} - z_{Q2} z_{P3}\,\delta z_{L2}) \quad \text{(C11)}$$

with

$$z_{Pj} = \delta z_{Lj} + 2\,\delta z_j \quad (j = 2, 3)$$

$$\delta z_{Lj} = z_{Lj} - z_{L1} \quad (j = 2, 3)$$

$$\delta z_j = z_{AB1} - z_{ABj} \quad (j = 2, 3)$$

and

$$z_{Qi} = \frac{V'_{1i}(0) + V'_{2i}(0)}{2[I_1(0) + I_2(0)]} \quad (i = 1, 2, 3).$$

References

[1] J. Riordan, "Current propagation in electric railway systems," *AIEE Trans.*, vol. 51, pp. 1011–1019, Dec. 1932.

[2] E. D. Sunde, "Currents and potentials along leaky ground-return conductors," *Electrical Engineering*, vol. 55, pp. 1338–1346, 1936.

[3] R. J. Hill, "Train position detection and track-train data transmission using audio frequency track circuits," *Journal of Electrical and Electronics Engineering, Australia*, vol. 5, no. 4, pp. 267–277, Dec. 1985.

[4] J. Holtz and H.-J. Klein, "The propagation of harmonic currents generated by inverter-fed locomotives in the distributed overhead supply system," *IEEE Trans. Power Electronics*, vol. PE-4, no. 2, pp. 168–174, April 1969.

[5] W. Machczynski, "Currents and potentials in earth-return circuits ex-

posed to alternating current electric railways," *IEE Proc.*, vol. 129B, pp. 279-288, Sep. 1982.
[6] A. Rosen, "Interference in railway lineside telephone cable circuits from 25 kV 50 Hz traction systems," *Institution of Railway Signal Engineers Proceedings*, pp. 55-79, 1958.
[7] F. Krittian, "Contribution to calculations of interference by thyristorized units to cables alongside a railway line," *Rail International*, vol. 12, no. 6, pp. 245-256, June 1981.
[8] D. C. Carpenter and R. J. Hill, "Rail impedance modelling for DC-fed railway traction simulation," in *IASTED International Symposium on Applied Modelling and Simulation*, Lugano, June 18-21, 1990. Anaheim CA: Acta Press 1990, pp. 105-108.
[9] E. D. Sunde, *Earth Conduction Effects in Transmission Systems*. New York: Dover 1968.
[10] L. M. Wedepohl, "Application of matrix methods to the solution of travelling-wave phenomena in polyphase systems," *Proc. IEE*, vol. 110, no. 12, pp. 2200-2212, Dec. 1963.
[11] R. J. Hill and S. L. Yu, "Computer modelling techniques for railway signalling interference," *International Journal of Modelling and Simulation*, vol. 9, no. 1, pp. 8-15, 1989.
[12] ——, "Mutual design of overhead transmission lines and railroad communications and signal system (Vols. I and II)." Tech. Rep., Electric Power Research Institute, Palo Alto, CA, Oct. 15, 1983, 398 pp. + 302 pp.
[13] R. J. Hill, S. L. Yu, and N. J. Dunn, "Rail transit chopper traction interference modeling using the SPICE circuit simulation package," *IEEE Trans. Vehicular Technology*, vol. 38, pp. 237-246, Nov. 1989.